DITHIENOPYRROLE-BASED ORGANIC MATERIALS FOR PHOTOVOLTAICS

Ph.D. THESIS

by

SUNIL KUMAR

DEPARMENT OF CHEMISTRY
INDIAN INSTITUTE OF TECHNOLOGY ROORKEE
ROORKEE - 247 667 (INDIA)
FEBRUARY, 2018

DITHIENOPYRROLE-BASED ORGANIC MATERIALS FOR PHOTOVOLTAICS

A THESIS

Submitted in partial fulfilment of the requirements for the award of the degree

of

DOCTOR OF PHILOSOPHY

in

CHEMISTRY

by

SUNIL KUMAR

DEPARMENT OF CHEMISTRY
INDIAN INSTITUTE OF TECHNOLOGY ROORKEE
ROORKEE-247 667 (INDIA)
FEBRUARY, 2018

INDIAN INSTITUTE OF TECHNOLOGY ROORKEE
ROORKEE

CANDIDATE'S DECLARATION

I hereby certify that the work which is being presented in the thesis entitled **"DITHIENOPYRROLE-BASED ORGANIC MATERIALS FOR PHOTOVOLTAICS"** in partial fulfilment of the requirements for the award of the Degree of Doctor of Philosophy and submitted in the Department of Chemistry of the Indian Institute of Technology Roorkee, Roorkee is an authentic record of my own work carried out during a period from July, 2013 to February, 2018 under the supervision of Dr. K. R. Justin Thomas, Associate Professor, Department of Chemistry, Indian Institute of Technology Roorkee, Roorkee.

The matter presented in the thesis has not been submitted by me for the award of any other degree of this or any other Institution.

(SUNIL KUMAR)

This is to certify that the above statement made by the candidate is correct to the best of my knowledge.

(K. R. Justin Thomas)
Supervisor

Dated:-

ACKNOWLEDGEMENTS

After an intensive period of four and an half years, today is the day: writing this note of thanks is the finishing touch on my thesis. It has been a period of intense learning for me, not only in the scientific arena, but also on a personal level. Writing this thesis has had a big impact on me. I would like to reflect on the people who have supported and helped me so much throughout this period.

First of all I would like to express my deep and sincere gratitude to my research supervisor ***Dr. K. R. Justin Thomas*** *(Associate Professor, Department of Chemistry, IIT Roorkee) for giving me the opportunity to do research and providing invaluable guidance throughout this research. His dynamism, vision, sincerity and motivation have deeply inspired me. He has taught me the methodology to carry out the research and to present the research works as clearly as possible. It was a great privilege and honor to work and study under his guidance. I am extremely grateful for what he has offered me. I would also like to thank him for his friendship, empathy, and great sense of humor. I am extending my heartfelt thanks to his wife* ***Mrs. Jeyaseeli Justin*** *for her blessings and wishes, family for their acceptance and patience during the discussion I had with him on research work. I also appreciate* ***Jeyaseeli*** *ma'am for providing a family atmosphere not only at the times with her family lunch and dinners, but also when I need moral and mental support.*

I am thankful to Head, Department of Chemistry, IIT Roorkee for all the necessary official support and for all the facilities in the department.

I thank my SRC (Student Research Committee) members, ***Dr. M.R. Maurya*** *(Professor, Department of Chemistry, IIT Roorkee),* ***Dr. Naseem Ahmed*** *(Associate Professor, Department of Chemistry, IIT Roorkee) and* ***Dr. P. Gopinath*** *(Associate Professor, Centre for Nanotechnology, IIT Roorkee) for their helpful suggestions and constant support and encouragement.*

Most of the results described in this thesis would not have been obtained without a close collaboration with few laboratories. I owe a great deal of appreciation and gratitude to ***Prof. Kuo-Chuan Ho****,* ***Dr. Chun-Ting Li*** *and* ***Miao-Syuan Fan*** *(Department of Chemical Engineering, National Taiwan University, Taipei, Taiwan), for performing DSSC fabrication and providing related studies to carry out my research work.*

I expend my thanks to ***Dr. Ritu Barthwal*** *(Professor, Department of Biotechnolgy, IIT Roorkee) for extending the NMR facility. Also, I sincerely acknowledge Department of Science and Technology (DST, FIST) for the financial support to procure Mass Spectral facility in the Department.*

*I take this opportunity to sincerely acknowledge the University Grant Commission (**UGC**), Government of India, New Delhi, for providing financial assistance in the form of Junior/Senior Research Fellowship which buttressed me to perform my work comfortably.*

*One of the most important persons who have been with me in every moment of my Ph. D. tenure is **Dr. Abhishek Baheti**, I would like to thank him to support and admire me for every step of life. His unwavering faith and confidence on my abilities and decisions provided me self-confidence to be a person like I am today.*

*I also would first like to thank my colleagues **Dr. Venkateswararao, Dr. Goverdhan, Dr. Karthik, Dr. Rajendra, Dr. Bhaskear, Dr. Snehasish, Sonu, Ankita, Joseph, Ambika, Tina, Anupriya, Abhishek & Anuj** for their wonderful collaboration and help when I asked. I am extending my thanks to the M.Tech. scholars Virender, Rashmi and M. Sc. students Somya and Diksha. You supported me greatly and were always willing to help me.*

*I would like to say thanks to my friends **Dr. Nishant Verma and Rekha bhabi ji, Dr. Varun Kundi, Surinder Kaur** (Simmi) and **Mandeep Kaur** for providing a stimulating and fun filled environment.*

*I am extremely grateful to my parents **Smt. Bimla Devi** and **Sh. Mohinder Pal** for their love, prayers, caring and sacrifices for educating and preparing me for my future. They are the most important people in my world and I dedicate this thesis to them. I am very much thankful to my wife **Mrs. Meenakshi Devi** for her love, understanding, prayers and continuing support to complete this research work. Also I express my thanks to my sisters, brother, sister in law and brother in laws for their support and valuable prayers.*

Thanks to God for this journey…

Sunil Kumar

Abstract

In order to efficiently function the dye molecule which is the heart of DSSC needs to fulfill some of the requirements such as low energy band gap, suitable LUMO energy level relative to the conduction band of the TiO_2 semiconductor for better electron injection, and sufficiently lower HOMO energy level as compared to the electrolyte redox potential for fast regeneration of the dye. Thus, the development of innovative and stable organic dyes with optical absorptions extending into red and/or near-IR regions of the solar spectrum is a challenging endeavor. In a D-π-A dye, modification of the donor (D) and conjugation pathway (π) is a useful strategy to alter the photophysical, electrochemical and photovoltaic performances. Therefore, the major approaches adopted for the improvement are the alternation of donor-acceptor motifs and modulation of the conjugation pathway to facilitate the intermolecular charge transfer (ICT). However, this approach suffers due to the large twist angle between the aromatic units in the conjugation pathway, which affect the ICT. The way to sort out this problem is the rigidification of neighboring aromatic units into planar segments. Thus, fused aromatic chromophores composed from the small aromatic units into planar and big π-conjugated systems facilitate the charge transfer and light harvesting in DSSCs. These rigid structures also possess less reorganization energy and reduce the steric congestion that allows the packing of dye more compact on TiO_2. The coplanar π-chromophore due to the intramolecular annulation results in promising properties such as photoluminescence efficiency and charge mobility. Thus, restriction for the twist and rotation allow the better electronic communication and better photo-induced charge transfer in the donor-acceptor dyads. However, more planarity for the chromophores also improves tendency of dye aggregation, low solubility in organic solvents, quenching of excited state sensitizers and recombination of the injected electrons. One way to alleviate this problem is to sterically demanding substituents or long hydrocarbon chains on rigidified chromophores, which retard dye aggregation and improve the solubility. In this regard, a plethora of new organic sensitizers containing several fused polyaryl/heteroaryl derivatives is registered. This thesis focuses on the importance of fusion of aryl groups by heteroatom in special context with dithienopyrrole and its use in DSSCs.

This thesis is divided into six chapters. First chapter introduces the importance of rigidification of chromophores by a heteroatom, a comprehensive survey on the organic

dyes containing dithienopyrrole either in the donor part or as a π-linker in the conjugation pathway in a conventional donor-π-acceptor molecular configuration and then presents the aim and scope of the work. From the literature background, it is understood that from fundamental viewpoint, molecules allow a more straightforward and reliable analysis of the structure-property relationships, an approach that remains the key tool for the design of new materials specifically designed for photovoltaic applications. Therefore, herein we believe that electron rich dithienopyrrole (DTP) unit can be explored towards systematic molecular engineering of organic materials for photovoltaic applications.

In second chapter, organic dyes based on dithienopyrrole (DTP) as a donor were synthesized in which thienyl/DTPs as π-linkers and cyanoacrylic acid acceptor were demonstrated. In comparison to thienyl, DTP-linkers showed remarkably improved light harvesting efficiency and reduced oxidation potentials for the dyes. The sufficient spatial separation between HOMO and LUMO orbitals establishes the presence of charge transfer on electronic excitation in the visible region for the DTP-linked dyes. The presence of bulky and electron rich DTP units in conjugating bridge for DTP donor dyes is found to be beneficial to retard the charge recombination processes. Therefore, the dye containing one DTP-linker showed the highest efficiency of 5.94% in the series attributable to its high J_{SC} and V_{OC} values. Irrespective of intense absorption, low efficiency was observed for the dye containing two DTP-linkers owing to its low charge collection efficiency and reduced electron lifetime.

In third chapter, DTP π-linker based organic dyes containing different arylamine/heterocyclic units as conjugating donors and cyanoacrylic acid as acceptor were synthesized and characterized. The effect of different conjugated donors such as triarylamine, carbazole and phenothiazine on the photophysical, electrochemical and photovoltaic properties is investigated. The optical and electrochemical properties of the dyes are strongly influenced by the nature of conjugating donor. The dye containing phenothiazine donor exhibited longer wavelength absorption and lowest oxidation potential in the series. The time dependent density functional calculations performed on the dye models reveal charge transfer character for their longer wavelength absorption. The dye-sensitized solar cells fabricated using a dye containing fluorenyldiphenylamine donor displayed highest power conversion efficiency (6.81%) in the series originating from the high short circuit current density (J_{SC} = 14.01 mA cm^{-2}) and high open circuit voltage (V_{OC} = 738 mV).

In fourth chapter, organic dyes featuring dithienopyrrole as a donor in D-A-π-A structural organization by employing different electron-demanding linkers such as benzothiadiazole, quinoxaline and benzotriazole besides phenyl/thienyl π-spacer and cyanoacrylic acid acceptor were synthesized. Further incorporation of TPA and DPF auxiliary donor on BTD dye with phenyl-linker extended the conjugation length and improved the spectral response for the dyes. Moreover, the position of BTD unit in the D-D-A-π-A to D-A-π-A molecular configurations adequately altered the absorption and electrochemical characteristics. The dyes, which possess BTD after DTP show negative solvatochromism in the absorption spectra, while the dyes containing BTD before DTP exhibit positive solvatochromism in the emission spectra. This clearly indicates that the former dyes are polar in ground state while the later are polarized only on electronic excitation. Theoretically, it was established that sufficient overlap of HOMO and LUMO of the dyes featuring BTD between donor and DTP units facilitate the charge transfer propensity form arylamine donor to acceptor and ensure high molar extinction coefficients in absorption. Among the dyes, the highest power conversion efficiency (η = 7.57%) for one of the dye is owed to its high photocurrent density and open circuit voltage. The superior performance of most efficient dye is attested to the sufficiently low charge transfer resistance by EIS studies.

From the work presented in Chapters 3 and 4, it is evident that the insertion of auxiliary donor increases electron lifetime and charge collection efficiency; however, introduction of BTD unit between arylamine and DTP linker (D-A-D-A) leads to low electron lifetime and high recombination resistance. This helps to realize high power conversion efficiency for this class of dyes.

In the fifth chapter, two sets of λ- and H-shaped dianchoring dyes are described which were synthesized either by tri-functionalization of dithienopyrrole or bridging two DTPs by fluorene. The λ- and H-shaped shaped dyes showed red shifted absorption maxima in comparison to previously known mono-anchoring congeners. Further, in case of λ-shaped dyes, decoration of conjugated electronic rich units at C7 position of fluorene was found to be beneficial for broadening the absorption. Also the insertion of different aromatic chromophores exerted similar effect on raising the HOMO and LUMO energy levels as a result of which energy band gap remained almost constant for all the dyes except for one dye. Theoretical calculation established that the HOMOs for λ-shaped dye remained spread over the electronic rich aromatic segments while LUMOs are

delocalized between two cyanoacrylic acids through DTP segments. The absorption maxima for the dye lacking auxiliary donor realized from HOMO to LUMO transitions while for the dyes λ-shaped dyes originated from HOMO-2 to LUMO transitions. Among the dyes, a fluorene containing H-shaped dye displayed highest power conversion efficiency due to high photocurrent density and open circuit voltage. The EIS studies revealed the large recombination resistance and small charge transfer resistance is responsible for the relatively superior performance. This work suggests that the strategy of synthesizing multi-anchoring dyes with the choice suitable aromatic system can be promising method to improve the efficiency of DSSCs.

In the sixth chapter, a summary of the work accomplished during the thesis work is presented. The relationship between the parameters such as absorption wavelength, short circuit current density (J_{SC}) and open circuit voltage (V_{OC}) is established. The role of molecular structure of the organic dyes on the photophysical and photovoltaic properties has clearly presented which may help the conceptual advancement in the development of future organic sensitizers to conquer the urgent challenges in DSSCs research.

Table of Contents

List of Figures

List of Schemes

List of Tables

List of Abbreviations

ACN	Acetonitrile
AM	Air mass
BOD	Benzooxadiazole
BT	Benzo[*b*]thiophene
BTD	Benzothiadiazole
BTZ	Benzotriazole
CA	Cyanoacrylic acid
CB	Conduction band
CDCA	Chenodeoxycholic acid
$CDCl_3$	Deuterated chloroform
CPDT	Cyclopentadithiophene
CT	Charge transfer
CV	Cyclic voltammetry
DCM	Dichloromethane
DFT	Density functional theory
DHO-TPA	dihexyloxy-triphenylamine
DMF	*N*,*N*-Dimethylformamide
DMSO	Dimethylsulphoxide
DPP	Diketopyrrolopyrrole
Dppf	1,2-Bis(diphenylphosphino)ferrocene
DPV	Differential pulse voltammetry
DPF	Diphenylaminofluorene
DSSC	Dye sensitized solar cell
DTP	Dithienopyrrole
DTBZ	Bithieno[3',2':3,4;2",3":5,6]benzo[1,2-*d*][1,2,3]triazole
EDOT	Ethylene dioxythiophene
BDT	Benzodithiophene
EIS	Electrochemical impedance spectroscopy
eV	Electron volt
FETs	Organic field effect transistors
Fl-DTP	4-(9,9-dibutyl-9*H*-fluoren-2-yl)-4*H*-dithieno[3,2-b:2',3'-*d*]pyrrole
FF	Fill factor
FTO	Fluorine doped tin oxide
HEYB	Hexenylbenzene
HOMO	Highest occupied molecular orbital
HT-HPA	4-(hexyloxy)-*N*-phenylaniline
HOP	Hexyloxypenyl
ICT	Intramolecular charge transfer
IPCE	Incident photon to current conversion efficiency
ITO	Indium tin oxide
I-V	Photocurrent-voltage
J_{SC}	Short circuit photocurrent density
LUMO	Lowest unoccupied molecular orbital
MeOH	Methanol
MLCT	Metal to ligend charge transfer
NHE	Normal hydrogen electrode
NIR	Near infra-red

NP	*N*-Annulated perylene
OLED	Organic light emitting diode
OPVs	Organic photovoltaic cells
OSCs	Organic solar cells
PCE (η)	Power conversion efficiency
PT	2-phenylthiophene
PTT	2-phenylthieno[3,2-*b*]thiophene
PV	Photo voltaic
Qx	Quinoxaline
R_{ct2}	Charge transport resistance
R_{rec}	Charge recombination resistance
TBT	Thieno[3,2-*b*] benzothiophene
TD-DFT	Time-dependent density functional theory
TEA	Triethylamine
TFA	Trifluoroacetic acid
THF	Tetrahydrofuran
TOL	Toluene
TPA	Triphenylamine
TPE	Tetraphenylethylene
TTA	tetrathienoacene
τ_e	Electron-life time
V_{OC}	Open circuit voltage
Z_w	Warburg diffusion

List of Publications

[1] Kumar S.; Thomas K.R.J.; Li C.-T.; Ho K.-C. Effect of electron-deficient linkers on the physical and photovoltaic properties of dithienopyrrole-based organic dyes. *J Mater. Sci.: Mater. Electron.* **2017**, *28*, 18404-18417.

[2] Kumar S.; Thomas K.R.J.; Li C.-T.; Ho K.-C. Synthesis and photovoltaic properties of organic dyes containing *N*-fluoren-2-yl dithieno[3,2-*b*:2′,3′-*d*]pyrrole and different donors. *Org. Electron.* **2015**, *26*, 109-116.

Chapter 1

Fused heterocyclic chromophore based organic dyes for dye sensitized solar cells: A literature review and aim & scope

1.1 Introduction

In 21st century, the most important issue is the energy scarcity, as the regular energy resources are depleting constantly. Therefore the mankind is deeply interested to find out a new clean and renewable energy resources to resolve this dilemma. The photovoltaic technology that converts the solar light into electricity is measured as an efficient tool to meet the global demand of energy [1-3]. Amongst various photovoltaic technologies, dye sensitized solar cells (DSSCs) [1] are one of the competitive candidates for energy production in order to satisfy the world's growing thirst of energy. The ease in fabrication and cost effectiveness of DSSCs has attracted the attentions of worldwide academic research groups and industrialists working on sustainable energy productions.

The major components of DSSCs are shown in Figure 1.1 (i) fluorine doped tin oxide (FTO) transparent conductive glass, on which mesoporous TiO_2 film is formed, (ii) a sensitizer adsorbed on mesoporous TiO_2 film to absorb the sunlight, (iii) a platinum counter electrode to collect electrons (iv) an electrolyte sandwiched in between working electrode and counter electrode to complete the electrical circuit. The different operational steps involved in a typical DSSC are described in Figure 1.1. Thus the absorption of photon, the sensitizers get excited from ground state to its higher energy state through photoexcitation process. From the excited state of sensitizers, electrons are pushed to the conduction band (CB) of metal oxide (TiO_2) semiconductor. Then electrons drift through the mesoscopic metal oxide film and get collected at transparent conducting substrate (FTO plate). After that, electrons go through external circuit and reach at the counter electrode. The oxidized sensitizers take electron from the redox couple and get regenerated to neutral species. In turn, oxidized half of the redox couple drifts to the counter electrode and get reduced to its original form. This cycle keeps on continuing to generate photocurrent continuously without any consumption of material. There are some

unwanted processes such as recombination of the electrons present in the conduction band of the metal oxide with oxidized dyes or constituents of the electrolyte. These processes reduce the photocurrent density (J_{SC}), open circuit voltage (V_{OC}), and overall power conversion efficiency (η).

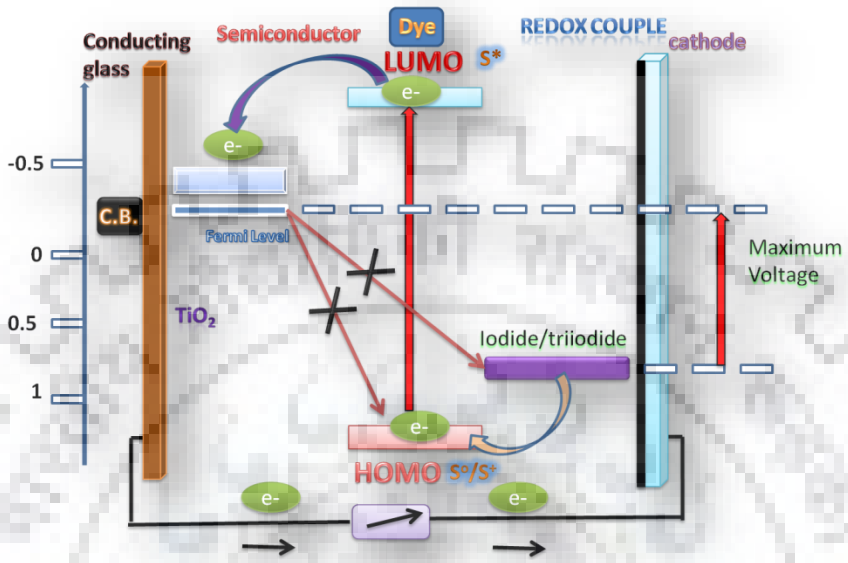

Figure 1.1 Schematic diagram and various operational processes involved in typical DSSC.

In DSSC, a sensitizer is a key element which harvests the photons of sunlight to pump the electrons from lower to higher energy states before dumping into the inorganic semiconductors [4-6]. Therefore it needs to fulfill some of the requirements such as low energy band gap, suitable high lying LUMO energy level from the conduction band of the TiO_2 semiconductor for better electron injection, and sufficient lower HOMO energy level for fast regeneration of the oxidized dye by electrolyte. As the Grätzel's crucial report on DSSC in which active material was ruthenium (II) polypyridyl complexes, revealed the overall power conversion efficiency (PCE) (η) of nearly 11% under standard (Global Air Mass 1.5) illumination, [3]. These Ru(II) complexes when adsorbed on TiO_2 possess strong metal-to-ligand charge transfer (MLCT) with extension of absorption wavelength to 700 nm [7]. However for Ru(II) complexes the longest wavelength MLCT transitions exhibited moderate molar extinction coefficients. Thus, immense attention is paid for molecular engineering of sensitizers to enhance their light harvesting ability in the red and near-IR region of sunlight and better conversion of photons into electricity [8-10]. Continuous efforts have led to progress to the extent of realizing metal-containing

dyes such as ruthenium-polypyridyl [11] complexes with 11.5% power conversion efficiency (PCE), and zinc-porphyrin [12] dyes achieving PCE as high as13.0%. But, low abundance and high cost of ruthenium metal, and complicated synthesis and purification of zinc porphyrin dyes limit their widespread application. On the other hand, metal free organic dyes displayed huge potential due to their easy and low cost synthesis from wide range of raw materials [4-10].

Figure 1.2 Pictorial representation of typical D-π-A configuration of organic sensitizers used in DSSCs.

The most efficient metal-free organic dyes are characterized by a donor-π-acceptor (D-π-A) architecture, in which the donor group (D) is an electron-rich unit, linked through a conjugated π-spacer to the electron-acceptor group (A) [13-15]. In DSSCs, unit A is bound to the TiO_2 surface usually through a carboxylic or pyridine fragment [16]. However, considerable effort were made to develop metal-free dipolar organic sensitizers to gain impressive high conversion efficiency and high stability for DSSCs [17,18] and recently organic dyes have been demonstrated to give PCE surpassing 12.5% without the use of any additive [19]. Despite this, the DSSCs fabricated with organic dyes are prone to some undesirable phenomena such as (i) aggregation on TiO_2 semiconductor surface due to π-π stacking interaction between the dye molecules (ii) decrease in the open circuit voltage (V_{OC}) due to the recombination of electrons from the conduction band of the TiO_2 with oxidized dye and/or oxidized half of the electrolyte [6]. Therefore, it is necessity to overcome these drawbacks of organic dyes to make them more efficient candidate for DSSCs applications.

1.2 Importance of rigidified chromophores in organic sensitizers used for DSSCs

Till date, the development of innovative and stable organic dyes with optical absorptions extending into red and/or near-IR regions of the solar spectrum is a challenging endeavor. Also, the modification in the donor and conjugated chromophores can be beneficial to improve their photophysical, electrochemical and photovoltaic performances. Therefore, the major approaches such as extension of conjugation length, rigidification of conjugating backbone and the introduction of donor-acceptor motifs being exploited to increase the light harvesting efficiencies of the dyes [20-23].

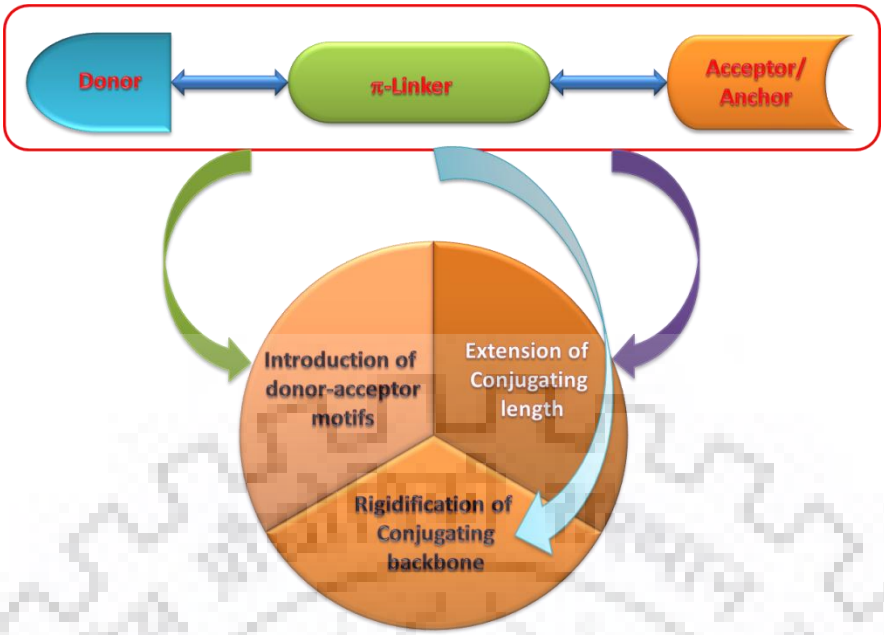

Figure 1.3 Pictorial representation of different methods for modification of donor or linker of organic sensitizers used in DSSCs.

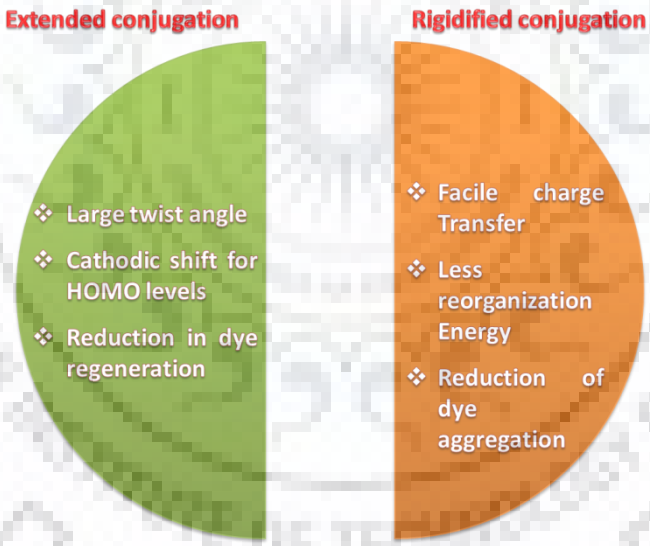

Figure 1.4 Pictorial representations of salient features of extended and rigidified conjugation.

Although, the major blows to the approach of enlargement of conjugation is the large dihedral angle between the neighboring conjugating units and cathodic shift of ground state oxidation potentials of the dyes which reduce the dye regeneration process [24,25]. So, the way to sort out this problem is the rigidification of neighboring aromatic units into fused planar segments. Thus, the fused aromatic chromophores composed from the small

aromatic units into planar and big π-conjugated systems facilitate the charge transfer and light harvesting in DSSCs [26-29] and hardly affect the dye regeneration along obvious cathodic shift of HOMO energy levels [24]. These rigid structures also possess less reorganization energy on photoexcitation of molecule and reduce the steric congestion that allows the packing of dye more compact on TiO_2 [30]. The coplanar π-chromophore due to the intramolecular annulation leads to interesting properties such as photoluminescence efficiency [31,32] and charge mobility [33]. Thus, restriction from the twist and rotation allows the better electronic communication and better photo-induced charge transfer. However, more planarity for the chromophores sometime introduces higher tendency of dye aggregation, low solubility in organic solvents, quenching of excited states and deterioration to the injected electrons. Therefore, the rigidification should be accomplished along with the introduction of sterically congested substituents and hydrocarbon chains in order to alleviate the dye aggregation and improve the solubility. In this regard, fused aromatic systems such as benzodithiophene (BDT) [34], carbazole [35], cyclopentadithiophene [36] (CPDT) and dithienopyrrole (DTP) [37] etc. have attracted considerable attention because of their electron richness, planarity and rigidity. These features lead to unique electronic properties such as high conductivity, field-effect mobility [38], and tunable stacking [39] in the solid state. Moreover, rigid structures hamper the roto-vibrational [25] modes responsible for the deactivation of the excited states in functional materials. In this regard, a plethora of new organic sensitizers containing several fused polyaryl/heteroaryl and their derivatives have come forward [40-42]. Therefore in the following discussion we will account the importance of fusion of three or more aryl rings and in particular dithienopyrrole.

1.3 Effect of fused polyaromatic/heteroaromatic chromophores (fluorene and carbazole) in DSSCs

Among the fused polyaryl systems, fluorene has taken a considerable attention [43-46]. Fluorene is a fused derivative of biphenyl which is being connected at 2,2'-position by means of on methylene bridge. This methylene bridge provides a high rigidity to fluorene and also other unique properties like high quantum efficiency etc. Therefore, fluorene-containing molecules represent an important class due to their exceptional photophysical properties and potential for chemical modification [43]. Fluorene and its derivatives are usually associated with relatively large band gaps and low HOMO energy levels, rendering them stable toward photo-degradation and thermal oxidation during

device operation [43]. The fluorene was widely used in DSSCs application as part of triarylamine donor or π-spacer [44-46]. The low-lying HOMO levels and high hole mobility character of fluorene derivatives are expected to achieve higher open circuit voltages and short-circuit currents, respectively.

Grätzel and co-workers [43] synthesized organic sensitizers **D1** and **D2** featuring fluorene units in the donor part. These dyes showed sufficient increase in photocurrent density, open-circuit voltage and hence power conversion efficiency when compared to the biphenyl congeners **R1** [44] and **R2** [45] (Figure 1.5). These dyes containing difluorenylaniline donor are found to be efficient candidates for DSSCs as it prompt enhanced photo- and thermal- stability for the sensitizers [46-48].

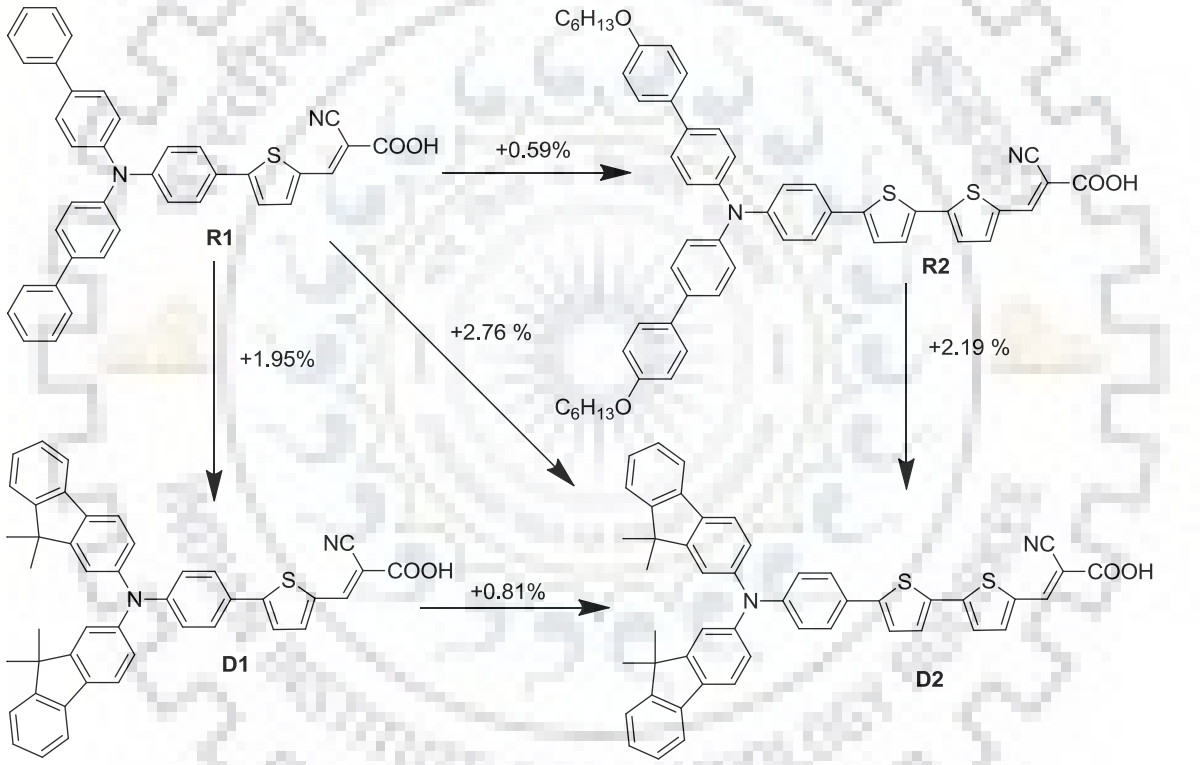

Figure 1.5 Effect of rigidified fluorene over biphenyl donor based dyes used in DSSCs [43-45].

Teng et al [49] synthesized organic sensitizers **R3-R5** and **D3-D5** featuring biphenyamine and carbazole as donors. It was observed that the conversion of biphenyl to carbazole augmented the light harvesting efficiencies and photo-current generation. However the rigidification of the biphenylamine donor for the dye **R6** [50] into carbazole donor for the dye **D5** [51] induced a slight blue shift, but enhanced the molar extinction coefficient by 47700 M^{-1} $cm^{-}1$.

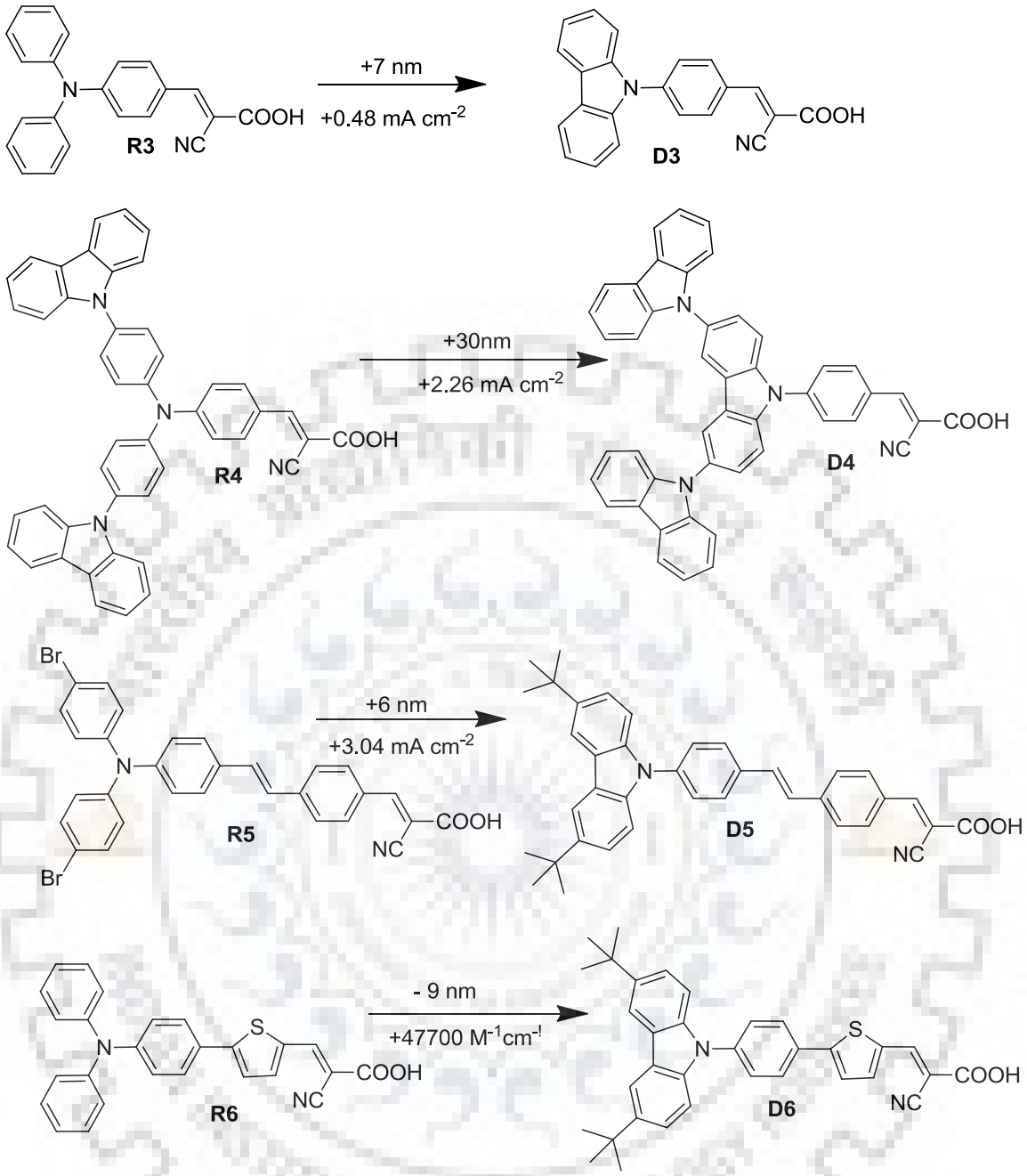

Figure 1.6 Effect of rigidified carbazole over biphenyl donor based dyes used in DSSCs [49-50].

1.4 Importance of polyheteroarene carbazole over polyarene fluorene based organic dyes for DSSCs

Though, the optical band gap of 9,9-dialkylfluorene derivatives is too high for efficient sunlight harvesting. However, the susceptibility of the oxidation of fluorene at 9-postion to the ketone make it little inefficient. But this unwanted oxidation process can be avoided by altering the bridging carbon atom with nitrogen a heteroatom during the process of rigidification can also reduce the undesired electronic and optical processes. As carbazole is being structurally analogous to fluorene, also known as 9-azafluorene, the central fused pyrrole ring with its donating nitrogen, makes it fully aromatic and electron-rich. Also the availability of sp^3-hybrid nitrogen in carbazole ensures its tri-functionalization to an alkyl chain to make it sufficient solubility in different organic solvents [52]. As a result, carbazole derivatives have been widely used as semiconductors [53-55] due to their ability to form stable radical cations, as well as their excellent thermal and photochemical stabilities, relatively high charge mobility, and easy availability. Carbazole due to its electron donating character normally strengthens the donor-acceptor interaction in dipolar compounds and benefits the optical properties such as absorption wavelength and molar extinction coefficient. Monofunctionaliztions at both C3 and N9 have been used to tether the carbazole as donor while difunctionalizations at C2, C7 and C3, C6 used for exploiting it as bridging segment [35,52,56-58]. Careful incorporation of electron rich carbazole as a donor/π-linker in a sensitizer tunes the HOMO and LUMO energy levels to produce high conversion efficiency [59-62].

Thomas and coworkers [63] synthesized fluorene π-linker based dyes **D7** and **D8** which possess red-shifted absorption and negative shift in oxidation. They demonstrated fluorene as an efficient π-linker to enhance the donor acceptor interactions and achieve red shifted absorption as compared to biphenyl congener **R6** [64] (Figure 1.7). However further rigidification of biphenyl unit by nitrogen atom i.e carbazole (**D9**) [52] instead of carbon atom (**D10**) not only induced red shifted absorption but also increased the efficiency when compared to respective biphenyl and fluorene counterparts.

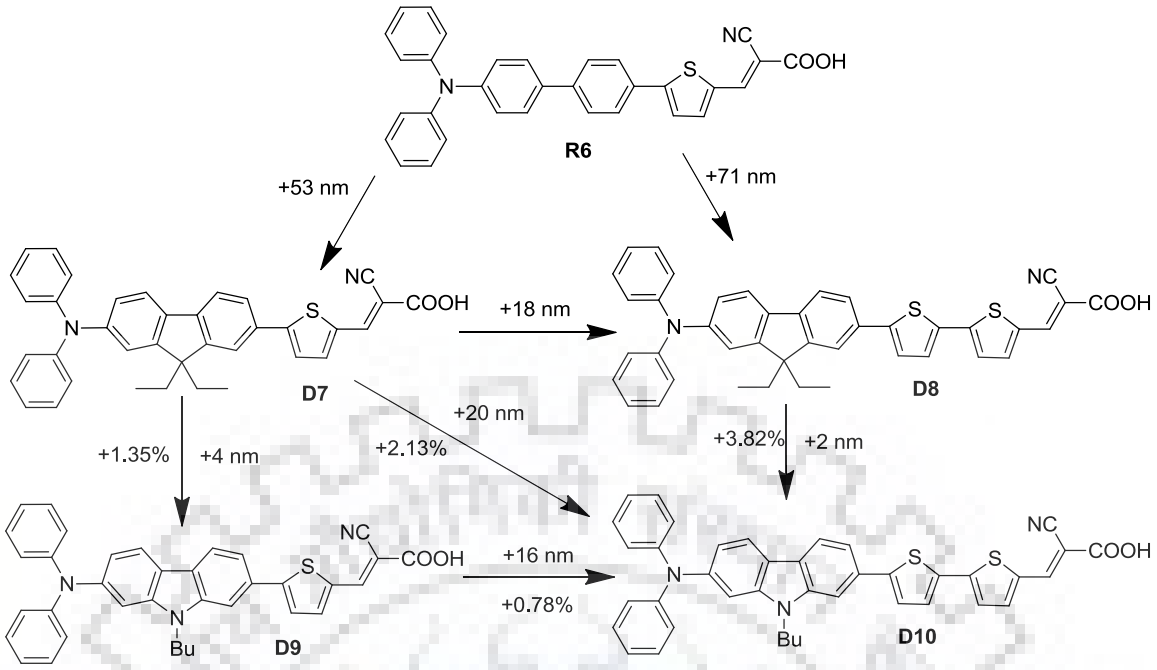

Figure 1.7 Comparison of rigidification of biphenyl unit by nitrogen atom and carbon atom in the organic dyes used in DSSCs [52,63,64].

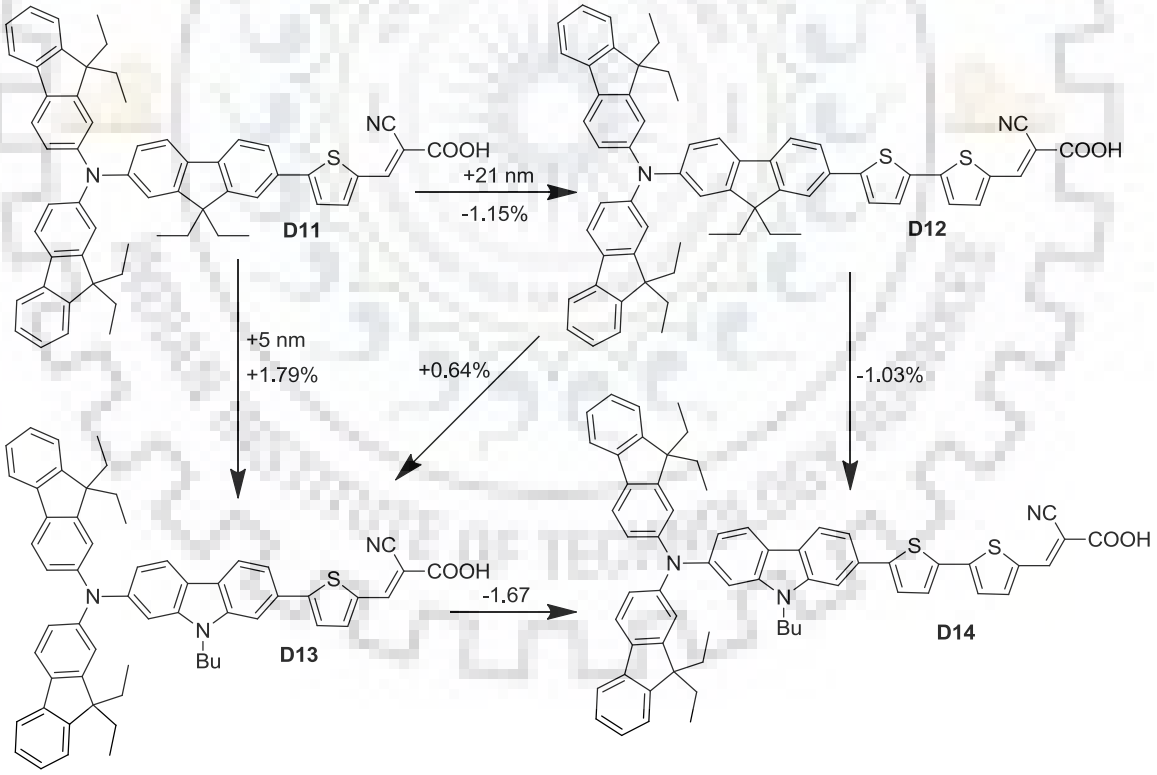

Figure 1.8 Comparison of fluorene and carbazole-based organic dyes used in DSSCs [48,65].

Thomas and coworkers [48,65] also synthesized fluorene and carbazole π-linker based dyes **D11**-**D14** containing fluoreneamine-based donor (Figure 1.8). It was observed

that the replacement of fluorene spacer (**D11**) by carbazole π-linker (**D13**) proved to be beneficial to increase absorption and photovoltaic efficiency than dyes **D11** and **D12**. Although extension of carbazole dyes **D4** by bithiophene linker resulted in the reduction of electron life-time and charge collection efficiency.

Hanaya and coworkers [60] synthesized carbazole donor based dyes **D15** and **D16** featuring cyanoacrylic acid and alkoxysilyl derivative anchoring group respectively (Figure 1.9). The dye **D16**, has a trimethoxysilyl group as the anchoring moiety to the TiO_2 electrode, was considered to be adsorbed on the electrode with the formation of three titanosiloxane (Si-O-Ti) bonds. Therefore, using this alkoxysilyl carbazole as a sensitizing dye and a $Co^{3+/2+}$ complex redox electrolyte the fabricated DSSC exhibited light-to-electric energy conversion efficiencies of over 12% with open-circuit photo voltage higher than 1000 mV.

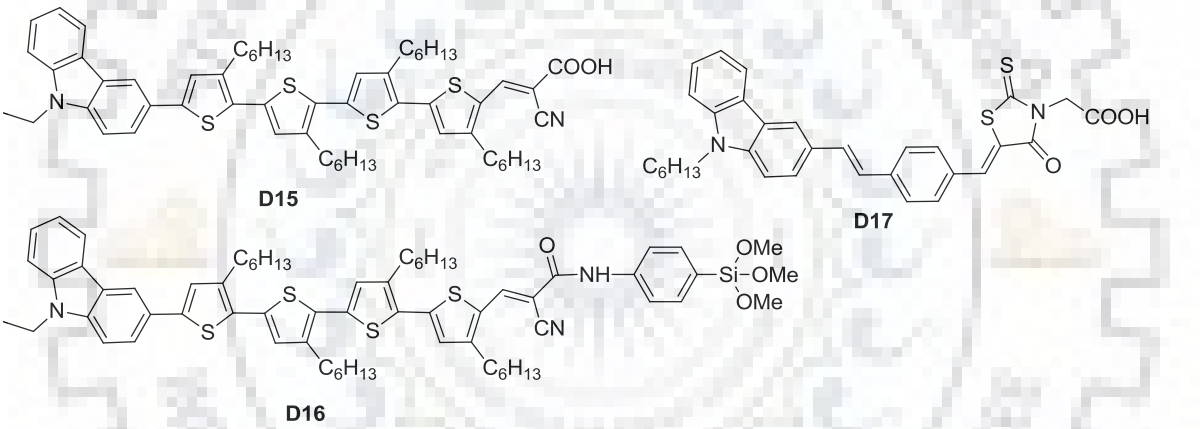

Figure 1.9 Structures of carbazole-donor based dyes used in DSSCs [27,28].

Soni and coworkers [61] synthesized D-π-A dye **D17** comprising of carbazole as a donor and vinylene-phenylene π-linker (Figure 1.9). The dye showed red shifted absorption on adsorption on titania surface due the lowering of the energy level of the π*-orbitals of the dyes by enhancement in conjugation. The high power conversion efficiency (PCE) of 9% was achieved for dye **D17** with a cobalt based redox shuttle. Zhu and coworker [62] demonstrated the detrimental effect of vinyl linkages on dipole moments and photo-stability in D-π-A dyes **D18**, **D19** and **D20** featuring carbazole as an auxiliary donor (Figure 1.10). Therefore, the dyes free from vinyl linkage on the adsorption on TiO_2 witnessed the up shift of conduction band (CB) edge of the TiO_2 and presented a slow charge recombination rate, which gave rise to high V_{OC} values for these

dyes. Thus, the overall power conversion efficiency 9.49% and 9.29% for the dyes **D19** and **D20** were obtained, respectively.

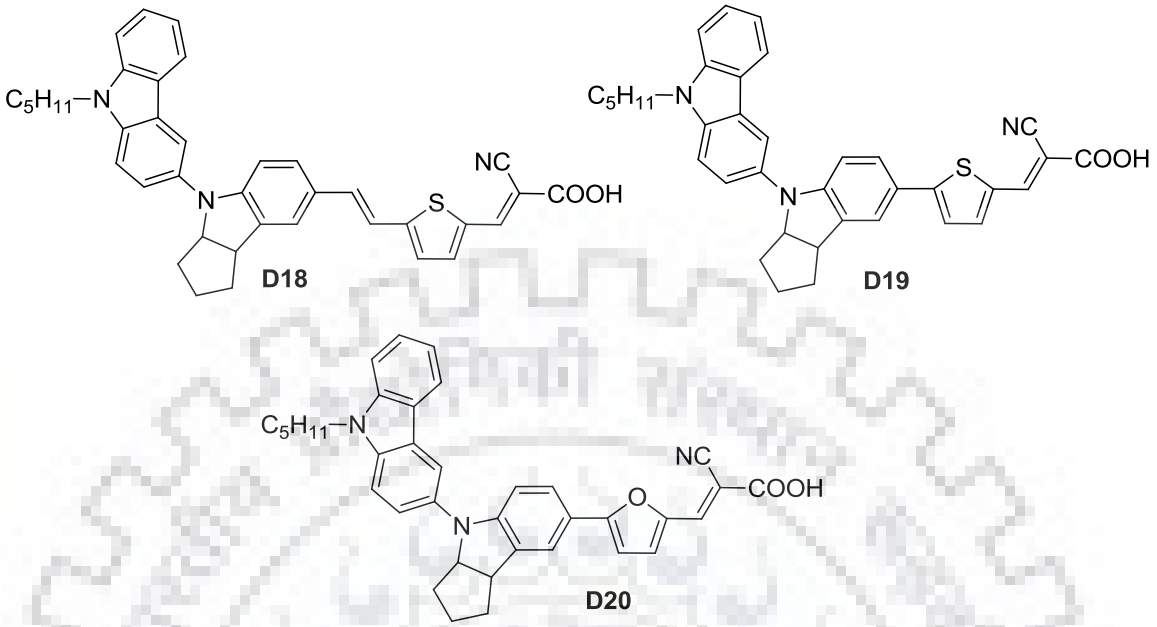

Figure 1.10 Structures of dyes containing carbazole as auxiliary donor [29,30].

1.5 Thiophene and multifused thiophene heteroarens (thieno[3,2-*b*]indole) based organic dyes for DSSCs

Besides, thiophene and multifused thiophenes possess electron rich coplanar structures [41,66]. Therefore, fused heteroacenes containing at least one thiophene ring always remained an efficient candidate for π-linkers in DSSCs [67-70]. Therefore, the fusion of heterocyclic thiophene ring instead of benzene ring of carbazole results in a new fused heterocyclic moiety thieno[3,2-*b*]indole. As thienoindole moiety features five membered thiophene ring attached at the 2,3-position of indole chromophore, serves as more electron rich with enhanced electron donating ability and coplanarity compared to the carbazole [71-73]. Thus, with the insertion of planar thienoindole in π-conjugation of the sensitizer a red shift and increased molar extinction coefficient can be expected and thus enhance the photocurrent generating efficiency of the dye.

Hara and co-worker [74] synthesized thieno[3,2-*b*]indole based organic dyes **D21-D23 (**Figure 1.11) comprised of oligothiophene π-bridge and cyanoacrylic acid acceptor/anchoring unit. As compared to carbazole dyes **D24** and **D25** [58], thienoindole based dyes demonstrated the stronger electron ability, planar confirmation and good long-

term stability as sensitizers. However, these thienoindole dyes showed shorter electron life time which resulted in low V_{OC} values in DSSCs.

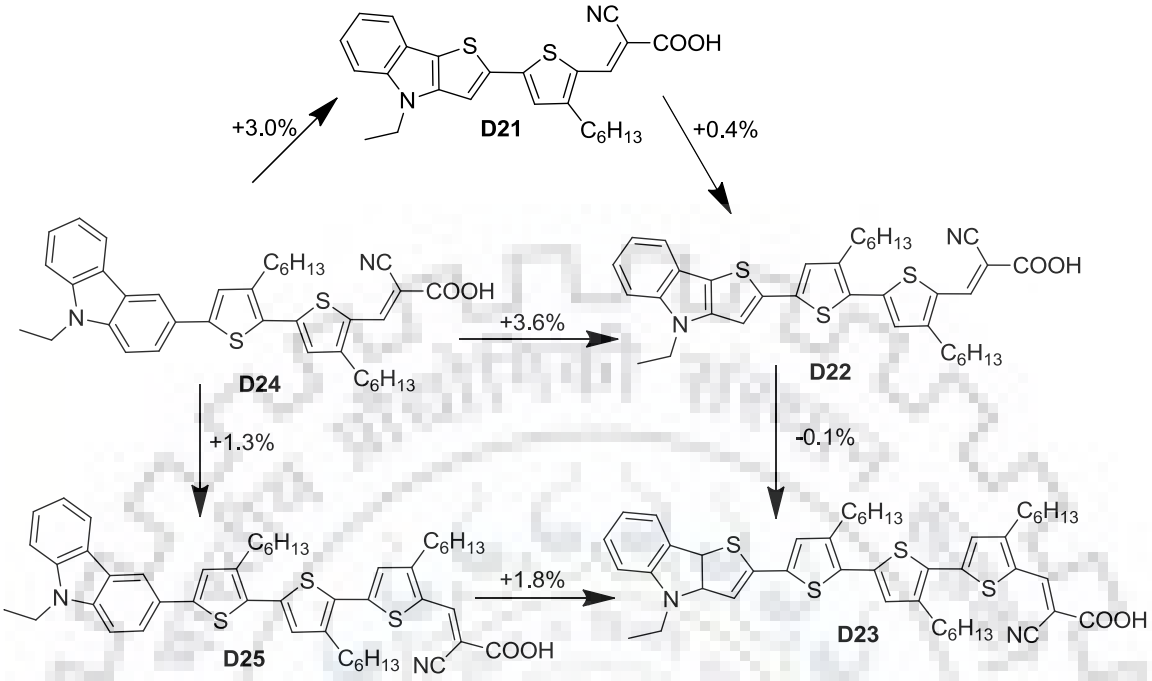

Figure 1.11 Structures of thienoindole donor in comparison to carbazole donor based dyes [58,74].

Lin and coworker [75] utilized thieno[3,2-*b*]indole as donor to synthesize the dye **D27** (Figure 1.12) by using dithieno[3',2':3,4;2'',3'':5,6]benzo[1,2-*d*][1,2,3]triazole (DTBZ) as the rigidified π-conjugated spacer. In comparison to carbazole congener **D26**, the former dye showed broad absorption and high molar extinction coefficient ~54,800 M^{-1} cm^{-1}. The dye **D27** exhibited the power conversion efficiency of 5.82% and 6.71% without and with CDCA, respectively.

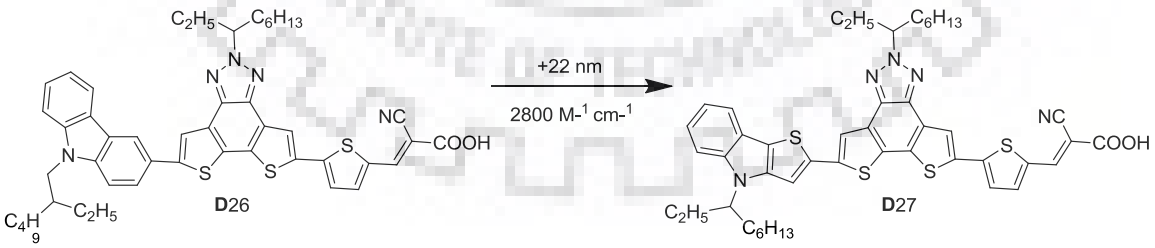

Figure 1.12 Comparison of thienoindole and carbazole-based dyes containing dithienobenzotriazole linker [75].

Recently, Kim and coworker [76] made an attempt to facilitate the electron transfer process from donor to acceptor by inserting thieno[3,2-*b*]indole in the conjugating bridge

(**D29** and **D30)** and compound with a dye containing thieno[3,2-*b*] benzothiophene (TBT), **D28** (Figure 1.12). Thus, the replacement bridging sulphur of TBT by nitrogen in thieno[3,2-*b*]indole moiety enhanced electron richness and increased the light harvesting efficiency for the later dyes. Further, the insertion of longer *n*-hexyl chain at nitrogen-bridged atom in the dye **D29**, instead of ethyl chain in dye **D30**, witnessed the more retardation of charge recombination and dye aggregation. Thus, by the use of above strategy they were able to get the maximum power conversion efficiency of 12.45% for the dye **D30**.

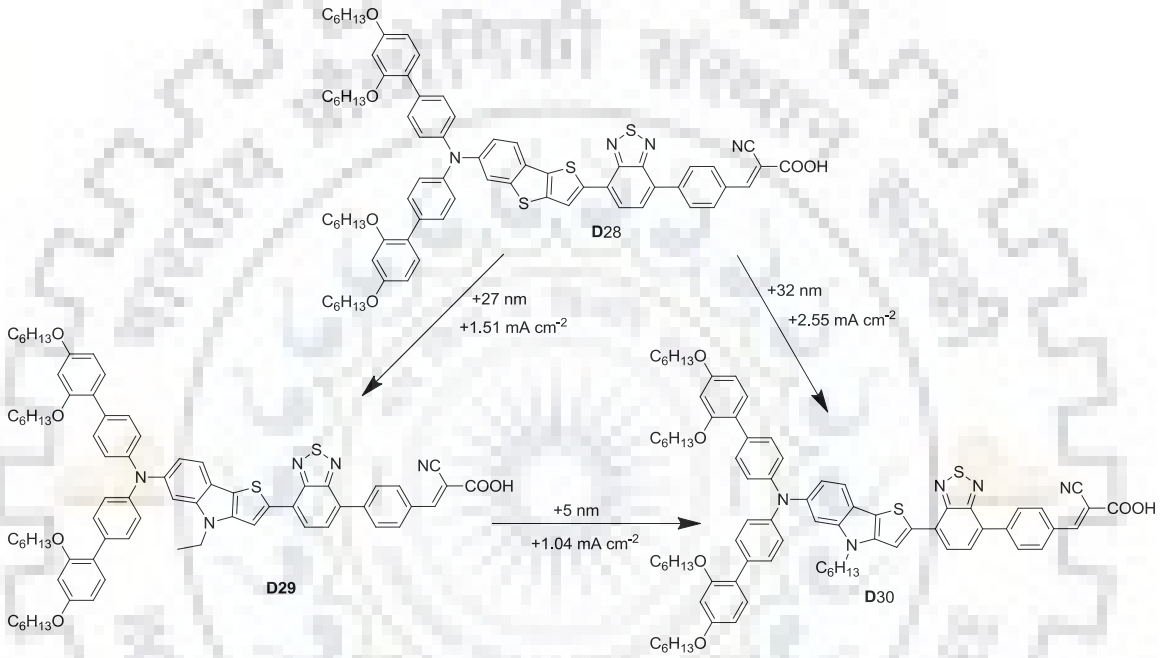

Figure 1.13 Structures of dye showing the effect of thienoindole [76].

1.6 Importance and properties of dithieno[3,2-*b*:2′,3′-*d*]pyrrole based organic semiconductors

Furthermore, the replacement of benzene ring of thieno[3,2-*b*]indole by thiophene results in dithieno[3,2-*b*:2′,3′-*d*]pyrrole (DTP), is highly accessible (up to 80% yield in one step) as showcased by Rasmussen et al. [77]. Thus the fusion of three five-membered heterocycles i.e. two thiophene and one pyrrole ring into DTP makes it more rich electronically. Due to the planarity of DTP units, their intriguing property derived from the presence of a bridging nitrogen atom contributes to the improvement of the hole-transport ability of the corresponding materials. Moreover, the substituents on pyrrole nitrogen of DTP moieties can be used to tune solubility and intermolecular packing without introducing significant torsions between adjacent aromatic units. As a result, this

position offers greater versatility toward the control of dye aggregation, which can make it attractive candidate for DSSC applications.

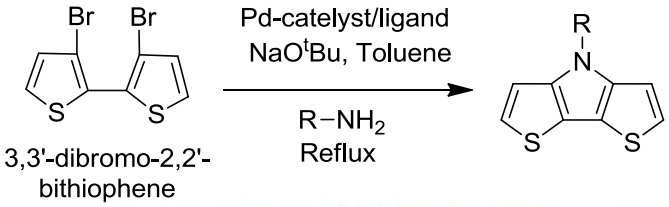

Scheme 1.1 Synthetic approach to achieve DTPs.

The easy and simple method of the synthesis of DTPs is the amination of dibromo bithiophene precursors via Pd-catalyzed Buchwald-Hartwig coupling in excellent yields [77-79]. DTP based scaffolds have been used as building blocks in various polymers, oligomers and molecular materials to provide high carrier mobilities, enhanced solution and solid-state fluorescence with low band gaps [37]. As a result, these materials have been applied to organic electronics such as organic photovoltaic cells (OPVs), [80-82] fluoroscent devices [83-85], and organic field effect transistors (FETs) [86-93]. DTP currently has been indicated as an alternative donor unit for the synthesis of low energy gap conjugated polymeric systems [94-106]. In recent years, several DTP based dyes were reported for application in organic solar cells (OSCs) [107-117] and emerged as potential candidate for dyes for DSSCs fabrication [45,118119,122,124-140].

1.7 *N*-Alkylated DTP based organic dyes in comparison with bithiophene and CPDT congeners for DSSCs

As compared to dye **R2,** the rigidification of bithiophene linker to dithienopyrrole in dye **DP1** led to increase absorption wavelength and pronounced molar extinction coefficient (Figure 1.14) [45]. As a result, the dye exhibited high photocurrent density and power conversion efficiency than **R2**.

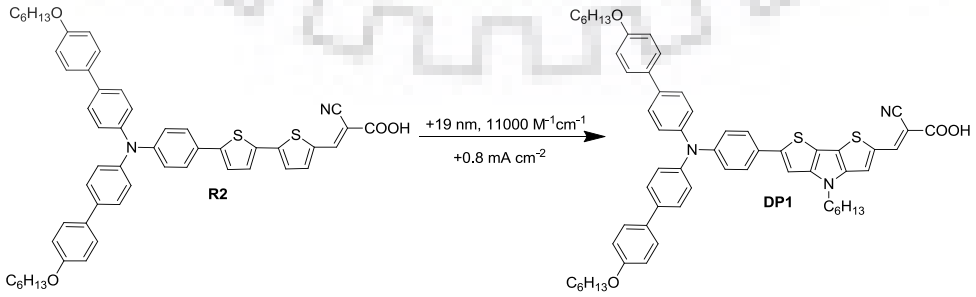

Figure 1.14 Trends in absorption maxima and molar extinction coefficient of DTP-dyes in comparison to bithiophene linker [45].

Angelis and coworkers [118] demonstrated the effect of rigidification of bithiophene conjugated bridge in the dye **D31**, by selecting three atoms Si, C and N to synthesize the dyes **D32**, **D33** and **DP2** respectively (Figure 1.15). This study revealed that rigidification of bithiophene not only affect the surface coverage and packing mode of the dye on titania, but also offers the opportunity to tune the photophysical properties and modulate the photovoltaic parameters. As compared to the dye **D31** the counterpart dyes **D32** and **D33** showed the bathochromic and hyperchromic absorptions for solar flux which is more pronounced for DTP dye **DP2**. The rigidification thus facile the increase in the short circuit current and hence the power conversion efficiency. However, the rigidification brought a fall in the open circuit voltage due to the adverse downward shift of CB of titania.

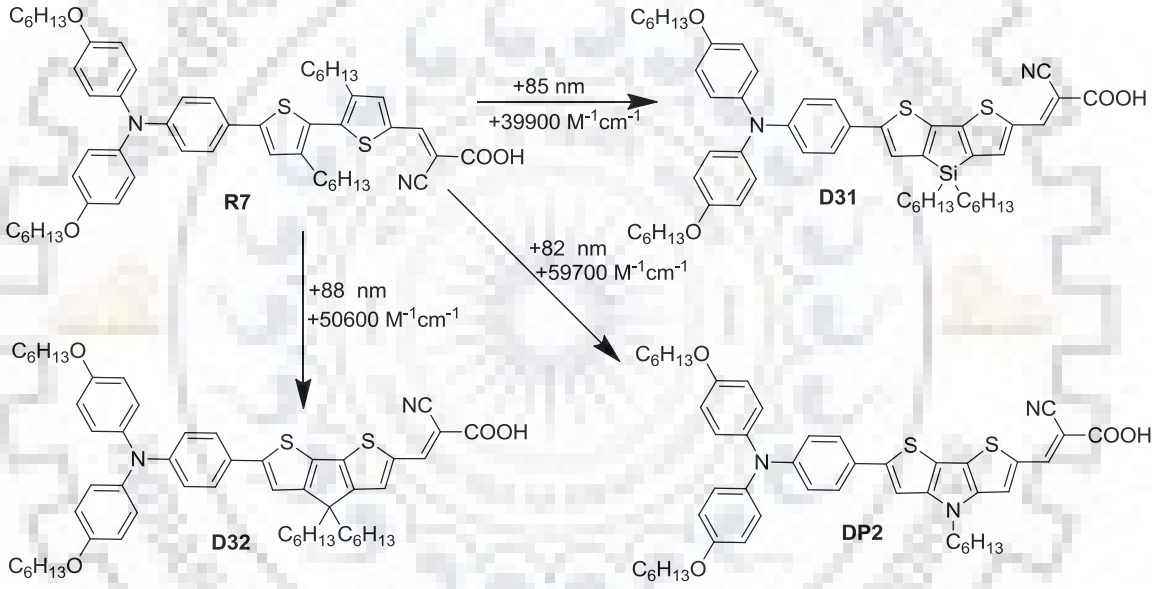

Figure 1.15 Trends in absorption maxima and molar extinction coefficient of the dyes demonstrating the effect of fusion [121].

Polander and coworkers [119] synthesized DTP-based dyes **DP3** and **DP4** (Figure 1.16). As compared to their bithiophene dye **R8** [120], DTP dyes showed enhanced molar extinction coefficient. However, in comparison to cyclopentadithiophene (CPDT) (**D33** and **D34**) [121], these dyes showed blue shifted absorption due to high lying LUMO, but exhibited augmented open circuit voltage and better charge transfer kinetics than CPDT dyes.

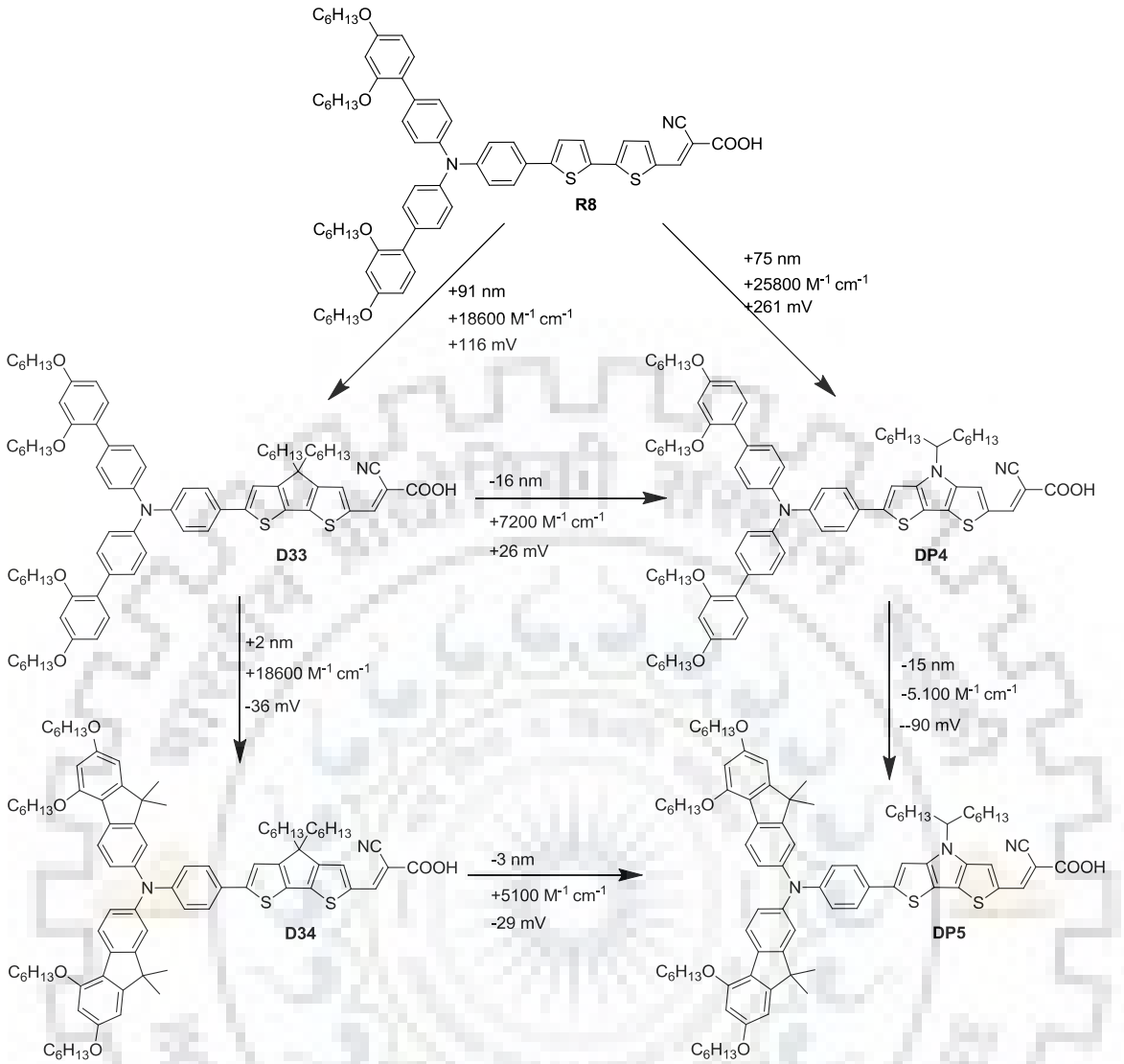

Figure 1.16 Structures of CPDT and DTP-based dyes [119-121].

El-Sayed and coworkers [122] synthesized squaraine dyes **DP5** and **DP6** (Figure 1.17) by DTP as spacer and cyanoacrylic acid (CA) and cyanophosphonic acid (PA) as two acceptor anchoring group respectively to achieve panchromatic absorption. But the PA-dye **DP6** exhibited low charge injection efficiency than CA dye **DP5** and hence 5.6% PCE was obtained for later dye. However in comparison to their CPDT counterpart **D35,** [123] these dyes **DP5** and **DP6** exhibited high electron life-time.

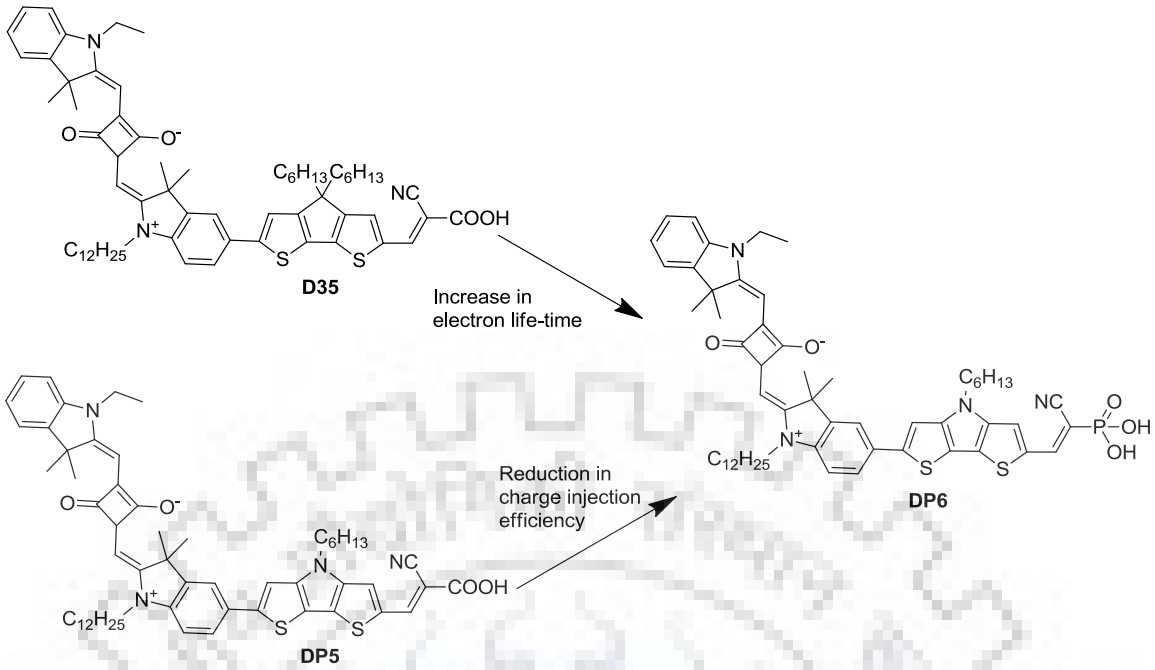

Figure 1.17 Structures of DTP-based dyes, **D24**, **DP2** and **DP3** [122,123].

Table 1.1 Optical and photovoltaic properties of DTP-based organic dyes **DP1-DP6** used in dye sensitized solar cells.

Entry	λ_{max} (nm (ε_{max} $\times 10^3$ $M^{-1}cm^{-1}$))	J_{SC} (mA cm^{-2})	V_{OC} (mV)	FF	η%	Ref
DP1	524 (75.0)	12.3	750	0.66	6.09	45
DP2	511 (68.0)	12.9	860	0.72	8.0	118
DP3	526 (57.7)	13.4	901	0.74	8.86	119
DP4	541 (52.6)	14.1	811	0.77	8.72	119
DP5	670 (160.0)	13.5	610	0.68	5.60	122
DP6	670 (204.0)	5.9	642	0.74	2.80	122

1.8 *N*-Alkylated DTP based organic dyes for DSSCs

Liang and coworkers [124] employed hexahexyltruxene-substituted 4-(hexyloxy)-N-phenylaniline (HT-HPA) segment as donor with DTP to construct two push-pull dyes **DP7** and **DP8** (Figure 1.18). In these dyes, HT-HPA segments adequately facilitate the recombination inhibition and prolonged the CB electron life time. However, no effect of DTP substituent was observed due to the bulkiness of HT-HPA segments. They further used TPA and DHO-TPA in place of biphenyl segment of triarylamine donor of **DP7** to improve the photocurrent density for the dyes **DP9** and **D10** [125]. Cyclic voltammetry revealed the poor driving for the dye regeneration for **DP10** as compared to **DP9**. On the

hand DSSCs based on **DP9** displayed a longer life time than **DP10**. Taking these two advantages, dye **DP9** was able to exhibit power conversion efficiency of 8.83%.

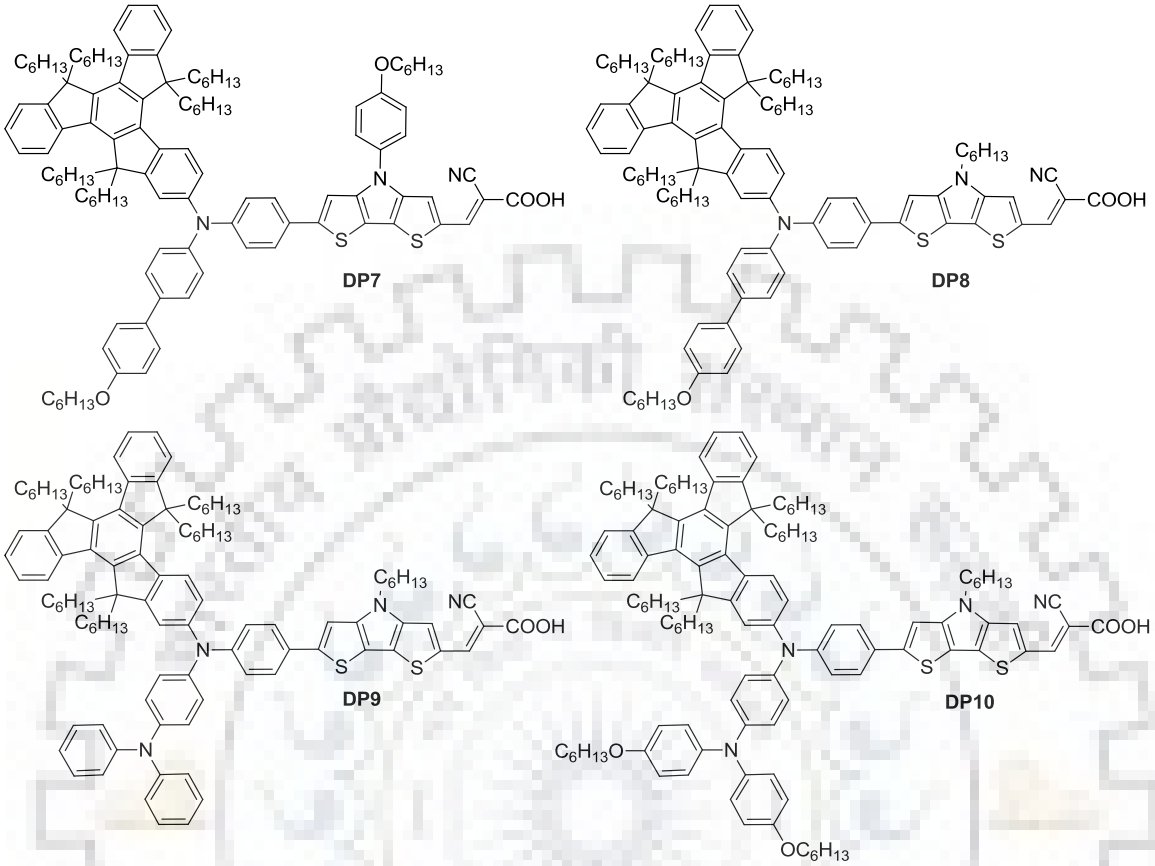

Figure 1.18 Structures of DTP-based dyes **DP7-DP10** containing truxene chromophore [124,125].

Table 1.2 Optical and photovoltaic properties of DTP-based organic dyes **DP7-DP10** used for dye sensitized solar cells.

Entry	λ_{max} (nm (ε_{max} $\times 10^3$ $M^{-1}cm^{-1}$))	J_{SC} (mA cm^{-2})	V_{OC} (mV)	FF	η%	Ref
DP7	534 (70.8)	12.0	917	0.72	7.90	124
DP8	532 (66.7)	12.2	948	0.73	8.50	124
DP9	531 (59.2)	14.3	907	0.68	8.83	125
DP10	543 (69.1)	12.8	885	0.69	7.81	125

Liang and coworkers realized that the lack of twist in fused thiophene organic dyes may be responsible for severe dye aggregation. Therefore, in order to overcome this demerit of fused thiophene dye, they introduced the hexenylbenzene (HEYB) unit in place of simple benzene rings of the dyes **DP11** and **DP13** to construct new dyes **DP12**

and **DP14** respectively [126] (Figure 1.19). This modification in the dyes **DP11** and **DP13,** however, induced only a little twist (~36°) between donors and acceptor but significantly improved the photophysical and photovoltaic properties due to suppression in dye aggregation and charge recombination. Moreover, irrespective of arylamine donor, the HEYB imparted the positive effect on the performances of the dyes.

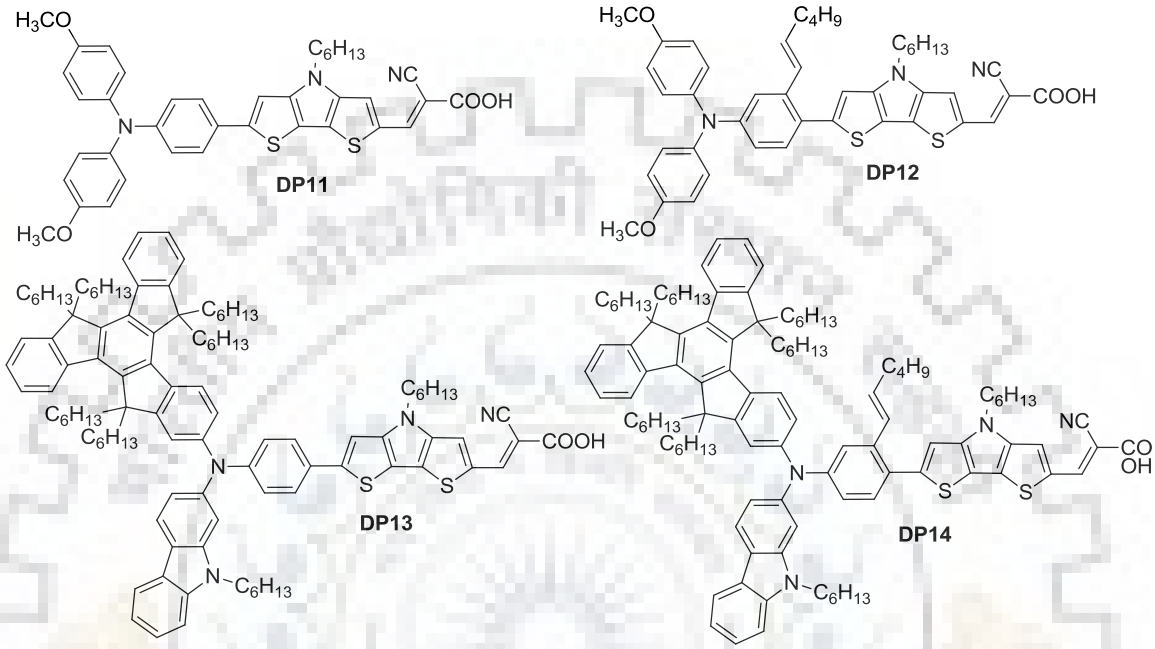

Figure 1.19 Structures of DTP-based dyes demonstrating the effect of twist by vinyl-butane [126].

Table 1.3 Optical and photovoltaic properties of DTP-based organic dyes **DP11-DP14** used for dye sensitized solar cells.

Entry	λ_{max} (nm (ε_{max} $\times 10^3$ $M^{-1}cm^{-1}$))	J_{SC} ($mAcm^{-2}$)	V_{OC} (mV)	FF	η%	Ref
DP11	502 (45.6)	14.2	843	0.66	7.90	126
DP12	492 (39.2)	15.5	866	0.68	9.13	126
DP13	538 (65.6)	15.4	920	0.67	9.49	126
DP14	518 (63.3)	15.4	945	0.67	9.75	126

1.9 Importance of *N*-aryl derivatives over *N*-alkyl substituent on DTP

As in the previous reports of Liang and co-workers used the bulky truxene based triarylamine donor to synthesize DTP π-linker dyes. Therefore, the bulkiness of the

truxene donor masked the exact impact of *N*-substituents on DTP segments. In order to unravel the effect of *N*-substituted DTP on the photovoltaic performances Liang and coworkers [127] synthesized a series of triarylamine-free organic dyes (**DP15**-**DP18**) synthesized, featuring only DTP segments with *n*-hexyl (H-DTP) and hexyloxypenyl (HOP-DTP) substituents (Figure 1.20). The systematic introduction of HOP group in place of *n*-hexyl chain improved the light harvesting ability, electrochemical and photovoltaic properties of the dyes. As a result, the dye **DP18** containing two consecutive HOP-DTP units displayed the best photovoltaic performances (4.21%) in the series.

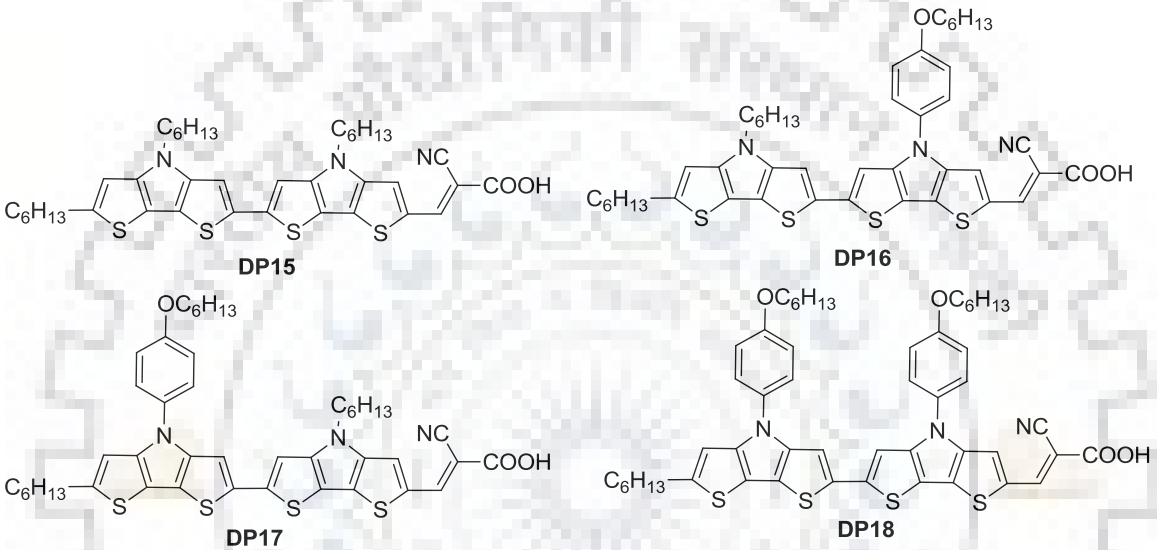

Figure 1.20 Structures of dyes containing DTP donor and linker [127].

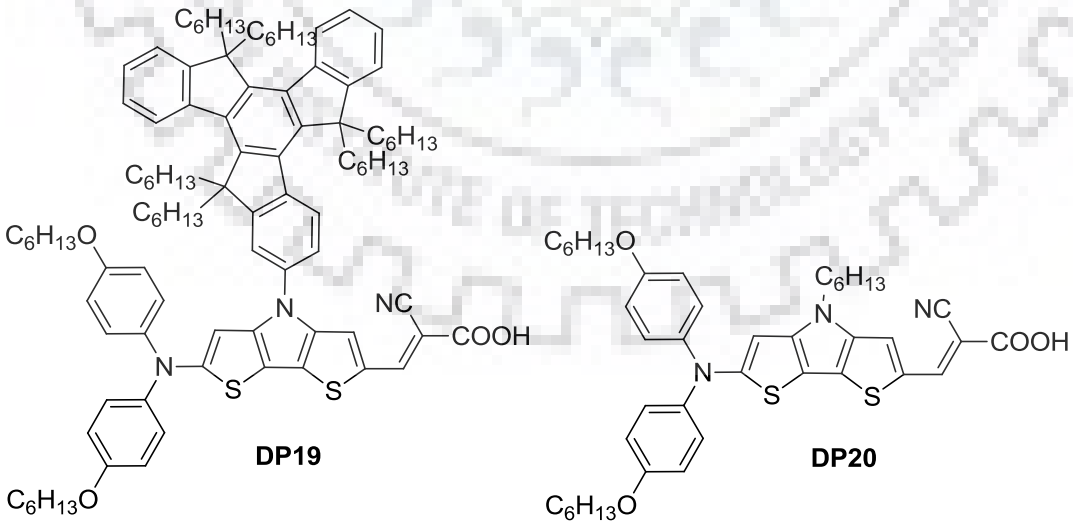

Figure 1.21 Structures of dyes containing DTP linker [128].

Liang and coworkers [128] used truxene substituted DTP to synthesize organic dye **DP19** (Figure 1.21). This dye exhibited increased light harvesting and charge recombination suppression when compared to its congener **DP20**. The dye **DP19** along with cobalt electrolyte exhibited J_{SC} = 12.1 mA cm^{-2}, V_{OC} = 758 mV, *FF* = 0.56 and hence PCE 5.1% outperforming **DP20**.

Table 1.4 Optical and photovoltaic properties of DTP-based organic dyes **DP15-DP20** used for dye sensitized solar cell.

Entry	λ_{max} (nm (ε_{max} ×10^3 M^{-1}cm^{-1}))	J_{SC} (mA cm^{-2})	V_{OC} (mV)	FF	η%	Ref
DP15	499 (22.6)	04.8	494	0.71	1.65	127
DP16	512 (32.1)	10.2	528	0.68	3.67	127
DP17	502 (32.8)	09.3	511	0.68	3.24	127
DP18	513 (38.9)	12.1	520	0.67	4.21	127
DP19	540 (54.7)	12.1	758	0.56	5.10	128
DP20	553 (41.5)	9.1	666	0.52	3.10	128

Zhang and coworkers [55] realized that despite of longer absorption wavelength and high molar extinction coefficient for the dye **DP1** less efficiency as compare to its congener dyes **D23** and **D24** can be improved by replacing the *n*-hexyl chain of DTP by means of some bulky insulation groups. In this regard, they synthesized 2′,6′-bis(octyloxy)-biphenyl substituted dithieno[3,2-b:2′,3′-d]pyrrole segment to use it as π-linker to make a 3D giant organic dye **DP22** (Scheme 1.2**)**. Alkylation of 2-iodobenzene[1,3]bisolate in acetone produced the substituted iodobenzene **2** which on cross coupling with 4-(4,4,5,5-tetramethyl-1,3,2-dioxaborolan-2-yl)benzenamine in the presence of Pd-catalyst yielded amine **3** in good yield. This amine underwent Buchward-Hartwig coupling with 3,3′-dibromo-2,2′-bithiophene to give key precursor **4**. The Vilsmeier-Haack reaction of **4** followed by the controlled monobromination yielded the brominated aldehyde precursor **6**. The dye **DP21** was synthesized by employing Suzuki-Miyaura cross coupling reaction between pinacol bisarylamino boronate and brominated aromatic aldehyde precursor **6** followed by Knovenegal condensation with cyanoacitic acid. The absorption spectra recorded for the dye **DP21** showed blue shifted and less intense absorption as compared to the dye **DP2** due torsional strain between phenyl ring and DTP unit. But, despite of reduced light harvesting efficiency the dye **DP21** could able to produce high power conversion efficiency. This enhanced efficiency was found to be

due to the porous organic coating by the dye on the surface of titania that was effective to slow down the kinetics of charge recombination on titania surface.

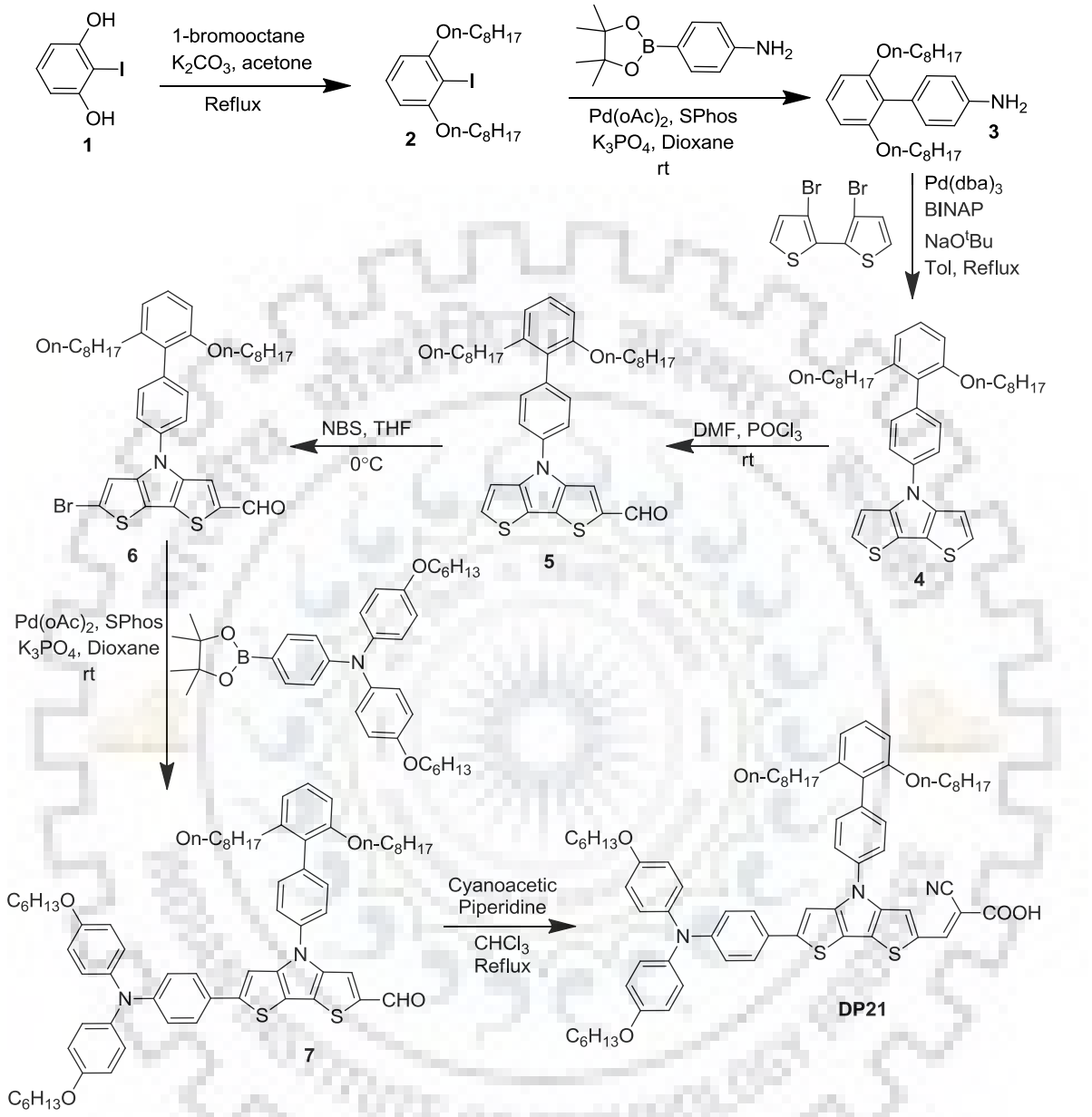

Scheme 1.2 Synthetic protocol for the dye **DP21** [129].

Next, they modified the **DP21** by extending the conjugation with thiophene on either side on DTP linker (**DP22**) or introducing another DTP (**DP23**) (Figure 1.22) [130]. However, the coplanarity of **DP23** displayed red-shifted absorption peak than **DP22**, but the positive oxidation potential reduced the energetic process for the dye regeneration by electrolyte. While, rise in the CB of TiO_2 was observed for **DP22** as a result, efficiency of 9.5% was obtained for **DP22** (Figure 1.22).

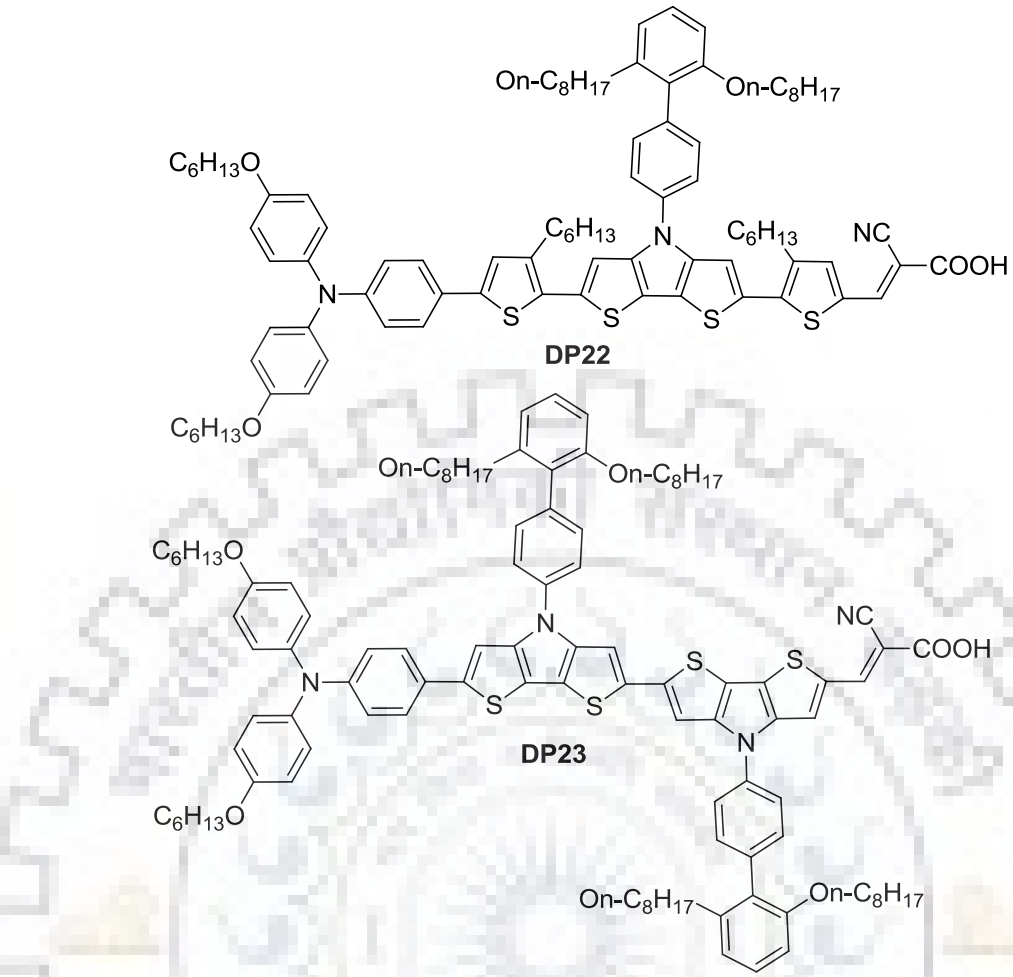

Figure 1.22 Structures of dyes containing bulky *N*-substituted DTP linker [130].

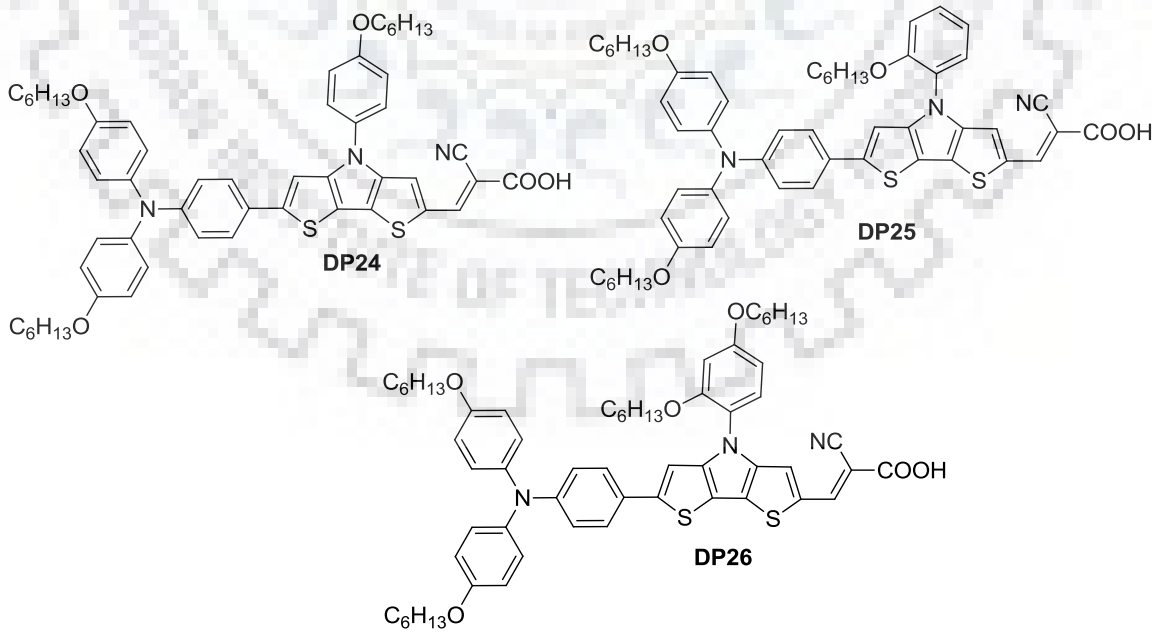

Figure 1.23 Structures of DTP-dyes showing the position effect of hexyloxy chain on *N*-phenyl [131].

Liang and coworkers [131] synthesized three DTP π-linker based dyes **DP24-DP26** with TPA donor and used as sensitizers in iodine-free DSSCs (Figure 1.23). The dye **DP24** having 4-hexyloxyphenyl on DTP unit displayed higher molar extinction coefficient, which contributed to high power conversion efficiency 8.14% for the dye as compared to other congeners.

Table 1.5 Optical and photovoltaic properties of DTP-based organic dyes **DP21-DP26**.

Entry	λ_{max} (nm (ε_{max} $\times 10^3$ $M^{-1}cm^{-1}$))	J_{SC} ($mAcm^{-2}$)	V_{OC} (mV)	FF	η%	Ref
DP21	511 (65.0)	13.5	960	0.72	9.3	129
DP22	512 (42.5)	15.4	861	0.71	9.5	130
DP23	542 (69.2)	12.3	745	0.73	6.7	130
DP24	520 (79.9)	13.5	850	0.71	8.14	131
DP25	510 (63.4)	11.2	950	0.70	7.45	131
DP26	522 (72.5)	11.6	935	0.69	7.48	131

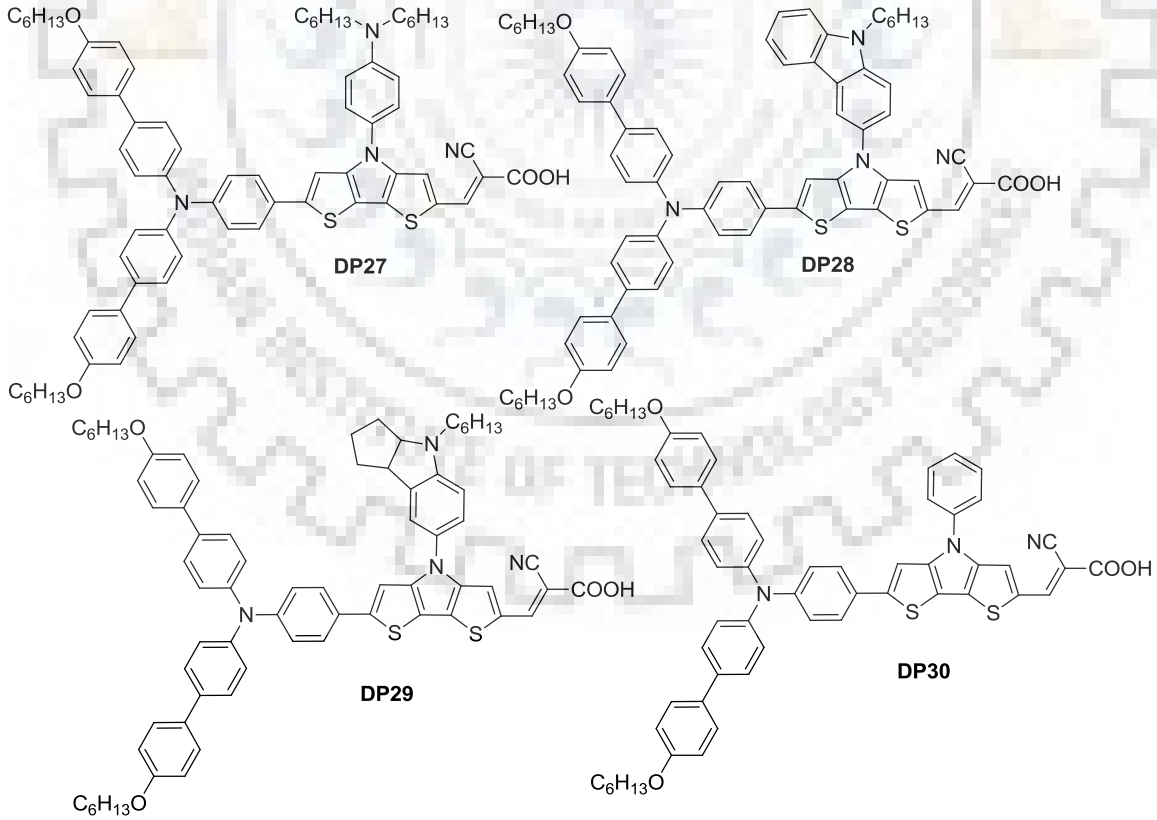

Figure 1.24 Structures of DTP-based dyes **DP26-DP30** with different *N*-chromophores [132].

Liang and coworkers [132] used *N*-heterocyclic substituted DTP as spacer in trarylamine based sensitizers **DP26-DP30** for iodine-free DSSCs (Figure 1.24). They utilized the dual effect of *N*-heterocyclic substituted DTP in order to tune charge transfer excitation and retarding the charge recombination. They also studied the effect of dye adsorption time on the performances of dyes. The highest efficiencies were observed for dihexylaniline (**DP27**) and hexylcarbazole (**DP30**) substituted DTP spacers respectively after stained for 36h.

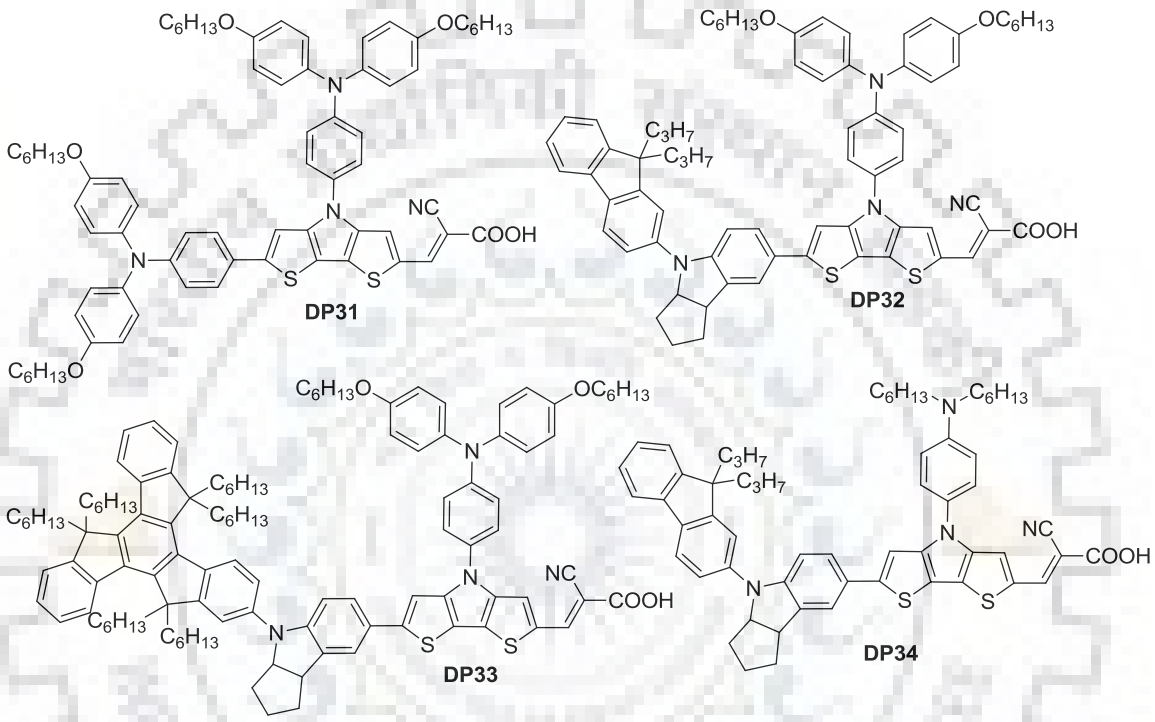

Figure 1.25 Structures of DTP-based dyes **DP31-DP34** with different donors [133].

Liang and coworkers [133] further used dihexyloxy-triphenylamine (DHO-TPA) substituted DTP as spacer to synthesize indoline donor based dyes **DP31-DP34** (Figure 1.25). Theoretical calculation revealed the contribution of DHO-TPA substituent to the electron donation capability of DTP segment. Also, the presences of DHO-TPA substituted DTP not only facilitate the light absorption properties for indoline dyes but also promoted the charge recombination resistance for TiO_2 electron. As result of which aiding the bulkiness truxene substituted indoline donor and DHO-TPA substituted DTP, the dye **DP33** displayed promising efficiency of 8.78% for indoline based dyes.

Table 1.6 Optical and photovoltaic properties of DTP-based organic dyes **DP27-DP34** containing different *N*-chromophores and donors.

Entry	λ_{max} (nm (ε_{max} $\times 10^3$ $M^{-1}cm^{-1}$))	J_{SC} ($mAcm^{-2}$)	V_{OC} (mV)	FF	η%	Ref
DP27	524 (54.9)	12.6	950	0.68	8.14	132
DP28	521 (60.9)	13.3	907	0.68	8.20	132
DP29	527 (60.5)	10.5	844	0.66	5.85	132
DP30	522 (64.2)	12.1	856	0.67	6.94	132
DP31	533 (53.7)	09.5	900	0.70	5.99	133
DP32	544 (69.8)	12.2	861	0.69	7.25	133
DP33	553 (73.5)	13.3	943	0.70	8.78	133
DP34	536 (61.3)	12.7	845	0.69	7.40	133

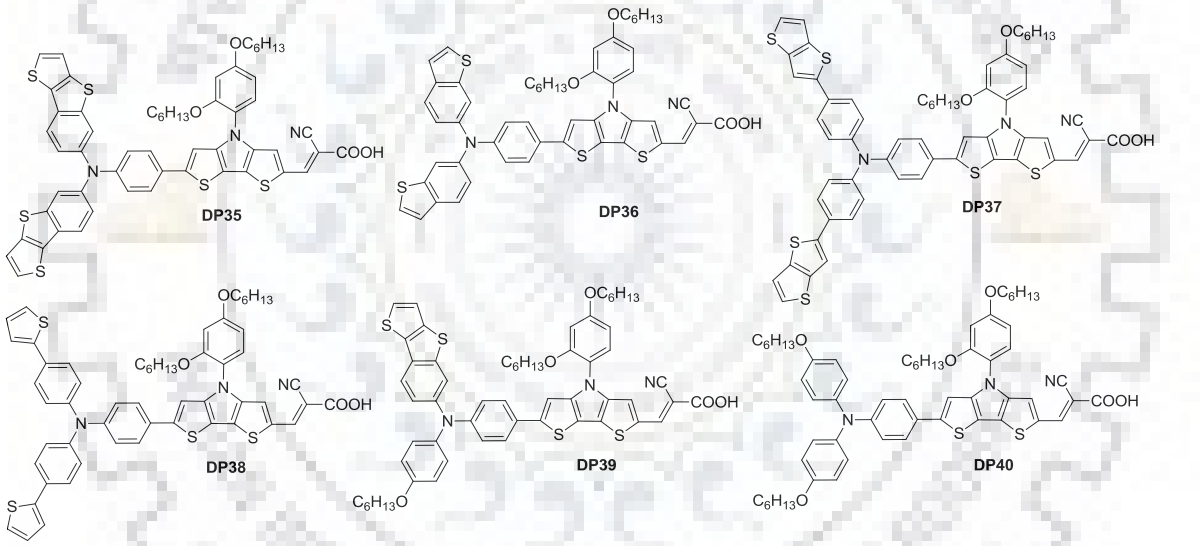

Figure 1.26 Structures of DTP-based dyes showing the effect of fusion of thiophenes in different donors **[**134].

Ge et al. [134] incorporated the fused thiophene derivatives thieno[3,2-*b*][1]benzothiophene (TBT), benzo[*b*]thiophene (BT), 2-phenylthieno[3,2-*b*]thiophene (PTT) and 2-phenylthiophene (PT) in triarylamine donor to synthesize DTP linker based dyes **DP35-DP39** in reference to **DP40** dye containing HOB unit in triarylamine donor (Figure 1.26). The fused thiophene derivatives were found to induce the positive shift for HOMOs and LUMOs which facilitate the dye regeneration and reduction in energy loss during the electron injection process. Moreover, a remarkable enhancement in the

chemical and photo stabilities for **DP35-DP39** were observed as compared to **DP40**. However BT unit containing dye **DP36** exhibited poorest efficiency.

Table 1.7 Optical and photovoltaic properties of DTP-based organic dyes **DP35-DP40** showing the effect of fusion of thiophenes in different donors**.**

Entry	λ_{max} (nm (ε_{max} $\times 10^3$ $M^{-1}cm^{-1}$))	J_{SC} ($mAcm^{-2}$)	V_{OC} (mV)	FF	η%	Ref
DP35	511 (60.5)	14.3	870	0.67	8.33	134
DP36	523 (36.0)	12.5	780	0.67	6.52	134
DP37	506 (50.5)	13.5	839	0.66	7.47	134
DP38	492 (56.8)	13.0	830	0.66	7.12	134
DP39	531 (56.1)	15.0	855	0.67	8.59	134
DP40	531 (50.2)	13.9	830	0.66	7.61	134

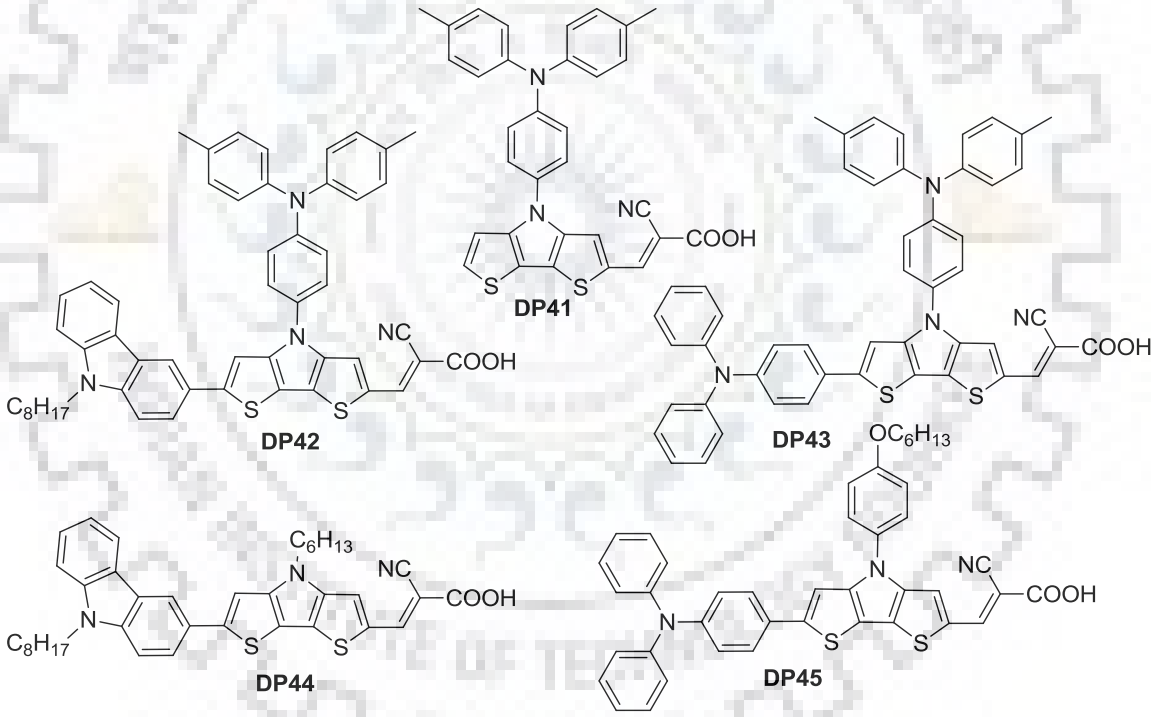

Figure 1.27 Structures of DTP-based dyes containing carbazole and triphenylamine donor [135].

Zhang *et al*. [135] synthesized five push-pull organic dyes **DP41-DP45** featuring carbazole or triphenylamine (TPA) donor, DTP as spacer and cyanoacrylic acid as acceptor (Figure 1.27). As compared to TPA dyes, small dihedral angle between carbazole and DTP unit was advantageous for high molar extinction coefficient and

stronger light capturing ability for carbazole dyes. Additionally the presence of benzene on DTP instead of alkyl chain is found to be beneficial to retard the charge recombination. Therefore, taking the benefits of above factors dye **DP42** was able to produce an efficiency of 6.63% with J_{SC} = 14.55 mA cm^{-2}, V_{OC} = 710 mV, *FF* = 0.64 in iodine based DSSC.

Table 1.8 Optical and photovoltaic properties of DTP-based organic dyes **DP41-DP45** containing carbazole and triphenylamine donor.

Entry	λ_{max} (nm (ε_{max} $\times 10^3$ M^{-1}cm^{-1}))	J_{SC} (mAcm^{-2})	V_{OC} (mV)	FF	η%	Ref
DP41	436(43.2)	07.1	620	0.79	3.68	135
DP42	492(56.4)	14.6	710	0.64	6.63	135
DP43	492(44.6)	13.4	690	0.65	5.96	135
DP44	496(62.5)	14.7	700	0.63	6.50	135
DP45	493(49.9)	14.8	720	0.61	6.44	135

1.10 Importance of auxiliary spacer in DTP based organic dyes for DSSCs

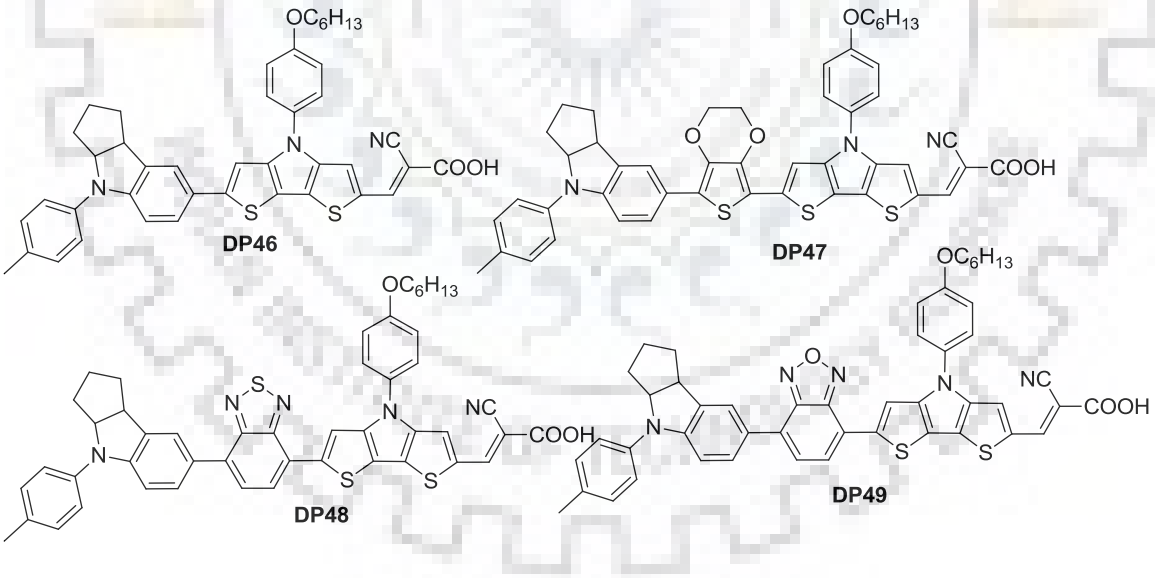

Figure 1.28 Structures of DTP-based dyes with indoline donor [136].

Xie et al [136] synthesized a new set of DTP-based organic dyes **DP46-DP49** featuring different auxiliary linker ethylenedioxythiophene (EDOT), benzothiadiazole (BTD) and benzooxadiazole (BOD) between indoline donor and DTP spacer, repectively (Figure 1.28). The insertion of electron rich EDOT unit lifted HOMO in upward direction without disturbing LUMO level for **DP47**. On the other hand, electron deficient BDT and

BOD units lowered the LUMOs for **DP48** and **DP49** with little effect on their HOMOs. Therefore, BDT and BOD units significantly customized the molecular energy levels for the dyes which reduced the energy waste for electron injection process. These advantages increased the efficiency of **DP49** to 9.4% from 0.24% in **DP47**.

Table 1.9 Optical and photovoltaic properties of DTP-based organic dyes **DP46-DP51** used for dye sensitized solar cells.

Entry	λ_{max} (nm (ε_{max} $\times 10^3$ $M^{-1}cm^{-1}$))	J_{SC} ($mAcm^{-2}$)	V_{OC} (mV)	FF	η%	Ref
DP46	549 (50.2)	7.9	640	0.68	3.44	136
DP47	570 (33.8)	1.22	440	0.48	0.24	136
DP48	563 (44.5)	15.8	660	0.68	7.14	136
DP49	558 (35.1)	19.7	678	0.70	9.46	136
DP50	571 (59.0)	14.4	807	0.56	6.50	137
DP51	567 (59.2)	18.0	809	0.56	8.14	137

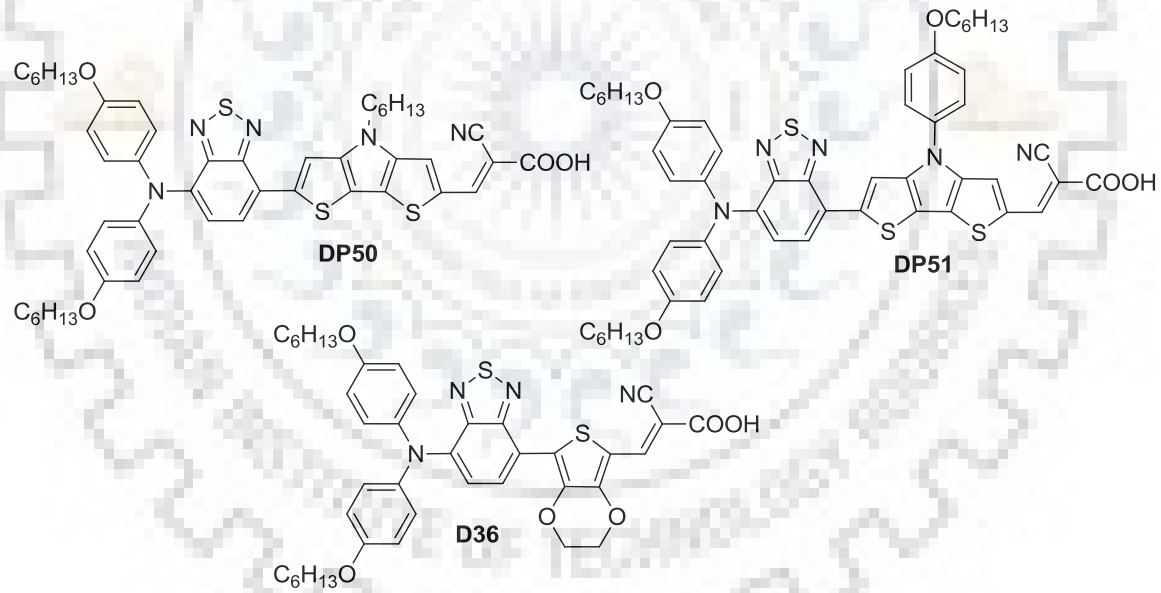

Figure 1.29 Structures of DTP-based dyes containing benzothiadiazole [137].

Li et al. synthesized [137] the BTD based three organic dyes incorporating DTP spacer (**DP50** and **DP51**) and EDOT π-linker (**D36**) (Figure 1.29). In comparison to EDOT linker, DTP dyes showed broad absorption owing to planar skeleton and reduced HOMO-LUMO energy gap. Also, DTP dyes **DP50** and **DP51** were found to be more conducive for electron injection and inhibition to charge recombination. Therefore, the

best performance was achieved for the dye **DP51** with a conversion efficiency of 8.14% in the series.

1.11 DTP dyes with auxiliary donor

Liang and coworkers [138] synthesized four DTP spacer based dyes **DP52-DP53** in which two dyes contaning DTP as a terminal donor in two different fashions via C-thiophene or *N*-pyrrolic linkage in a D-D-π-A configuration (**DP54** and **DP55**) (Figure 1.30). However C-linkage proved to be beneficial for extending the absorption edge, molar extinction coefficients and charge transfer interactions than *N*-linkage. This made the dye **DP54** to exhibit high photocurrent generation in DSSC with Co-electrolyte.

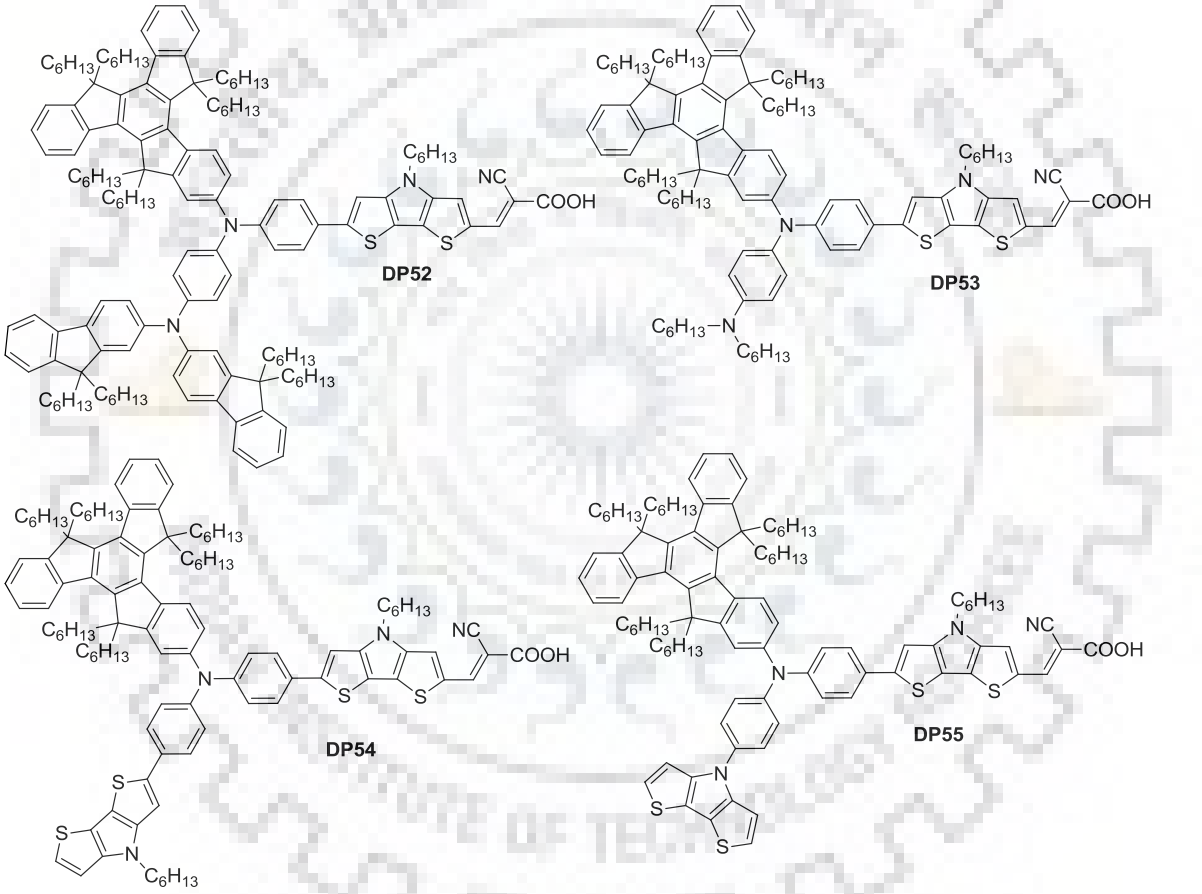

Figure 1.30 Structures of DTP-linker based dyes containing truxene and DTP as auxiliary donor [138].

Table 1.10 Optical and photovoltaic properties of dithienopyrrole based organic dyes **DP53-DP56** used for dye sensitized solar cells.

Entry	λ_{max} (nm (ε_{max} $\times 10^3$ $M^{-1}cm^{-1}$))	J_{SC} ($mAcm^{-2}$)	V_{OC} (mV)	FF	η%	Ref
DP52	529 (60.3)	11.2	915	0.68	6.97	138
DP53	535 (58.4)	5.6	765	0.69	2.95	138
DP54	521 (79.6)	15.3	867	0.68	9.02	138
DP55	510 (69.3)	7.97	760	0.71	4.30	138

1.12 DTP-based dianchoring organic dyes for DSSCs

Lin and co-workers [139] used the DTP first time to synthesize A-π-D-π-A di-anchoring organic dyes in which DTP was utilized as donor and linker. Later on the DTP was exploited as a conjugating spacer in A-π-D-π-A di-anchoring configuration, showed a high molar extinction coefficient for the dyes [140].

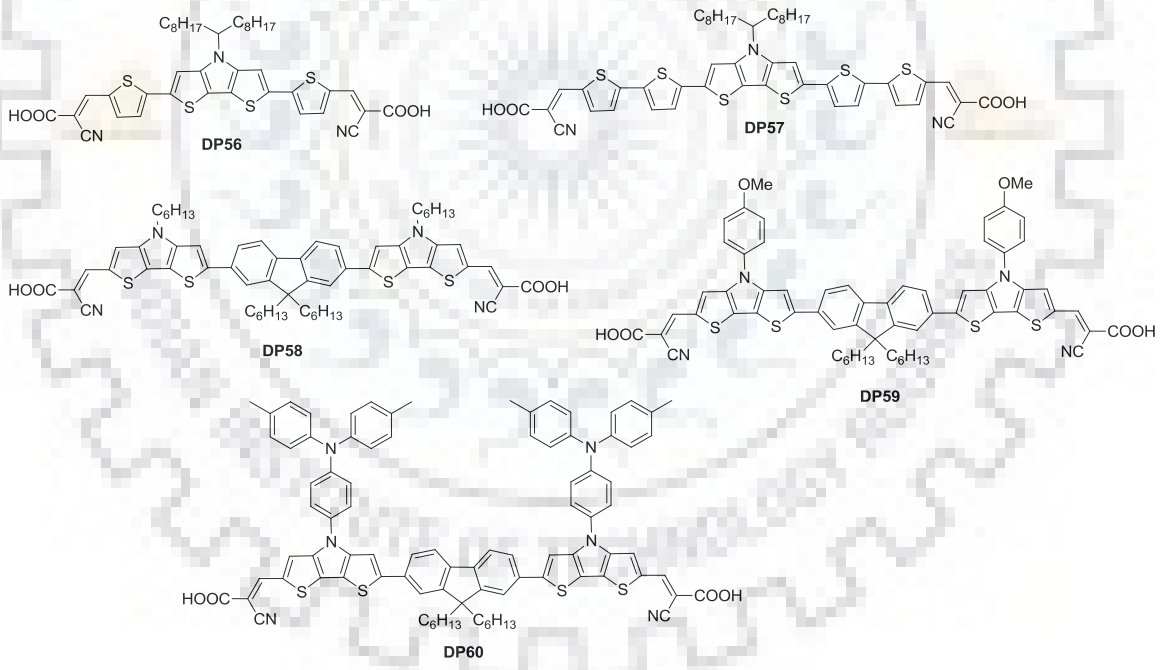

Figure 1.31 Structures of the DTP based di-anchoring dyes [139,140].

Table 1.11 Optical and photovoltaic properties of DTP-based di-anchoring dyes **DP56-DP60**.

Entry	λ_{max} (nm (ε_{max} $\times 10^3$ $M^{-1}cm^{-1}$))	J_{SC} ($mAcm^{-2}$)	V_{OC} (mV)	FF	η%	Ref
DP56	557 (74.6)	9.8	580	0.65	3.70	139
DP57	564 (79.0)	3.8	500	0.65	1.24	139
DP58	520 (145.0)	13.1	629	0.69	5.66	140
DP59	514 (116.0)	13.8	669	0.69	6.36	140
DP60	516 (108.0)	10.8	664	0.69	4.95	140

1.13 Conclusion

Organic dyes as an effectual alternate of the metallic ruthenium- and zinc-dyes have achieved the maximum efficiency of 12.5%. Likewise, the modification of conventional D-π-A architecture of the organic sensitizers achieved by extending the conjugation, insertion of donor-acceptor motif and rigidification of conjugating backbone effectively improved the light harvesting efficiency and photovoltaic performances. The rigidification approach has the advantages over the approach of extending the conjugation such as less dihedral angle, less reorganization energy, reduction in the steric congestion, high photoluminescence efficiency and charge mobility etc. In this regard, the rigidified chromophores have gained immense attention for the development of efficient sensitizers for the DSSCs applications. Further, fused heteroarenes have over ruled the fused poly aryl derivatives due to their electron rich character owing to the presence of at least one heteroatom. Moreover, heteroarens are being chemically and thermally stable, and less susceptible for oxidation. Among fused heteroarenes, thiophene derivatives specially DTP possess more coplanar and electron rich character reminiscent to the fusion of two thiophene and one pyrrole rings. Contrary to the CPDT, which is synthetically costly, not only DTP is more accessible, but possesses similar electronic properties with respect to CPDT and allows to incorporate a variety of *N*-substituents. *N*-substituted DTP based electronic materials have been used as building blocks in various polymers, oligomers and molecular materials to provide high carrier mobilities, enhanced solution and solid-state fluorescence with low band gaps. Moreover, the substituents of DTP moieties can be used to improve the materials solubility and intermolecular packing without introducing significant torsions between adjacent aromatic units.

As a result, this position offered a greater versatility toward the control of dye aggregation, which made it particularly attractive for DSSC applications. DTP-dyes have possessed high light harvesting efficiency, dye regeneration, reduced dye aggregation, and suppressed the quenching of photo-excited electrons and hence high photovoltaic performances. Therefore, in this point of view, several DTP based dyes have emerged as potential candidate for DSSCs fabrication.

Dithienopyrrole based organic dyes for dye sensitized solar cells: Aim & scope

In the present scenario, natural energy sources are depleting continuously and therefore, in order to meet the global demand of energy, photovoltaic technology is considered an imminent alternative. Despite the dominance of silicon-based photovoltaic technologies, dye sensitized solar cell (DSSC) [1] invented by Grätzel has gained much impetus in recent years due to its structural modularity which allows the conversion of solar flux into electric power with high power conversion efficiency and low cost. Light absorbers possessing optical absorptions extending into red and near-IR regions of the solar spectrum and effectively injecting electrons into the conduction band of semiconductor metallic oxides are actively searched [2]. The sensitizer adsorbed on the TiO_2 mediates the interaction between inorganic semiconductor and redox couple and control the overall performances of DSSCs. For the DSSCs technology, metal free organic sensitizers containing rigidified are achieving immense attention over the dyes lacking rigidified segments, because of their facile properties such as high extinction co-efficient and less reorganization energies etc..

Also from the literature background, it is understood that from fundamental viewpoint, molecules allow a more straightforward and reliable analysis of the structure-property relationships, an approach that remains the key tool for the design of new materials specifically designed for photovoltaic applications. Therefore, herein we believe that electron rich rigidified DTP unit can be explored towards systematic molecular engineering of organic materials for photovoltaic applications. We speculate that the fluorene-based dyes are more redox stable than the corresponding biphenyl derivatives. So, we felt that incorporation of fluorene on DTP may enhance the electron richness and may have positive impact on the detrimental processes such as electron recombination and dye aggregation. Therefore, the schematic representation of structural diversity

expected from the various possibilities with design strategies for the *N*-functionalized with fluorene DTP-based target dyes is illustrated in Figure 1.28.

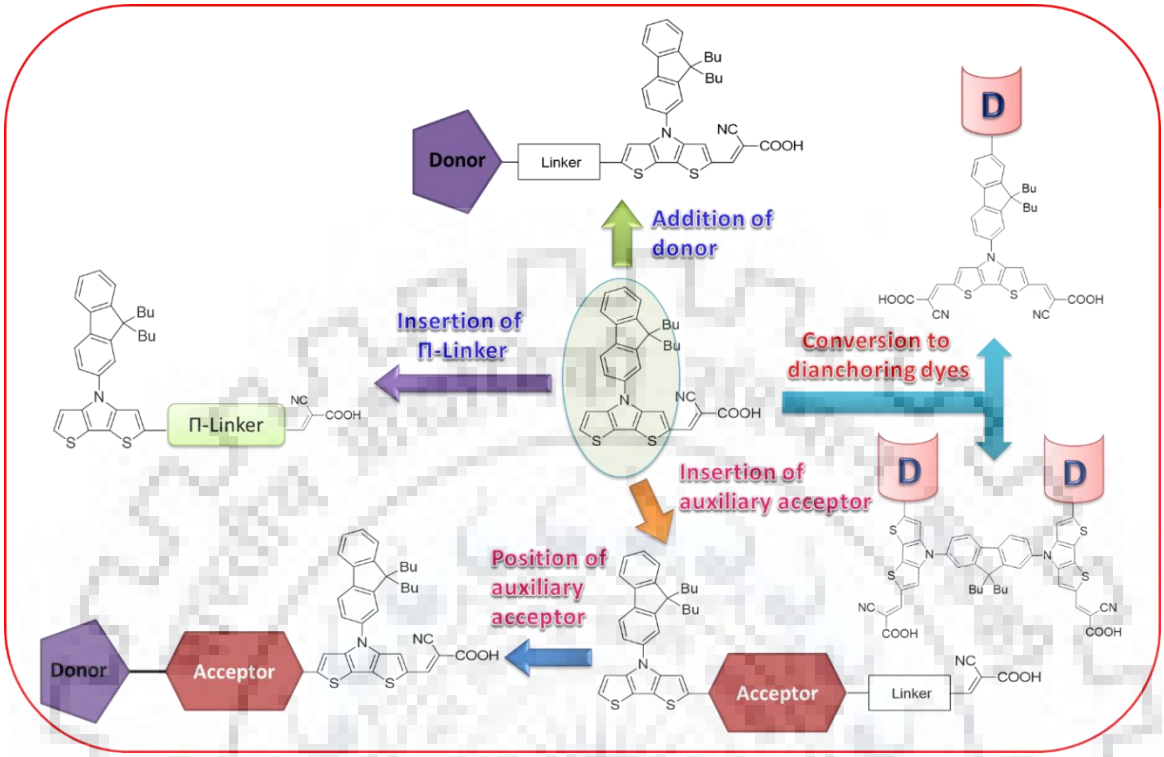

Figure 1.32 Pictorial representation of designs and strategies for different sensitizer targets.

Effect of π-spacer: The coplanar and electron rich π-spacers are advantageous for the delocalization of electron and charge transfer from donor to acceptor. So herein, we want to do structural modification to the DTP dyes by increasing the length of the conjugated system by thiophene/bithiophene and fused thiophene (DTP itself) to achieve the extended absorption, charge transfer probabilities and reduce the oxidation potentials for the dyes. The use of bulky and electronic rich DTP units in conjugating bridge for DTP donor-based dyes are expected to enhance the molar extinction coefficient and will be beneficial to retard the charge recombination processes. Owing to this hypothesis we desire for improved photovoltaic parameters J_{SC} and V_{OC} in the dyes.

Effect of donor: Electron rich donor units on the sensitizer may be a better choice to broaden the absorption spectra and introduction of energy delocalizing chromophore, which cause prolongation of excited state and eventually can compete with several deactivating processes. Therefore, we have designed new organic dyes featuring triphenylamine, diphenylaminofluorene and heterocycles as donors, DTP conjugation and cyanoacetic acid, acceptor. As it is well documented that arylamines featuring

triphenylamine act as an efficient donor. By replacing the phenyl linker with fluorene moiety, the absorption spectra can be broadened. Moreover, phenothiazine and carbazole are aromatic heterocyclic compounds with electron-rich nitrogen or sulfur hetero atoms, and have attracted great interest for their excellent hole-transporting ability, rigid structure and large π conjugated arrangements. The two phenyl groups in these heterocyles are arranged nearly coplanar, so that a π-delocalization can be extended over the entire chromophore. We believe that thiophene group in conjugation pathway can stabilize the charge separated state and therefore enhance the value of open-circuit photovoltage.

Effect of Acceptor: It is well known that the increase in the acceptor strength results in increase in the charge transfer propensity and consequently can lead to the longer wavelength absorption. There are several reports where benzothiadiazole, benzotriazole and quinoxaline have been used as acceptor in linker and it was found to be helpful in bathochromically shifting the absorption spectra as well as in increasing the efficiency for device. In our work, we want to introduce these units directly attached with donor unit in order to induce the better/efficient electronic communication between the donor and acceptor segments. We assume that this architecture will helpful to retard back electron transfer in DSSC. Also, we believe that change in the position of BTD units will further improve the photophysical and electrochemical properties. Introduction of aromatic moiety in between the auxiliary donor and cyanoacrylic acceptor can reduce the propensity of trapping for the flow of electrons towards the TiO_2.

Effect of Dianchoring: We also want to synthesize two set of dianchoring dyes through design featuring λ-shaped and H-shapes. In λ-shaped di-anchoring system, in which DTP has been tri-functionalized with three substituents, one is attached at pyrrole nitrogen atom other two are cyanoacrylic acid at the C2 and C6-positions. For H-shaped dyes, fluorene has been used as bridge through the pyrrolic nitrogen of DTPs to connect two monoanchoring dyes. We expected that the di-anchoring dye would be able to bring the structural variety for panchromatic response, extension of π-conjugation and to enhance the binding capacity to the TiO_2 nanoparticles. Also, these type of molecules can retard the approach of the oxidized dye/oxidized half of the redox couple to TiO_2. By the use of this protocol, the dark current can be reduced and open circuit voltage will increase.

Briefly, in this dissertation we provide a systematic description about the key parameters those decide the efficiency of DSSCs can be well-adjust by judicious molecular engineering of DTP-based sensitizers. We anticipate building up insights on different possible chemical modifications such as increase in conjugating bridge, insertion of auxiliary donors/acceptors and dianchoring motifs in the composition with various chromophores can modulate the electronic structure of the organic dyes and tune the power conversion efficiency. We believe that our studies will provide systemic information to future experimental investigations to continue the research on rigidification and electronic rich DTP-based organic dyes.

Chapter 2

Effect of nature of electron rich π-linkers in the functional properties of dithienopyrrole-based sensitizers

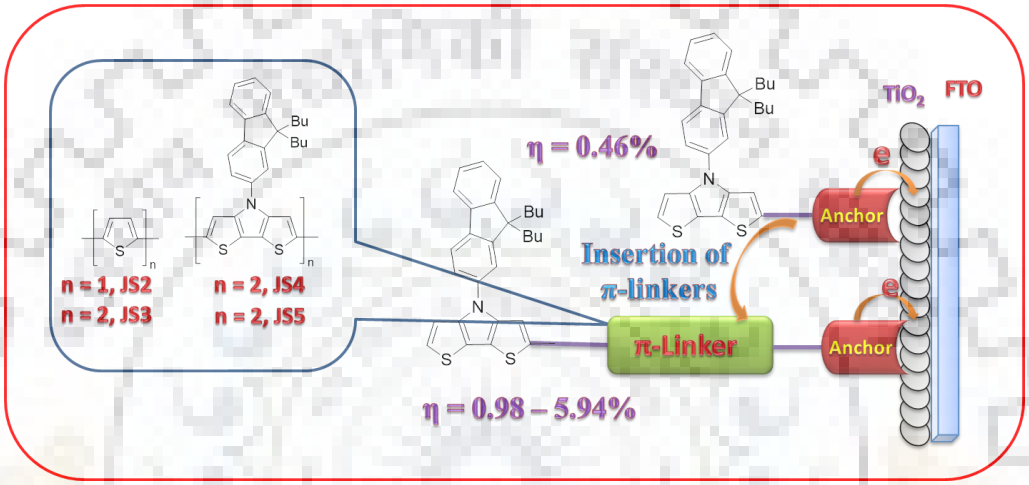

2.1 Introduction

It has been found that the presence of bulky groups and introduction of longer alkyl chains on the donor or linker can reduce the charge recombination and dye aggregation [141] but these are not enough criteria to achieve high performance solar cells. There are also other molecular engineering methods to improve the light harvesting efficiency of the organic dyes which involve the increase in the electron richness of the donor moieties [142] and introduction of the electron deficient acceptors [18]. However, the introduction of electron-rich moieties in conjugation with donor segment, not only help to broaden the absorption spectra but also leads to prolongation of excited state which facilitates the electron injection into the conduction band of TiO_2 [143]. Therefore, the nature of conjugated bridging segment (π) play a significant role in controlling the light-harvesting performance of the dyes as it effectively tunes the donor-acceptor interactions [144] Furthermore, it has been found in the literature that the incorporation of electron rich or deficient chromophores in suitable positions relative to the donor and acceptor segments can induce the desirable changes in electronic structures of the dyes. The coplanarity of π-bridge produces red shift in the absorption profiles of the dyes [145,146], while the

twisted π-bridge is beneficial for the charge separation and electron injection propensity [147]. Moreover, conjugating π-bridge controls the dynamics of the charge separation [148]. A number of π-conjugated aromatic segments such as substituted thiophene [149] or thienothiophene [41,67] derivatives have been reported to result remarkable power conversion efficiencies.

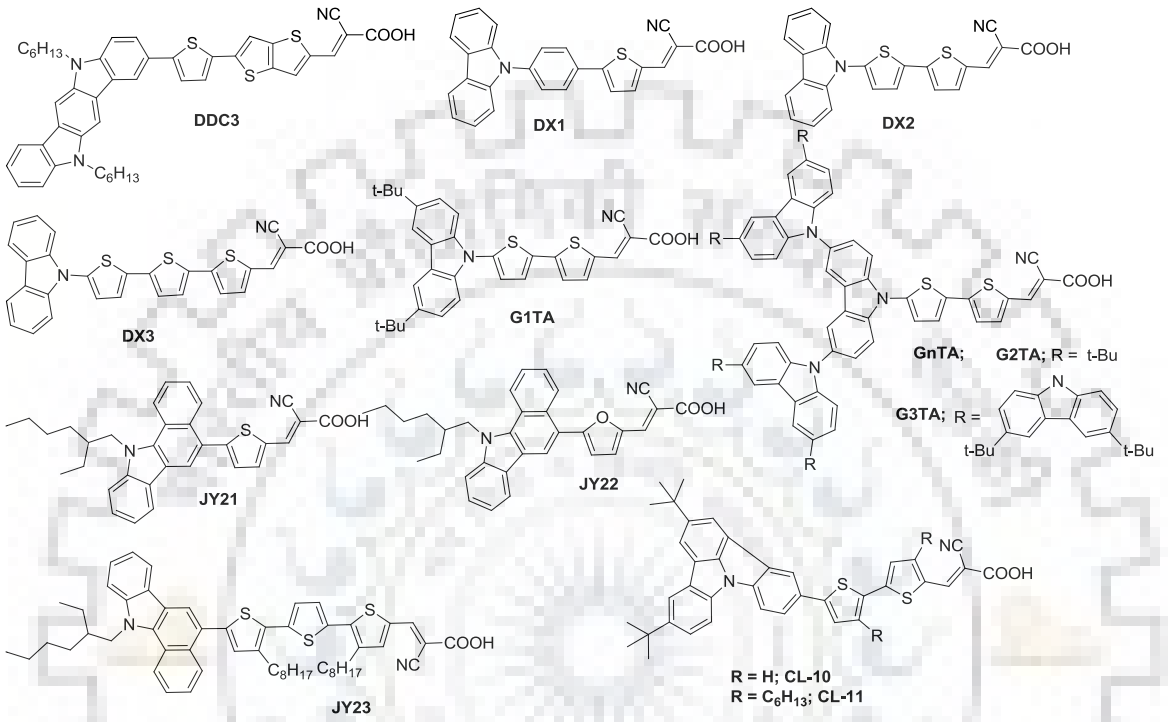

Figure 2.1 Structures of dyes containing thienothiophene/thiophene/oligothiophene π-linkers [67,150-153].

Liu and coworkers [150] reported dyes **DX1-DX3** containing carbazole donor with benzene/thiophene or oligothiophene as π-linker and cyanoacrylic acid acceptor (Figure 2.1). The presence of benzene/thiophene spacer not only helps to retard the charge recombination and dye aggregation for **DX1**, but also the extension of conjugation by thiophene produces bathochromic shift in absorption of **DX2** and **DX3**. Promarak and coworkers [151] developed dyes featuring carbazole dendrons as donor with bithiophene as π-linker, and cyanoacrylic acid as acceptor. It was observed that on increasing the dendritic donor size light harvesting ability increases along with reduction in the amount of dye uptake per unit TiO_2 area because of increase in the molecular volume. As a result of which the dye **G1TA** (Figure 2.1) having lowest molecular volume exhibited the highest power conversion efficiency of 5.16%. Zhu and coworkers [152] incorporated benzo[*a*]carbazole as donor to synthesize a series of dyes **JY21-JY23** based on different

heteroaromatic spacers (Figure 2.1). Among these dyes, **JY23** containing oligothiophene π-linker showed most red shifted absorption due to longer conjugation length. Also IPCE response for the dye **JY23** was observed up to 740 nm covering the entire region of the UV-visible light and lead to high efficiency of 7.54% under standard AM 1.5 G irradiation. Li et al. [153] reported the dyes **CL-10** and **CL-11** containing a *tert*-butyl-capped indolo[3,2,1-*jk*]carbazole unit as a donor with or without hexyl chain substituted bithiophene units as π-linkers (Figure 2.1). They demonstrated that although the presence of hexyl chains at non-ortho β-position of the bithiophene unit do not disturb the planarity of the dye structure but cause the reduction in dye loading amount on TiO_2 surface. Thus the dye **CL-10** without hexyl chain showed power conversion efficiency up to 4.68% by the addition of chenodeoxylic acid (CDCA) as a co-adsorbent.

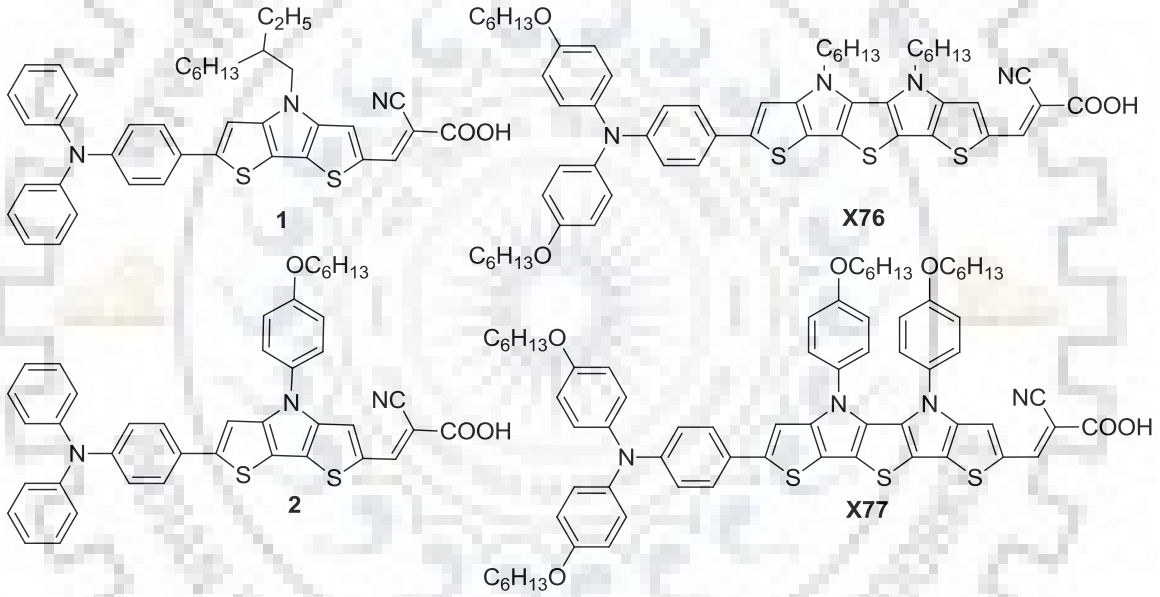

Figure 2.2 Structures of the dyes containing DTP as π-linkers [154,155].

Further fusethienyl systems such as benzodithiophene (BDT) [34], cyclopentadithiophene [36] (CPDT) and dithienopyrrole (DTP) [37] have attracted attention because of their electron richness, planarity and rigidity. Gupta and coworkers synthesized *N*-substituted-DTP π-linker based organic dyes **1-2**. They found that the rigidification of π-spacer (such as by DTP here) in enhancement of the spectral response of the dyes (Figure 2.2). As a result, the dye **2** containing an *N*-arylsubtituted DTP π-linker exhibited the power conversion efficiency of 6.2% [154]. Liang and coworkers further prepared organic dyes **X76** and **X77** using modified DTP dithieno[2,3-*d*:2′,3′-*d*′]-thieno[3,2-*b*:3′,2′-*b*′]dipyrrole (DTDP) unit into D-π-A architectures (Figure 2.2). These

dyes exhibit good light harvesting ability. Furthermore, the *N*-substituents on DTDP core were found to play a crucial role in electrochemical and photovoltaic properties and helped to hinder the dye aggregations on TiO_2. Thus, the dye **X77** containing *N*-aryl substituents on DTDP core, showed cell efficiency of 7.2% with Co-bpy electrolyte [155].

From above discussion it is evident that the dye containing thiophene/oligothiophene and DTPs as linker are promising entries. In this chapter we have designed and synthesized organic dyes featuring *N*-fluorene-2-yl dithieno[3,2-*b*:2',3'-*d*]pyrrole as a donor and thienyl, bithienyl and DTP as linkers and cyanoacrylic acid as acceptor in a D-π-A molecular arrangement (Fig. 2.3). Our aim is to elucidate the role of fluoreny DTP on improving the dye characteristics relevant to DSSC applications. The newly developed dyes showed significant enhancement in optical and electrochemical properties for DTP-linker when compared to the analogous derivatives with or without thienyl/bithienyl spacer functionalized DTP between the donor and acceptor and consequently served as efficient sensitizers in DSSCs.

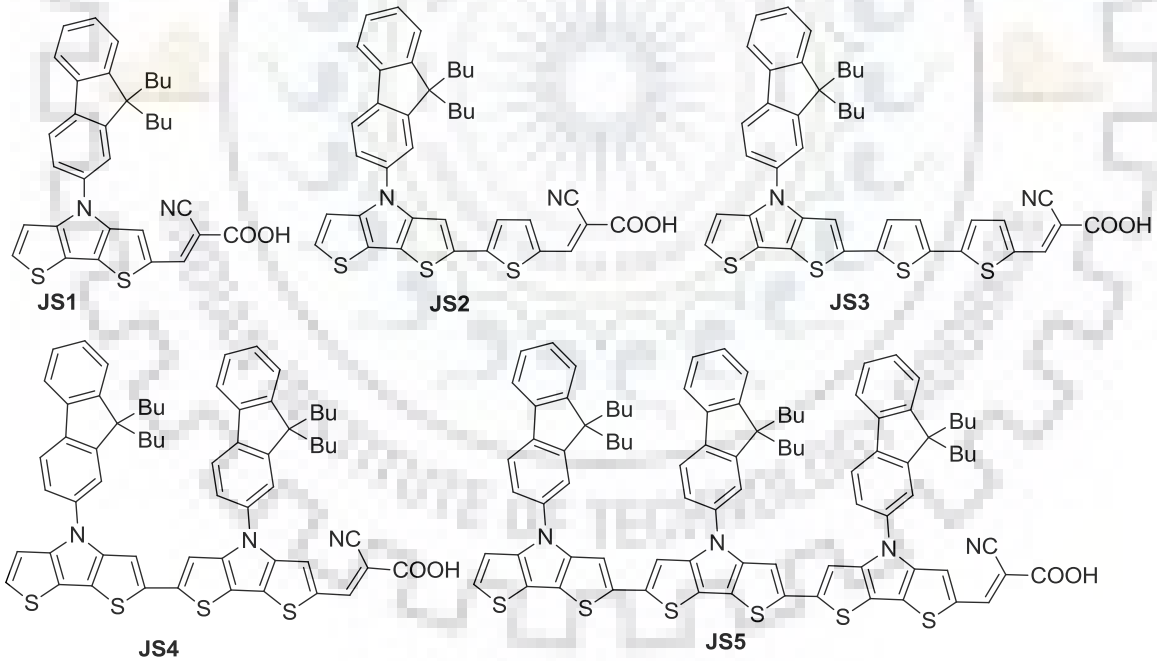

Figure 2.3 Structures of DTP- based dye, **JS1-JS5** containing different π-linkers.

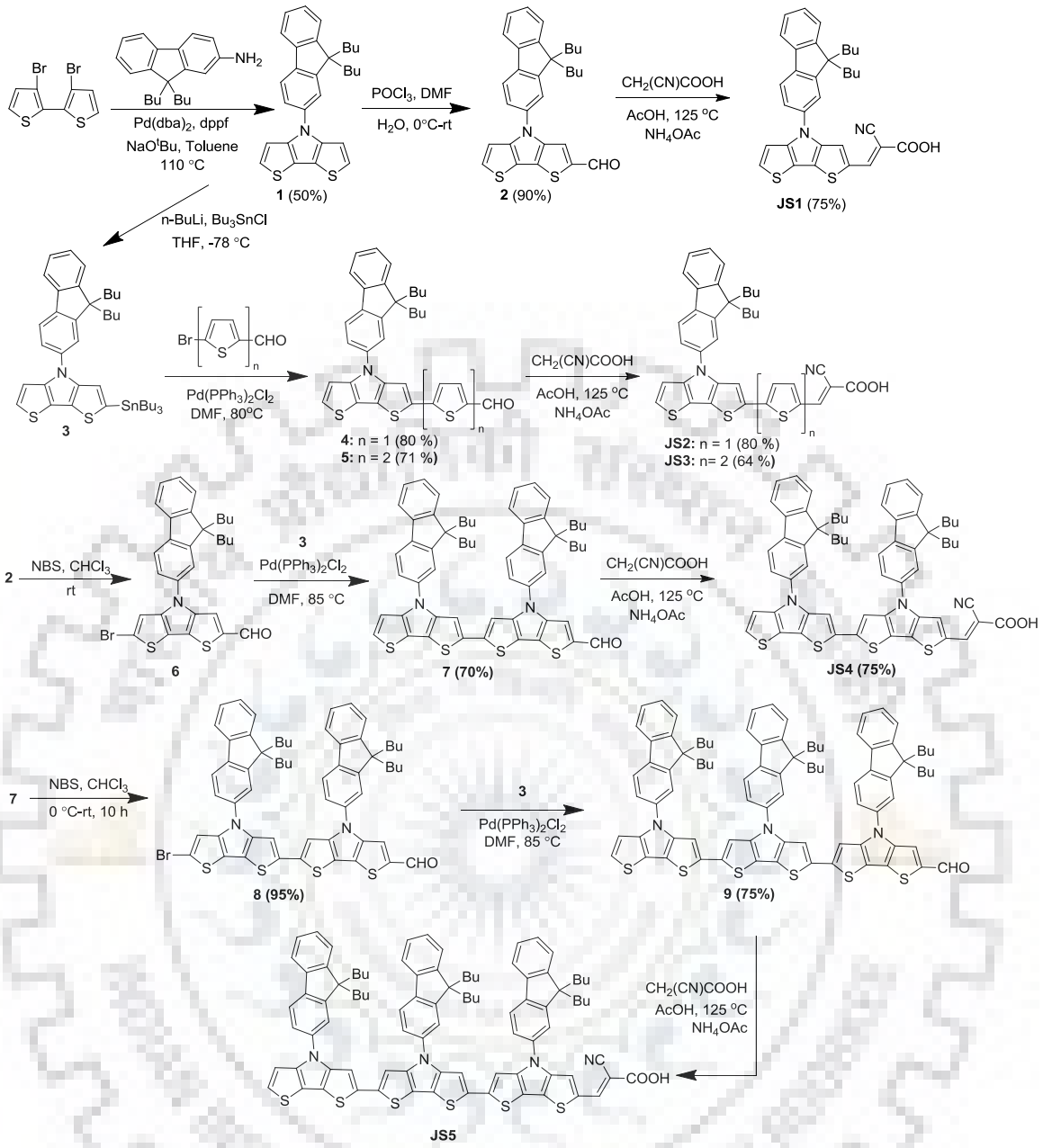

Scheme 2.1 Synthetic scheme of DTP-based dyes, **JS1-JS5**.

2.2 Result and discussion

2.2.1 Molecular design and synthesis

The structures of the newly synthesized organic dyes featuring dithienopyrrole as donor in conjugation with different electronic rich thienyl-linkers and cyanoacrylic acid as acceptor are displayed in Figure 2.3. The synthetic pathway adopted to produce new dyes is shown in Scheme 2.1. The parent chromophore, 4-(9,9-dibutyl-9*H*-fluoren-2-yl)-4*H*-dithieno[3,2-b:2',3'-*d*]pyrrole (Fl-DTP) was synthesized by palladium catalyzed Buchwald-Hartwig C-N cross coupling [156] reaction between 9,9-dibutyl-9*H*-fluoren-2-

amine and 3,3'-dibromo-2,2'-bithiophene. Subsequent Vilsmeier-Haack formylation of Fl-DTP using DMF/$POCl_3$ in suitable stoichiometric ratios yielded the 4-(9,9-dibutyl-9*H*-fluoren-2-yl)-4*H*-dithieno[3,2-*b*:2',3'-*d*]pyrrole-2-carbaldehyde (**2**) in reasonable yield. Further, another key precursor 4-(9,9-dibutyl-9*H*-fluoren-2-yl)-2-(tributylstannyl)-4*H*-dithieno[3,2-*b*:2',3'-*d*]pyrrole (**3**) was obtained from **1** by adopting literature procedure [157]. Then, the precursor aldehydes 5-(4-(9,9-dibutyl-9H-fluoren-2-yl)-4H-dithieno[3,2-b:2',3'-d]pyrrol-2-yl)thiophene-2-carbaldehyde (**4)** and 5'-(4-(9,9-dibutyl-9H-fluoren-2-yl)-4H-dithieno[3,2-b:2',3'-d]pyrrol-2-yl)-[2,2'-bithiophene]-5-carbaldehyde (**5)** were obtained by performing Stille reactions [158] between **3** and monobromo-derivatives of thienyl/bithienyl aldehydes. On the other hand, the bromination with controlled addition of NBS to the solution of **2** in DCM produced 6-bromo-4-(9,9-dibutyl-9*H*-fluoren-2-yl)-4*H*-dithieno[3,2-b:2',3'-*d*]pyrrole-2-carbaldehyde (**6**). The precursor 4,4'-bis(9,9-dibutyl-9*H*-fluoren-2-yl)-4*H*,4'*H*-[2,2'-bidithieno[3,2-*b*:2',3'-*d*]pyrrole]-6-carbaldehyde (**7)** was obtained from **3** and **6** under Stille coupling reaction conditions. Further, 6'-bromo-4,4'-bis(9,9-dibutyl-9*H*-fluoren-2-yl)-4*H*,4'*H*-[2,2'-bidithieno[3,2-*b*:2',3'-*d*]pyrrole]-6-carbaldehyde (**8**) was produced by the bromination of **7** in DCM with the addition of NBS. Next, the Stille reactions between **3** and **8** yielded 4,4',4"-tris(9,9-dibutyl-9*H*-fluoren-2-yl)-4*H*,4'*H*,4"*H*-[2,2':6',2"-terdithieno[3,2-b:2',3'-d]pyrrole]-6-carbaldehyde (**9**). Finally, by applying Knoevenagel condensation using cyanoacetic acid and catalytic amount of ammonium acetate in acetic acid, all the aldehyde precursors **2**, **4, 5, 7** and **9** were converted into respective cyanoacrylic acids **JS1-JS5** in reasonable yield. The structures of the newly synthesized compounds were confirmed by ^{1}H, ^{13}C NMR spectroscopy and mass spectral techniques. The spectral data are found to be consistent with proposed structures of the molecules.

2.2.2 Optical properties

To study the photophysical properties of the newly synthesized dyes, absorption spectra for the dyes were recorded in tetrahydrofuran (THF) and displayed in Figure 2.4. The corresponding data is compiled in Table 2.1. The absorption bands shown by the dyes in high energy region (< 400 nm) can be assigned to π-π* transitions originating from different aromatic units present in the dyes. The absorption peaks appeared in the lower energy region (400-600 nm) is probably a intramolecular charge transfer (ICT) transition from DTP donor to cyanoacrylic acid acceptor. The dye **JS1** displayed shortest wavelength absorption at 431 nm in the series. The ICT absorption wavelength and its

molar extinction coefficient progressively increased on moving from **JS1** to **JS5**. Further, the insertion of different thienyl/fused-thienyl derivatives as π-linkers between DTP unit and cyanoacrylic acid induced a red shift and enhancement in the molar extinction coefficient for this band. This may be due to increase in effective conjugation length and electron richness by thienyl and its derivatives which further enhance the CT from donor to acceptor. However, extension in conjugation from one thiophene unit (**JS2**) to bithiophene unit (**JS3**) induced the both bathochromic and hyperchromic effect, but a distinct effect was established when bithiophene linker was further exchanged by the rigidified DTP segment (**JS4**). This is due to increase in electron richness and planarization of conjugation pathway on insertion of thiophene and DTP as spacer which is beneficial for the donor-acceptor interactions [133]. Interestingly, in comparison to **JS4** the insertion of second DTP segment in conjugation-bridge increased the absorption maxima 25 nm and molar extinction coefficient 31.7 $\times 10^3$ M^{-1} cm^{-1} for **JS5**. This observation suggested that the rigidified and extended conjugating bridge through DTP units is beneficial for improving the light harvesting efficiencies of present dyes.

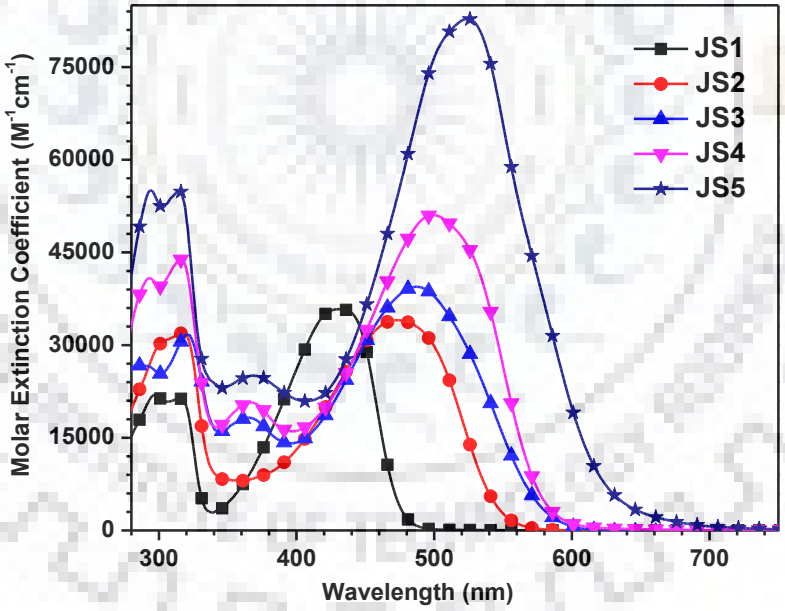

Figure 2.4 Absorption spectra of the dyes **JS1-JS5** recorded in THF.

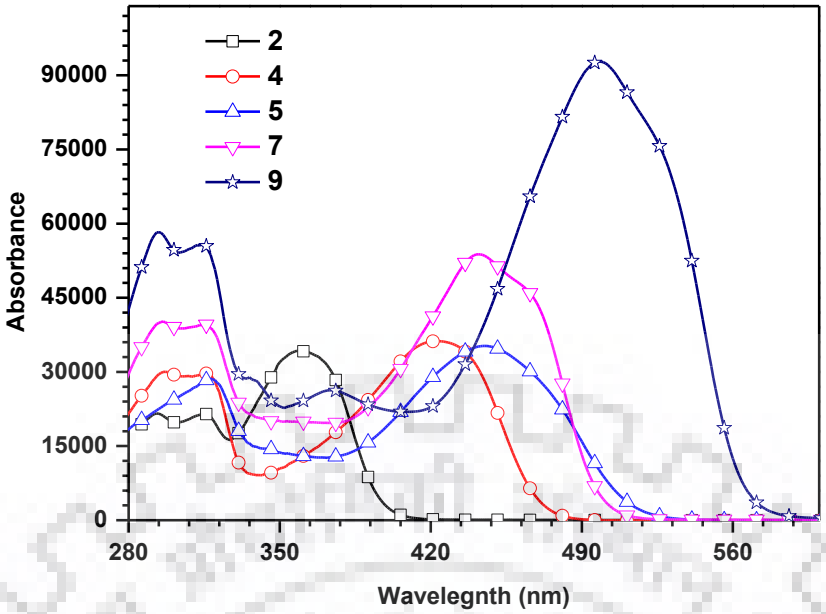

Figure 2.5 Absorption spectra of the aldehyde precursors **2, 4, 5, 7** and **9** recorded in THF.

The charge transfer nature of the absorption maxima was confirmed by comparing the absorption of the dyes with their respective aldehyde precursors (Figure 2.5). In comparison to the aldehydes, the absorption of the dyes shows red shift. This was attributable to the strong electron accepting nature of cyanoacrylic acid than carbaldehyde. Further, an acid/base equilibrium study involving the addition of triethylamine (TEA) and trifluoroacetic acid (TFA) to the THF solutions of the dyes was performed (Figure 2.6). All the dyes exhibited blue/red shift for longer wavelength absorption with TEA/TFA addition respectively. This was owing to the increment and decrement of electron withdrawing capacity of carboxylic acid resulted from protonation/deprotonation by TFA/TEA respectively. All the dyes displayed negative solvatochromism for the solvent of increasing polarities attributable to the stabilization of polar ground state by polar solvents (Figure 2.7) [159]. However, the dyes displayed the most blue shift absorption in DMF solvent due to its basic nature which caused the deprotonation of carboxylic acid. Also the fast reorganization of excited electrons in chlorinated DCM solvent generated the most red shift for the dyes [160].

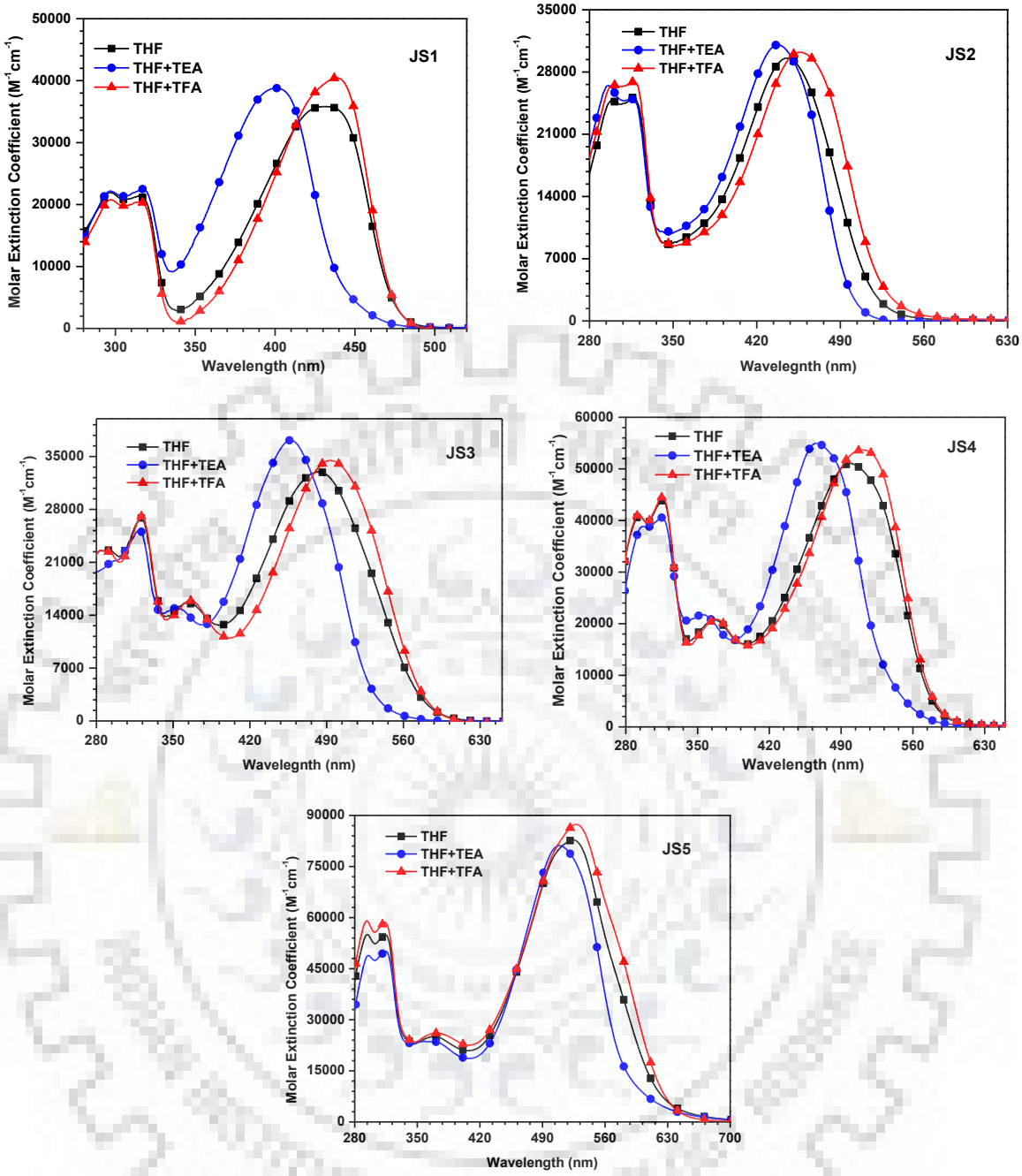

Figure 2.6 Absorption spectra of the dyes **JS1-JS5** recorded in THF before and after the addition of TEA/TFA.

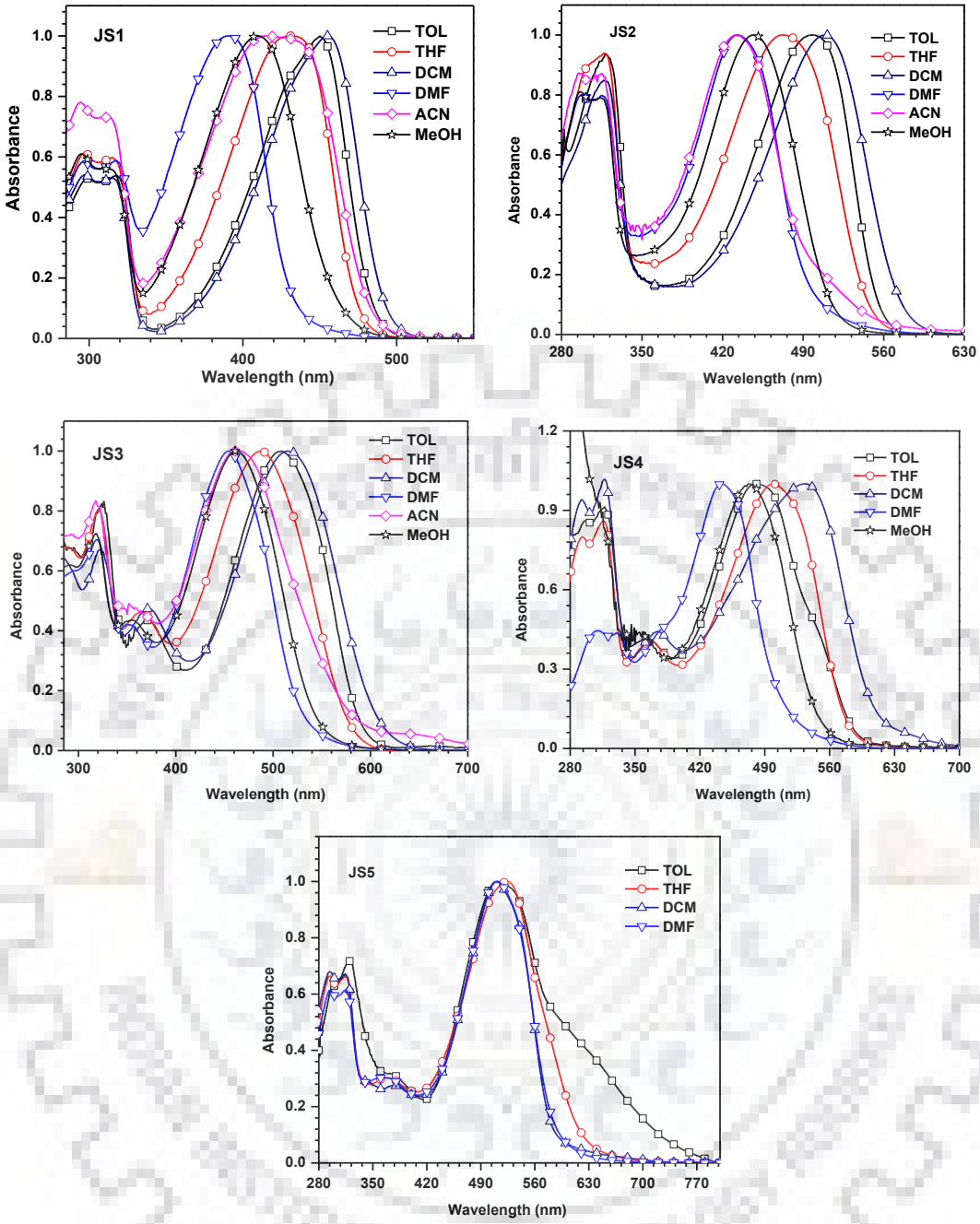

Figure 2.7 Absorption spectra of the dyes **JS1-JS5** recorded in the solvents of different polarities (Due to poor solubility **JS5** was not measured in MeOH and ACN).

The absorption spectra of the dyes anchored on mesoporous thin film of nanocrystalline TiO_2 were also recorded and displayed in Figure 2.8. As compared to solution, all the dyes showed broad and red shifted absorption on solid states which are due to the *J*-type of aggregation of the dyes in solid state [161]. This would be beneficial to enhance the light harvesting efficiency of the dyes. The emission spectra of the dyes were also recorded in THF and showed the similar trend as observed for the absorption maxima (Figure 2.9). Interestingly, the dye **JS5** showed less significant solvatochromism

in absorption and narrow emission with relatively small Stokes-shift in the series. Which indicate poor charge polarization in the molecule in both ground and excited state. This is probably because of conjugation saturation effect which prevents donor-acceptor interaction.

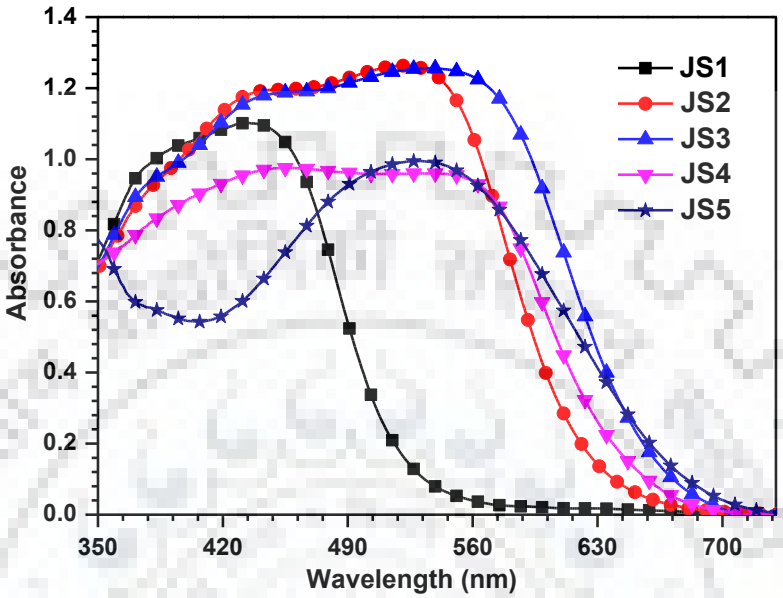

Figure 2.8 Absorption spectra of the dyes **JS1-JS5** anchored on nanocrystalline TiO_2.

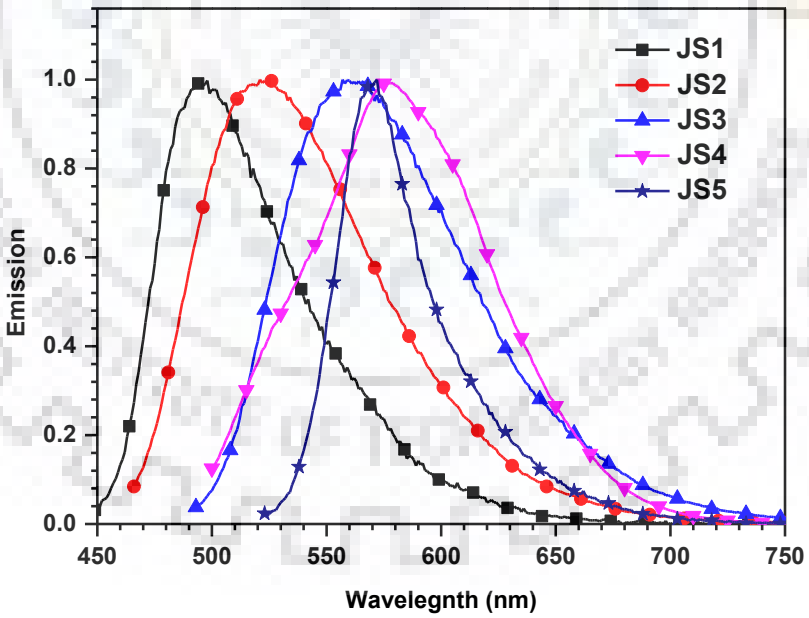

Figure 2.9 Emission spectra of the dyes **JS1-JS5** recorded in THF.

Table 2.1 Optical and electrochemical data of the dyes **JS1-JS5**.

Dyes	$\lambda_{abs.}$ (nm ($\varepsilon_{max} \times 10^3$ $M^{-1}cm^{-1}$))	λ_{max}^{TiO2} (nm)	E_{OX} (mV (ΔE_p, mV)) [a]	E_{OX} (V) (Vs NHE)	HOMO (eV)[b]	LUMO (eV)[c]	$E_{0\text{-}0}$ (eV)[d]	E_{OX}* (V)[e]
JS1	431 (35.8), 315 (21.4), 292 (21.9)	434	808	1.578	-5.608	-2.964	2.644	-1.066
JS2	473 (34.0), 317 (31.9)	520	540	1.310	-5.340	-2.87	2.470	-1.160
JS3	487 (39.5), 365 (18.3), 320 (31.8), 283 (26.8)	536	436	1.206	-5.236	-2.896	2.340	-1.134
JS4	499 (51.1), 367(20.7), 315 (43.9), 293 (40.9)	545	346 (85)	1.116	-5.146	-2.845	2.301	-1.185
JS5	524 (82.8), 363 (25.1), 314 (54.9), 294 (55.0)	531	188 (125), 399 (111)	0.958	-4.988	-2.762	2.226	-1.268

[a] Oxidation potentials are reported with reference to the ferrocene internal standard.
[b] Deduced from the oxidation potential using the formula HOMO = -(4.8 + E_{OX})
[c] Deduced using the formula LUMO = HOMO + $E_{0\text{-}0}$.
[d] Calculated from intersection of absorption & emission spectra.
[e] Calculated from E_{OX}* = E_{OX} - $E_{0\text{-}0}$ (Vs. NHE).

2.2.3 Electrochemical properties

The redox properties give insightful information about the ground and excited state oxidation potentials of the dyes. Through these potentials, it is possible to ascertain the feasibility of electron injection into the conduction band (CB) of TiO_2 and regeneration of the oxidized dyes by electrolyte. Therefore, the redox parameters were estimated by carrying out cyclic voltammetry (CV) (Figure 2.10) and differential pulse voltammetry (DPV) (Figure 2.11) measurements on the dyes **JS1-JS5**. The dyes **JS1-JS3** exhibited irreversible oxidations while the dyes **JS4** and **JS5** showed quasi-reversible oxidation waves. The irreversible oxidation for the dyes might be due to the severe reorganization of dyes after the removal of electrons. The **JS1** showed a high oxidation potential value 1.57 V due to the removal of electron from DTP donor present adjacent to the cyanoacrylic acid. Further insertion of the thienyl and bithienyl between DTP and cyanoacrylic acid reduced the E_{OX} for **JS2** and **JS3** owing to separation between DTP donor and cyanoacrylic acceptors and electron richness. However, a pronounced fall in oxidation potentials was observed by altering the thienyl/bithienyl linkers by DTP moieties. This was due to the fact the electronic rich and rigid planar DTP units not only induce the separation between donor and acceptor but also share its electron density with donor and facilitate the removal of electron. For this reason dye **JS5** possess lowest oxidation potential in the series owing to the presence of three DTP units in conjugation.

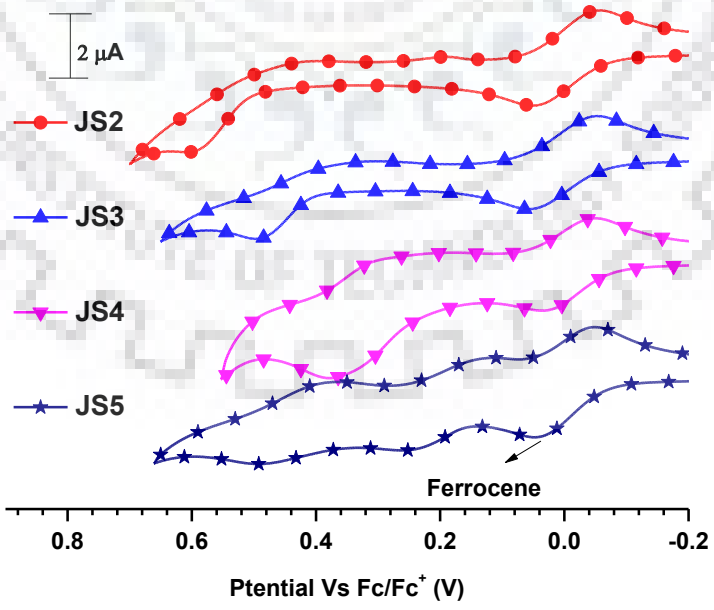

Figure 2.10 Cyclic voltammograms of the dyes **JS1-JS5** recorded in THF.

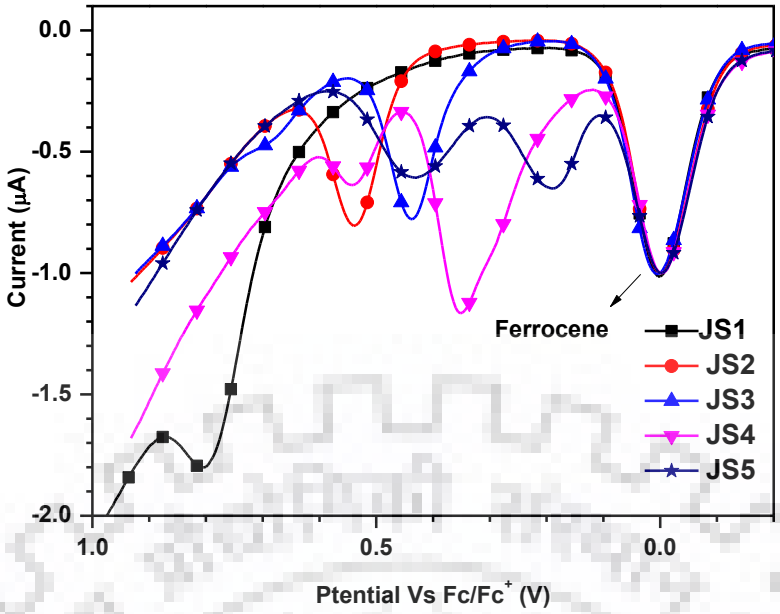

Figure2.11 Differential pulse voltammograms of the dyes **JS1-JS5** recorded in THF.

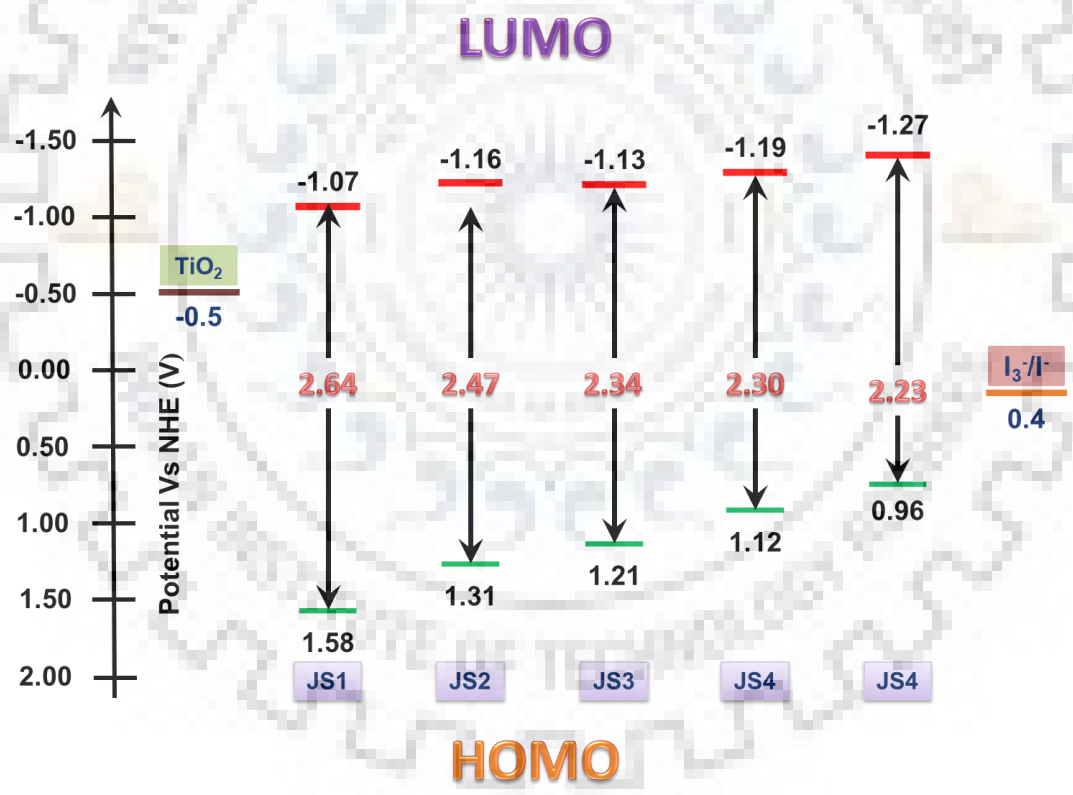

Figure 2.12 Energy level diagram for the dyes **JS1-JS5.**

An equation $E_{OX}^* = E_{OX} - E_{0\text{-}0}$ was used to calculate the excited state oxidation potentials (E_{OX}^*) of the dyes, in which $E_{0\text{-}0}$ was obtained from intersection of normalized absorption and emission spectra. The nature and size of the conjugating bridges not only affected the ground state oxidation potentials, but in the similar way raise the excited state

oxidation potentials for the dyes. Due to the absence of π-linker in **JS1** it displays lower E_{OX}* value while more electronic rich conjugation fetched a highest E_{OX}* value for the dye **JS5**. All the dyes possessed the ground state oxidation potential 0.98 - 1.58 V (*vs.* NHE) were sufficiently more positive than the redox potential of I^-/I^{3-}electrolyte (0.4 V *vs.* NHE) [162], suggest thermodynamically feasible regeneration of the oxidized dyes by electrolyte. The excited state potentials for the dyes observed from -1.07 to -1.27 V (*vs.* NHE) are sufficiently more negative than the conduction band edge (-0.5 V *vs.* NHE) [163] of TiO_2, which energetically ensure the excited state electron injection of the sensitizers into the CB of the TiO_2.

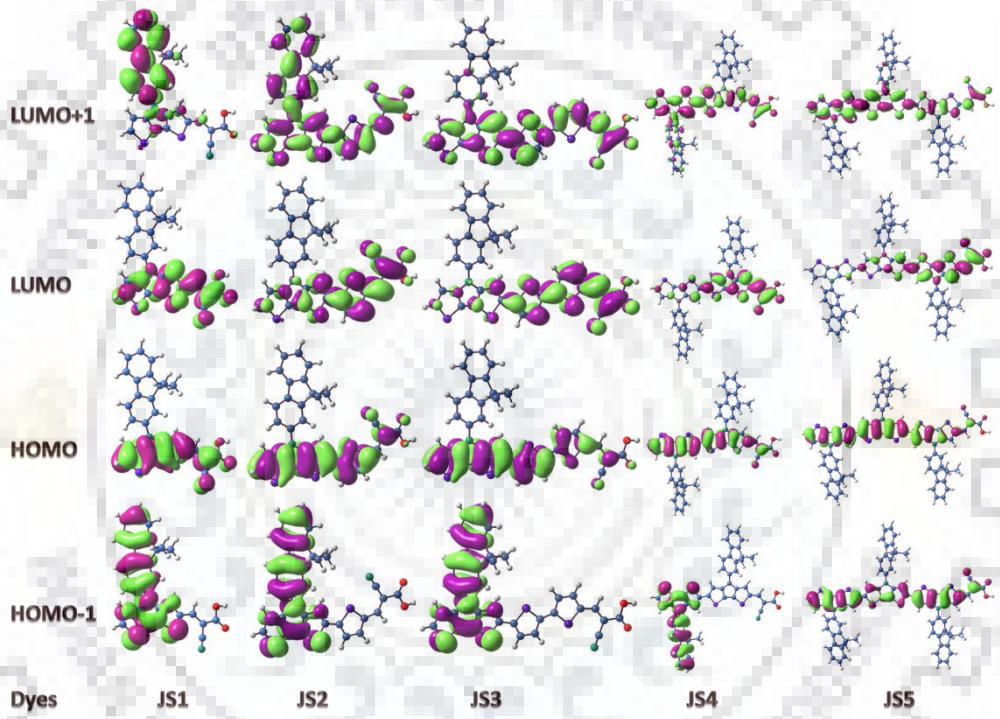

Figure 2.13 Electronic distributions in the frontier molecular orbitals of the dyes **JS1-JS5**.

2.2.4 Theoretical calculations

To further understand the photophysical and redox behaviors of the dyes, density functional theory [164,165] at B3LYP/6-31g(d,p) level was performed. Thus, the obtained electronic distributions for the highest occupied molecular orbitals (HOMOs) and lowest unoccupied molecular orbitals (LUMOs) for the dyes featuring different thienyl-linkers are given in Figure 2.13. Except **JS1**, the HOMOs for other dyes are constituted by DTP donor with the extension into π-conjugating linkers. While, for **JS1** it is being delocalized over DTP and cyanoacrylic acid. The LUMOs for the dyes are

contributed mainly by cyanoacrylic acids and stretched upto thienyl/DTP linkers. Consequently, the enough separation of HOMOs and LUMOs for the dyes **JS3-JS4** ensures active charge transfer from DTP donor to cyanoacrylic acid acceptor [150]. But in case of **JS1**, a significant overlap between HOMO and LUMO hamper the effective charge transfer form donor to acceptor. These observations are consistent with the absorption of the dyes recorded in the solutions.

The time-dependent density functional theory (TD-DFT) employing BMK functional and DGDZVP basis set was used to forecast the absorption wavelengths and electronic excitation parameters among the compounds. The computed vertical excitation energies, molecular orbital assignments and their oscillator strength (*f*) are listed in Table 2.2. The calculated absorption follow the trend **JS1** < **JS2** < **JS4** < **JS3** < **JS5** nearly similar to their solution. The longer wavelength absorption confirmed charge transfer originated from DTP donor to cyanoacrylic acid as involved the HOMO to LUMO transitions.

Table 2.2 Computed vertical transition energies and their oscillator strengths and configurations for the dyes **JS1-JS5**.

Dye	λ_{max}^{abs} (nm)	*f*	Configuration	HOMO (eV)	LUMO (eV)	Band gap (eV)
JS1	410	1.22	HOMO→LUMO (98%) HOMO-5→LUMO (2%)	-6.53	-2.26	4.26
JS2	478 281	1.29 0.99	HOMO→LUMO (96%) HOMO-1→LUMO+1 66%), HOMO-1→LUMO+2 (25%)	-6.19	-2.44	3.68
JS3	534 287	1.69 0.48	HOMO→LUMO (93%) HOMO-3→LUMO (29%), HOMO-1→LUMO+1(35%), HOMO-1→LUMO+2 (26%)	-5.89	-2.52	3.37
JS4	499 284	1.96 0.53	HOMO→LUMO (93%) HOMO→LUMO+2(42%) HOMO-4→LUMO (12%)	-5.93	-2.36	3.57
JS5	548	2.78	HOMO→LUMO (83%)	-5.63	-2.40	3.23

2.2.5 Photovoltaic properties

Finally, the photovoltaic parameters were investigated from photoelectrochemical cells fabricated with synthesized dyes as sensitizers and the performance parameters summarized in Table 2.3. The incident photon-to-current conversion efficiencies (IPCE) as function of different irradiation wavelengths for photoelectrochemical cells are displayed in Figure 2.14. The IPCE spectra for the dyes **JS2-JS5** extend upto 700 nm, while for **JS1** it remains within 580 nm which is in accordance with absorption spectra recorded for their respective photoanodes. Although, light harvesting efficiency of the dyes highly influence the IPCE value, but surprisingly the poorest IPCE shown by **JS5** may be due to the lack of effective ICT as inferred by solvent insensitive absorption and narrow emission spectrum (*vide supra*). However, the dye **JS4** displays highest IPCE value 75% in the series is reminiscent of its higher molar extinction coefficient.

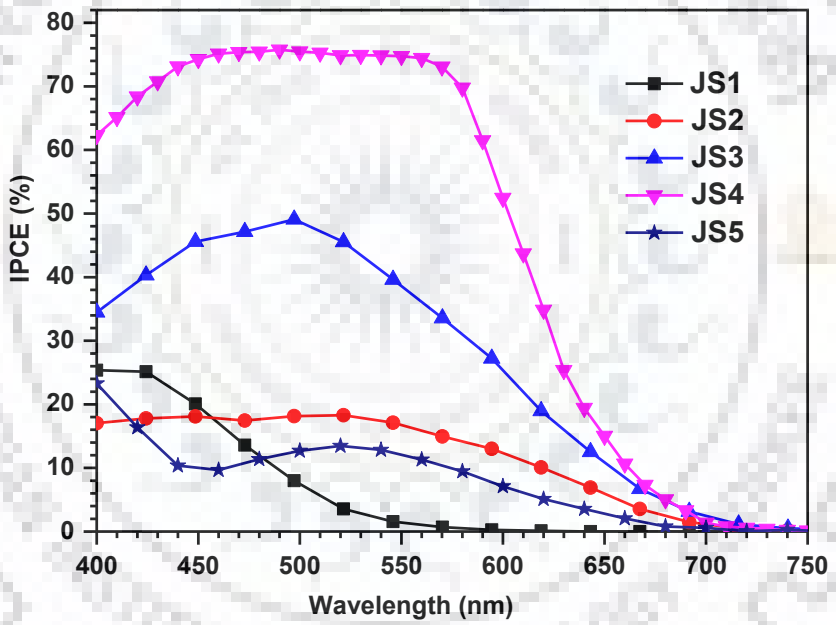

Figure 2.14 IPCE spectra of the DSSCs fabricated with synthesized dyes **JS1-JS5**.

The current-voltage measurements under the one sun condition are presented by Figure 2.15.The photocurrent density of the dyes follow the order **JS4** > **JS3** > **JS5** > **JS2** > **JS1**. It will be worthy to mention that approximately two-fold growth in J_{SC} value is observed on every step of extension of conjugation by thienyl or fused-thienyl linkers which support their impact on photocurrent of DSSCs. The high J_{SC} value for **JS4** is owing to its broad and intense absorption and low value for **JS1** is attributable to its inferior molar extinction coefficients. However, the molar extinction coefficient and electron injection cannot elucidate the poor J_{SC} for **JS5** as both are high in this dye. The

poor J_{SC} for **JS5** can be describes on the basis of low charge collection efficiency and reduced electron lifetime for increasing number of thiophene units (*vide infra*). The open circuit voltage of the dyes assume the trend **JS4** > **JS3** > **JS2** > **JS1** > **JS5**. In the series, the dye **JS4** possessed the highest open circuit voltage 710 V among the present dyes due to the presence of DTP unit containing alkylated fluorene. This is one of highest V_{OC} values obtained so far for DTP-dyes in iodine electrolyte based DSSCs [166,136]. The insulated fluorene moiety with butyl chains is found to be beneficial for retarding the charge recombination process of injected electrons with oxidized dye/electrolyte. Also, the effective electron injection may have increased the electron density in the TiO_2 conduction band and upwardly shifted the fermi energy for the dye **JS4**. In contrast, the dye **JS5** showed inferior open circuit voltage due to poor regeneration of the oxidized dye by electrolyte after the injection of photo-excited electron into photocathode. This may be due to the reduction in thermodynamic feasibility of electron downhill process from electrolyte to high lying HOMO of the dye **JS5**. The efficiency for the dyes follow the order **JS4** > **JS3** > **JS2** > **JS5** > **JS1** which is almost similar to the order of V_{OC} values. The highest efficiency of 5.94% is reminiscent to its high J_{SC} and V_{OC} values. It will be worthy to compare the efficiency of **JS4** with previously reported related DTP-dyes **DP24-DP27** [127]. In comparison to later dyes, the present dye **JS4** showed superior photovoltaic performances. It is witnessed that presence of suitable number of bulky and electronic rich *N*-substituted DTP unit in conjugating bridge for DTP donor-based dyes is beneficial to increase the efficiency.

Table 2.3 Performance parameters of the DSSCs fabricated with the dyes **JS1-JS5.**

Dye	η (%)	V_{OC} (mV)	J_{SC} (mA cm^{-2})	*FF*	R_{ct2} (ohm)	τ_e (ms)	R_{rec} (ohm)
JS1	0.46	497	2.46	0.37	60.73	1.71	21.84
JS2	1.53	560	4.72	0.58	41.50	2.54	28.76
JS3	3.47	604	8.88	0.65	24.15	3.34	38.96
JS4	5.94	710	13.34	0.63	21.39	1.71	52.91
JS5	0.98	392	6.98	0.36	75.41	0.44	47.37

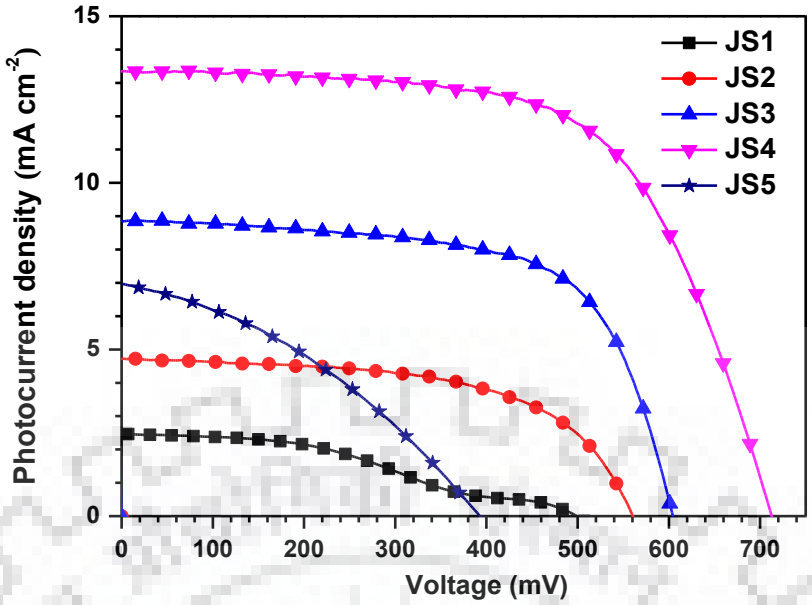

Figure 2.15 I-V characteristics of the DSSCs fabricated with the dyes **JS1-JS5**.

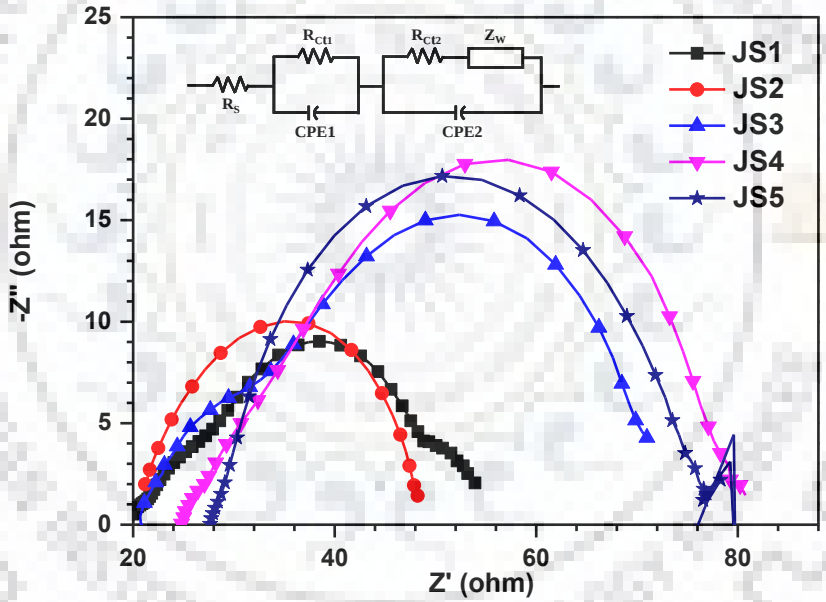

Figure 2.16 Nyquist plots observed for the DSSCs fabricated with the dyes **JS1-JS5** under dark condition.

2.2.6 Electrochemical impedance spectroscopy

To further elucidate the fate of photogenerated electrons at the interfaces of photoelectrochemical cells, the electrochemical impedance spectroscopy (EIS) measurements under dark and one sun illumination conditions were carried out. The Nyquist plots obtained in dark and illumination conditions are displayed in Figure 2.16 and 2.17, respectively. The electron recombination resistances (R_{rec}) at the interfaces of TiO_2/dye/electrolyte correspond to the second semicircle in Figure 2.16.The order of R_{rec}

is **JS4** > **JS5** > **JS3** > **JS2** > **JS1.** The largest R_{rec} value obtained for the dye **JS5** and **JS4** suggests that the presence *n*-butylated fluorene unit on DTP are useful to suppress the recombination of electrons with the oxidized half of electrolyte (*vide supra*). On the other hand, low charge recombination exhibited by the **JS1** can be attributed to the smaller size of the dye molecule which leads to low surface coverage for the approach of oxidized electrolyte.

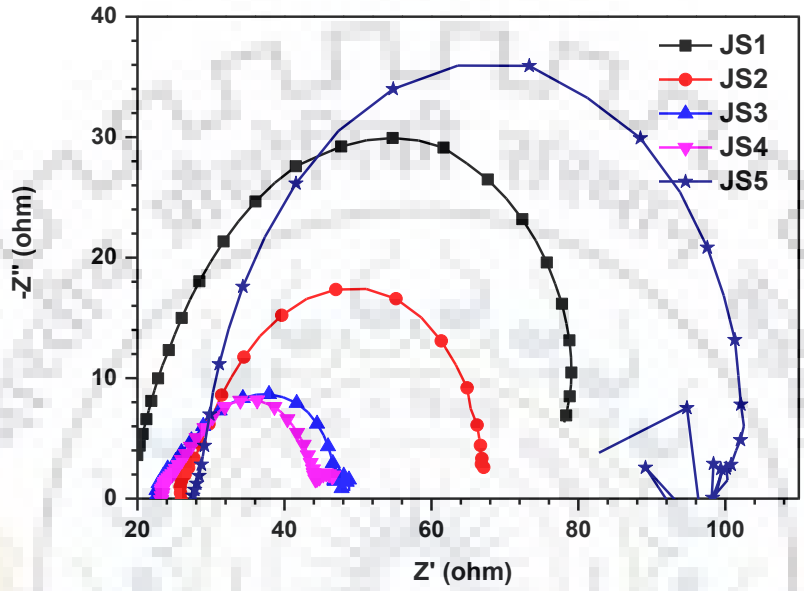

Figure 2.17 Nyquist plots observed for the DSSCs fabricated with the dyes **JS1-JS5** under illumination.

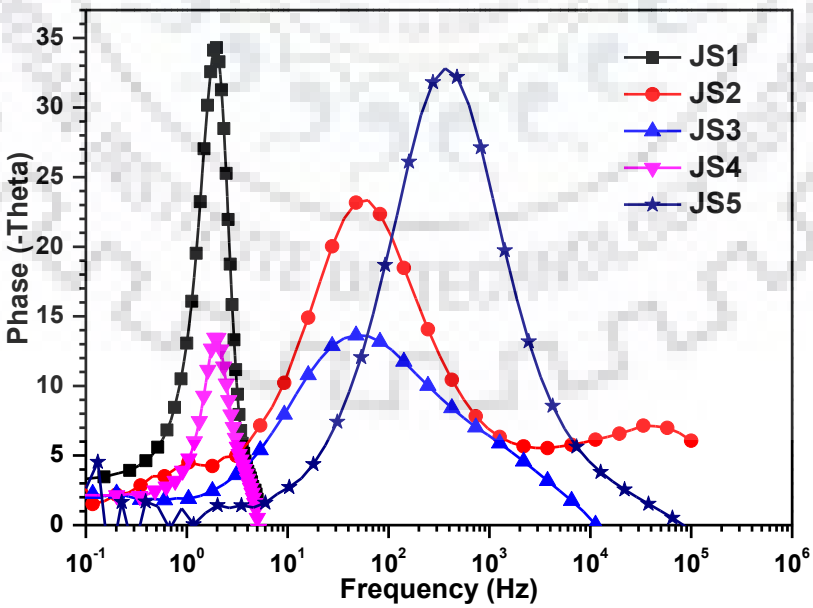

Figure 2.18 Bode phase plots for the DSSCs fabricated with the dyes **JS1-JS5** under illumination.

The large semicircles of the Nyquist plots under the one sun illumination conditions (Figure 2.17) give the charge-transport resistances *(R_{ct2})* for the DSSCs. The R_{ct2} of the dyes followed the order **JS5** > **JS1** > **JS2** > **JS3** > **JS4**. The dye **JS5** possessed larger R_{ct2} value which suggests low charge collection in the respective devices. In comparison to other dyes, the large number of thienyl unit in **JS5** may boost interaction with I^- species of electrolyte [66]. Similarly, large R_{ct2} value for **JS1** originated from the unfavorable thermodynamic condition for electron injection due to the relatively low-lying LUMO energy level [167,168]. The comparatively smaller R_{ct2} values for the dyes **JS3** and **JS4** suggest efficient charge collection in the respective devices. From the mid-frequency peaks of the Bode phase plot (Figure 2.18) the electron life time (τ_e) in the device can be measured by the equation $\tau_e = 1/\omega_{min}$ in which ω_{min} is the angular frequency of low frequency peak [169,170]. The dye bithiophene linker based dye **JS3** showed highest τ_e value reminiscent of more effective suppression of the back electron transfer in the series as compared to the DTP-linked dyes **JS4** and **JS5** which show the low electron life time for the devices.

2.3 Conclusions

In summary, we demonstrated the use of dithienopyrrole as a donor in organic dyes featuring thienyl/DTPs as π-linkers and cyanoacrylic acid acceptor. In comparison to thienyl, DTP-linkers showed remarkably improved light harvesting efficiency and reduced oxidation potentials for the dyes. The sufficient separation between HOMO and LUMO energy level further confirmed facile charge transfer probabilities for the dyes **JS4** and **JS5**. The presence of bulky and electronic rich DTP units in conjugating bridge for DTP donor-based dyes is found to be beneficial to retard the charge recombination processes. Therefore the dye **JS4** showed the highest efficiency 5.94% in the series attributable to its high J_{SC} and V_{OC} values. The V_{OC} value obtained for **JS4** is one of highest among DTP-dyes in iodine electrolyte based DSSCs. Irrespective of intense absorption, low efficiency was observed for the **JS5** owing to its low charge collection efficiency and reduced electron lifetime due to the increase in number of thienyl units as revealed by EIS measurements.

2.4 Experimental

2.4.1 General methods

All the chemicals and reagents were received from commercial sources and used without further purification. Organic solvents were purified by following the standard distillation techniques prior to use. Column chromatography purification of the synthesized compounds was carried out by using silica gel (100-200 mesh) or neutral alumina as stationary phase in a column of 40 cm length and 3.0 cm diameter. NEXUS FT-IR spectrometer (Thermonicolet) was used to collect IR spectra for the compounds as KBr pellets. The ^{1}H and ^{13}C NMR spectra were recorded on JEOL ECX 400 MHz spectrometer and deuterated chloroform ($CDCl_3$) and dimethyl sulfoxide (DMSO-d_6) were used as solvents. The mass spectra were obtained in a positive ion mode on a Bruker micrOTOF-QII ESI mass spectrometer. UV-visible absorption spectra were obtained by using a Cary 100 spectrophotometer using spectroscopic grade solvents at room temperature in quartz cuvettes. Emission spectra were obtained by using Shimadzu RF5301 spectrofluorimeter. Cyclic voltammetry (CV) and differential pulse voltammetry (DPV) studies were conducted by using BASi Epsilon electrochemical analyzer with a conventional three-electrode configuration consisting of a glassy carbon working electrode, a platinum wire auxiliary electrode, and a non-aqueous $Ag/AgNO_3$ reference electrode. The experiments were performed in dichloromethane at room temperature under nitrogen atmosphere with Bu_4NClO_4 (0.1 M) as supporting electrolyte and the potentials are quoted against the ferrocene which was used as an internal standard.

2.4.2 Synthesis

*Synthesis of 4-(9,9-dibutyl-9H-fluoren-2-yl)-4H-dithieno[3,2-b:2',3'-d]pyrrole (**1**)*

A mixture of 9,9-dibutyl-*9H*-fluoren-2-amine (5.0 g, 15.4 mmol), 3,3'-dibromo-2,2'-bithiophene (4.98 g, 17.0 mmol) and sodium *tert*-butoxide (11.86 g, 123.4 mmol) in 30 mL of toluene was maintained under nitrogen atmosphere. To this mixture, bis(dibenzylideneacetone)palladium(0); $Pd(dba)_2$ (0.44 g, 0.8 mmol) and 1,1'-bis(diphenylphosphino)ferrocene; dppf (1.28 g, 2.3 mmol) were added and refluxed at 110 °C for 12 h. On completion of the reaction, volatiles were removed under vacuum from the reaction mixture. The resulting residue was extracted with chloroform, washed with water and finally with brine solution. The organic layer was dried over anhydrous Na_2SO_4 and evaporated by rotary evaporation. The crude product obtained was further

purified by column chromatography on neutral alumina using hexane as eluent: white solid; yield (3.64 g, 50%); mp 125-127 °C; ^{1}H NMR (500 MHz, $CDCl_3$) δ 0.65-0.73 (m, 10 H), 1.08-1.15 (m, 4 H), 1.99-2.03 (m, 4 H), 7.19-7.22 (m, 4 H), 7.32-7.39 (m, 3 H), 7.55-7.57 (m, 2 H), 7.73-7.74 (m, 1 H), 7.83 (d, *J* = 8.0 Hz, 1 H); ^{13}C NMR (123.55 MHz, $CDCl_3$) δ 152.6, 150.7, 144.1, 140.3, 139.2, 138.8, 127.2, 127.0, 123.5, 123.0, 121.3, 120.7, 119.7, 117.3, 116.8, 112.3, 55.3 40.2, 26.1, 23.1, 13.9. HRMS calcd for $C_{29}H_{29}NS_2$ $[M+H]^+$ m/z 456.1814, found 456.1813.

Synthesis of 4-(9,9-dibutyl-9H-fluoren-2-yl)-4H-dithieno[3,2-b:2',3'-d]pyrrole-2-carbaldehyde ***(2)***

Phosphoryl oxychloride (0.45 mL, 4.83 mmol) was added drop wise to a stirring mixture of **1** (2.0 g, 4.39 mmol) and DMF (8 mL) maintained at 0 °C. After complete addition, the stirring was continued for further 2 h at room temperature. Then the reaction was quenched by addition of ice-water and neutralized with sodium hydroxide solution. The organic product was extracted with chloroform, washed with brine solution and dried over anhydrous Na_2SO_4. The combined organic extracts were concentrated to obtain a residue. It was purified by column chromatography on alumina using hexane:chloroform (3:2) mixture as eluent; light yellow solid; yield (1.90 g, 90%); mp 182-183 °C; IR (KBr, cm^{-1}) 1654 ($\nu_{C=O}$); ^{1}H NMR (500 MHz, $CDCl_3$) δ 0.67-0.75 (m, 10 H), 1.09-1.17 (m, 4 H), 2.01-2.05 (m, 4 H), 7.18 (d, *J* = 5.0 Hz, 1 H), 7.35-7.41 (m, 3 H), 7.45 (d, *J* = 5.5 Hz, 1 H), 7.53-7.56 (m, 2 H), 7.75-7.77 (m, 1 H), 7.81 (s, 1 H), 7.86 (d, *J* = 8.0 Hz, 1 H), 9.88 (s, 1 H); ^{13}C NMR (123.55 MHz, $CDCl_3$) δ 183.0, 152.9 150.8 148.1, 143.6, 140.7, 140.1, 140.0, 137.6, 128.9, 127.6, 127.5, 123.0, 121.7, 121.0, 119.9, 117.6, 112.1, 55.4, 40.1, 26.1, 23.1, 14.0. HRMS calcd for $C_{30}H_{29}NOS_2$ $[M]^+$ m/z: 484.1763 found 484.1750.

Synthesis of 5-(4-(9,9-dibutyl-9H-fluoren-2-yl)-4H-dithieno[3,2-b:2',3'-d]pyrrol-2-yl)thiophene-2-carbaldehyde ***(4)***.

A mixture **3** (1.30 mmol), 5-bromothiophene-2-carbaldehyde (0.128 g, 0.67 mmol), $Pd(PPh_3)_2Cl_2$ (0.004 g, 0.05 mmol), and dry DMF (3 mL) was heated at 85 °C under a nitrogen atmosphere for 24 h. On the completion of reaction, the reaction mixture was poured into water and organic compound was extracted with chloroform. The organic layer was washed with brine solution followed by water and dried over anhydrous Na_2SO_4. The combined organic extracts were concentrated and further purified by alumina column chromatography using a hexanes:chloroform (1:1) as eluent. Yellow

solid; yield (0.235 g, 80%); mp 135-138 °C; IR (KBr, cm^{-1}) 1649 ($\nu_{C=O}$); ^1H NMR (399.78 MHz, $CDCl_3$) δ 0.67-0.76 (m, 10 H), 1.12-1.17 (m, 4 H), 2.03 (dd, *J* = 8.0, 5.6 Hz, 4 H), 7.16 (d, *J* = 5.2 Hz, 1 H), 7.27 (s, 1 H), 7.30 (d, *J* = 5.2 Hz, 1 H), 7.35-7.41 (m, 3 H), 7.45 (s, 1 H), 7.54-7.56 (m, 2 H), 7.67 (d, *J* = 4.0 Hz, 1 H), 7.74-7.77 (m, 1 H), 7.86 (d, *J* = 8.0 Hz, 1 H), 9.84 (s, 1 H); ^{13}C NMR (100.53 MHz, $CDCl_3$) δ 182.3, 152.9, 150.8, 148.7, 144.1, 141.1, 140.2, 139.9, 138.1, 137.6, 133.4, 127.5, 127.2, 125.7, 123.1, 121.7, 121.0, 119.9, 117.6, 116.8, 112.3, 111.0, 55.4, 40.2, 29.8, 26.2, 23.2, 14.0. HRMS calcd for $C_{34}H_{31}NOS_3$ $[M+H]^+$ m/z 566.1641 found 566.1641.

Synthesis of 5'-(4-(9,9-dibutyl-9H-fluoren-2-yl)-4H-dithieno[3,2-b:2',3'-d]pyrrol-2-yl)-[2,2'-bithiophene]-5-carbaldehyde ***(5)***.

It was obtained from **3** (1.3 mmol) and 5'-bromo-[2,2'-bithiophene]-5-carbaldehyde (0.189 g, 0.68 mmol) by following a procedure same as described above for the synthesis of **2**. Red solid; yield (0.250 g, 71%); mp 153-155 °C; IR (KBr, cm^{-1}) 1658 ($\nu_{C=O}$); ^1H NMR (399.78 MHz, $CDCl_3$) δ 0.69-0.78 (m, 10 H), 1.12-1.19 (m, 4 H), 2.03-2.07 (m, 4 H), 7.15-7.17 (m, 1 H), 7.18 (s, 1 H), 7.21 (d, *J* = 3.6 Hz, 1 H), 7.27 (d, *J* = 3.6 Hz, 1 H), 7.29 (d, *J* = 3.6 Hz, 1 H), 7.31 (s, 1 H), 7.36-7.42 (m, 3 H), 7.56-7.58 (m, 2 H), 7.67 (d, *J* = 3.6 Hz, 1 H), 7.75-7.77 (m, 1 H), 7.87 (d, *J* = 8.8 Hz, 1 H), 9.86 (m, 1 H); ^{13}C NMR (100.53 MHz, $CDCl_3$) δ 181.8, 152.1, 150.2, 143.9, 143.3, 140.8, 139.6, 137.7, 136.9, 133.4, 126.8, 126.5, 124.1, 123.24, 123.23, 122.4, 121.0, 120.2,119.2, 116.9, 111.6, 108.8, 54.7, 39.6, 29.1, 25.5, 22.5, 13.4. HRMS calcd for $C_{38}H_{33}NOS_4$ $[M+Na]^+$ m/z 645.1699 found 645.1703.

Synthesis of 6-bromo-4-(9,9-dibutyl-9H-fluoren-2-yl)-4H-dithieno[3,2-b:2',3'-d]pyrrole-2-carbaldehyde ***(6)***

N-Bromosuccinimide (NBS) (0.861, 4.84 mmol) was added batch-wise to a stirring mixture of **2** (1.8 g, 3.72 mmol) and dichloromethane (20 mL) maintained at 0 °C. After complete addition, the stirring was continued for further 8 h at room temperature. On completion of reaction, it was poured into water. The product was extracted with dichloromethane, washed with water followed by brine solution and dried over anhydrous sodium sulfate. The combined organic extracts were concentrated to obtain a residue. It was purified by column chromatography on alumina using a hexane:dichloromethane (1:1) mixture as eluent: Yellow solid; yield (1.78 g, 85%); mp 195-196 °C; IR (KBr, cm^{-1}) 1658 ($\nu_{C=O}$); ^1H NMR (500 MHz, $CDCl_3$) δ 0.68-0.75 (m, 10 H), 1.11-1.16 (m, 4 H),

2.02 (t, *J* = 8.5 Hz, 4 H), 7.22 (s, 1 H), 7.34-7.40 (m, 3 H), 7.46-7.51 (m, 2 H), 7.75-7.77 (m, 2 H), 7.86 (d, *J* = 8.0 Hz, 1 H), 9.87 (s, 1 H); ^{13}C NMR (123.55 MHz, $CDCl_3$) δ 183.0, 153.0, 150.9, 145.7, 142.6, 141.0, 140.5, 139.8, 137.1, 127.7, 127.2, 124.3, 121.8, 121.1, 120.8, 120.0, 117.7, 116.6, 116.0, 155.6, 55.4, 40.1, 26.2, 23.1, 14.0. HRMS calcd for $C_{30}H_{28}BrNOS_2$ $[M+H]^+$ m/z: 562.0868, found: 568.0870.

Synthesis of 4,4'-bis(9,9-dibutyl-9H-fluoren-2-yl)-4H,4'H-[2,2'-bidithieno[3,2-b:2',3'-d]pyrrole]-6-carbaldehyde ***(7)***.

It was obtained **6** (0.150 g, 0.27 mmol) and **3** (1.3 mmol) by following a procedure same as described above for the synthesis of **4**. Orange microcrystalline solid; yield (0.176 g, 70%); mp 183-185 °C; IR (KBr, cm^{-1}) 1643 ($\nu_{C=O}$); ^{1}H NMR (399.78 MHz, $CDCl_3$) δ 0.637-0.77 (m, 20 H), 1.10-1.20 (m, 8 H), 2.02-2.07 (m, 8 H), 7.16 (d, *J* = 5.2 Hz, 1 H), 7.25 (s, 1 H), 7.27 (s, 1 H), 7.37-7.42 (m, 7 H), 7.55-7.58 (m, 4 H), 7.73-7.78 (m, 3 H), 7.85-7.90 (m, 2 H), 9.86 (s, 1 H); ^{13}C NMR (100.53 MHz, $CDCl_3$) δ 182.9, 153.1, 152.8, 150.9, 150.8, 148.2, 144.6, 144.0, 143.4, 141.9, 140.6, 140.21, 140.15, 140.1, 139.7, 138.3, 137.4, 135.3, 127.7, 127.5, 127.2, 127.1, 125.0, 124.8, 124.7, 123.3, 123.10,121.06, 121.9, 121.4, 121.1, 120.9, 120.6, 119.9, 119.63, 119.57, 117.8, 117.5, 116.9, 116.6, 115.0, 112.3, 109.3, 109.22, 109.18, 107.3, 55.5, 55.4, 40.3, 40.2, 26.2, 23.2, 14.1. HRMS calcd for $C_{59}H_{56}N_2OS_4$ $[M+H]^+$ m/z 937.3349 found 937.3334.

Synthesis of 6'-bromo-4,4'-bis(9,9-dibutyl-9H-fluoren-2-yl)-4H,4'H-[2,2'-bidithieno[3,2-b:2',3'-d]pyrrole]-6-carbaldehyde ***(8).***

It was obtained from **7** (0.150 g, 0.160 mmol) and NBS (0.340 g, 0.192 mmol) by following a procedure same as described above for the synthesis of **6.** Yellow microcrystalline solid; yield (0.145g, 95%). mp 186-188 °C; IR (KBr, cm^{-1}) 1644 ($\nu_{C=O}$). ^{1}H NMR (400 MHz, $CDCl_3$): δ 0.61-0.76 (m, 20 H), 1.07 (d, *J* = 6.8 Hz, 8 H), 2.00 (s, 8 H), 6.92 (s, 1 H), 7.37-7.39 (m, 7 H), 7.45-7.47 (m, 2 H), 7.50-7.52 (m, 2 H), 7.57 (s, 1 H), 7.75-7.79 (m, 3 H), 7.82 (d, *J* = 8.4 Hz, 1 H), 7.84-7.86 (m, 1 H), 9.85 (s, 1 H); ^{13}C NMR (123.55 MHz, $CDCl_3$) δ 183.3, 151.9, 151.0, 146.3, 141.5, 140.1, 135.4, 134.9, 127.9, 127.2, 127.1, 125.9, 123.1, 122.9, 122.7, 120.2, 120.1, 120.0, 115.4, 115.3, 55.5, 55.4, 40.2, 40.1, 31.1, 26.1, 23.1. HRMS calcd for $C_{59}H_{55}BrN_2OS_4$ $[M]^+$ m/z: 1014.2375 found 1014.2368.

Synthesis of 4,4',4''-tris(9,9-dibutyl-9H-fluoren-2-yl)-4H,4'H,4''H-[2,2':6',2''-terdithieno[3,2-b:2',3'-d]pyrrole]-6-carbaldehyde ***(9).***

It was obtained from **8** (0.140 g, 0.14 mmol) and **3** (1.3 mmol) by following a procedure same as described above for the synthesis of **2**. Red solid; yield (0.145 g, 75%); mp 153-155 °C; IR (KBr, cm^{-1}) 1642 ($\nu_{C=O}$); ^{1}H NMR (399.78 MHz, $CDCl_3$) δ 0.70-0.75 (m, 30 H), 1.11-1.20 (m, 12 H), 2.01-2.08 (m, 12 H), 7.13 (s, 2 H), 7.20 (s, 2 H), 7.37-7.46 (m, 11 H), 7.50 (d, *J* = 7.4 Hz, 2 H), 7.55 (d, *J* = 4.4 Hz, 3 H), 7.65 (s, 2 H), 7.69-7.75 (m, 3 H), 7.78 (d, *J* = 8.0 Hz, 1 H), 7.83 (d, *J* = 8.0 Hz, 2 H), 9.74 (s, 1 H); ^{13}C NMR (100.53 MHz, $CDCl_3$) δ 182.2, 152.7, 139.9, 139.7, 139.5, 127.2, 126.8, 126.7, 126.5, 122.7, 121.4, 120.7, 119.6, 117.5, 55.1, 39.84. 39.77, 25.8, 25.4, 22.8, 22.7, 13.1, 13.6. HRMS calcd for $C_{88}H_{83}N_3OS_6$ $[M+Na]^+$ m/z 1412.4753 found 1412.4744.

Synthesis of (E)-2-cyano-3-(4-(9,9-dibutyl-9H-fluoren-2-yl)-4H-dithieno[3,2-b:2',3'-d]pyrrol-2-yl)acrylic acid ***(JS1).***

A mixture of **2** (0.15 g, 0.31 mmol), cyanoacetic acid (0.034 g, 0.40 mmol), acetic acid (5 mL) and ammonium acetate (10 mg) was heated at 125 °C for 12 h. The resulting solution was poured into ice-cold water to get precipitates. These precipitates were filtered and washed thoroughly with water and dried. The solid was further crystallized from hot chloroform to get pure compound. Brown solid; yield (0.128 g, 75%); mp 233-235 °C; IR (KBr, cm^{-1}) 2214 ($\nu_{C\equiv N}$); ^{1}H NMR (500 MHz, $CDCl_3$) δ 0.68-0.75 (m, 10 H), 1.13 (sex, *J* = 5.5, 4 H), 2.00-2.04 (m, 4 H), 7.16 (d, *J* = 5.5 Hz, 1 H), 7.36-7.40 (m, 3 H), 7.51-7.54 (m, 3 H), 7.75-7.76 (m, 1 H), 7.87 (d, *J* = 8.0 Hz, 1 H), 7.92 (s, 1 H), 8.35 (s, 1 H); ^{13}C NMR (100.53 MHz, DMSO-d_6) δ 172.3, 164.2, 152.4, 150.4, 147.9,142.9, 139.8, 139.3, 137.2, 133.2, 131.4, 127.1, 125.4, 122.9, 121.4, 120.1, 117.3, 116.7, 112.2, 95.2, 55.1, 25.1, 22.5, 21.5, 13.9. HRMS calcd for $C_{33}H_{30}N_2O_2S_2$ $[M+Na]^+$ m/z 573.1640 found 573.1674.

Synthesis of (E)-2-cyano-3-(5-(4-(9,9-dibutyl-9H-fluoren-2-yl)-4H-dithieno[3,2-b:2',3'-d]pyrrol-2-yl)thiophen-2-yl)acrylic acid ***(JS2).***

It was obtained from **4** (0.140 g, 0.24 mmol) by following a procedure same as described above for the synthesis of **JS1.** Brown solid; yield (0.106 g, 80%); mp 176-178 °C; IR (KBr, cm^{-1}) 2215 ($\nu_{C\equiv N}$); ^{1}H NMR (399.78 MHz, DMSO-d_6) δ 0.50-0.60 (m, 4 H), 0.66-0.69 (m, 6 H), 1.04-1.12 (m, 4 H), 1.96-2.05 (m, 2 H), 2.12-2.17 (m, 2 H), 7.25 (d, *J* = 5.6 Hz, 1 H), 7.34-7.39 (m, 2 H), 7.47-7.50 (m, 1 H), 7.53-7.57 (m, 2 H), 7.59 (d, *J* = 8.0 Hz, 1 H), 7.64 (dd, *J* = 2.4, 8.0 Hz, 1 H), 7.79, (d, *J* = 1.6 Hz, 1 H), 7.86-7.88 (m, 1 H), 7.94 (d, *J* = 4.0 Hz, 1 H), 8.01 (d, *J* = 8.4 Hz, 1 H), 8.43 (s, 1 H); ^{13}C NMR (100.53

MHz, DMSO-d_6) δ 164.1, 152.8, 151.1, 150.9, 146.6, 145.6, 144.6, 143.8, 143.7, 140.1, 134.4, 133.5, 128.8, 127.9, 127.6, 127.1, 125.3, 125.2, 124.8, 123.4, 122.0, 121.9, 120.5, 117.7, 117.4, 117.2, 116.9, 116.6, 112.8, 110.5, 55.5, 55.4, 26.4, 23.0, 14.3. HRMS calcd for $C_{37}H_{32}N_2O_2S_3$ $[M]^+$ m/z 632.1620 found 632.1619.

Synthesis of (E)-2-cyano-3-(5'-(4-(9,9-dibutyl-9H-fluoren-2-yl)-4H-dithieno[3,2-b:2',3'-d]pyrrol-2-yl)-[2,2'-bithiophen]-5-yl)acrylic acid ***(JS3).***

It was prepared from **5** (0.140 g, 0.22 mmol) by following a procedure similar to that described above for **JS1**. Brown solid; yield (0.100 g, 64%); mp 177-179 °C; IR (KBr, cm^{-1}) 2214 ($\nu_{C\equiv N}$); ^{1}H NMR (399.78 MHz, DMSO-d_6) δ 0.50-0.59 (m, 4 H), 0.63-0.68 (m, 6 H), 1.01-1.09 (m, 4 H), 1.99-2.05 (m, 2 H), 2.10-2.16 (m, 2 H), 7.23 (d, *J* = 5.2 Hz, 1 H), 7.35-7.37 (m, 3 H), 7.46-7.48 (m, 1 H), 7.57 (d, *J* = 4.0 Hz, 1 H), 7.63-7.69 (m, 4 H), 7.80 (d, *J* = 1.6 Hz, 1 H), 7.86-7.88 (m, 1 H), 7.94 (m, 1 H), 8.01 (d, *J* = 8.0 Hz, 1 H), 8.43 (s, 1 H); ^{13}C NMR (100.53 MHz, DMSO-d_6) δ 164.2, 152.8, 150.9, 147.8, 145.4, 143.9, 142.1, 140.3, 139.6, 138.0, 133.9, 133.1, 128.3, 128.0, 127.6, 124.8, 123.5, 122.1, 121.9, 120.5, 118.3, 117.8, 117.2, 117.0, 112.8, 112.2, 55.6, 26.4, 23.0, 14.4. HRMS calcd for $C_{41}H_{34}N_2O_2S_4$ $[M]^+$ m/z 714.1498 found 714.1480.

Synthesis of (E)-3-(4,4'-bis(9,9-dibutyl-9H-fluoren-2-yl)-4H,4'H-[2,2'-bidithieno[3,2-b:2',3'-d]pyrrol]-6-yl)-2-cyanoacrylic acid ***(JS4).***

It was prepared from **7** (0.150 g, 0.16 mmol) by following a procedure similar to that described above for **JS1**. Brown solid; yield (0.120 g, 75%); mp 280-282 °C; IR (KBr, cm^{-1}) 2210 ($\nu_{C\equiv N}$); ^{1}H NMR (399.78 MHz, DMSO-d_6) δ 0.49-0.61 (m, 20 H), 1.00-1.05 (m, 8 H), 1.95-2.02 (m, 4 H), 2.07-2.13 (m, 4 H), 7.16 (d, *J* = 5.2 Hz, 1 H), 7.35-7.38 (m, 5 H), 7.45-7.48 (m, 3 H), 7.50 (d, *J* = 5.2 Hz, 1 H), 7.57-7.62 (m, 2 H), 7.74 (s, 1 H), 7.80-7.84 (m, 3 H), 7.93-7.96 (m, 2 H), 8.00 (s, 1 H), 8.35 (s, 1 H). 13C NMR is not recorded due to poor solubility in solvent. HRMS calcd for $C_{62}H_{57}N_3O_2S_4$ $[M]^+$ m/z 1003.3228 found 1003.3314.

Synthesis of (E)-2-cyano-3-(4,4',4''-tris(9,9-dibutyl-9H-fluoren-2-yl)-4H,4'H,4''H-[2,2':6',2''-terdithieno[3,2-b:2',3'-d]pyrrol]-6-yl)acrylic acid ***(JS5).***

It was prepared from **9** (0.120 g, 0.09 mmol) by following a procedure similar to that described above for **JS1**. Brown solid; yield (0.090 g, 72%); mp 238-240 °C; IR (KBr, cm^{-1}) 2204 ($\nu_{C\equiv N}$); ^{1}H NMR (399.78 MHz, $CDCl_3$); 0.71-0.88 (m, 30 H), 1.14 (s, 12 H), 2.06 (s, 12 H), 7.4 (s, 15 H), 7.52-7.50 (m, 5 H), 7.73-7.84 (m, 9 H); ^{13}C NMR could not

be recorded due to poor solubility in solvent. HRMS calcd for $C_{91}H_{84}N_4O_2S_6$ $[M]^+$ m/z 1456.4913 found 1456.4940.

2.4.3 Computational methods

All the computational calculations were performed using Gaussian 09 program package. The ground-state geometries of the dyes were optimized without any symmetry constraints by employing a Becke's hybrid correlation functional B3LYP and 6-31 G(D,P) basis set for all atoms. The vertical excitation energies and oscillator strengths for the lowest 10 singlet-singlet transitions for the optimized geometry in the ground state were obtained by TD-DFT calculations using the DGDZVP basis set and BMK hybrid functional.

2.4.4 Fabrication and characterization of DSSC

The dye sensitized TiO_2 photoanodes were prepared by following the procedures present in the literature. A transparent and scattering layers of TiO_2 with different sizes were coated on a pretreated fluorine-doped SnO_2 conducting glass (FTO, 7 Ω $sq.^{-1}$, transmittance ~80%, NSG America, Inc., New Jersey, USA) by doctor blade technique. During the coating process the dried TiO_2 films firstly was heated at 450 °C in an air flow and then sintered at same temperature for 30 min. The scanning electron microscopic images were used to judge the thickness of TiO_2 layers. It was found that the TiO_2 photoanodes of the DSSCs were composed of a 12 μm thick transparent TiO_2 (20 nm) layer and a scattering layer of 4 μm thickness of TiO_2 (300 nm). After sintering at 450 °C and cooled to 80 °C, The dyes were adsorbed on the TiO_2 film by immersing it in a 3×10^{-4} M dye solution for 24 h, at room temperature. A solvent mixture containing acetonitrile (ACN), *tert*-butyl alcohol and dimethyl sulfoxide (DMSO) (volume ratio of 3.5:3.5:3) was used to prepare the dye bath. The absorption spectra of the dye coated on ~4 μm TiO_2 (20) nm were recorded by using a JASCO UV-visible spectrophotometer (V-570) equipped with an integrating sphere. After that, the TiO_2/dye photoanode was placed over a platinum-sputtered ITO coated glass (7 U Ω $sq.^{-1}$, Ritek Corporation, Hsinchu, Taiwan) and then two electrodes were sandwiched with a 25 mm-thick Surlyn® (SX1170-25, Solaronix S.A., Aubonne, Switzerland) at the edges and sealed by heating. A mixture of 1.2 M 1-propyl-2,3-dimethylimidazolium iodide (DMPII), 0.035 M I_2, 0.5 M *tert*-butylpyridine (TBP) and 0.1 M guanidine thiocyanate dissolved in acetonitrile/3-methoxypropionitrile mixture (8:2) were used as electrolyte. The electrolyte was injected

in the gap between the two electrodes through hole which was already made on the counter electrode by drilling machine. After injection of electrolyte the hole was sealed with hot melt-glue to obtain the working DSSC.

The active surface area of the DSSC was restricted to 0.16 cm^2 by using a mask. The DSSC was illuminated by a class-A solar simulator (XES-301S, AM 1.5 G, San-Ei Electric Co., Ltd.). A standard silicon cell (PECSI01, Peccell Technologies, Inc.) was used to calibrate the incident light intensity of simulator and maintained at 100 mW cm^{-2}. A potentiostat/galvanostat (PGSTAT30, Autolab, Eco-Chemie, Netherlands) was used to characterize the Photocurrent-voltage curves of the DSSC. A potentiostat/galvanostat equipped with an FRA2 module was employed to analyze electrochemical impedance spectral (EIS) analysis of the DSSCs. The applied bias voltage was set at the open-circuit voltage between the working photoanode and Pt-counter electrode of the DSSC under a constant light illumination 100 mW cm^{-2}. Incident photocurrent conversion efficiency (IPCE) spectrum was obtained using a monochromated light (Oriel Instrument,model 74100) at short-circuit condition. The IPCE (λ) is defined by IPCE (λ) = 1240 (J_{SC}/λφ), where λ is the wavelength, J_{SC} is short-circuit photocurrent density (mA cm^{-2}) recorded with a potentiostat/galvanostat, and φ is the incident radiative flux (Wm^{-2}) measured with an optical detector (Oriel Instrument, model 71580) and a power meter (Oriel Instrument, model 70310).

Chapter 3

Tuning the dithienopyrrole-based organic dyes for dye-sensitized solar cells by different auxiliary donors

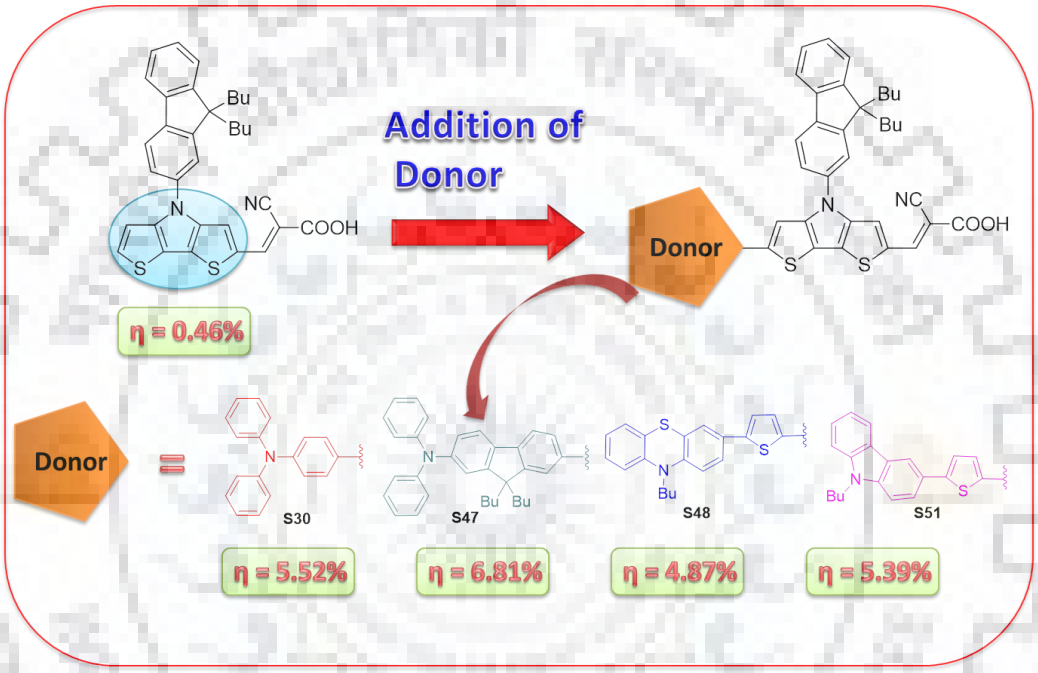

3.1 Introduction

Among the various methods involved in molecular engineering of organic dyes to improve the light harvesting efficiency, increase in electronic richness of donor moiety [142] and insertion of bulky groups or longer alkyl chains which reduces the dye aggregation [141,171] and have been found to be useful to improve the performance of the solar cells. In general, triarylamine, indoline, tetrahydroquinoline, phenothiazine, phenoxazine and carbazole are routinely being used as donors [42] and cyanoacrylic acid, rhodanine, acetic acid or pyridine as acceptor/ anchoring group [172]. Likewise, the introduction of electron-rich moieties on the donor segment help to broaden the absorption spectra and attachment of energy delocalizing chromophores cause prolongation of excited state and make the electron injection easy [143].

Chen and coworkers [173] synthesized 3D bulky organic sensitizers **TP1-TP4** featuring triphenylamine (TPA) donor with *N*-substituted phenothiazine core as π-linker (Figure 3.1). This bulky configuration of dyes showed strong UV-visible absorption and found to be beneficial for retarding the charge recombination. Thus the dye **TP3** containing as *N*-carbazole substituent yielded the best conversion efficiency of 8.00%. Bedzyk and coworkers [70] synthesized a series of the dyes **TPA-TTART-A 1-3** containing TPA donor in conjugation with tetrathienoacene (TTA) as the π-bridge (Figure 3.1). All of these dyes exhibited high absorption intensities owing to extended and rigid π-conjugated bridge. The dye **TPA-TTART-A (3)** witnessed an improved electron delocalization and self-assembly on TiO_2 surface and yielded an efficiency of 10.1%. Wang and coworkers [174] synthesized organic sensitizers **NPS-1** and **NPS-4** based TPA derivatives with *N*-annulated perylene (NP) derivatives as π-linker and different number of thiophene as conjugated linkers (Figure 3.1). The dye **NPS-4** showed broad absorption spectra and better photovoltaic performance with power conversion efficiency of 8.28%.

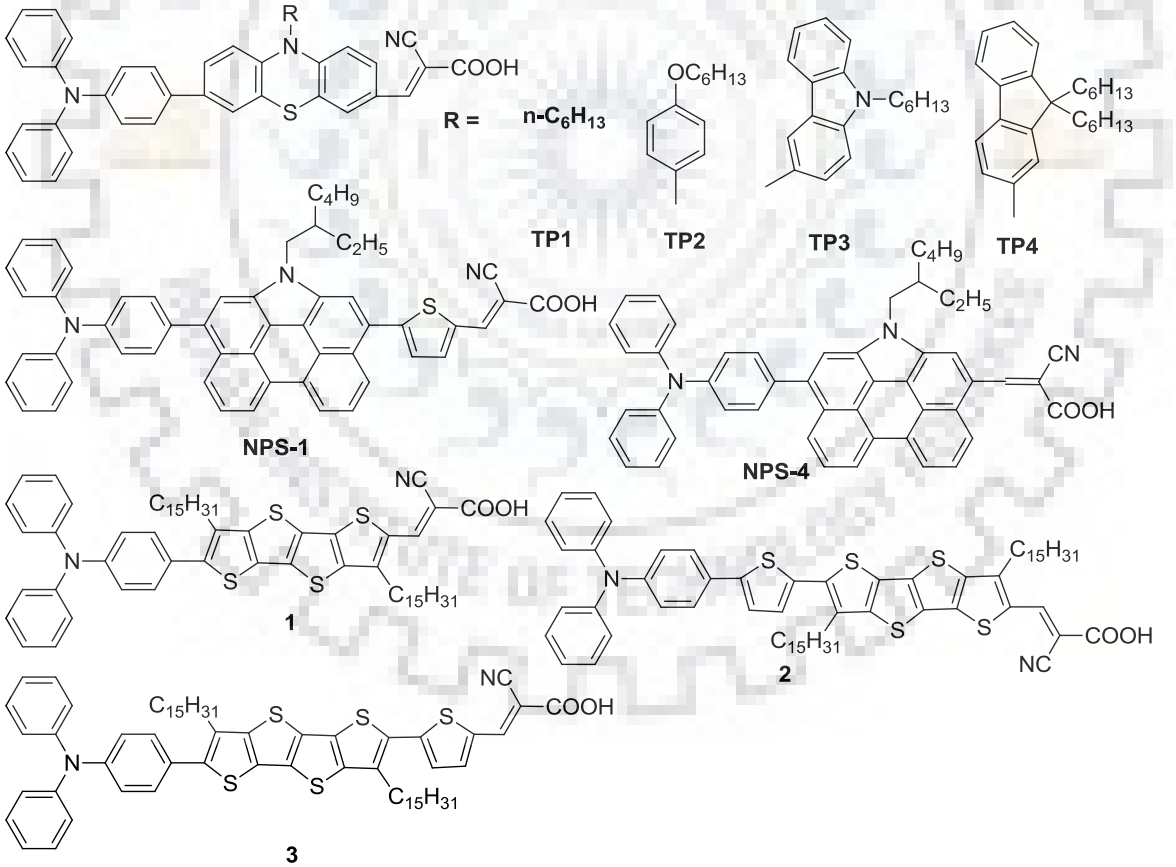

Figure 3.1 Structures of reported dyes containing triphenylamine donors and rigid linkers [173,70,174].

Thomas and coworkers [48] recently developed several organic dyes featuring fluorene appendad triarylamine donors such as diphenylaminofluorene (DPF) (**DA1** and **DA2**) and trifluorenylamine (**JA1** and **JA2**) in conjugation with bithiophene as π-linker (Figure 3.2). Here fluorene along with bithiophene served as efficient π-linker and showed stronger donor-acceptor interactions and favoured the upward shift of fermi level of TiO_2 and rendered hindrance of electron recombination process. They also synthesized organic dyes **3a-c** containing DPF donor and ethynylbenzene or ethynylthiophene as π-linker (Figure 3.2) [175]. In which ethynylthiophene linker based dye **3b** showed longer absorption wavelength while ethynylbenzene based dyes exhibited impressive photovoltaic characteristics.

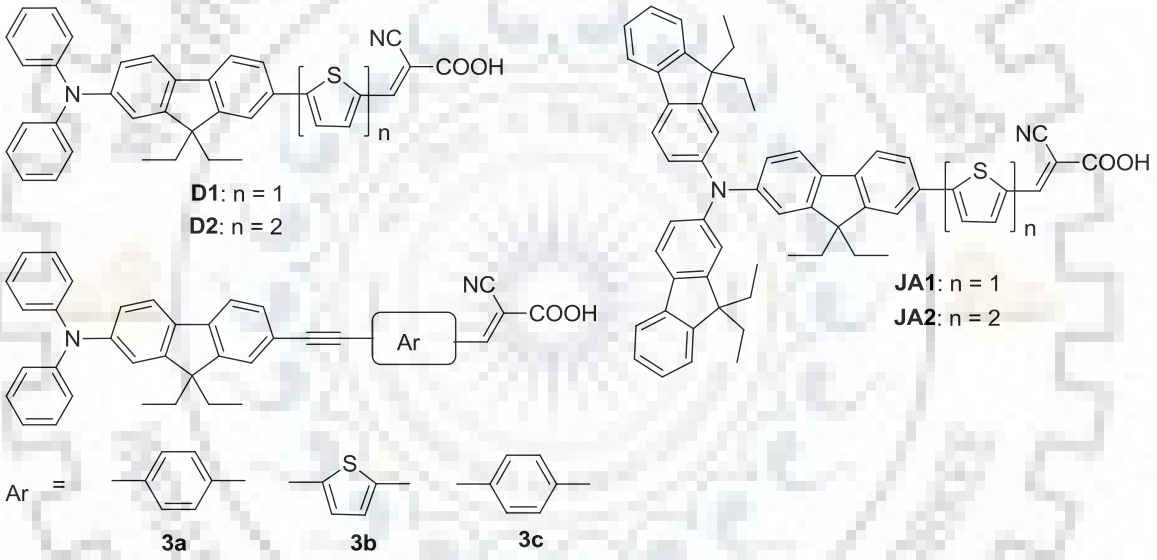

Figure 3.2 Structures of the dyes containing fluorene based triarylamine donors [48,175].

Hanaya and coworkers [60] utilized the carbazolethienyl moiety with alkylated oligothiophene π-linkers to synthesize high performing dyes **ADEKA-1** and **ADEKA-2** (Figure 3.3). The dye **ADEKA-1**, has a trimethoxysilyl group as the anchoring moiety to the TiO_2 electrode, exhibited light-to-electric energy conversion efficiency of over 12% with open-circuit photovoltages higher than 1000 mV. Soni and coworkers [61] synthesized D-π-A dyes comprising of carbazole as a donor, vinylene-phenylene as π-linker (Figure 3.3). The dye showed red shifted absorption on adsorption on titania surface due the lowering of the energy level of the π*-orbitals of the dyes by enhancement in conjugation. The high power conversion efficiency (PCE) of 9% was achieved with dye **SK3** and a cobalt based redox shuttle.

Tan, Yang and coworkers [176,177] synthesized the dyes in which phenothiazine was used as donor and thiophene spacer (Figure 3.3). The insertions of benzothiadizole (BTD) as an auxiliary acceptor lead to the charge trapping and retarded charge injection. This results in lowering of J_{SC} values and efficiency of the devices. Thus the dyes **DX1** and **JH305** containing oligothiophene in conjugation path afforded high efficiencies of 5.69% and 7.5% respectively. Kuang and coworkers [178] studied the influence of trilateral π-conjugation extensions by thiophene and furan spacer in phenothiazine donor based dyes (Figure 3.3). The dye **TLEP-2** containing thiophene as π-linker lead to broad photo-response and produced an efficiency of 7.33%.

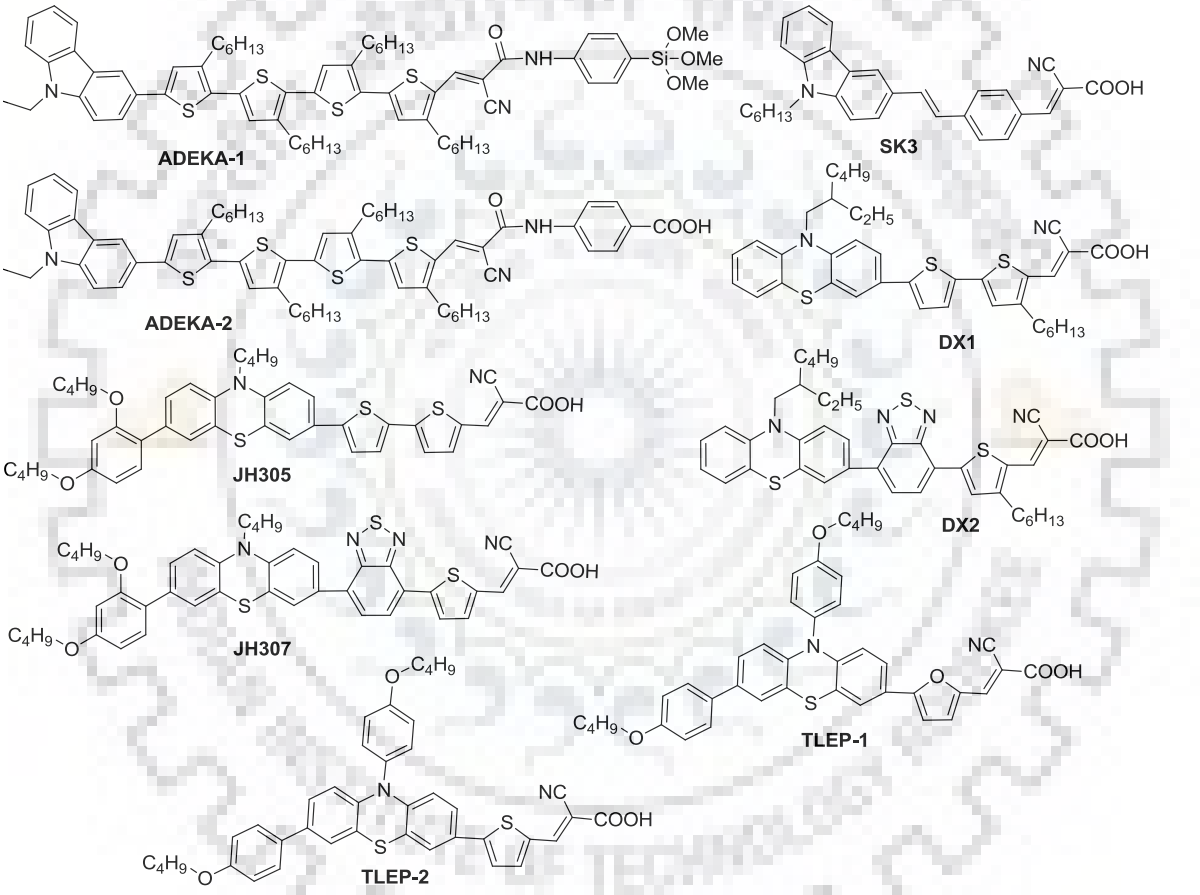

Figure 3.3 Structures of the dyes containing carbazole or phenothiazine donor in conjugation with thiophene [60,60,176-178].

Therefore, in the context of above discussion, we have designed and synthesized a series of dyes featuring DTP *N*-functionalized with fluorene. Promising donor groups such as triarylamine, carbazole and phenothiazine and cyanoacrylic acid acceptor were attached either sides of DTP moiety to achieve D-π-A molecular arrangement in the dyes. The aim of the work is to unravel the supplementing effect of auxiliary donors on the

functional properties. The newly developed dyes showed significant enhancement in optical and electrochemical properties when compared to the analogous derivatives containing simple bithiophene spacer or alkyl group functionalized DTP between the donor and acceptor and consequently served as efficient sensitizers in DSSCs.

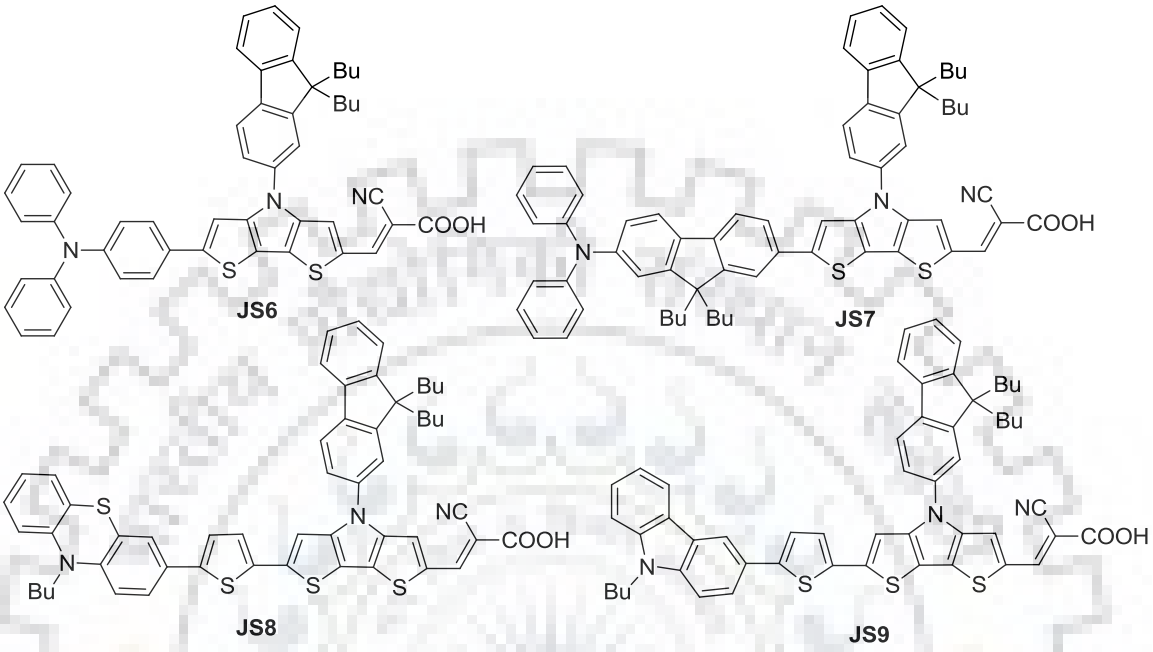

Figure 3.4 Structures of DTP-based dyes with different donors.

3.2. Results and discussion

3.2.1. Synthesis and characterization

The structures of newly synthesized dyes featuring *N*-fluorene-2-yl dithieno[3,2-*b*:2',3'-*d*]pyrrole in the conjugation pathway with different donors are shown in Figure 3.4. The synthetic scheme used for the synthesis of dyes is shown in Scheme 3.1. All the target dyes were obtained by conventional reactions such as Suzuki-Miyaura [179]/Stille [158] cross-coupling and Knoevenegal condensation. The Suzuki coupling of the suitable boronic acids with 6-bromo-4-(9,9-dibutyl-9*H*-fluoren-2-yl)-4*H*-dithieno[3,2-b:2',3'-*d*]pyrrole-2-carbaldehyde (**6**) formed the aldehyde precursors **10** and **11** and on the other hand Stille coupling of the **6** with appropriate arylstannylenes produced the required aldehyde precursors **12** and **13** in reasonable yield. Finally, Knoevenegel condensation of aldehyde derivatives with cyanoacetic acid in the presence of ammonium acetate yielded the target dyes **JS6-JS9**. The dyes were thoroughly characterized by ^{1}H and ^{13}C NMR and mass spectral methods. The spectral data are consistent with the proposed structures.

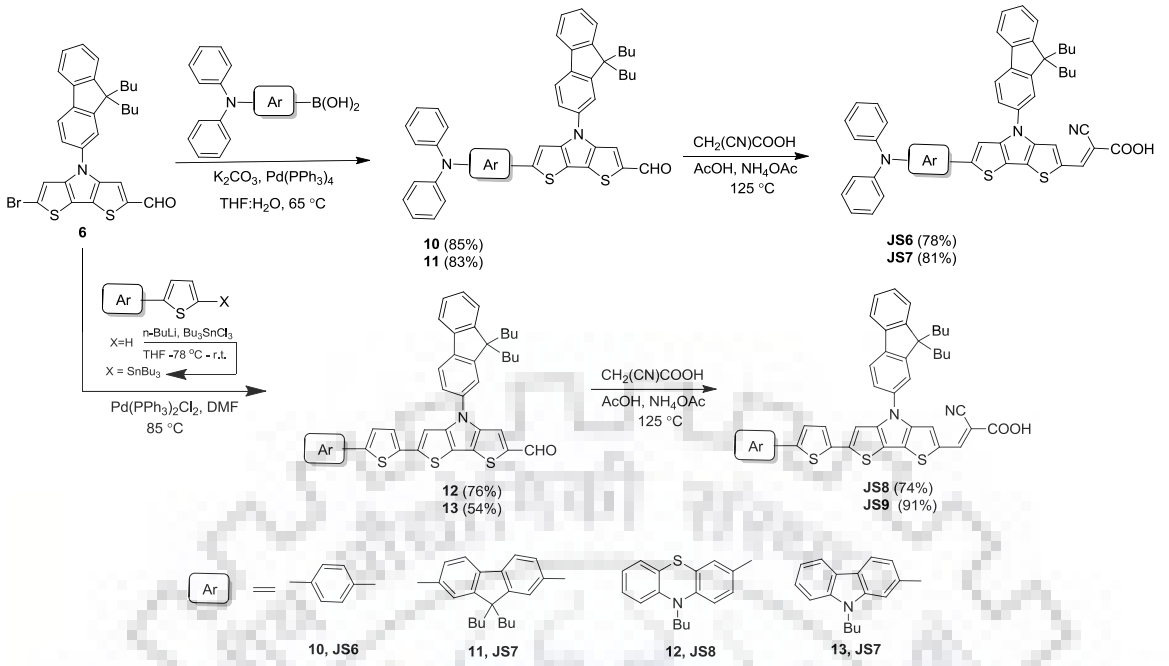

Scheme 3.1 Synthetic scheme of DTP-based dyes **JS6-JS9** containing different donors.

3.2.2 Photophysical properties

To elucidate the photophysical properties of the dyes the optical spectra were recorded in THF and displayed in Figure 3.5. The pertinent data listed in Table 3.1. The optical spectra of the dyes showed two prominent absorption bands extending from 280 nm to 590 nm. The peaks appearing at the higher energy region can be assigned to the localized π-π* transitions originating from different aromatic segments present in the dyes and the lower energy absorption peaks in between 340-590 nm can be attributed to intramolecular charge transfer (ICT). As we discussed in chapter 2, the absorption maxima recorded for the dye **JS1** at 431 nm is attributed to the ICT from DTP unit to cyanoacrylic acid acceptor moiety. Therefore, further addition of auxiliary conjugating chromophores at C6-position of the DTP unit in **JS6-JS9**, led to red shift and enhancement in the molar extinction coefficient for the low energy band. This may be due to the increase in effective conjugation length. This absorption band is attributed to ICT between arylamine/heterocyclic donor units to cyanoacrylic acid acceptor moiety with some contribution from DTP unit. The heterocyclic donor-based derivatives (**JS8** and **JS9**) showed most red-shifted absorption when compared to the triarylamine derivatives (**JS6** and **JS7**). This may be due to the thiophene unit which increases the donor strength of the heterocyclic segments due to the delocalization of the contributing molecular orbitals and render a planar bridge comprising thiophene and DTP. Electron richness and

planar conjugation pathway are beneficial for the donor-acceptor interactions and consequently red-shifted charge transfer absorption [133]. The DPF based dye **JS7** exhibited red-shifted and enhanced molar extinction coefficient when compared to its congener dye **JS6** containing phenylene linker. Incorporation of fluorene unit in place of phenyl extends the conjugation length and increases the electron donating strength of π-bridge between diphenylamine and DTP units [48]. Extension in conjugation benefits the π-π* transitions and increase in electron donor strength of the π-bridge which enhances the ICT probability. The absorption spectrum of thienylphenothiazine-based dye, **JS8** is slightly blue shifted than carbazole-based dye **JS9**, may be due to the loss of coplanarity, which affects the donor-acceptor interactions [180].

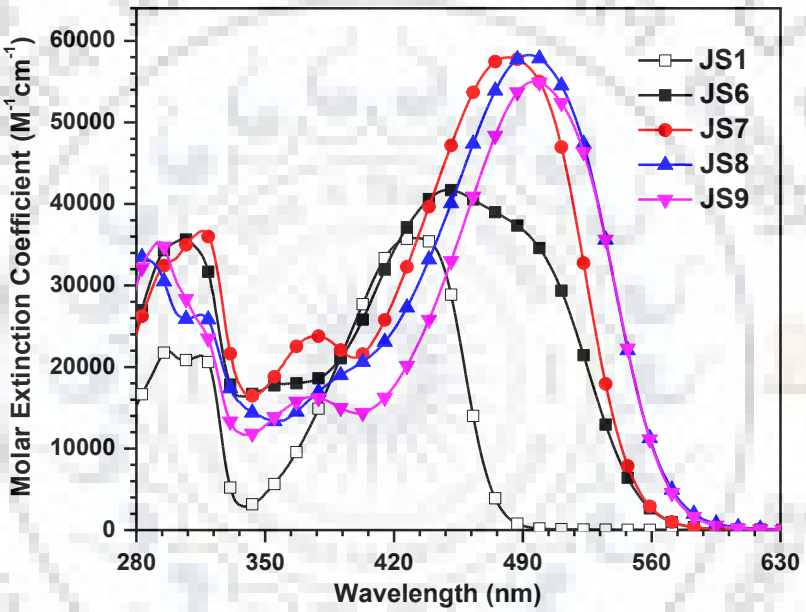

Figure 3.5 Absorption spectra of the dyes **JS6-JS9** recorded THF.

It is interesting to compare the absorption spectra of these dyes with structurally related dyes (*E*)-2-cyano-3-(5'-(4-(diphenylamino)phenyl)-[2,2'-bithiophen]-5-yl)acrylic acid **1b** [181], (*E*)-2-cyano-3-(5'-(9,9-dibutyl-7-(diphenylamino)-9*H*-fluoren-2-yl)-[2,2'-bithiophen]-5-yl)acrylic acid **D2** [63] and (*E*)-2-cyano-3-(5''-(9-ethyl-9*H*-carbazol-3-yl)-[2,2':5',2''-terthiophen]-5-yl)acrylic acid **MK-3** [182] containing oligothiophene as π-linker instead of DTP (**5b**, **5c**, and **5e** respectively). In general, red shifted and enhanced molar extinction coefficient is observed in the present dyes when compared to the reported dyes due to the effective conjugation by DTP unit in comparison with oligothiophene π-linker. All these observations suggest the electronic richness and effective conjugation rendered by DTP unit which facilitate the charge transfer/electronic

interactions between the donor and acceptor. On the other hand, dye **JS6** exhibited red-shifted and broad absorption when compared to the analogous dyes (*E*)-2-cyano-3-(6-(4-(diphenylamino)phenyl)-4-(2-ethylhexyl)-4*H*-dithieno[3,2-*b*:2',3'-*d*]pyrrol-2-yl)acrylic acid **1** and (*E*)-2-cyano-3-(6-(4-(diphenylamino)phenyl)-4-(4-(hexyloxy)phenyl)-4*H*-dithieno[3,2-*b*:2',3'-*d*]pyrrol-2-yl)acrylic acid **2** [155] containing ethylhexyl or phenoxy substituent at the *N*-position of DTP. This observation indicates that *N*-fluorenyl moiety on DTP unit is substantially beneficial for the light harvesting property of the dye [183].

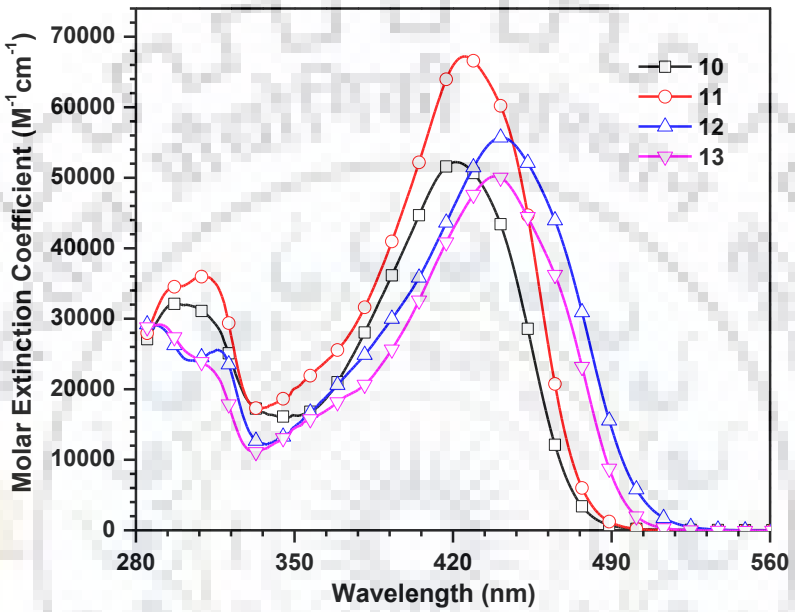

Figure 3.6 Absorption spectra of the aldehyde intermediates **10-13** recorded in THF.

The charge transfer nature of the longer wavelength absorption in the dyes is confirmed by close examination of the absorption spectra of the precursor aldehydes **10-13** (Figure 3.6) and comparing with that of the dyes (Figure 3.5). The absorption maximum shows red-shift on moving from the aldehyde to the cyanoacrylic acid derivative. Further, existence of the acid-base equilibrium is confirmed by the addition of the triethylamine (TEA) and trifluoroacetic acid (TFA) to the THF solution of the dyes (Figure 3.7). In general, bathochromic and hypsochromic shift for the low energy absorption band is observed with the addition of TEA and TFA respectively to the dye solution. All the dyes in THF solution showed hypsochromic shift for longer wavelength absorption on addition of TEA. On the other hand, no noticeable change is observed on TFA addition. This indicates that all the dyes are in protonated form in THF solution [184]. As expected for the ICT transition, the absorption spectra of the dyes exhibited negative solvatochromism (Figure 3.8) which suggests efficient solvation of the dyes in

the ground state by the polar solvents [159]. The hypsochromic shift in the DMF solution for all the dyes is attributed to the basic nature of DMF [175]. Exceptional red shift observed for the dyes in DCM may be due to instant stabilization of the excited state by the solvent dipoles during the electronic excitation [160].

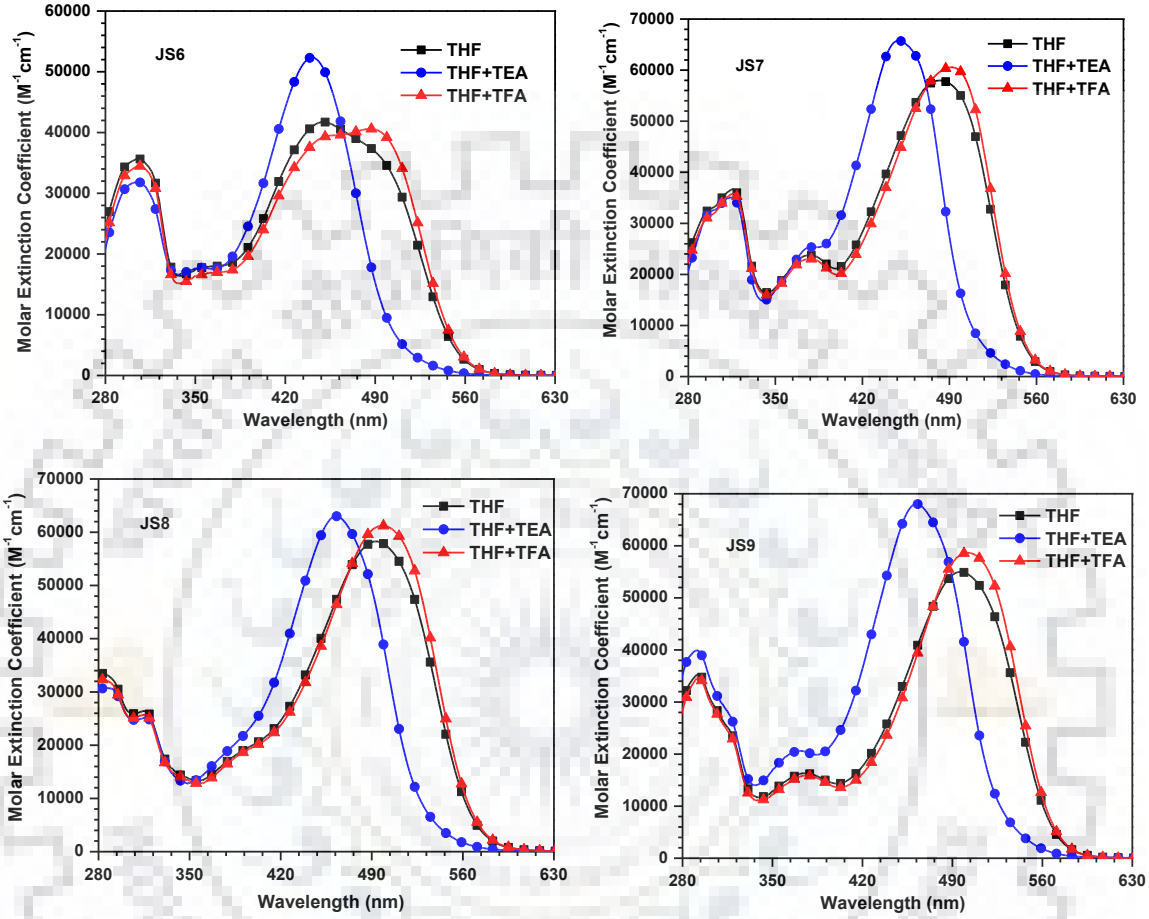

Figure 3.7 Absorption spectra of the dyes **JS6-JS9** recorded in THF before and after the addition of TEA/TFA.

Generally, organic dyes aggregate at TiO_2 surface and result in either red shift or blue shift in the absorption spectrum based on the aggregation type [161]. In the present study, the absorption spectra of the dyes anchored on the surface of TiO_2 (Figure 3.9) exhibited broad red shifted absorption profiles when compared to those recorded in THF solution. This can be attributed to the formation of *J*-aggregates [161] or the large thickness of the TiO_2 films [185]. The emission peak values recorded for the dyes in THF solution follow the trend, **JS8** < **JS7** < **JS6** < **JS9** (Figure 3.10). The red shifted emission peaks for dyes **JS6**, **JS7** and **JS9** may be due to more dipole-dipole relaxation for these dyes in the excited state [186].

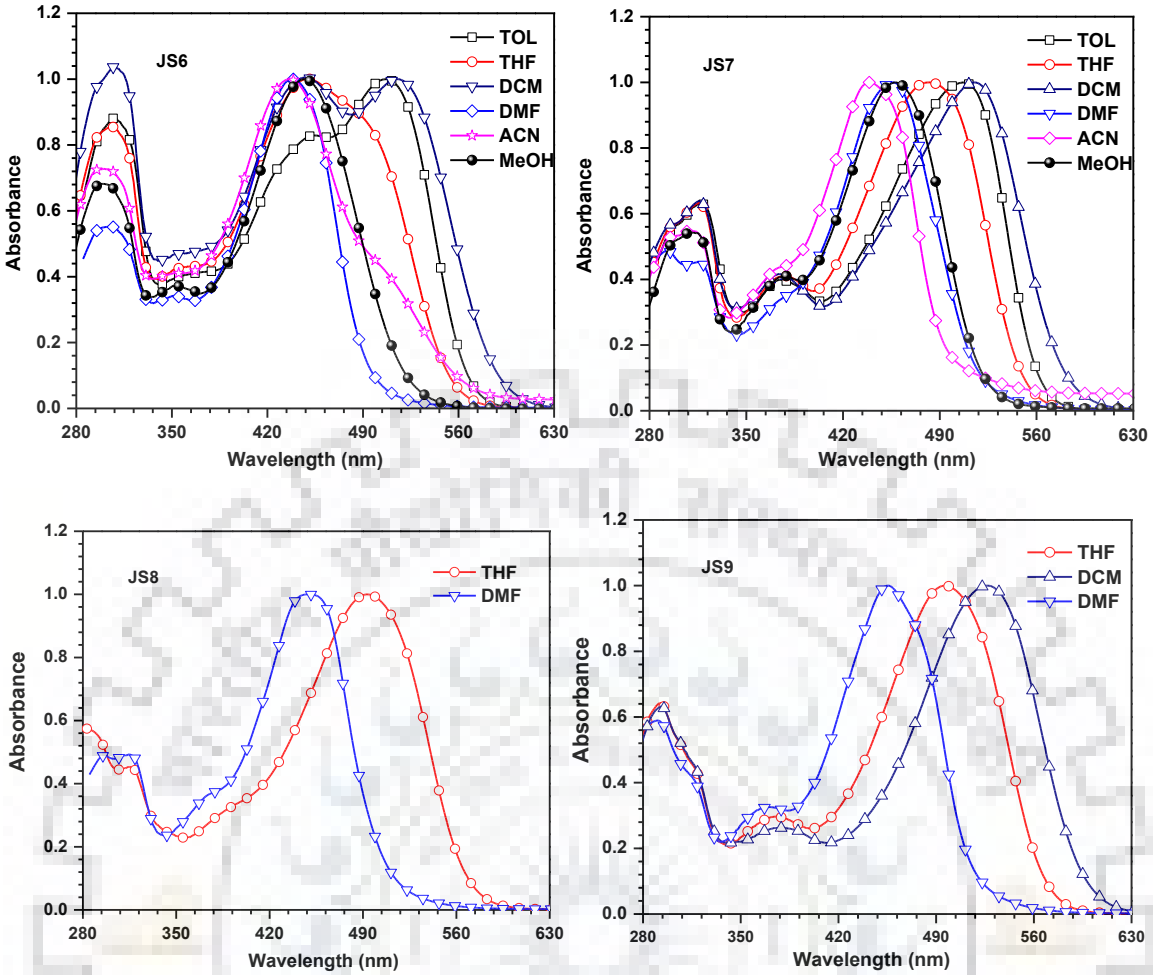

Figure 3.8 Normalized absorption spectra of the dyes **JS6-JS9** recorded in the solvents of different polarities (Due to poor solubility solvatochromism studies of **JS8** and **JS9** are restricted to few solvents).

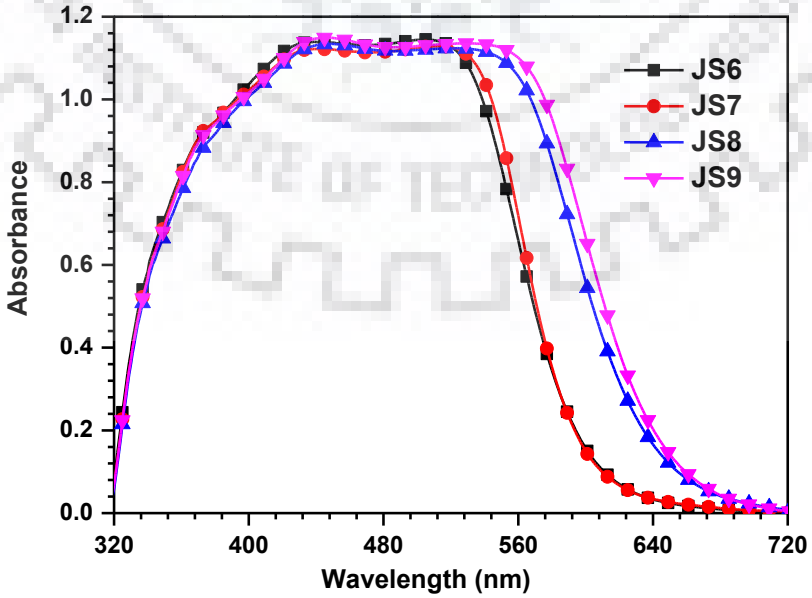

Figure 3.9 Absorption spectra of the dyes **JS6-JS9** anchored on nanocrystalline TiO_2.

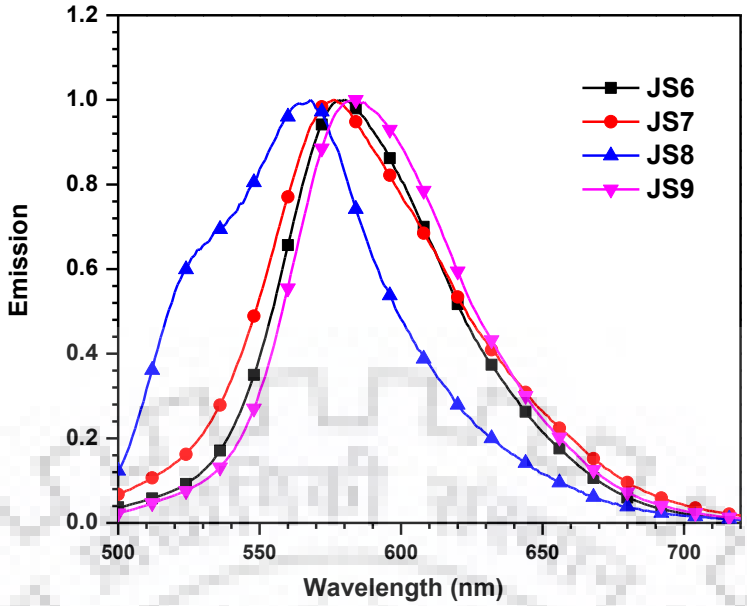

Figure 3.10 Normalized emission spectra of the dyes **JS6-JS9** recorded in THF.

3.2.3. Electrochemical properties

Electrochemical studies were employed to investigate the redox characteristics of the dyes in THF. The redox parameters deduced from the electrochemical measurements are listed in Table 3.1 and recorded cyclic voltammograms (CV) and differential pulse voltammograms (DPV) shown in Figures 3.11 and 3.12. All the dyes **JS6-JS9** containing additional donors displayed two quasi-reversible oxidation couples. The oxidation potentials of the dyes are more positive than that observed for ferrocene under identical conditions. The first oxidation potential of the dyes originates from the removal of electron from the donor segment. The E_{OX} values follow the order, **JS9** > **JS6** > **JS7** > **JS8**, reminiscent of the donor strength. The second oxidation potential which is more positive than the previous one is arises from the conjugating back-bone including arylamine/heterocyclic units and DTP unit. This oxidation is substantially influenced by the nature of the conjugation pathway. Comparison of oxidation potential of the dye **JS1** (Chapter 2) with the second oxidation potentials of the present dyes (**JS6-JS9**) reveals that the DTP oxidation is easier in the later compounds. This suggests that the tethering donor moiety on one side of DTP unit increased the electron-donating propensity approximately two-fold. As hypothesized, incorporation of donor is beneficial for the push of electrons toward the acceptor via the DTP linkage.

Table 3.1 Optical and electrochemical data of the dyes **JS6-JS9**.

Dye	$\lambda_{abs.}$ (nm ($\varepsilon_{max} \times 10^3$ $M^{-1}cm^{-1}$))	λ_{max}^{TiO2} (nm)	E_{OX} (mV (ΔE_p, mV)) [a]	E_{OX} (V) (Vs NHE)	HOMO (eV)[b]	LUMO (eV)[c]	$E_{0\text{-}0}$ (eV)[d]	E_{OX}* (V)[e]
JS1	431 (35.8), 315 (21.4), 292 (21.9)	434	808	1.578	-5.608	-2.964	2.644	-1.066
JS6	495 (35.7), 450 (41.7), 306 (35.7)	505	427 (92), 568 (65)	1.197	-5.227	-2.956	2.271	-1.07
JS7	483 (57.9), 379 (23.8) 316 (36.7)	515	442 (72), 555 (49)	1.212	-5.242	-2.958	2.284	-1.07
JS8	493 (58.3), 315 (26.4)	524	225 (138), 485 (130)	0.995	-5.025	-2.758	2.267	-1.28
JS9	496 (55.0), 375 (16.3), 293 (35.4)	529	335 (90), 576 (94)	1.105	-5.135	-2.909	2.226	-1.13

[a] Oxidation potentials are reported with reference to the ferrocene internal standard.

[b] Deduced from the oxidation potential using the formula HOMO = -(4.8 + E_{OX})

[c] Deduced using the formula LUMO = HOMO + $E_{0\text{-}0}$.

[d] Calculated from intersection of absorption & emission spectra.

[e] Calculated from $E_{OX}^* = E_{OX} - E_{0\text{-}0}$ (Vs. NHE).

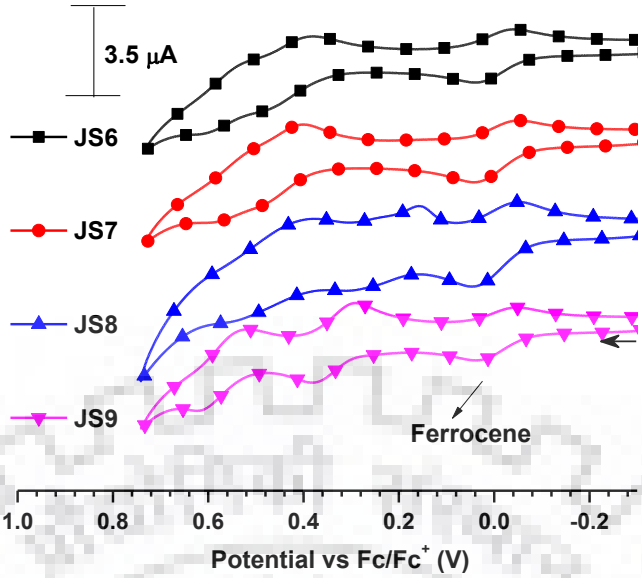

Figure 3.11 Cyclic voltammograms of the dyes **JS6-JS9** recorded in THF.

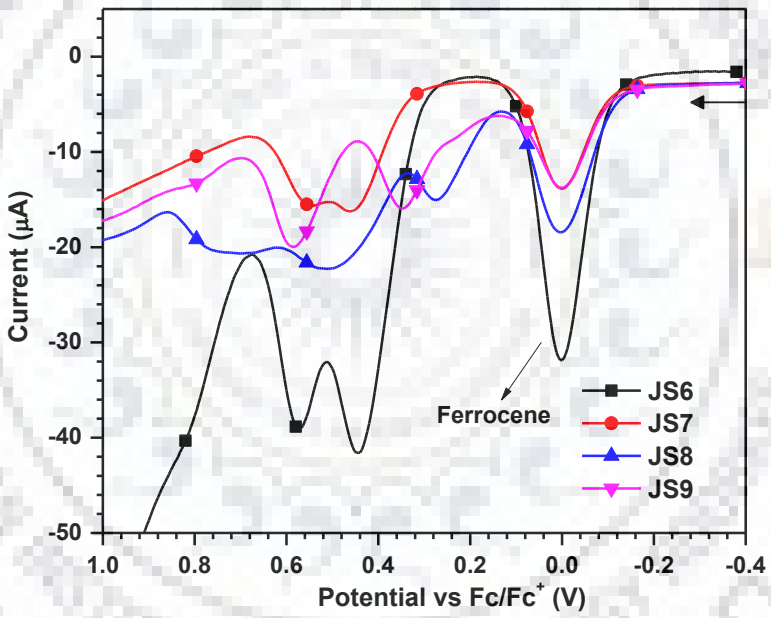

Figure 3.12 Differential pulse voltammograms of the dyes **JS6-JS9** recorded in THF.

To predict the electron injection propensity of the dyes into conduction bands of titania, the excited state oxidation potentials of the dyes were calculated from the equation $E_{OX}^* = E_{OX} - E_{0\text{-}0}$ where $E_{0\text{-}0}$ is the optical energy gap obtained from the intersection of normalized absorption and emission spectra of the dyes. The excited state oxidation potentials for the dyes are more negative (-1.06 to -1.28 V *vs*. NHE) [162] than the conduction band edge of the TiO_2 (-0.5 V *vs*. NHE) which ensures efficient electron injection from the photo-excited dyes into the conduction band of TiO_2. Similarly, the ground state oxidation potentials of the dyes are more positive (0.99 to 1.58 V *vs*. NHE)

than the redox potential of I_3^-/I^- electrolyte (~ 0.4 V) [163] which suggests thermodynamically feasible regeneration of the oxidized dye by the electrolyte.

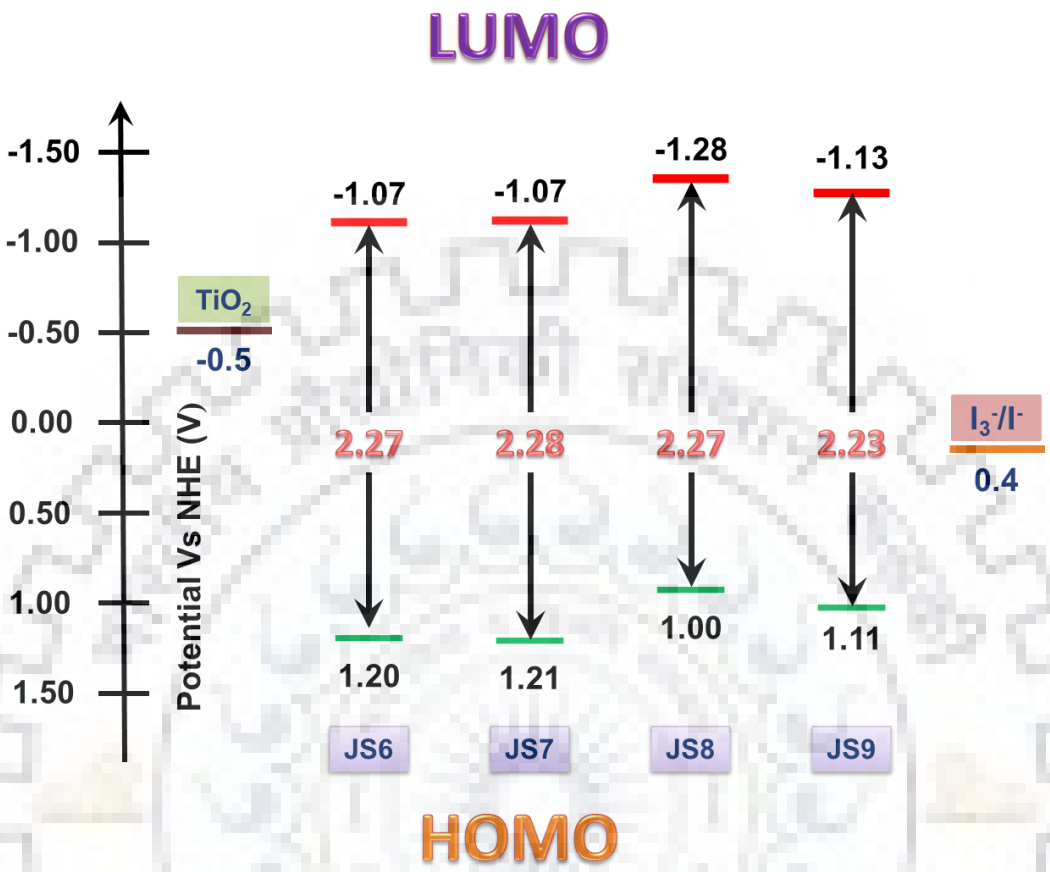

Figure 3.13 Energy level diagram of the dyes **JS6-JS9**.

3.2.4 Theoretical calculations

To get correlation between the molecular structure and electronic properties of dyes, density functional theory (DFT) [164,165] calculations were performed. The ground state geometries of the dyes (**JS6-JS9**) were optimized by B3LYP functional and 6-31g(d,p) basis set while the vertical electronic excitation parameters computed at the TD-DFT level by using BMK functional and DGDZVP basis set [187,188]. The electronic distribution for HOMO-1, HOMO and LUMO for dyes is displayed in Figure 3.14. The computed vertical transition energies and orbital contribution for the respective transitions are listed in Table 3.2. The fluorene and DTP units are perpendicular to one another which may be beneficial to hinder the aggregation of the dyes and retard the recombination of the electrons. The HOMOs for the dyes **JS6-JS9** are constituted by arylamine segment and DTP spacer. The LUMO for the dyes are spread over the cyanoacrylic and DTP units. For all the dyes, the HOMO and LUMO are overlapping

reasonably; however, suggest efficient charge transfer propensity. Since the lower energy vertical excitation predicted by the theoretical computations involves major contribution from the HOMO to LUMO electronic transition, the longer wavelength absorption can be described to possess charge transfer character. Inspection of electronic distribution of HOMO-1 for the dye **JS7** suggests appreciable π-π* character as well. The computed lower energy transition λ_{max} matched closely with the experimental values.

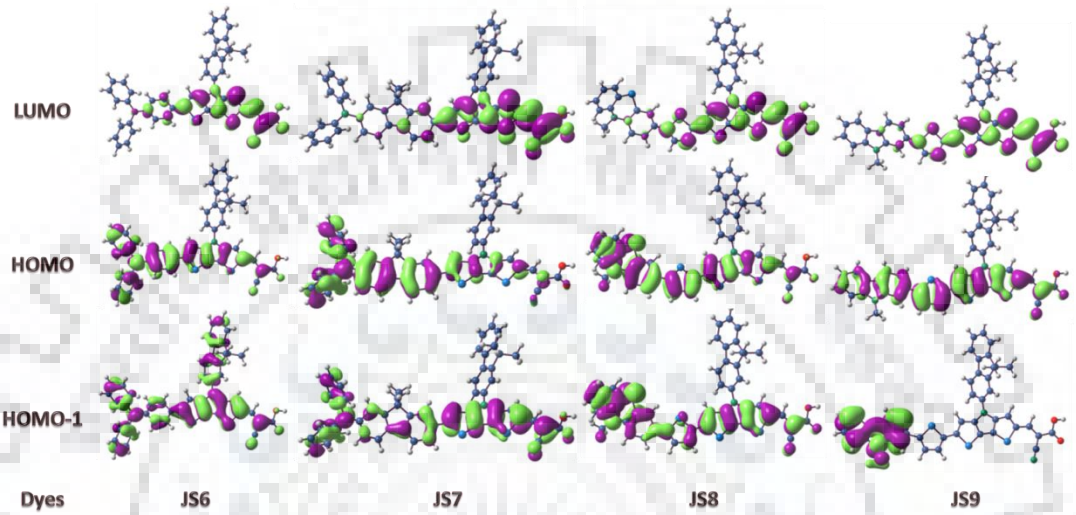

Figure 3.14 Electronic distribution in the selected molecular orbitals of the dyes **JS6-JS9.**

Table 3.2 Computed vertical transition energies and their oscillator strengths and configurations for the dyes **JS6-JS9**.

Dye	λ_{max}^{abs} (nm)	*f*	Configuration	HOMO (eV)	LUMO (eV)	Band gap (eV)
JS6	492	1.84	HOMO→LUMO (88%) HOMO-1→LUMO (6%)	-5.79	-2.30	3.49
JS7	488	2.11	HOMO→LUMO (71%) HOMO-1→LUMO (24%),	-5.73	-2.33	3.40
JS8	513	2.15	HOMO→LUMO (83%) HOMO-1→LUMO (12%),	-5.79	-2.40	3.39
JS9	504	2.31	HOMO→LUMO (93%) HOMO-3→LUMO (2%), HOMO→LUMO+1 (2%)	-5.93	-2.40	3.53

3.2.5. Photovoltaic performance of DSSCs

As the DTP based organic dyes showed promising photophysical and electrochemical properties, we evaluated the photovoltaic performance of them using as sensitizers for nanocrystalline TiO_2-based dye-sensitized solar cells. The performance parameters of the DSSCs under AM 1.5 G simulated solar light at a light intensity of 100 mW cm^{-2} are

collected in Table 3.3. Figure 3.15 shows incident photon-to-current conversion efficiencies (IPCE) of the dyes. The IPCE spectrum is broadened and extended upto 790 nm for the dye **JS9** which is consistent with its absorption spectra (THF solution as well on the TiO_2). Figure 3.16 shows the photocurrent-voltage (*I-V*) curves of the cells. The photocurrent density (J_{SC}) for the dyes follow the trend **JS7** > **JS9** > **JS6** > **JS8**. The high J_{SC} for **JS7** and **JS9** is attributable to their high molar extinction coefficients in absorption spectra. It is interesting to notice that dye **JS8** produced comparatively low J_{SC} despite possessing high molar extinction coefficient in absorption spectra. This may be due to inefficient charge collection efficiency from the excited dye to conduction band of TiO_2 (*vide infra*) [189]. Similarly, open circuit voltage (V_{OC}) for the dyes follows the order, **JS9** < **JS8** < **JS6** < **JS7**. The larger V_{OC} observed for the dye **JS7** is probably arising from the two *n*-butyl chains on the fluorene segment, which effectively reduces the possibility of charge recombination by retarding the approach of triiodide ion (I_3^-) at the TiO_2 surface [190]. However, small V_{OC} realized for **JS9** is attributed to relatively high recombination rate of electron present in the conduction band of TiO_2 (*vide infra*) [191]. The high photocurrent density, open-circuit potential and fill factor exhibited by the DPF donor containing dye **JS7** produced the overall high efficiency for the device (6.81%). As compared to the dye **JS1**, the introduction of donors in the dyes **JS6**-**JS9** significantly improved the optical and electrochemical properties which enhanced the photo-induced electron generation, electron injection and dye regeneration.

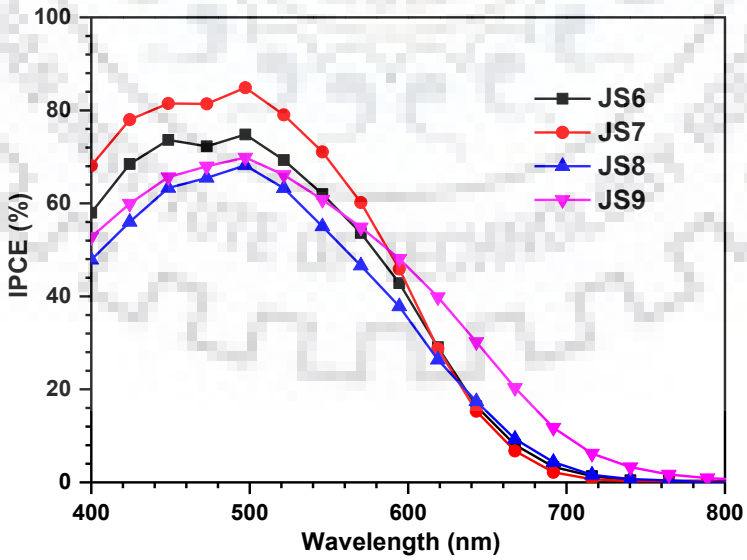

Figure 3.15 IPCE spectra of the DSSCs fabricated using the dyes **JS6**-**JS9**.

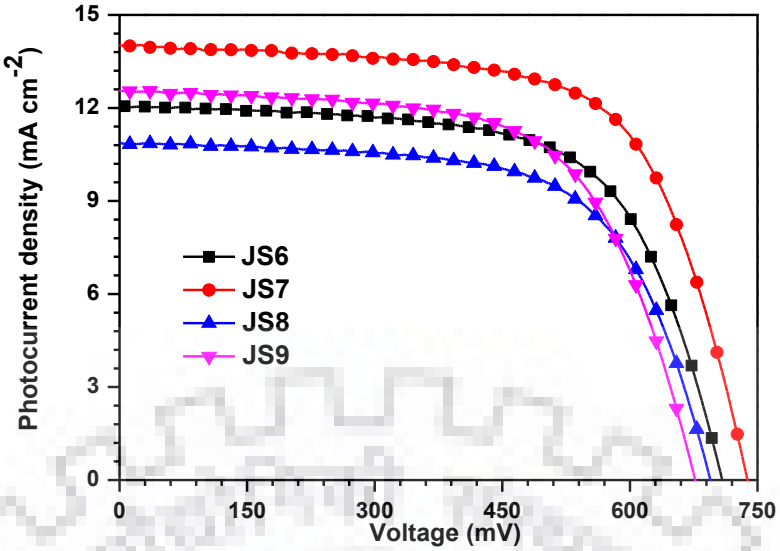

Figure 3.16 I–V characteristics of the DSSCs fabricated using the dyes **JS6-JS9**.

Table 3.3 Performance parameters of the DSSCs fabricated using the dyes **JS6-JS9**.

Dye	η (%)	V_{OC} (mV)	J_{SC} (mA cm^{-2})	*FF*	R_{ct2} (ohm)	τ_e (ms)	R_{rec} (ohm)
JS1	0.46	497	2.46	0.37	60.73	1.71	21.84
JS6	5.52	708.2	12.03	0.65	20.31	6.00	50.34
JS7	6.81	738.1	14.01	0.66	14.20	7.92	57.53
JS8	4.87	694.4	10.88	0.65	24.01	4.54	48.23
JS9	5.39	676.6	12.57	0.63	19.74	1.96	42.97

3.2.6. Electrochemical impedance spectroscopy

To understand the structural effect of dyes on electron transfer kinetics at different interfaces of DSSCs, electrochemical impedance spectroscopy (EIS) measurements were performed. These EIS measurements were carried out under dark and illumination conditions and corresponding Nyquist plots are displayed as Figure 3.17 and 3.18 respectively. In general, three semicircles are seen in the EIS spectrum which corresponds to the resistance for the different electron transfer processes at the TiO_2 (R_{ct2}), TiO_2/dye/electrolyte interface (R_{rec}) and Warburg diffusion process of electrolyte (Z_w) in DSSCs. From the Nyquist plot (Figure 3.17) obtained for dark measurements the electron recombination resistance (R_{rec}) can be deduced from the radius of second semicircle. The R_{rec} for the dye follows the order **JS7** > **JS6** > **JS8** > **JS9**. Based on this order, **JS7** is expected to display large V_{OC}. The order of R_{rec} is exactly matching with the trend observed for V_{OC} (**JS9** < **JS8** < **JS6** < **JS7**). From the Nyquist plot (Figure 3.18) constructed from the measurements under the illumination conditions (100 mW cm^{-2}, AM 1.5G) the charge transport resistance can be estimated from the radius of intermediate frequency semicircle. Large semicircle observed for the dye **JS8** indicates high charge-

transport resistance (R_{ct2}) for the corresponding device. The order for R_{ct2} is **JS8** > **JS9** > **JS6** > **JS7**. The lowest R_{ct2} for **JS7** can be interpreted as relatively better electron collection efficiency for the device over the other dyes.

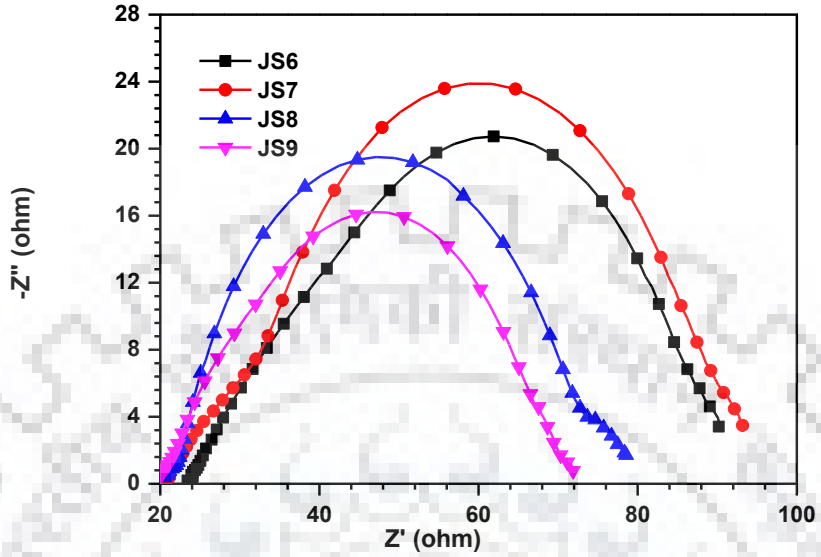

Figure 3.17 Nyquist plots observed for the DSSCs fabricated using the dyes **JS6-JS9** under dark condition.

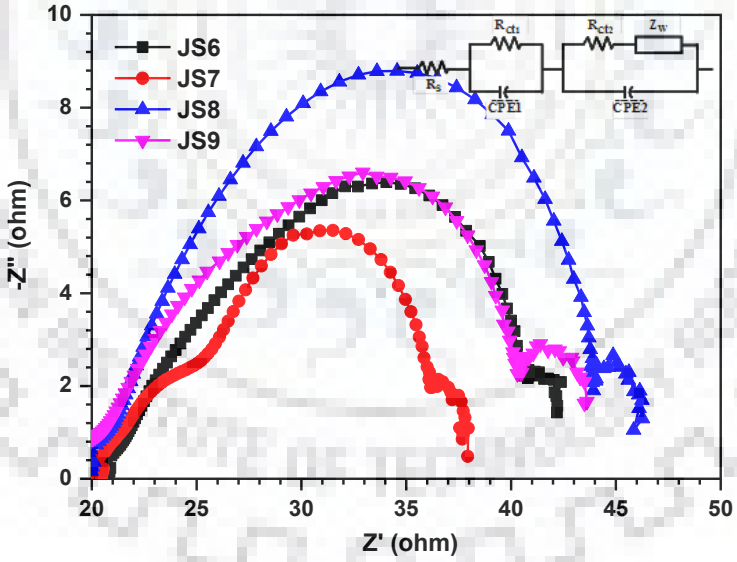

Figure 3.18 Nyquist plots observed for the DSSCs fabricated using the dyes **JS6-JS9** under illumination.

The mid-frequency peak in the Bode phase plot (Figure 3.19) corresponds to the electron-life time τ_e ($\tau_e = 1/\omega_{min}$, where ω_{min} is the angular frequency of the low-frequency peak) in the devices. The electron life time is a measure of suppression of back reaction of injected electrons with I_3^- in the electrolyte. The τ_e for the dyes assume the trend, **JS7** >

JS6 > **JS8** > **JS9** which is consistent with the order observed for V_{OC}. The large electron-life time is essential to improve the J_{SC} and V_{OC} and subsequently enhances the power conversion efficiency of the DSSC.

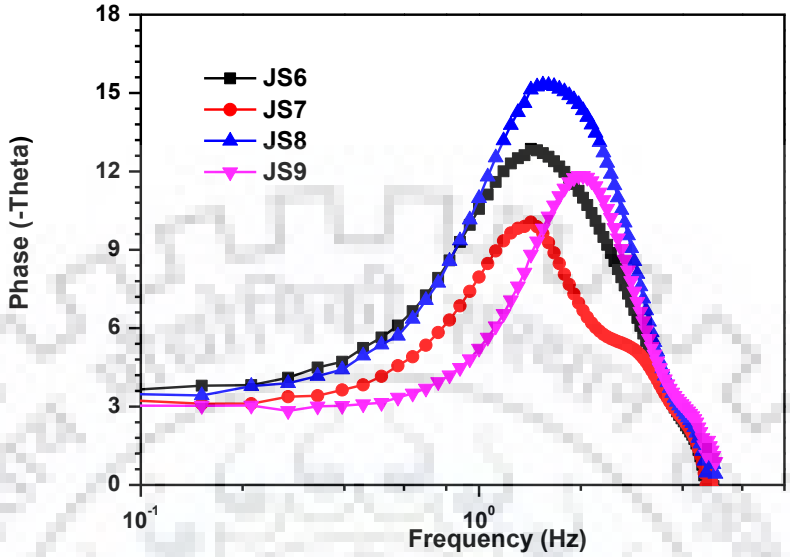

Figure 3.19 Bode phase plots for the DSSCs fabricated using the dyes **JS6-JS9** measured under illumination.

3.3 Conclusions

We have synthesized new organic dyes containing DTP as a linker in conjugation with different donors (triphenylamine, fluorenyldiphenylamine, carbazole and phenothiazine). The dyes showed red shifted absorption and high molar extinction coefficients when compared to the control dye lacking donor. Electron richness of the fluorene appended DTP considerably influenced the optical and electrochemical properties of the dyes. From theoretical calculations, the absorption in the visible region is presumed to result in migration of charge from the arylamine/heterocyclic donor to cyanoacrylic acid acceptor. Non-planar fluorene moiety on the DTP unit could be beneficial for retarding the aggregation of the dyes and impeding the electron recombination. The DSSC fabricated using fluorenyldiphenylamine donor-based sensitizer showed promising higher power conversion efficiency (6.81 %) in the series attributable to the high recombination resistance (R_{rec}) and low charge transfer resistance (R_{ct2}).

3.4 Experimental

3.4.1 Materials and methods

The general methodology is similar to that described in Chapter 2.

3.3.2 Synthesis

*Synthesis of 4-(9,9-dibutyl-9H-fluoren-2-yl)-6-(4-(diphenylamino)phenyl)-4H-dithieno[3,2-b:2',3'-d]pyrrole-2-carbaldehyde **(10)***

A mixture of **6** (0.563 g, 1.00 mmol), (4-(diphenylamino)phenyl)boronic acid (0.318 g, 1.10 mmol), potassium carbonate (0.42 g, 3 mmol), THF (24 mL) and water (6 mL) was maintained under a nitrogen atmosphere. After the addition of $Pd(PPh_3)_4$ (0.058 g, 5 mol%), this mixture was heated at 65 °C for 12 h. The mixture was poured into water and extracted with chloroform. The organic layer was washed with water followed by brine solution and dried over anhydrous Na_2SO_4. The residue obtained on evaporation of the organic extract was purified by column chromatography on alumina using hexane:chloroform (1:4) mixture as eluent; Yellow solid; yield (0.623 g, 85%); mp 156-158 °C; IR (KBr, cm^{-1}) 1657 ($\nu_{C=O}$); ^{1}H NMR (500 MHz, $CDCl_3$) δ 0.73 (t, *J* = 8.0 Hz, 10 H), 1.10-1.15 (m, 4 H), 2.03 (t, *J* = 8.0 Hz, 4 H), 7.05-7.08 (m, 4 H), 7,13 (d, *J* = 8.0 Hz, 4 H), 7.28-7.30 (m, 5 H), 7.35-7.40 (m, 3 H), 7.50 (d, *J* = 8.0 Hz, 2 H), 7.56 (d, *J* = 10.0 Hz, 2 H), 7.76 (d, *J* = 4.0 Hz, 2 H), 7.87 (d, *J* = 7.5 Hz, 1 H), 9.86 (s, 1 H); ^{13}C NMR (123.55 MHz, $CDCl_3$) δ 182.8, 152.9, 148.7, 147.2, 140.3, 137.5, 129.4, 127.6, 127.2, 126.6, 125.3, 124.8, 123.5, 123.2, 123.0, 121.8, 121.0, 120.0, 117.8, 106.7, 55.4, 40.1, 26.1, 23.1, 13.9. HRMS calcd for $C_{48}H_{42}N_2O_2S_2$ $[M]^+$ m/z 742.2682 found 742.2680.

*Synthesis of 6-(9,9-dibutyl-7-(diphenylamino)-9H-fluoren-2-yl)-4-(9,9-dibutyl-9H-fluoren-2-yl)-4H-dithieno[3,2-b:2',3'-d]pyrrole-2-carbaldehyde **(11)***

It was obtained from **6** (0.38 g, 0.68 mmol) and (9,9-dibromo-7-(diphenylamino)-9*H*-fluoren-2-yl)boronic acid (0.40 g, 0.74 mmol) by following a procedure described above for **4a**. Yellow solid; yield (0.520 g, 83%); mp 215-218 °C; IR (KBr, cm^{-1}) 1655 ($\nu_{C=O}$); ^{1}H NMR (500 MHz, $CDCl_3$) δ 0.65-0.77 (m, 20 H), 1.06-1.11 (m, 4 H), 1.13-1.18 (m, 4 H), 1.84-1.95 (m, 4 H), 2.04-2.07 (m, 4 H), 7.01-7.04 (m, 3 H), 7.11-7.14 (m, 5 H), 7.21 -7.24 (m, 3 H), 7.27 (s, 1 H), 7.36-7.42 (m, 4 H), 7.54-7.62 (m, 6 H), 7.77-7.78 (m, 2 H), 9.88 (s, 1 H); ^{13}C NMR (123.55 MHz, $CDCl_3$): δ 182.7, 153.0, 150.9, 148.2, 145.9, 143.2, 141.1, 141.0, 140.5, 140.2, 140.0, 137.4, 135.5, 127.6, 127.2, 126.1, 125.3, 125.0, 124.8, 123.7, 123.3, 123.0, 122.6, 121.8, 121.0, 120.4, 120.0, 119.2, 117.8, 117.5, 115.0,

109.1, 109.0, 107.4, 55.4, 43.0, 40.2, 31.2, 26.2, 23.1, 20.6, 14.0, 13.9. HRMS calcd for $C_{63}H_{62}N_2OS_2$ $[M+Na]^+$ m/z 949.4146 found 949.4175.

Synthesis of 6-(5-(10-butyl-10H-phenothiazin-3-yl)thiophen-2-yl)-4-(9,9-dibutyl-9H-fluoren-2-yl)-4H-dithieno[3,2-b:2',3'-d]pyrrole-2-carbaldehyde ***(12)***

A mixture **6** (0.563 g, 1.00 mmol), 10-butyl-3-(5-(tributylstannyl)thiophen-2-yl)-10*H*-phenothiazine prepared from **I1** (1.2 mmol) and dry DMF (5 mL) was maintained under nitrogen atmosphere. After the addition of $Pd(PPh_3)_2Cl_2$ (0.07 g, 1 mol%), this mixture was heated at 80 °C for 24 h. On completion of the reaction, the mixture was poured into water and extracted with chloroform. The organic layer was washed with water followed by brine solution and dried over anhydrous Na_2SO_4. The combined organic extracts were concentrated and further purified by alumina column chromatography using a hexane/chloroform (1:4) mixture as eluent, Yellow solid; yield (0.620 g, 76%). mp 200-202°C; IR (KBr, cm^{-1}) 1655 ($\nu_{C=O}$); ^{1}H NMR (500 MHz, $CDCl_3$) δ 0.77-0.82 (m, 10 H), 0.97 (t, *J* = 7.5 Hz, 3 H), 1.17-1.20 (m, 4 H), 1.45-1,49 (m, 2 H), 1.80 (quin, *J* = 7.0 Hz, 2 H), 2.04-2.07 (m, 4 H), 3.86 (t, *J* = 8.0 Hz, 2 H), 6.87 (q, *J* = 8.5 Hz, 2 H), 6.92 (t, *J* = 8.0 Hz , 1 H), 7.12-7.17 (m, 3 H), 7.21 (d, *J* = 4.0 Hz, 2 H), 7.33-7.41 (m, 2 H), 7.55 (dd, *J* = 2.0, 3.6 Hz, 2 H), 7.75-7.7.78 (m, 2 H), 7.89 (d, *J* = 8.5 Hz, 1 H), 9.86 (s, 1 H); ^{13}C NMR (123.55 MHz, $CDCl_3$): δ 182.7, 153.0, 150.9, 148.0, 144.9, 144.7, 142.28, 142.23, 140.2, 140.0, 137.4, 136.0, 128.0, 127.6, 127.5, 127.4, 127.2, 125.4, 125.1, 124.9, 124.5, 124.1, 124.0, 123.0, 122.9, 122.6, 121.7, 121.0, 120.0, 117.7, 115.5, 115.4, 115.1, 107.5, 47.2, 40.2, 28.9, 26.2, 23.1, 20.2, 14.0, 13.9. HRMS calcd for $C_{50}H_{46}N_2OS_4$ $[M]^+$ m/z 818.2487 found 818.2490.

Synthesis of 6-(5-(9-butyl-9H-carbazol-3-yl)thiophen-2-yl)-4-(9,9-dibutyl-9H-fluoren-2-yl)-4H-dithieno[3,2-b:2',3'-d]pyrrole-2-carbaldehyde ***(13)***

It was obtained from **6** (0.150 g, 0.21 mmol) and 9-butyl-3-(5-(tributylstannyl)thiophen-2-yl)-9*H*-carbazole prepared from **I2** (1.2 mmol) by following a procedure described above for **12**. Orange solid; yield (0.130 g, 78%); mp 196-198 °C; IR (KBr, cm^{-1}) 1650 ($\nu_{C=O}$); ^{1}H NMR (500 MHz, $CDCl_3$): δ 0.73-0.81 (m, 10 H), 0.88-1.06 (m, 4 H), 1.17-1.22 (m, 4 H), 1.39-1.44 (m, 2 H), 1.87 (t, *J* = 7.5 Hz, 2 H), 2.07 (quin, *J* = 5.0 Hz, 3 H), 4.32 (s, 2 H), 7.25 (d, *J* = 8.0 Hz, 2 H), 7.28-7.29 (m, 2 H), 7.39-7.43 (m, 5 H), 7.47-7.49 (m, 1 H), 7.57-7.58 (m, 2 H), 7.71 (dd, *J* = 1.5, 8.0 Hz, 1 H), 7.76-7.79 (m, 2 H), 7.9 (s, 1 H), 8.11 (d, *J* = 7.5 Hz, 1 H), 8.29 (d, *J* = 7.0 Hz, 1 H), 9.86 (s, 1 H); ^{13}C

NMR (123.55 MHz, $CDCl_3$) δ 182.7, 153.0, 150.9, 148.2, 145.9, 143.2, 141.1, 140.2, 140.0, 137.4, 135.5, 127.6, 126.1, 125.3, 125.0, 124.8, 123.7, 123.3, 123.0, 122.7, 121.8, 120.4, 120.0, 119.2, 117.8, 117.5, 115.0, 109.1, 109.0, 107.4, 55.4, 43.0, 40.1, 31.2, 26.2, 23.1, 20.6, 14.0, 13.9. HRMS calcd for $C_{50}H_{46}N_2OS_3$ $[M]^+$ m/z 786.2767 found 786.2748.

Synthesis of (E)-2-cyano-3-(4-(9,9-dibutyl-9H-fluoren-2-yl)-6-(4-(diphenylamino)phenyl)-4H-dithieno[3,2-b:2',3'-d]pyrrol-2-yl)acrylic acid ***(JS6)***

It was prepared from **10** (0.56 g, 1.00 mmol) by following a procedure similar to that described above for **JS1**. Red solid; yield (0.130 g, 78%); mp 244-246 °C; IR (KBr, cm^{-1}) 2211 ($\nu_{C\equiv N}$); ^{1}H NMR (399.78 MHz, DMSO-d_6) δ 0.55-0.64 (m, 10 H), 1.02-1.07 (m, 4 H), 1.99-2.05 (m, 2H), 2.14-2.19 (m, 2H), 6.94 (d, *J* = 8.4 Hz, 2 H), 7.40-7.10 (m, 5 H), 7.30-7.34 (m, 5 H), 7.46-7.50 (m, 2 H), 7.55-7.61 (m, 3H), 7.78-7.88 (m, 2H), 8.01 (d, *J* = 8.0 Hz, 1 H), 8.11 (s, 1 H), 8.31 (s, 2 H), 8.45 (s, 1 H); ^{13}C NMR (100.53 MHz, $CDCl_3$) δ 164.6, 152.9, 151.0, 148.0, 147.7, 147.1, 143.0, 140.2, 139.8, 137.7, 137.5, 136.7, 130.2, 129.1, 124.3, 123.5, 122.2, 121.9, 120.6, 117.7, 108.0, 55.6, 26.4, 22.9, 14.3. HRMS calcd for $C_{51}H_{43}N_3O_2S_2$ $[M+Na]^+$ m/z 816.2689 found 816.2669.

Synthesis of (E)-2-cyano-3-(6-(9,9-dibutyl-7-(diphenylamino)-9H-fluoren-2-yl)-4-(9,9-dibutyl-9H-fluoren-2-yl)-4H-dithieno[3,2-b:2',3'-d]pyrrol-2-yl)acrylic acid ***(JS7)***

It was prepared from **11** (0.150 g, 0.16 mmol) by following a procedure used for **JS1.** Ddark red solid; yield (0.130 g, 81%); mp 260-263 °C; IR (KBr, cm^{-1}) 2211 ($\nu_{C\equiv N}$); ^{1}H NMR (399.78 MHz, $CDCl_3$): δ 0.69-0.76 (m, 20 H), 1.07-1.19 (m, 8 H), 1.87-1.93 (m, 4 H), 2.02-2.07 (m, 4 H), 7.01-7.02 (m, 5 H), 7.12-7.14 (m, 5 H), 7.24 (s, 1 H), 7.28, (s, 1 H), 7.39-742 (m, 3 H), 7.53-7.61 (m, 6 H), 7.77 (d, *J* = 6.8 Hz, 2 H), 7.87-7.92 (m, 2 H), 8.33 (s, 1H);); ^{13}C NMR (100.53 MHz, $CDCl_3$) δ 153.0, 152.3, 151.6, 150.8, 149.7, 147.8, 147.7, 144.1, 141.9, 140.3, 139.9, 137.3, 135.3, 133.2, 132.2, 132.3, 129.2, 127.6, 127.1, 124.9, 124.03, 123.96, 123.2, 123.0, 122.7, 121.8, 121.1, 120.9, 120.6, 119.94, 119.87, 119.6, 118.7, 117.6, 115.6, 107.0, 55.4, 40.1, 26.0, 23.1, 13.9. HRMS calcd for $C_{66}H_{63}N_3O_2S_2$ $[M]^+$ m/z 993.4356 found 993.4326.

Synthesis of (E)-3-(6-(5-(10-butyl-10H-phenothiazin-3-yl)thiophen-2-yl)-4-(9,9-dibutyl-9H-fluoren-2-yl)-4H-dithieno[3,2-b:2',3'-d]pyrrol-2-yl)-2-cyanoacrylic acid ***(JS8)***

It was prepared **12** (0.150 g, 0.18 mmol) by following a procedure similar to that described above for **JS1**. Black solid; yield (0.120 g, 81%); mp 269-270 °C; IR (KBr, cm^{-1}) 2212 ($\nu_{C\equiv N}$); ^{1}H NMR (500 MHz, DMSO-d_6) δ 0.55-0.62 (m, 4 H), 0.70 (t, *J* = 7.5 Hz,

6 H), 0.80 (t, *J* = 7.5 Hz, 3 H), 1.11 (quint, *J* = 4.5 Hz, 4 H), 1.14 (sex, *J* = 7.5 Hz, 2 H), 1.67 (quin, *J* = 7.0 Hz, 2 H), 2.00-2. 05 (m, 2 H), 2.17-2.21 (m, 2 H), 3.88 (t, *J* = 7.0 Hz, 2 H), 6.95 (t, *J* = 7.5 Hz, 1 H), 7.03-7.05 (m, 2 H), 7.15-7.16 (m, 1 H), 7.19-7.22 (m, 1 H), 7.36-7.39 (m, 3 H), 7.41-7.47 (m, 4 H), 7.49-7.51 (m, 1 H), 7.66-7.68 (m, 1 H), 7.86 (d, *J* = 1.5 Hz, 1 H), 7.91-7.93 (m, 1 H), 8.04-8.06 (m, 1 H), 8.15 (s, 1 H), 8.49 (s, 1 H); ^{13}C NMR (100.53 MHz, $CDCl_3$) δ 153.3, 150.8, 140.9, 139.9, 137.0, 127.9, 127.3, 123.1, 122.4, 121.1, 120.1, 120.0, 118.9, 117.9, 116.1, 113.3, 110.4, 55.5, 40.2, 26.2, 23.1, 14.0. HRMS calcd for $C_{53}H_{47}N_3O_2S_4$ $[M+H]^+$ m/z 886.2623 found 886.2602.

Synthesis of (E)-3-(6-(5-(9-butyl-9H-carbazol-3-yl)thiophen-2-yl)-4-(9,9-dibutyl-9H-fluoren-2-yl)-4H-dithieno[3,2-b:2',3'-d]pyrrol-2-yl)-2-cyanoacrylic acid ***(JS9)***

It was obtained from **13** (0.150 g, 0.18 mmol) by following a procedure similar to that described above for **JS1**. Black solid; yield (0.150 g, 90%); mp 252-254270 °C; IR (KBr, cm^{-1}) 2210 ($\nu_{C\equiv N}$); ^{1}H NMR (500 MHz, DMSO-d_6) δ 0.56-0.67 (m, 4 H), 0.71 (t, *J* = 7.5 Hz, 3 H), 1.13 (sex, *J* = 7.5 Hz, 4 H), 1.29 (sex, *J* = 7.5 Hz, 2 H), 2.17-2.22 (m, 2 H), 4.39 (t, *J* = 7.0 Hz, 2 H), 7.22 (t, *J* = 7.22 Hz, 1 H), 7.36-7.39 (m, 3 H), 7.46-7.47 (m, 2 H), 7.49-7.51 (m, 1 H), 7.54 (d, *J* = 6.5 Hz, 1 H), 7.60-7.64 (m, 2 H), 7.67-7.69 (m, 1 H), 7.73 (d, *J* = 8.0 Hz, 1 H), 7.87 (d, *J* = 1.5 Hz, 1 H), 7.91-7.93 (m, 1 H), 8.14 (s, 1 H), 8.18, (d, *J* = 7.5 Hz, 1 H), 8.44 (s, 1 H), 8.46 (s, 1 H); ^{13}C NMR (100.53 MHz, DMSO-d_6) δ 164.7, 152.9, 151.0, 148.3, 145.4, 143.2, 141.4, 141.1, 140.3, 140.0, 137.4, 135.2, 134.1, 128.0, 127.7, 126.3, 124.6, 123.8, 123.1, 122.4, 122.2, 121.9, 120.9, 120.7, 118.0, 117.8, 117.4, 115.5, 110.3, 110.1, 95.0, 79.8, 79.6, 55.6, 42.6, 31.2, 26.4, 23.0, 20.3, 14.4, 14.2. HRMS calcd for $C_{53}H_{47}N_3O_2S_3$ $[M+Na]^+$ m/z: 876.2723 found 876.2731.

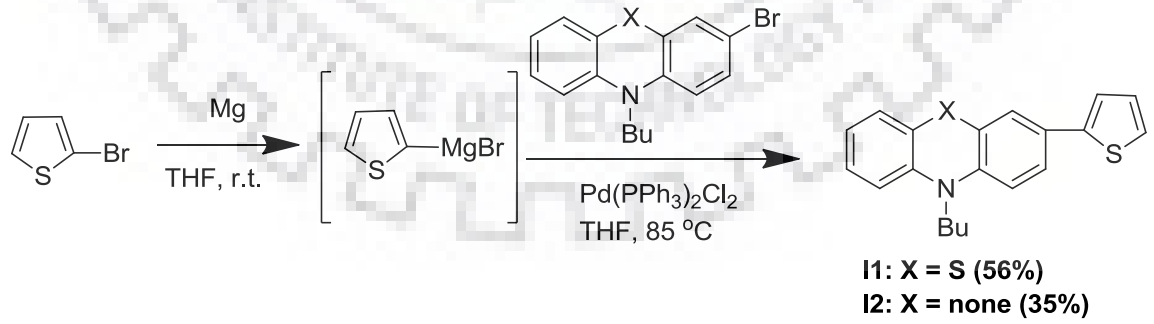

Scheme 3.2 Synthesis of thienylheterocyclic derivatives.

Synthesis of 10-butyl-3-(thiophen-2-yl)-10H-phenothiazine ***(I1)***

A mixture of activated Mg (0.472 g, 19.62 mmol), and dry 20 mL of THF under the N_2 atmosphere was stirred for 10 minutes at room temperature. Then to this reaction

mixture (2.60 g, 15.95 mmol) 2-bromothiophene was added drop wise by syringe at 10-20 °C. After the completion of addition reaction mixture was allowed to stir for 60 minutes. This Grignard reagent formed was added to another 250 mL two neck RB. which had already contained (4.1 g, 12.26 mmol) 3-bromo-10-butyl-10*H*-phenothiazine, $Pd(PPh_3)_2Cl_2$ (0.129 g, 0.184 mmol) in 40 mL THF under N_2 atmosphere immediately and finally it was kept at 85 °C under refluxed conditions for 24 hrs. The reaction was monitored by TLC. After the completion of reaction, reaction mixture was diluted with chloroform and washed with water three times and finally with brine solution. The organic layer was separated and dried over Na_2SO_4 and solvent was evaporated by rotary evaporator. The crude product obtained after the evaporation further purified by column chromatography. Light green solid; yield (2.0 g, 56%). mp 66-68 °C; ^{1}H NMR (399.78 MHz, DMSO-d_6): δ 0.86 (t, *J* = 7.2 Hz, 3H), 1.35-1.40 (m, 2H), 1.65 (t, *J* = 7.2 Hz, 2 H), 3.86 (t, *J* = 7.2 Hz, 2 H), 6.91-6.95 (m, 1 H), 7.1 (d, *J* = 8.0 Hz, 2 H), 7.07-7.09 (m, 1H), 7.13-7.15 (m, 1 H), 7.17-7.21 (m, 1 H), 7.40-7.46 (m, 4 H)); ^{13}C NMR (100.53 MHz, $CDCl_3$): δ 144.47, 144.11, 142.42, 128.57, 128.36, 127.85, 127.28, 124.99, 124.90, 124.40, 123.73, 123.02, 122.97, 122.69, 116.21, 115.94, 46.25, 28.40, 19.47, 13.73. HRMS calcd for $C_{20}H_{19}NS_2$ $[M]^+$ m/z 337.0959 found 337.0943.

Synthesis of 9-butyl-3-(thiophen-2-yl)-9H-carbazole ***(I2)***

It was prepared from 3-bromo-9-butyl-9*H*-carbazole (5.0 g, 16.5 mmol) by following a procedure similar to that described above for **I1.** green colored solid; yield (1.4g, 35%); mp 42-43 °C; ^{1}H NMR (500 MHz, $CDCl_3$) δ 0.98 (t, *J* = 7.5 Hz, 3 H) 1.38-1.44 (m, 2 H), 1.84-1.90 (m, 2 H), 7.12 (dd, *J* = 2.0, 3.5 Hz, 1 H), 7.25-7.28 (m, I H), 7.35 (dd, *J* = 1.0, 2.5 Hz, 1 H), 7.38-7.42 (m, 2 H), 7.47-7.50 (m, 1 H), 7.73 (dd, *J* = 1.0, 6.5 Hz, 1 H), 8.15 (d, *J* = 7.5 Hz, 1 H), 8.34 (d, *J* = 7.0 Hz, 1 H);); ^{13}C NMR (123.55 MHz, $CDCl_3$): δ 145.90, 140.96, 140.06, 128.03, 125.97, 125.71, 124.33, 123.65, 123.29, 122.84, 122.06, 120.57, 119.05, 117.94, 109.00, 108.93, 42.97, 31.19, 20.61, 13.93. HRMS calcd for $C_{50}H_{46}N_2OS_3$ $[M]^+$ m/z 3.5.1238 found 305.1246.

3.4.3 Computational methods

The computational methodology used is similar to that described in Chapter 2.

3.4.4 Fabrication and characterization of DSSC

The DSSCs were fabricated and characterized by following the procedures detailed in Chapter 2 for the dyes **JS1-JS5**.

Chapter 4

Effect of electron deficient π-linkers and position of benzothiadiazole in the optical and photovoltaic properties of dithienopyrrole-based sensitizers

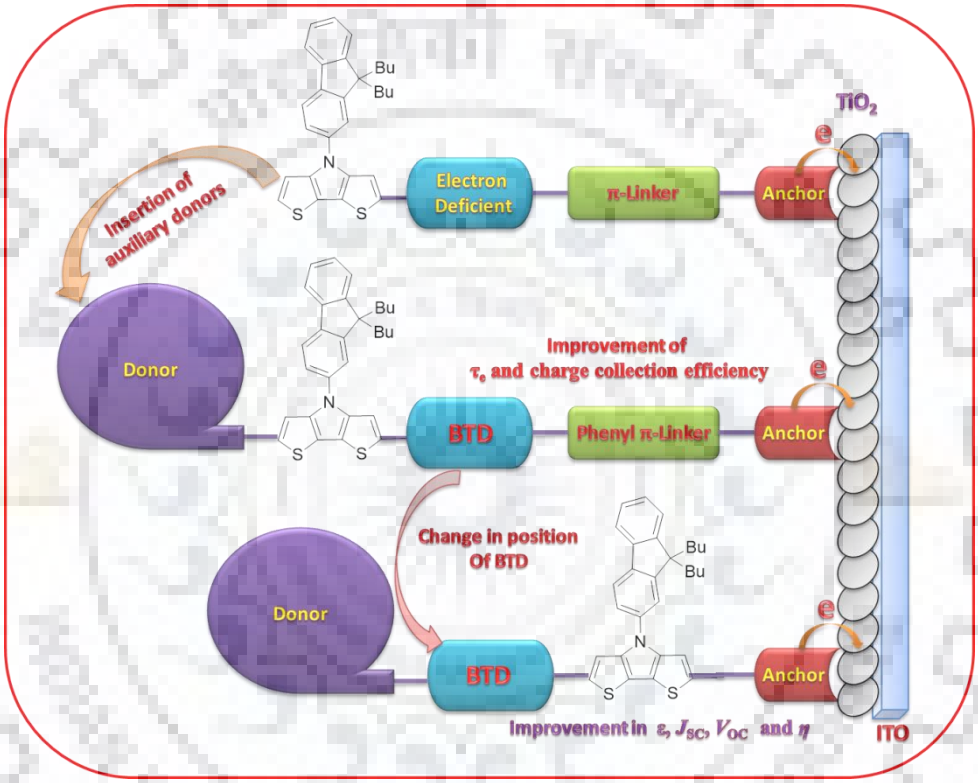

4.1 Introduction

Organic dyes usually feature a D-π-A molecular configuration which contains an electron-rich donor (D), π-conjugation linker (π) and electron-deficient acceptor (A) [13,14,42]. So far many attempts have been made to modify the structural elements either by increasing the electron donor or acceptor ability or efficiently extending the conjugation between donor and acceptor to optimize the light-harvesting of organic dyes in solar photon-flux spectrum effectively [4,5]. In comparison to the extension of conjugation by simple aromatic ring, insertion of an auxiliary acceptor between donor and π-linker can modulate the band gap of the dyes effectively [136]. Moreover, the shifting of absorption from visible to NIR can be obtained when the π-conjugating donor connect

with auxiliary acceptor covalently in organic dyes [1,192]. Thus, in D-A-π-A framework, an auxiliary acceptor decreases the HOMO-LUMO gap and improves the light absorption profile. The D-A-π-A architecture imposes the advantages not only (a) efficient tuning of the energy band, but also (b) facilitate charge transfer (c) enhance the dye-stability and (d) photovoltaic efficiency with additional acceptor [193]. In this regard Zhu and coworkers incorporated an auxiliary acceptor in D-A-π-A motif to synthesize the dyes **WS-1**–**WS-4** (Figure 4.1) [18]. The incorporation of auxiliary acceptors was found to be favorable for improving the photophysical, electrochemical and photovoltaic properties along with photo and thermal stabilities of the dyes as compared to the D-π-A reference dye **LS-1**.

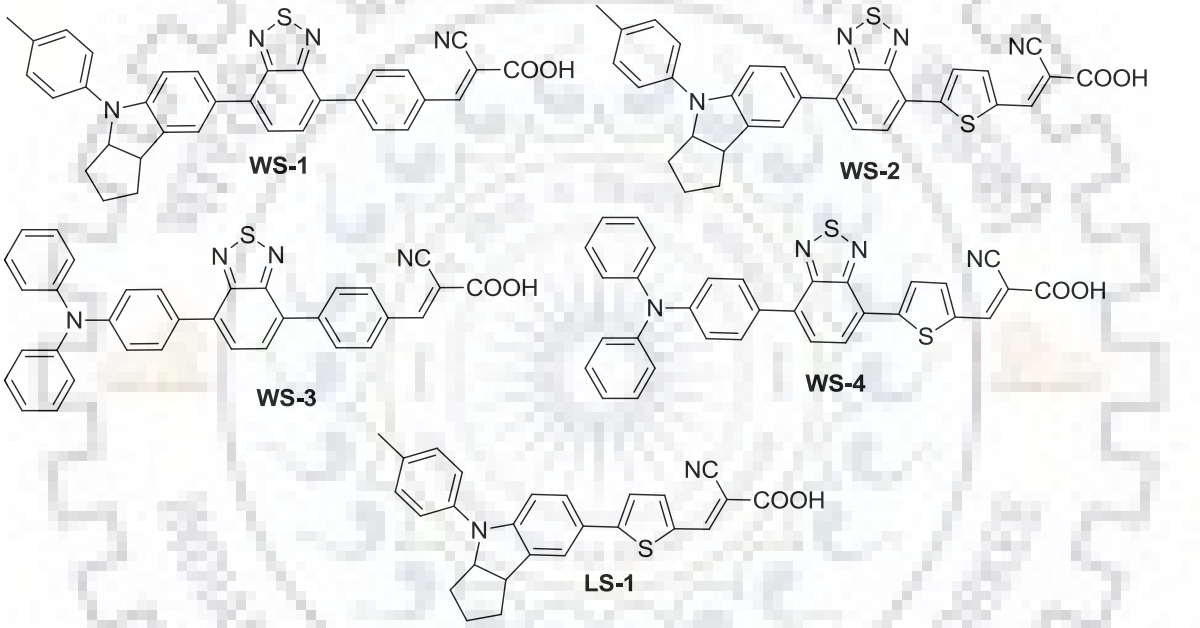

Figure 4.1 Structure of the dyes containing benzothiadiazole [192].

Thereafter, a number of organic dyes in D-A-π-A motif were developed and studied as sensitizers for DSSCs [193]. The most common acceptors such as benzothiadiazole (BTD) [194,195], benzotriazole (BTZ) [196-198] quinoxaline (Qx) [199,200], diketopyrrolopyrrole (DPP) [201,202], benzoxadiazole (BOD) [203,204], etc. were extensively used in D-A-π-A configuration of the dyes. Zhu and coworkers [193] also systematically summarized the use of benzothiadiazole (BTD), benzotriazole (BTZ), quinoxaline (Qx), and benzoxadiazole (BOD) in D-A-π-A motif containing electron rich indoline derivative as donor and thienyl as π-linker (Figure 4.2). It was found that the electron accepting nature of auxiliary acceptor made a significant impact on the HOMO of donor and LUMO for acceptor part. The light harvesting efficiency and IPCE for the

dyes followed the order of BOD > BTD > Qx > BTZ. This trend was exactly matching with the electron accepting natures of the acceptor as BOD > BTD > Qx > BTZ, calculated from theoretical simulations and experimental evidences [205,206].

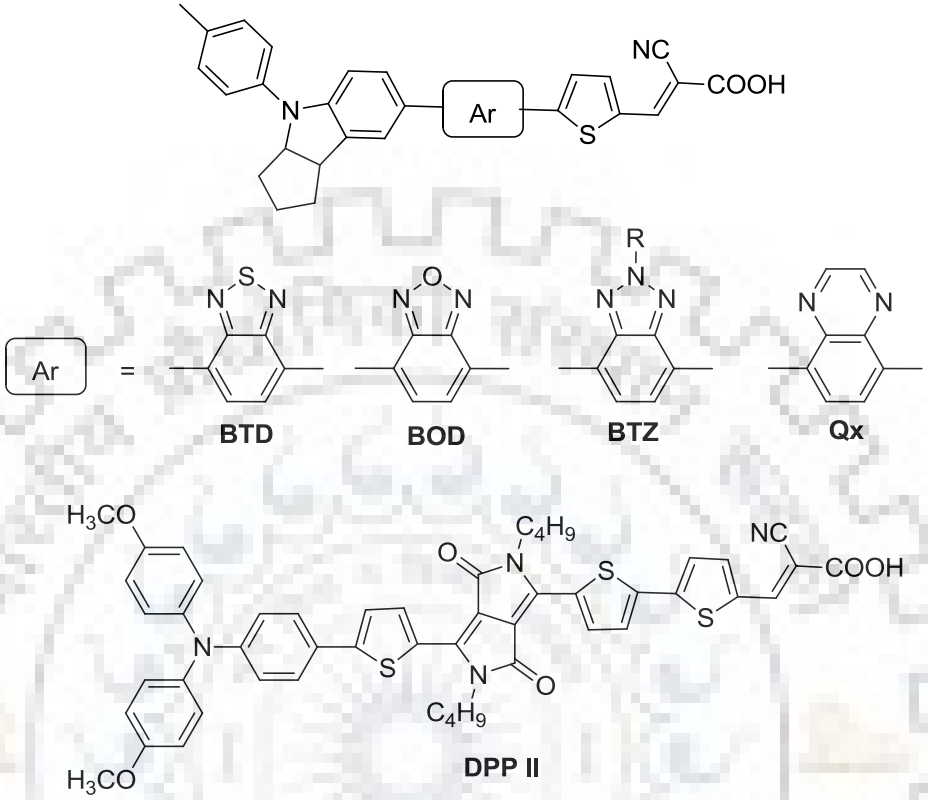

Figure 4.2 D-A-π-A Motif of the dyes with different electron withdrawing units [207].

However, Tian et al. [207] utilized strong electron-withdrawing diketopyrrolopyrrole (DPP) unit to develop **DPP II** dye (Figure 4.2). Apart from the extended absorption upto 627 nm, the inferior photocurrent density 2 mA cm^{-2} and efficiency < 0.7% were obtained for **DPP II**. Here, strong withdrawing nature of DPP unit lowered the LUMO energy level to -0.56 V that suppressed the electron injection into the conduction band of TiO_2. Even though, DPP unit have been extensively used as building block for developing the sensitizers for DSSCs to its utilized strong electron withdrawing nature [208-211].

Bäurle and Grätzel et al. [212] synthesized **Dye I** and **Dye II** (Figure 4.2) in which BTD unit was used in two D-A-π-A and D-π-A-A motifs, respectively and compared the electron injection and recombination dynamics. It was recognized that the **Dye I** containing BTD unit close to the anchoring group showed red shifted absorption as compared to **Dye II** having phenyl unit between BTD and anchoring group. Although

both dyes showed almost 95% injection yield, the **Dye I** exhibited poor photovoltaic performance. The transient laser photolysis experiments exposed the rapid recombination of the injected electrons with oxidized dye which is responsible for the inferior performance of the **Dye I**. Further Grätzel and coworkers explored the importance of phenyl unit between BTD and anchoring group to develop the Zn-porphyrin based **GY21** and **GY50** dyes to achieve the high efficiency [213].

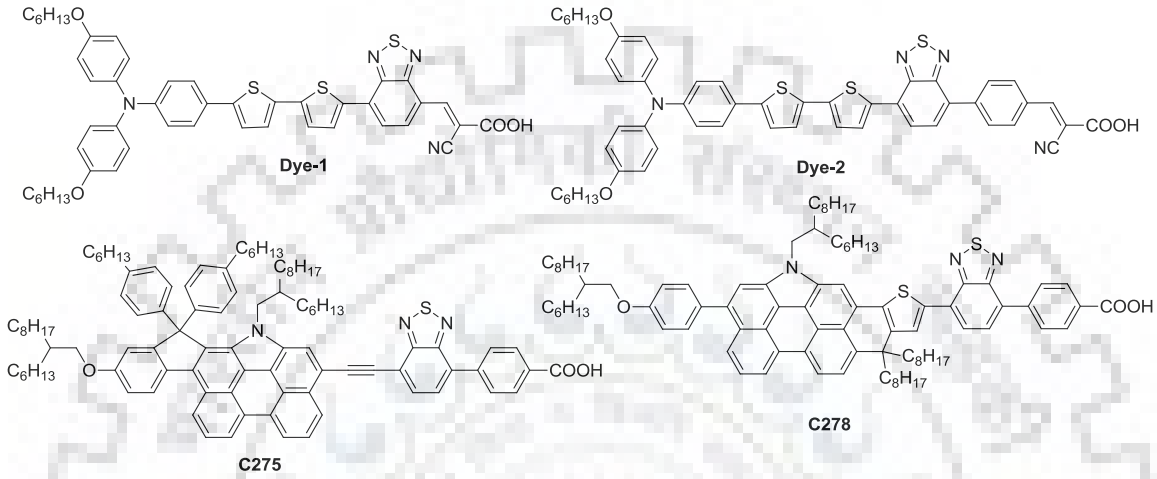

Figure 4.3 Structures of the organic dyes containing BTD units [212,23].

Moreover the use of BTD unit in D-A-π-A based sensitizer have produced the long term stability of 5000h in aging test at 65 °C under one sun condition [214]. Thus the development of D-A-π-A is the reliable strategy to develop the efficient and stable sensitizers for DSSCs. A record efficiency >12.0% was achieved from the D-A-π-A motif dyes by utilizing benzothiadiazole as auxiliary acceptor and *N*-annulated indenoperylene (dye **C275**) [19] or *N*-annulated thienocyclopentaperylene (dye **C278**) [23] as donor (Figure 4.3).

By keeping the aforementioned points in our mind, in this Chapter, we explored the hitherto unknown dyes D-A-π-A where DTP was used as a donor via *C*-linkage. Auxiliary acceptors such as BTZ, Qx and BTD were used along with thiophene or phenyl unit to compose the conjugation bridge. However, the use of auxiliary acceptors in combination with thienyl linker proved to be beneficial for broadening the absorption spectra. But, the importance of BTD unit in conjugation with phenyl linker [212,213] was utilized to further develop D-D-A-π-A dyes by the addition of TPA and DPF donors at C6 position of DTP in BTD dye **JS14**. Here, we also synthesized regioisomers, by varying the position of BTD in D-π-D-A dyad which resulted in strong improvement in

photophysical, electrochemical and photovoltaic performances. A dye containing BTD amidst of TPA and DTP chromophores led to highest efficiency 7.57% in the series owing to the favorable thermodynamic driving force for electron injection and structural elements helpful to retard electron recombination.

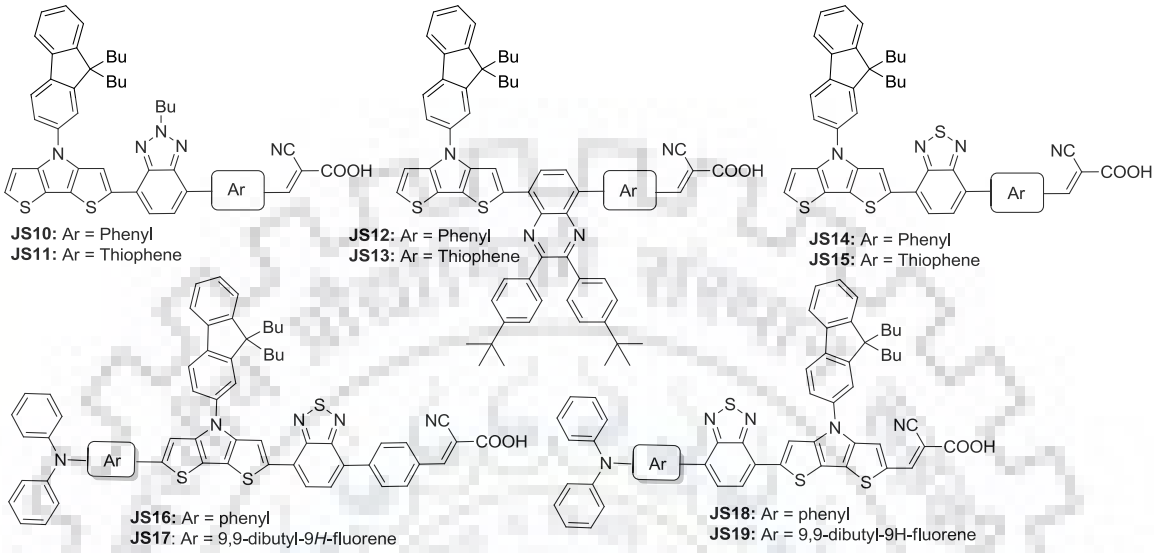

Figure 4.4 Structures of DTP donor based dyes containing different electron deficient π-spacers.

4.2 Result and discussion

4.2.1 Molecular design and synthesis

The structures of the newly synthesized organic dyes containing dithienopyrrole donor and different π-conjugation bridges and cyanoacrylic acid acceptor are displayed in Figure 4.4. The methodology used to obtain the target dyes is outlined in Schemes 4.1 and 4.2. All the target dyes were obtained by multi-step sequence involving conventional reactions such as Vilsmeier-Haack formylation, Suzuki-Miyaura [179]/Stille [158] cross-coupling and Knoevenegal condensation. The aldehyde precursors **14-17** were synthesized by following Stille coupling protocol involving **3** and different bromo-arene/heteroarene-aldehydes **S1-S4**. The intermediate, 4-(7-(4-(9,9-dibutyl-9*H*-fluoren-2-yl)-4*H*-dithieno[3,2-*b*:2',3'-*d*]pyrrol-2-yl)benzo[*c*][1,2,5]thiadiazol-4-yl)benzaldehyde **(18)** was synthesized in reasonable yield by stochiometric controlled Stille coupling reactions between **3** and 4,7-dibromobenzo[*c*][1,2,5]thiadiazole. Subsequently, Suzuki or Stille reaction of **18** with (4-formylphenyl)boronic acid and (5-(1,3-dioxolan-2-yl)thiophen-2-yl)tributylstannane followed by acid hydrolysis gave corresponding aldehydes **19** and **20** precursors respectively.

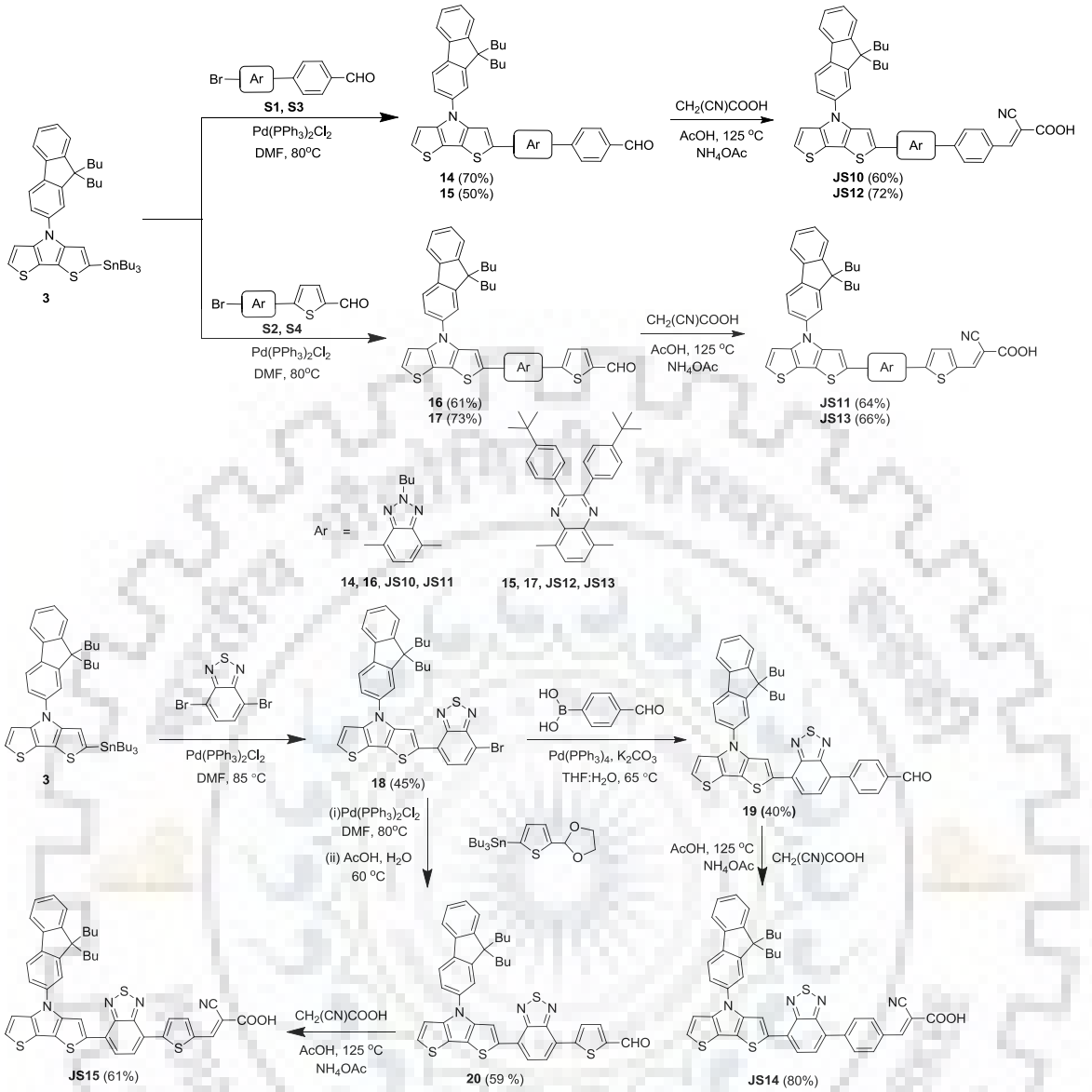

Scheme 4.1 Synthetic scheme of DTP donor based dyes **JS10-JS15** in D-A-π-A configuration.

On the other hand, the bromination of **19** by NBS yielded 4-(7-(6-bromo-4-(9,9-dibutyl-9*H*-fluoren-2-yl)-4*H*-dithieno[3,2-*b*:2',3'-*d*]pyrrol-2-yl)benzo[*c*][1,2,5]thiadiazol-4-yl)benzaldehyde (**21**) in reasonable amount. Whereas the 6-(7-bromobenzo[*c*][1,2,5]thiadiazol-4-yl)-4-(9,9-dibutyl-9*H*-fluoren-2-yl)-4*H*-dithieno[3,2-*b*:2',3'-*d*]pyrrole-2-carbaldehyde (**24**) was obtained by Vilsmeier-Haack formylation of **18**. Suzuki coupling reaction of (4-(diphenylamino)phenyl)boronic acid and (9,9-dibutyl-7-(diphenylamino)-9*H*-fluoren-2-yl)boronic acid with **21** and **24** produced the aldehydes **22**, **23**, **25** and **26** respectively.

Finally, all the precursor aldehydes **14-17, 22**, **23**, **25** and **26** were converted into the target dyes **JS10-JS19** respectively by reacting with cyanoacetic acid in the presence of catalytic amount of ammonium acetate. The new compounds were thoroughly characterized by NMR spectroscopy, FT-IR, and HR mass spectra. The proposed structures of the newly synthesized compounds were found to be consistent with the observed spectral data.

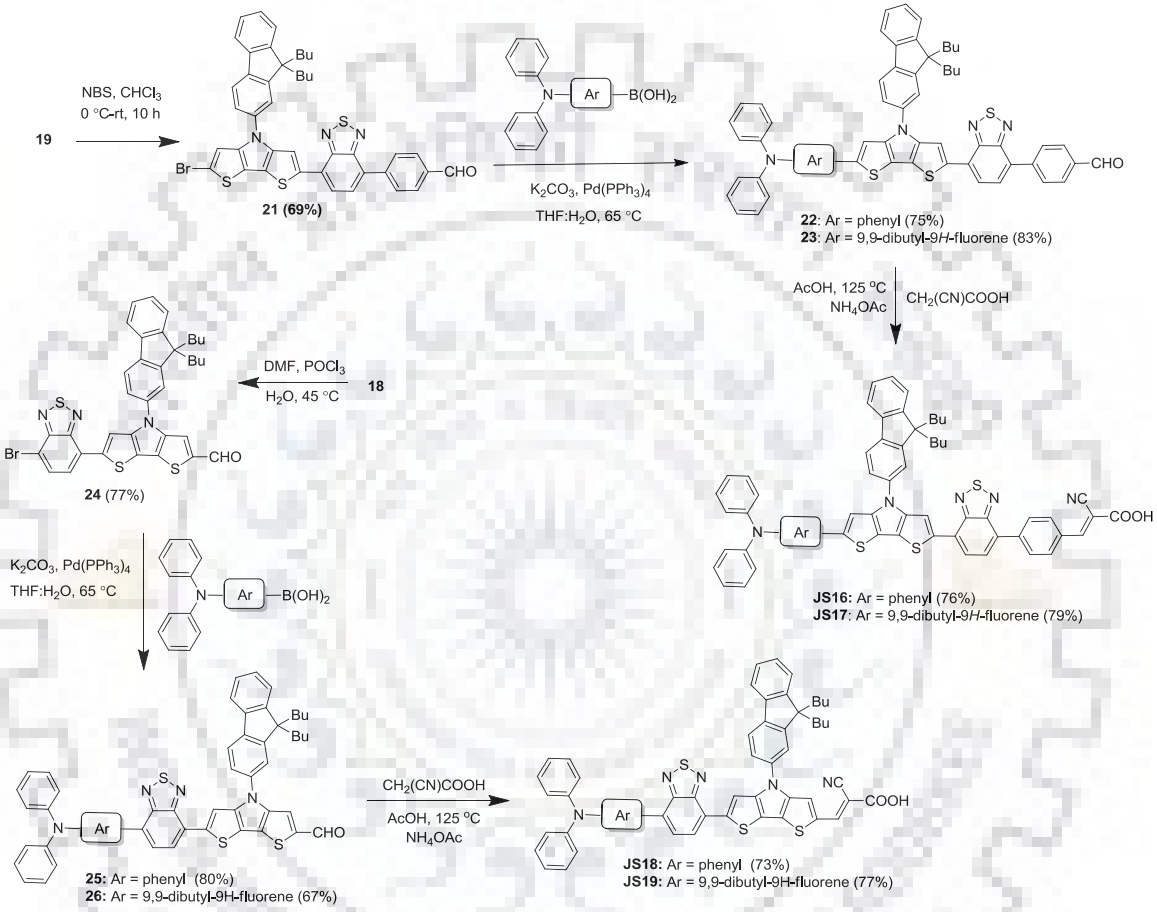

Scheme 4.2 Synthetic scheme of DTP based dyes **JS16-JS19** in D-A-D-A configuration.

4.2.2 Optical Properties

To investigate the light harvesting efficiency of the synthesized dyes, the absorption spectra were recorded in THF and displayed in Figures 4.5 and 4.6 and the pertinent data are compiled in Table 4.1. Generally, all the dyes exhibited prominent absorption peaks in the region of 285-650 nm. The absorption peaks appearing at shorter wavelength region (<400 nm) can be assigned to π-π* electronic transition arising from different aromatic segments present in the dyes. The absorptions in the longer wavelength region (above 403 nm) are ascribed to the intramolecular charge transfer (CT) from DTP donor to the cyanoacrylic acid acceptor [42]. Amongst the first set of D-A-π-A dyes, the dyes

containing thienyl π-linker (**JS11, JS13** and **JS15)** exhibited broader absorption profile as compared to phenyl-linked dyes (**JS10, JS12** and **JS14)**. This may be due to the presence of electron-rich thienyl π-linker which facilitate the electronic communication between DTP donor and cyanoacrylic acceptor due to its planar arrangement [205]. On the other hand in case of **JS10, JS12** and **JS14** dyes, the twisted phenyl units reduced the donor-acceptor interactions and shift the ICT absorption band to the high energy region. Further, the BTD dyes (**JS14** and **JS15**) when compared to the similar BTZ and Qx-dyes displayed relatively bathochromic shift for the ICT band. This behavior could be rationalized to the high electron-accepting nature of BTD unit than BTZ or Qx units, [193,205] which was beneficial for enhancing the donor-acceptor interactions, and to shift the absorption to longer wavelength [206]. Next, the addition of auxiliary TPA and DPF donor at peripheral C6-position of the DTP unit of **JS14** into D-D-A-π-A dyad induced a bathochromic shift for longer wavelength along with reduction in molar extinction coefficient for absorption maxima for the dyes **JS16** and **JS17**. However, this hypochromic effect on absorption maxima was compensated by the appearance of new intense bands ca. 390 nm due to the new charge transfer propensities auxiliary aryl amine donor to BTD acceptor (*vide infra*). Moreover, isomeric change of BTD position from D-D-A-π-A dyad to amidst of donor and DTP in D-A-D-A motif not only exerted the bathochromic shift for the longer absorption but also rendered the enhancement in the molar extinction coefficient for the dyes **JS18** and **JS19.** This was attributable to the effective conjugation and charge transfer propensity from arylamine donor to cyanoacrylic acceptor through DTP unit. In comparison to TPA congeners, the DPF dyes exhibited high molar extinction coefficient due to the presence of electron rich fluorene conjugating bridge which increases the charge transfer probability of DTP donor to cyanoacrylic acceptor [139,192].

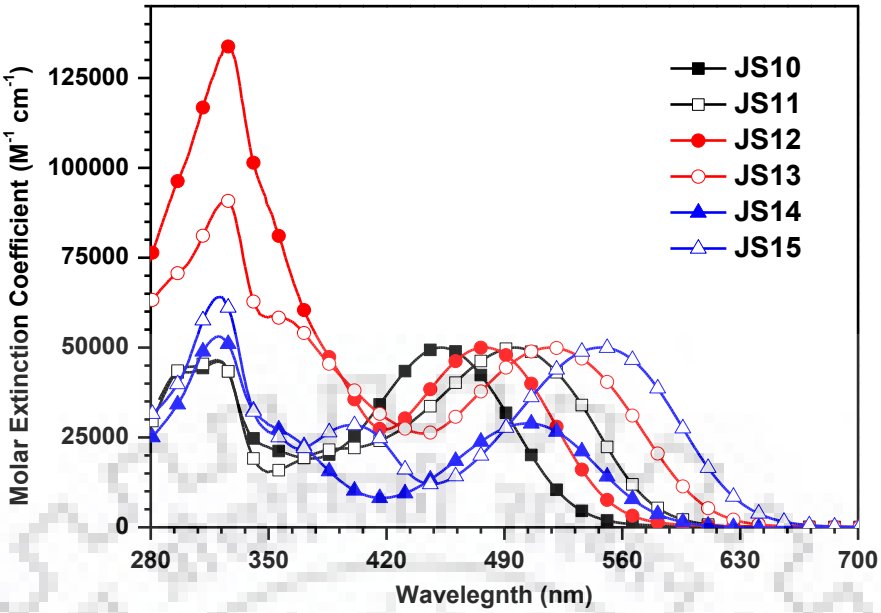

Figure 4.5 Absorption spectra of the dyes **JS10-15** recorded in THF.

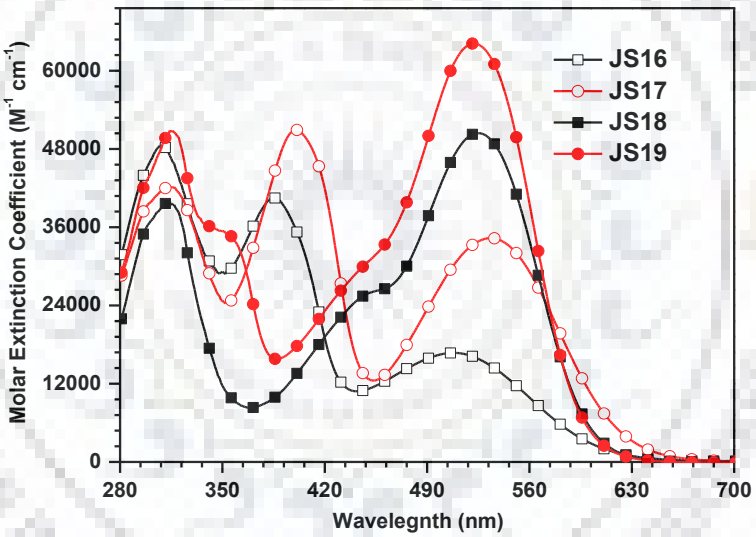

Figure 4.6 Absorption spectra of the dyes **JS16-19** recorded in THF.

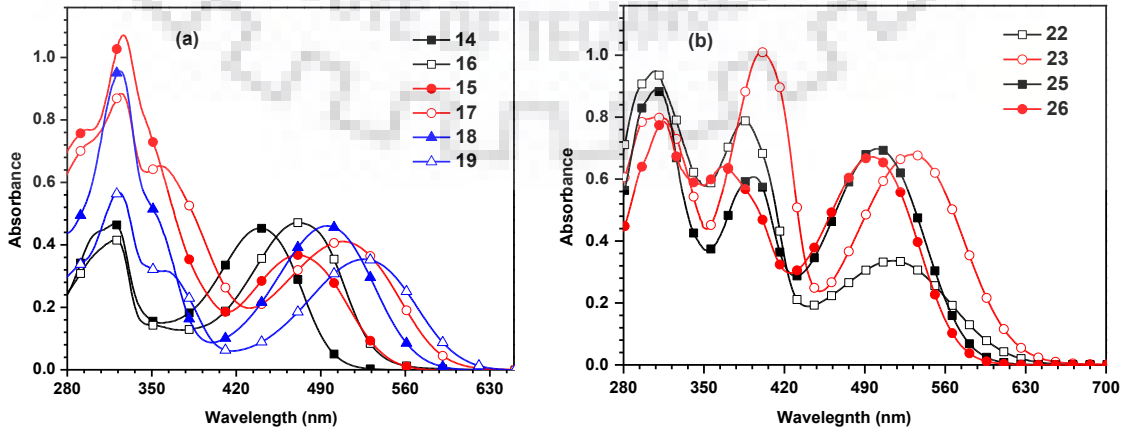

Figure 4.7 Absorption spectra of the aldehyde precursors (a) **14-19** and (b) **22-26**.

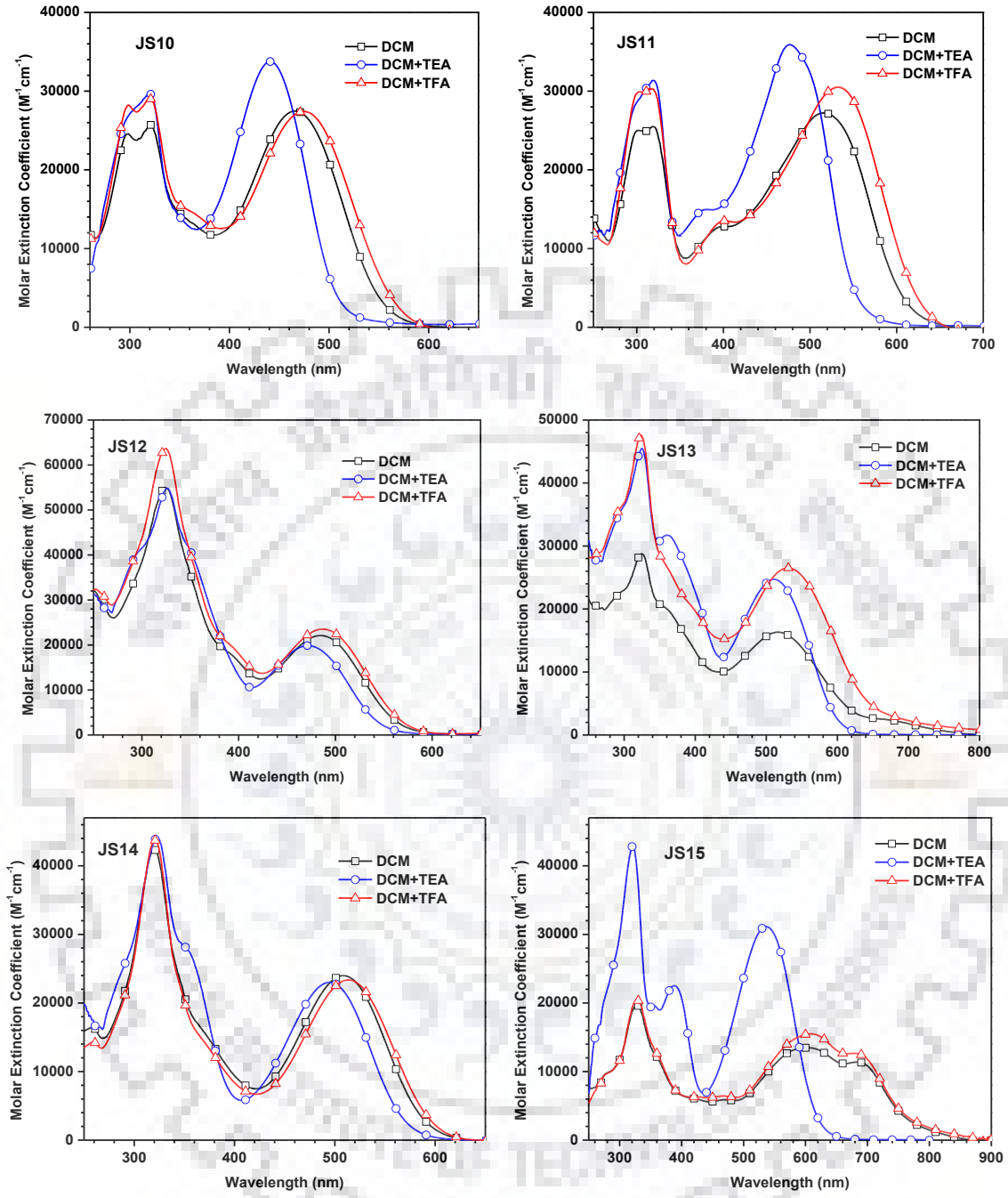

Figure 4.8 Absorption spectra of the dyes **JS10-15** recorded in DCM before and after the addition of TEA/TFA.

The charge-transfer character of the longer wavelength absorptions was confirmed by comparing the absorption spectra with their respective aldehyde precursors (Figure 4.7). A bathochromic shift for the absorptions was noticed on converting the aldehyde to cyanoacrylic acid group. This could not be aroused only due to the extension in conjugation. Further, the acid-base equilibrium analyses by recording the absorption

spectra of the dyes in the presence of TFA/TEA were carried out. The dyes **JS10-JS15** displayed blue-shift on addition of TEA and a slight red-shift with TFA for the CT absorption (Figure 4.8). These were attributed to decrement/increment in the acceptor strength originating from the deprotonation/protonation on addition of TEA/TFA. In contrast, no such a significant effect was observed with TEA/TFA addition for the dyes **JS16-JS19** (Figure 4.9). All the dyes exhibited negative solvatochromism in the ground state attributable to the effective solvation of the dyes in ground state by more polar solvents (Figure 4.10 and 4.11) [159]. Also, these dyes showed distinctively blue-shifted absorption in MeOH and DMF arising from the hydrogen-bonding and basic nature of the solvent, respectively. Additionally, the most red-shifted absorption was observed in chlorinated solvent (DCM) owing to the fast reorganization of polarized electrons in the excited state of the dyes [160].

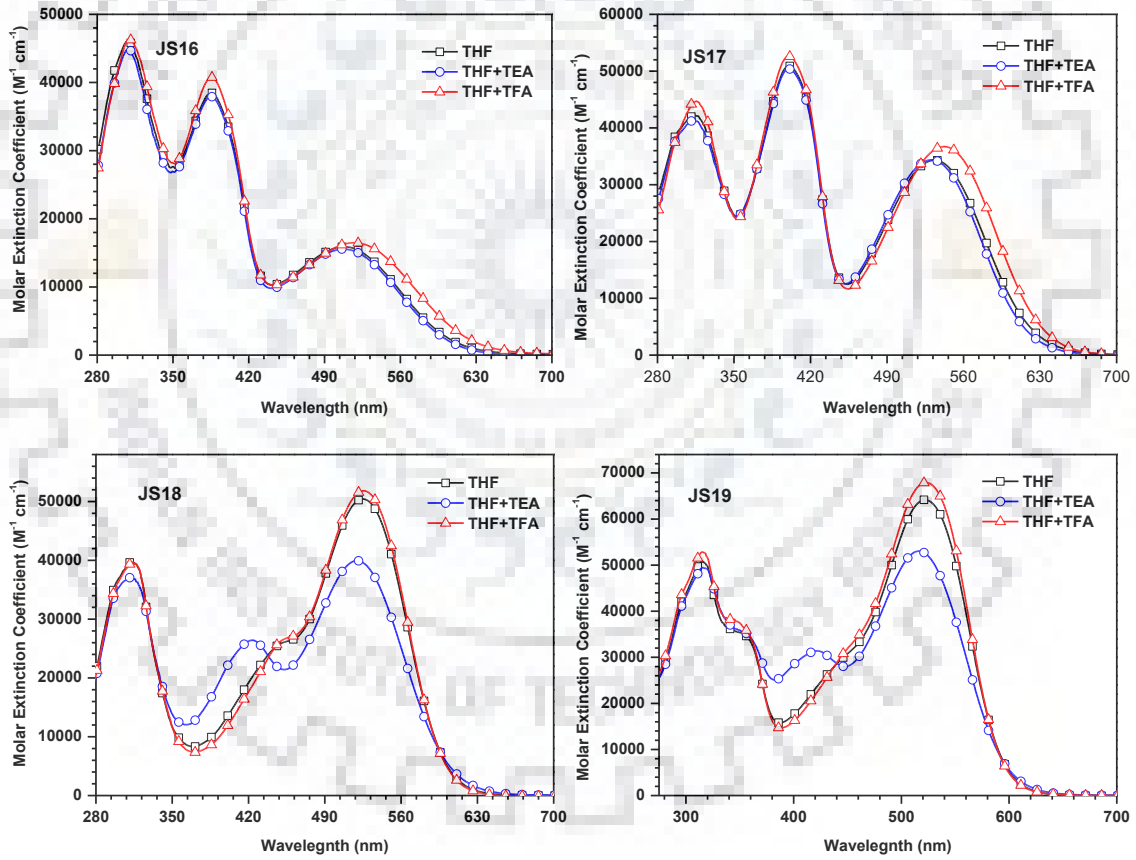

Figure 4.9 Absorption spectra of the dyes **JS16-JS19** recorded in THF before and after the addition of TEA/TFA.

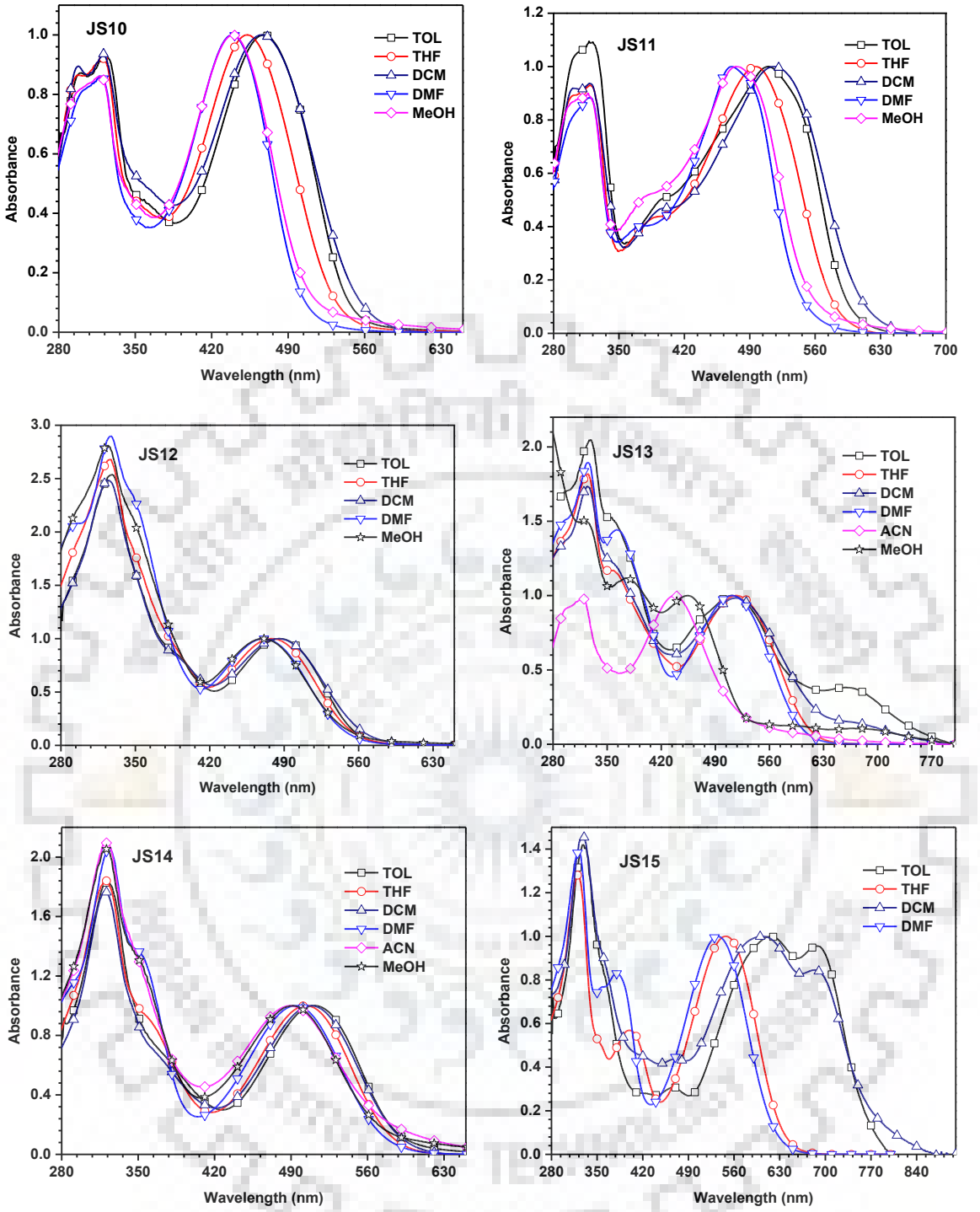

Figure 4.10 Normalized absorption spectra of the dyes **JS10-JS15** recorded in the solvents of different polarities.

The absorption spectra of the dyes recorded on mesoporous thin film of nanocrystalline TiO_2 and displayed in Figure 4.12. The absorption maxima recorded on TiO_2 were red-shifted and broadened as compared to the absorptions of the dyes in solution. This can be attributed to the *J*-aggregation of the dyes on TiO_2 surfaces [161]. The D-A-π-A dyes (**JS18** and **JS19**) were weakly emissive (Figure 4.13a) in the solution

and the trend of emission peaks is similar to that observed for absorption. But the dyes **JS16-JS19** showed opposite emission trend from the absorptions in THF (Figure 4.13b) and also the positive solvatochromism for emission in the solvents of varying polarities (Figure 4.14). This behavior of the dyes specified the polar excited states for the dyes **JS16-JS19** which were prone to dipole-dipole relaxation with the solvent dipoles [186].

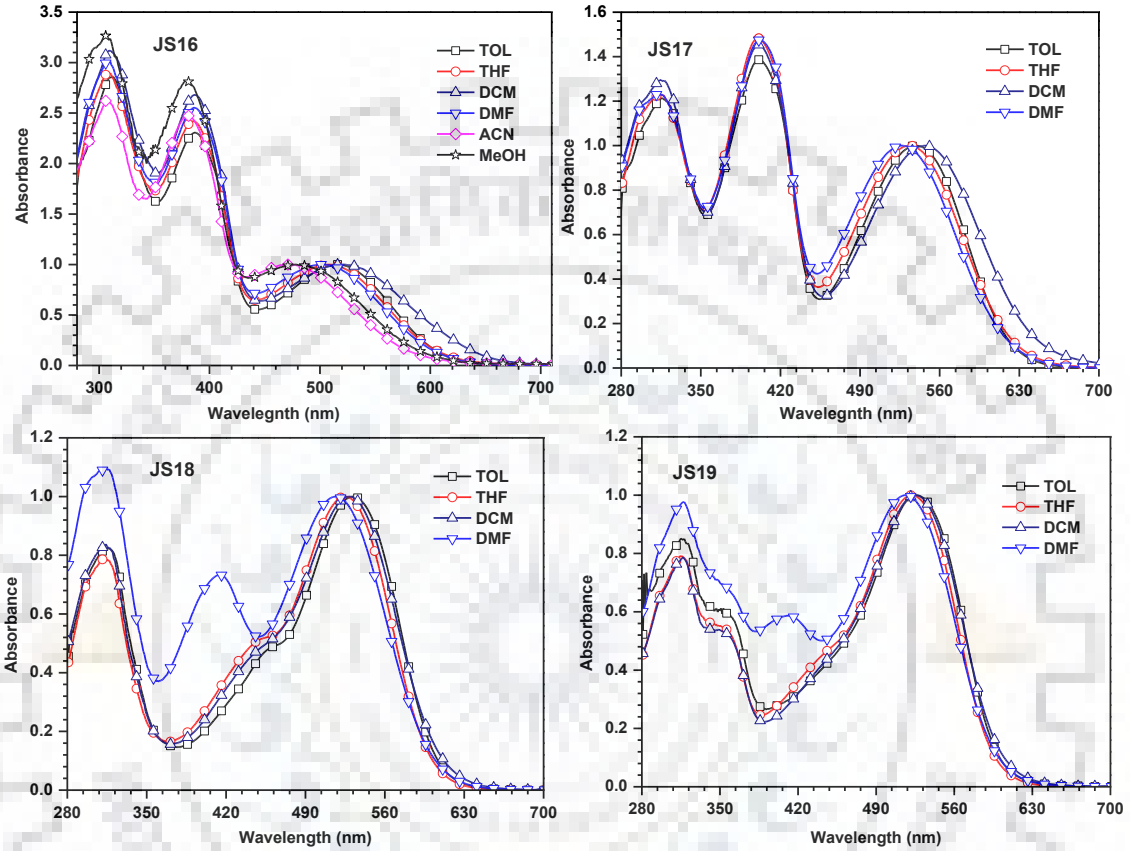

Figure 4.11 Normalized absorption spectra of the dyes **JS16-JS19** recorded in the solvents of different polarities.

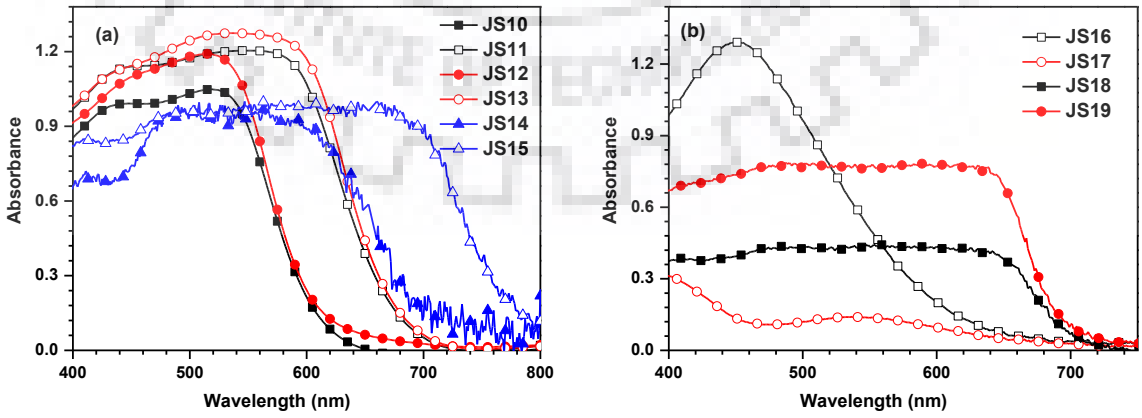

Figure 4.12 Absorption spectra of the dyes (a) **JS10-JS15** and (b) **JS16-JS19** anchored on nanocrystalline TiO_2

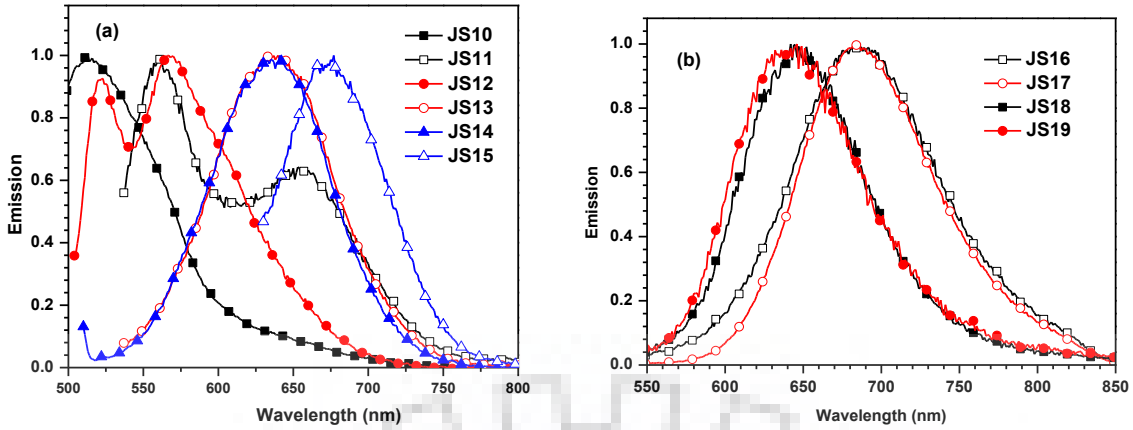

Figure 4.13 Emission spectra of the dyes (a) **JS10-JS15** and (b) **JS16-JS19** recorded in THF.

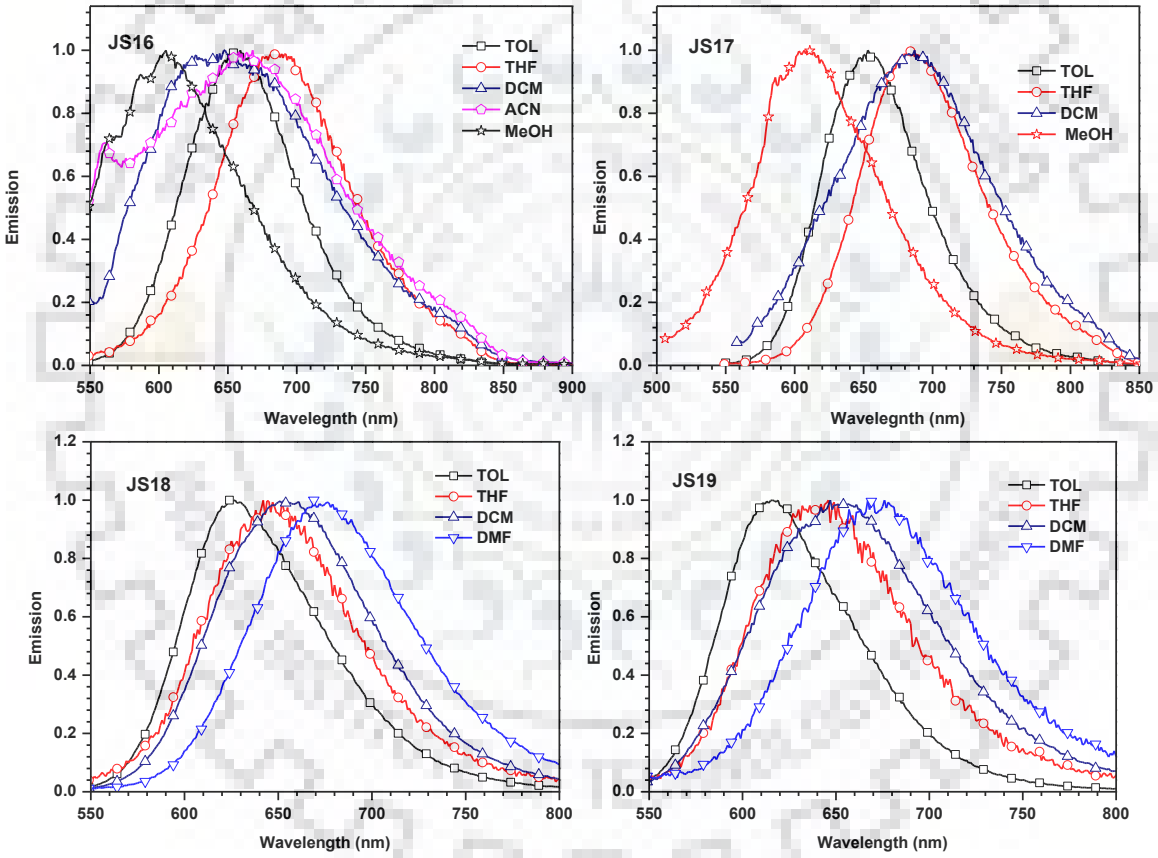

Figure 4.14 Emission spectra of the dyes **JS16-JS19** recorded in solvents of varying polarities.

Table 4.1 Optical and electrochemical data of the dyes **JS10-JS19**.

Dyes	$\lambda_{abs.}$ (nm ($\varepsilon_{max} \times 10^3$ $M^{-1}cm^{-1}$))	λ_{max}^{TiO2} (nm)	E_{OX} (mV (ΔE_p, mV)) [a]	E_{OX} (V) (Vs NHE)	HOMO (eV) [b]	LUMO (eV) [c]	$E_{0\text{-}0}$ (eV) [d]	E_{OX}* (V) [e]
JS10	452 (50.0), 320 (40.1), 298 (43.3)	520	425 (136)	1.195	-5.225	-2.720	2.505	-1.231
JS11	496 (50.0), 319 (46.6)	545	434 (135)	1.204	-5.234	-2.975	2.259	-1.055
JS12	478 (50.0), 327 (13.4)	515	428 (086)	1.198	-5.228	-2.816	2.412	-1.214
JS13	517 (50.0), 358 (58.8), 325 (90.9)	535	431 (083)	1.201	-5.231	-3.122	2.109	-0.908
JS14	503 (28.9), 321 (53.2)	581	480 (113)	1.250	-5.228	-3.052	2.172	-0.922
JS15	548 (50.), 400 (28.5), 322 (64.1)	617	504 (053)	1.274	-5.304	-3.414	1.890	-0.616
JS16	509 (16.7), 385 (40.5), 308 (48.5)	449	303 (75)	1.073	-5.103	-3.043	2.060	-0.987
JS17	534 (34.3), 400 (50.9),314 (42.2)	539	376 (104)	1.154	-5.180	-3.175	2.009	-0.855
JS18	525 (50.4), 445 (25.4), 312 (39.8)	642	556 (150)	1.326	-5.356	-3.244	2.112	-0.789
JS19	522 (64.2), 353 (35.0), 314 (50.8)	646	482 (135)	1.252	-5.282	-3.155	2.127	-0.875

[a] Oxidation potentials are reported with reference to the ferrocene internal standard.
[b] Deduced from the oxidation potential using the formula HOMO = -(4.8 + E_{OX})
[c] Deduced using the formula LUMO = HOMO + $E_{0\text{-}0}$.
[d] Calculated from intersection of absorption & emission spectra.
[e] Calculated from $E_{OX}^* = E_{OX} - E_{0\text{-}0}$ (Vs. NHE).

4.2.3 Electrochemical Properties

The molecular orbital energies give insightful information about the propensity of electron injection from the excited dyes into the CB of TiO_2 and regeneration of oxidized dyes by electrolyte. These parameters can be calculated from the oxidation and reduction potentials which correspond to HOMO and LUMO respectively. Therefore, we carried out the CV and DPV measurements on the dyes **JS10-JS15** and **JS16-JS19** in DCM and THF solutions respectively. The relevant parameters and the derived orbital energies are presented in Table 4.1. BTD and BTZ-based dyes showed a quasi-reversible oxidation while the Qx-containing dyes exhibited an irreversible oxidation attributable to the removal of an electron from dithienopyrrole donor (Figure 4.15 and 4.16). Irreversibility of the oxidation in Qx-based dyes indicates that they undergo severe reorganization upon oxidation. However for D-A-π-A dyes, the oxidation potentials for BTZ and Qx-dyes did not show variations attributable to the nature of electron-withdrawing linker. It apparently pointed that the electron-accepting ability of BTZ and Qx units were almost same [206]. However for the BTD-dyes showed high oxidation potentials attributable to the relatively high electron-accepting ability of BTD. Further, the nature of linker such as phenyl and thiophene units marked their presence in the oxidation potentials of the dyes. A slightly lower oxidation potentials were observed for the dyes containing phenyl linker attributable to the poor electronic communication between the donor and acceptor because of the tilting in the phenyl ring. Lack of strong interaction between the donor and acceptor makes the donor comparatively electron-rich and so oxidized easily. Further, addition of TPA and DPF donor lowered the oxidation potential due to augmented the electron density which facilitates the removal of electron for the dyes **JS16** and **JS17**. Conversely, position variations of BTD units significantly increase the oxidation potentials of the dyes **JS18** and **JS19** due the electron withdrawing ability of BTDs in the vicinity of arylamine donor. However, this effect is less pronounced in **JS18** due to twisted phenyl conjugation which suppress the donor-acceptor communication and facilitate the extraction of electron as compared to **JS19** (*vide supra*)**.**

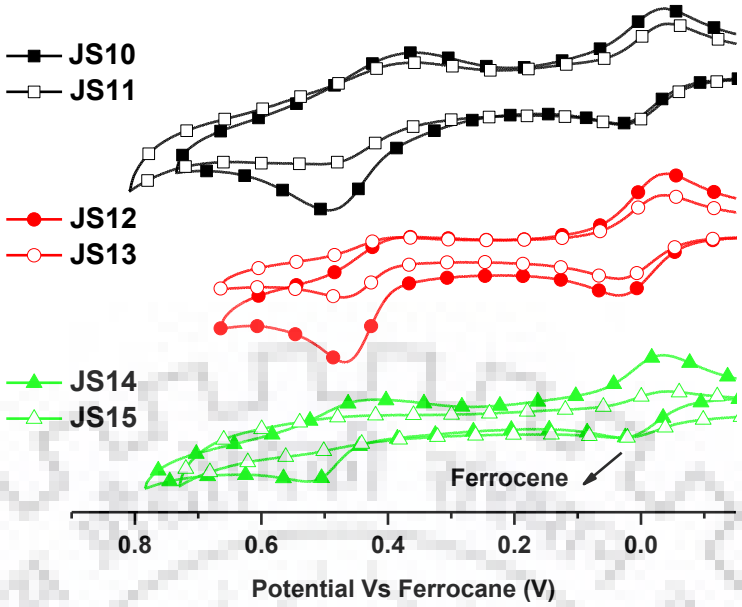

Figure 4.15 Cyclic voltammograms of the dyes **JS10-JS15** recorded in DCM.

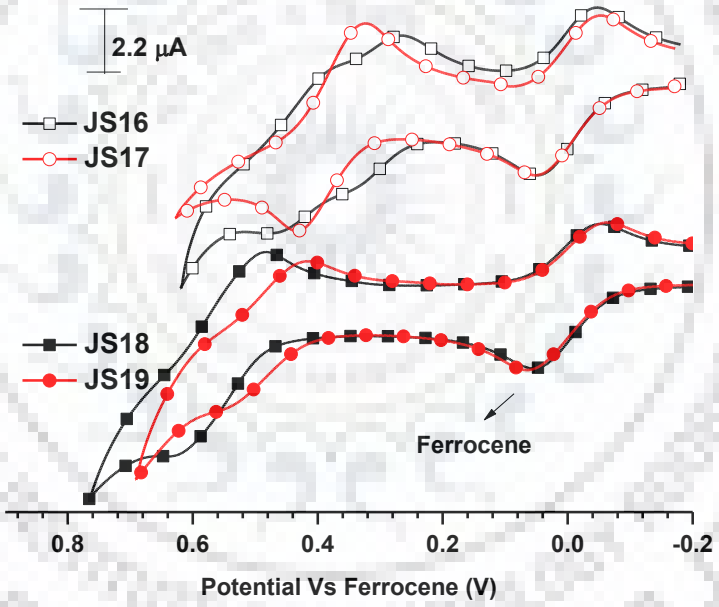

Figure 4.16 Cyclic voltammograms of the dyes recorded in THF.

It is interesting to note that the thienyl-linked dyes (**JS11, JS13** and **JS15**) exhibited lower E_{OX}* values than the corresponding phenyl analogues due to the better donor-acceptor interactions induced by the planar thienyl linker. The lowering of the E_{OX}* values resulted in decrease in the energy band gap for these dyes which is consistent with the absorption of these dyes. Similarly, better donor-acceptor interactions also affected the E_{OX}* values for the dyes **JS16-JS19**. Thus, as compared to the dye **JS18**, facile electronic communication in the **JS19** elevated the E_{OX}* values cathodically. The ground

state oxidation potentials for the dyes were sufficiently more positive (~1.20 V *vs.* NHE) than the redox potential of I^-/I^{3-}electrolyte (0.4 V *vs.* NHE) [162] which attests the thermodynamic feasibility for the regeneration of the oxidized dye by the electrolyte (Figure 4.17 and 4.18). The excited state oxidation potentials of the sensitizers were more negative (-0.91 to -1.23 V *vs.* NHE) than the conduction band edge (-0.5 V *vs.* NHE) [163] of TiO_2, which energetically permits the injection of electron from the excited state of the sensitizers into the conduction band of the TiO_2.

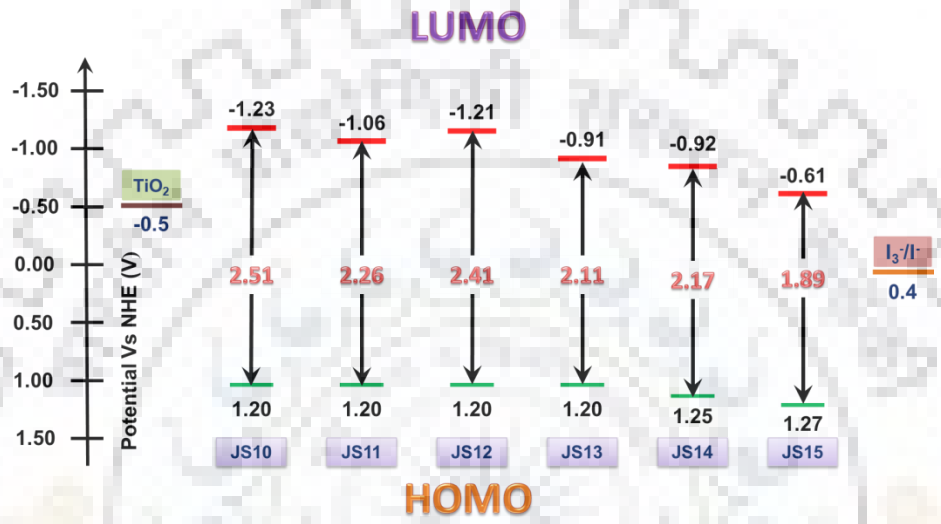

Figure 4.17 Energy level diagram for the dyes **JS10-JS15**.

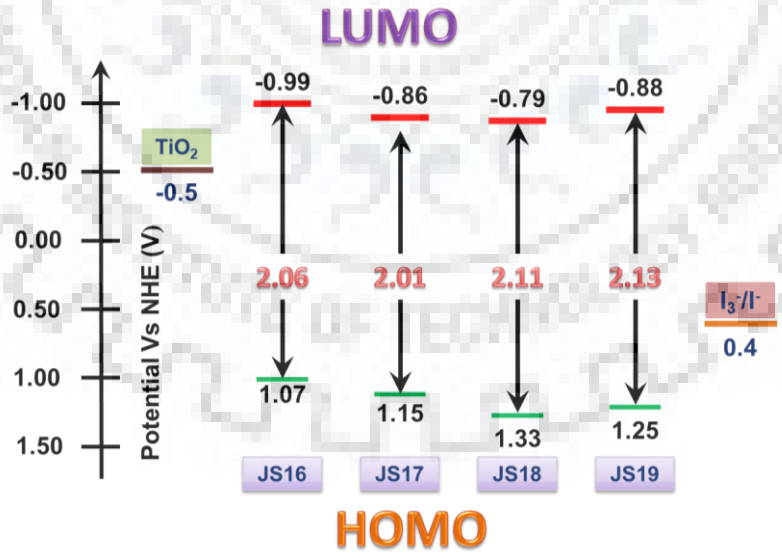

Figure 4.18 Energy level diagram for the dyes **JS16-JS19.**

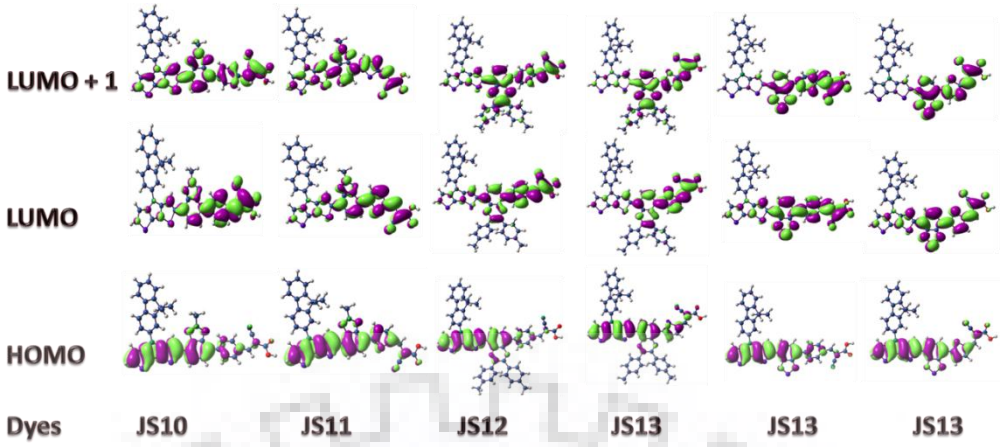

Figure 4.19 Electronic distributions in the frontier molecular orbitals of the dyes **JS10-JS15**.

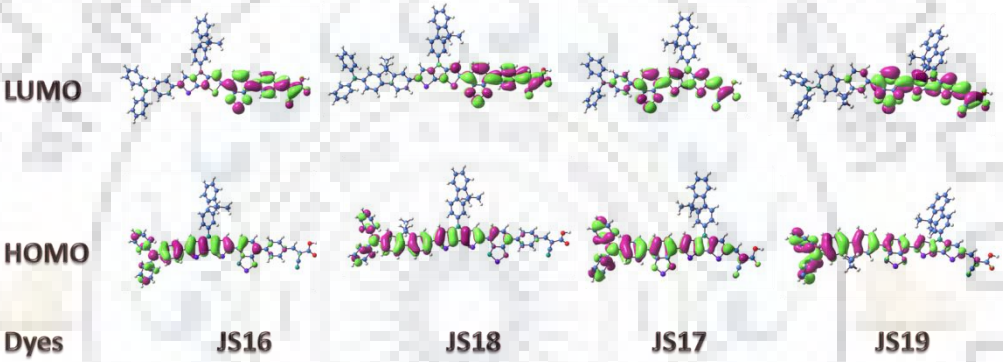

Figure 4.20 Electronic distributions in the frontier molecular orbitals of the dyes **JS16-JS19**.

4.2.4 Theoretical calculations

To elucidate the nature of oxidation and absorption in the dyes, the electronic structure calculations were performed at the density functional theory [164,165] level using B3LYP/6-31g(d,p) hybrid functional. The HOMO and LUMO electronic distributions for the dyes containing different π-conjugation are depicted in Figures 4.19 and 4.20. For the dyes **JS10-JS15**, the HOMOs are mainly contributed by the DTP unit and spread over the benzene ring of the electron deficient units (BTZ, Qx and BTD). The LUMOs are mainly concentrated on cyanoacrylic acid and spread up to the auxiliary acceptor via the phenyl or thiophene linker. The significant overlap of HOMO and LUMO over the auxiliary acceptor ensures the migration of charge from the DTP donor to the cyanoacrylic acid acceptor via π-linkers. However, the twisting of phenyl π-linkers in **JS10**, **JS12** and **JS14** may reduce the transition probability of charge transfer. The

observation of blue shift in absorption for the phenyl-linked dyes attests this hypothesis. Moreover, the HOMOs are constituted by arylamine donor and DTP units for the dyes **JS16** and **JS17** and the LUMOs remain concentrated on cyanoacrylic acid and BTD units. On the other hand, for the dyes **JS18** and **JS19**, HOMOs are composed by arylamines and BTD units with small extension to DTPs and LUMOs spread upto BTD units through DTPs in case of **JS17** and **JS19** dyes. Thus, in comparison to **JS16** and **JS17**, enough overlapping of HOMO and LUMO for the dyes **JS18** and **JS19** ensures the facile charge transfer propensity from arylamine donor to acceptor. This observation is consistent with the intense absorption maxima recorded for later dyes in solution.

Table 4.2 Computed vertical transition energies and their oscillator strengths and configurations for the dyes **JS10-JS19**.

Dye	λ_{max}^{abs} (nm)	f	Configuration	HOMO (eV)	LUMO (eV)	Band gap (eV)
JS10	482	1.73	HOMO→LUMO (89%)	-5.93	-2.37	3.57
JS11	536	1.74	HOMO→LUMO (93%)	-5.93	-2.59	3.34
JS12	481	1.18	HOMO→LUMO (83%), HOMO→LUMO+1(13%)	-5.91	-2.32	3.59
JS13	539	1.29	HOMO→LUMO (92%)	-5.93	-2.37	3.57
JS14	540	1.22	HOMO→LUMO (92%)	-5.97	-2.58	3.39
JS15	603	1.33	HOMO→LUMO (95%)	-5.95	-2.82	3.12
JS16	572	1.72	HOMO→LUMO (81%), HOMO-1→LUMO (11%)	-5.69	-2.58	3.11
	363	1.20	HOMO→LUMO+2(84%)			
JS17	567	1.87	HOMO→LUMO (71%) HOMO-1→LUMO (20%)	-5. 70	-2.58	3.12
	374	1.50	HOMO→LUMO+2(87%)			
JS18	538	1.85	HOMO→LUMO (83%), HOMO-1→LUMO (9%)	-5.94	-2.56	3.38
JS19	537	2.03	HOMO→LUMO (60%) HOMO-1→LUMO (33%)	-5.86	-2.59	3.265

To predict the absorption wavelengths and estimate the trend among the compounds the electronic excitation parameters were computed using the time-dependent density functional theory (TD-DFT) employing BMK functional and DGDZVP basis set. The computed excitation energies, their oscillator strength (*f*) and molecular orbital contributions are listed in Table 4.2. For the dyes **JS10-JS15**, the calculated maximum absorption wavelength follows the trend **JS15** > **JS14** > **JS13** > **JS11** > **JS12** > **JS10** which is similar to the observed values in THF. All the dyes show the charge transfer nature for the longer wavelength absorption originating from HOMO to LUMO transitions i.e. from arylamine donors to cyanoacrylic acceptors. Also the intense absorption ca. 370 nm involved HOMO→LUMO+2 transitions for **JS16** and **JS19** attest the additional charge transfer arylamines to BTD as observed in solution for these dyes.

4.2.5 Photovoltaic properties

To investigate the photovoltaic properties of the dyes, we fabricated the DSSCs by employing the dyes as sensitizers and the performance parameters summarized in Table 4.3. The incident photon-to-current conversion efficiencies (IPCE) of the DSSCs as function of different irradiation wavelengths are plotted in Figure 4.21. The IPCE spectrum of a particular dye depends on the light harvesting efficacy and extends up to 750 nm for the D-A-π-A dyes and for the isomeric dyes, tails upto 650 nm which is consistent with the absorption spectra of their respective photoanodes. In D-A-π-A dyes, BTZ-based dyes exhibited superior spectral response as compared to the Qx and BTD-based dyes. Also, the thiophene-linked dyes (**JS11, JS13** and **JS15)** exhibited longer wavelength onset for IPCE which is in accordance with the low energy tailing of their absorption. Further, the extension of conjugation in D-D-A-π-A architecture by TPA and DPF at C6-postion of DTP of **JS14** increases the IPCE values to 75% for **JS16**. Furthermore, the isomeric positional variations of BTD unit from D-D-A-π-A to D-A-D-A upgraded the IPCE response for the dyes **JS18** and **JS19** in accordance with their absorption in solutions. The current-voltage (I-V) characteristics were measured under simulated solar light conditions and presented in Figure 4.22. The photocurrent density of the dyes assume the order, **JS18** > **JS19** > **JS16** = **JS17** > **JS14** > **JS11** > **JS10** > **JS15** > **JS13** > **JS12**. The high J_{SC} observed for the dyes **JS18** and **JS19** is attributed to their broad and intense absorption. On the other hand, inferior molar extinction coefficients and poor electronic coupling with the TiO_2 nanoparticles may be responsible for low photocurrent density observed for the dyes, **JS12** and **JS13** [216]. However, amongst the

JS10-JS15 dyes, the high photocurrent density observed for **JS14** might be due to the kinetically fast injection of electron from low lying LUMO energy level to the CB of TiO_2. The presence of TPA and DPF in D-D-A-π-A and D-A-D-A are expected to retard the approach of electrolyte and dye aggregation on the TiO_2 surface and improve the open circuit voltage. The trend for the open circuit voltage of the dyes is, **JS19** > **JS18** > **JS16** > **JS14** > **JS11**> **JS17** > **JS12** > **JS10** = **JS13** > **JS15**. In comparison to **JS16** and **JS17**, the high open circuit voltage for **JS18** and **JS19** explain the beneficial role of BTD present before DTP to suppress the recombination process effectively. The **JS14** exhibited the highest V_{OC} among the D-A-π-A dyes due to its low-lying HOMO energy levels which ensures fast thermodynamically feasible regeneration by electrolyte than other congeners. However, the lowest V_{OC} for the dye **JS15** can be explained on the basis of electron life time and charge collection efficiency (*vide infra*).

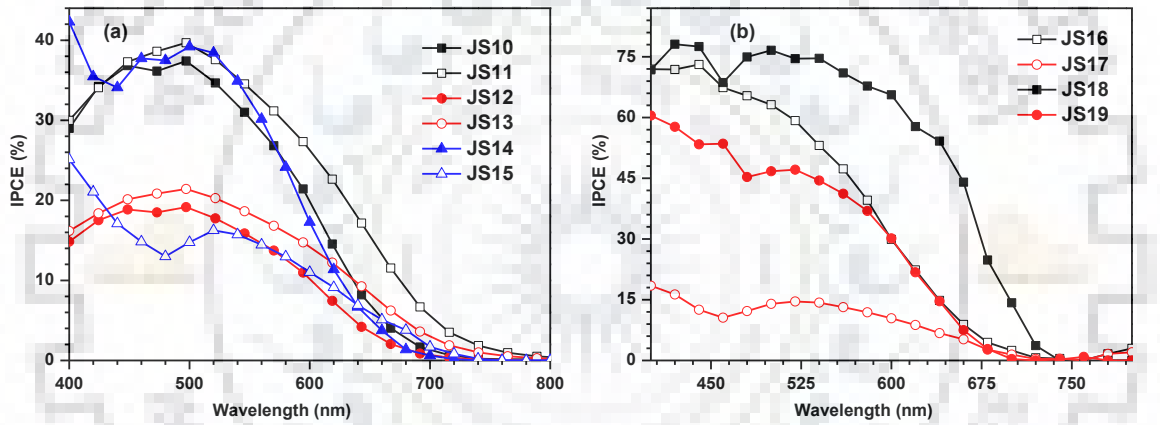

Figure 4.21 IPCE spectra of the DSSCs fabricated with dyes (a) **JS10-JS15** and (b) **JS16-JS19.**

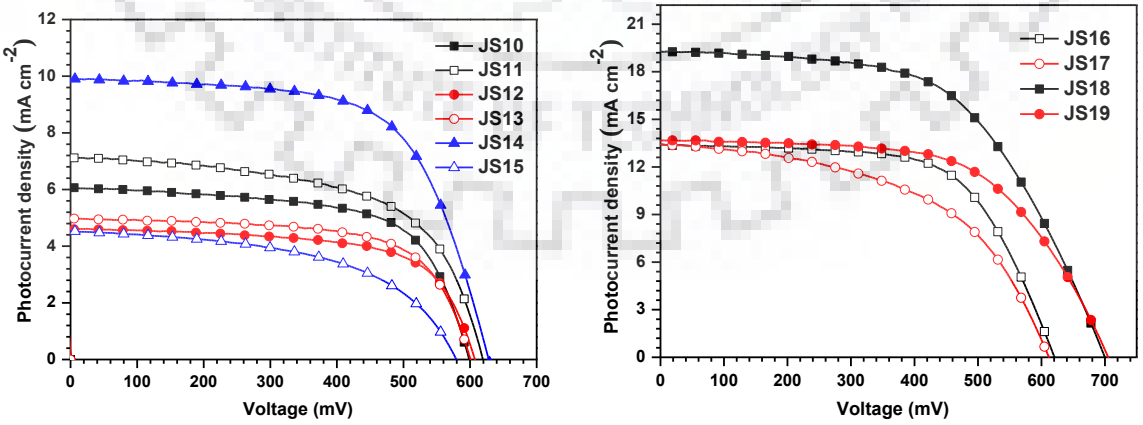

Figure 4.22 I-V characteristics of the DSSCs fabricated with dyes (a) **JS10-JS15** and (b) **JS16-JS19.**

The efficiency of the dyes follow the order **JS18** > **JS19** > **JS16** > **JS17** > **JS14** > **JS11** > **JS10** > **JS13** > **JS12** > **JS15**, which is almost similar to the order of J_{SC} values. Amongst all the dyes, **JS18** showed highest efficiency of 7.57% can be attributed to the high J_{SC} and V_{OC} values. It will be worthy to compare the efficiency of **JS18** with previously reported related DTP-dyes **WS54, F16** and **F17** [136,137] containing indoline and dipenylamine donors respectively. In comparison to **WS54**, our dye **JS18** and **F16** showed superior photovoltaic performances while with **F17** it is comparable. Therefore, it is advisable that the insertion of suitable electronic rich donor and bulky units at DTP-chromophore in D-A-π-A design is beneficial to increase the efficiency. Also, the isomeric position variation of BTD unit amidst of arylamine donor and DTP linker is suitable strategy to further improve the J_{SC}, V_{OC} and hence the efficiency.

Table 4.3 Performance parameters of the DSSCs fabricated with dyes **JS10-JS19.**

Dye	η (%)	V_{OC} (mV)	J_{SC} (mA cm^{-2})	*FF*	R_{ct2} (ohm)	τ_e (ms)	R_{rec} (ohm)
JS10	2.33	599	06.07	0.64	29.63	3.34	45.79
JS11	2.61	618	07.13	0.59	28.25	4.39	37.76
JS12	1.83	606	04.62	0.65	42.11	3.34	39.75
JS13	1.97	599	04.98	0.66	39.52	3.34	37.76
JS14	3.98	626	09.91	0.64	22.01	0.44	19.12
JS15	1.38	577	04.53	0.53	62.14	0.76	15.43
JS16	5.26	619	13.42	0.63	12.77	1.31	23.28
JS17	4.20	610	13.42	0.51	18.81	2.26	34.90
JS18	7.57	699	19.29	0.56	20.34	0.25	28.27
JS19	5.78	704	13.65	0.60	24.41	0.33	36.40

4.2.6 Electrochemical impedance spectroscopy

To further understand the structural effect of different π-linkers and axillary donors on the fate of electrons at the interfaces of the DSSCs, we carried out the electrochemical impedance spectroscopy (EIS) measurements under dark and one sun illumination conditions. The Nyquist plots obtained in dark and illumination conditions are displayed in Figure 4.23 and 4.24, respectively. The electron recombination resistances (R_{rec}) at the interfaces of TiO_2/dye/electrolyte correspond to the second semicircle in Figure 4.23. The diameter of this semicircle is the measure of recombination resistance. The order of R_{rec} is **JS10** > **JS12** > **JS11** = **JS13** > **JS19** > **JS17** > **JS18** > **JS16** > **JS14** > **JS15**. The largest R_{rec} values obtained for the dyes **JS10** and **JS12** suggest that the presence of *n*-butyl group on BTZ unit in conjunction with thienyl linker and bulky *tert*-butylphenyl group on Qx respectively are effective in suppressing the recombination of electrons with the

oxidized half of electrolyte. Also, the effective electron injection ability of these dyes may also increase the electron density in the TiO_2 conduction band and upwardly shift the Fermi energy. On the other hand for BTD-isomers, the DPF dyes (**JS17** and **JS19**) showed high R_{rec} than TPA-dyes (**JS16** and **JS18**) as observed for V_{OC} values it explains the ability of DPF chromophores with two *n*-hexyl chains to suppress the recombination process effectively than TPA chromophores. Charge-transport resistances *(Rct2)* for the DSSCs are estimated from the large semicircle of the Nyquist plots under the one sun illumination conditions (Figure 4.24). The R_{ct2} of the dyes followed the order, **JS15** > **JS12** > **JS13** > **JS10** > **JS11** > **JS14** > **JS19** > **JS18** > **JS17** > **JS16.** The dye **JS15** possessed larger R_{ct2} values, originated from the unfavorable thermodynamic condition for electron injection due to the relatively low-lying LUMO energy level [167,168]. The comparatively smaller R_{ct2} values for the dyes **JS16** and **JS17** suggest efficient charge collection in the respective devices.

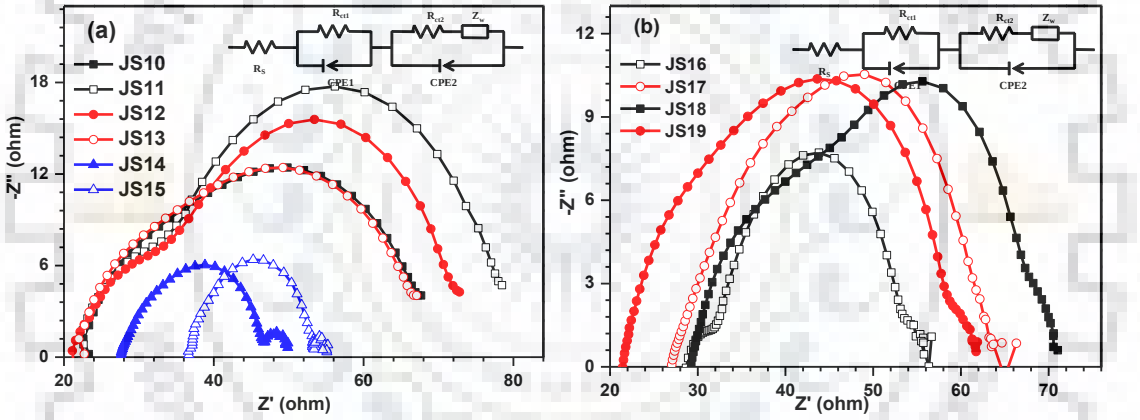

Figure 4.23 Nyquist plots observed for the DSSCs fabricated with the dyes (a) **JS10-JS15** and (b) **JS16-JS19** under dark condition.

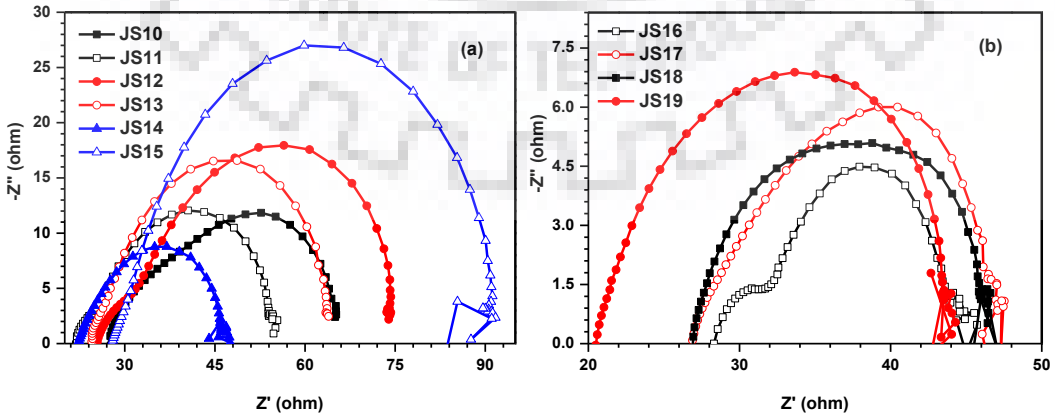

Figure 4.24 Nyquist plots observed for the DSSCs fabricated with the dyes (a) **JS10-JS15** and (b) **JS16-JS19** under illumination.

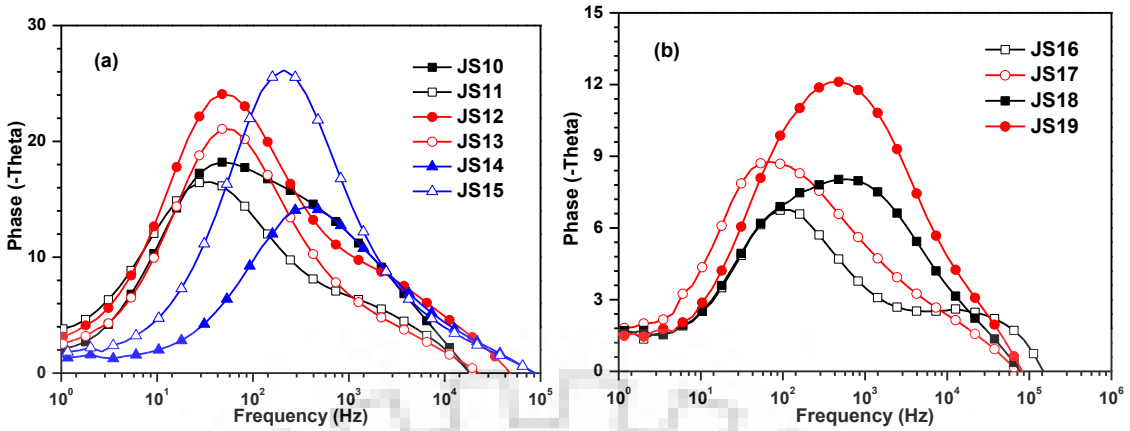

Figure 4.25 Bode phase plots for the DSSCs fabricated with the dyes (a) **JS10-JS15** and (b) **JS16-JS19** measured under illumination.

The electron life time (τ_e) in the device can be measured by the mid-frequency peaks of the Bode phase plot (Figure 4.25) from the equation $\tau_e = 1/\omega_{min}$, where ω_{min} is the angular frequency of low frequency peak [169,170]. The dye **JS11** showed highest τ_e value suggestive of more effective suppression of the back electron transfer when compared to the other dyes. Thus, the BTZ-thiophene dyad constitutes to an efficient conjugation pathway leading to improved electronic coupling between the donor and acceptor and inhibition of recombination of electrons. While in case of isomeric dyes **JS16-JS19**, the large τ_e value for **JS16** and **JS17** suggests that presence of BTD unit between DTP and phenyl-linker is however beneficial to attain the high electron lifetime and charge collection efficiency as compared to **JS18** and **JS19**.

4.3 Conclusions

In summary, we demonstrated the use of dithienopyrrole as a donor in organic dyes featuring D-A-π-A structural organization by employing different electron-demanding linkers such as BTZ, Qx and BTD along phenyl/thienyl π-spacer with cyanoacrylic acid acceptor. We further incorporated TPA and DPF auxiliary donor on BTD dye with phenyl-linker (**JS14**) to extend the conjugation length in order to improve the spectral response for the dyes. Moreover, further isomeric positional variation of BTD unit from D-D-A-π-A to D-A-π-A architecture adequately improved the absorption and electrochemical characteristics. The D-A-π-A dyes were found to be sufficiently polar in ground state as confirmed by the negative solvatochromism exhibited by them in the absorption spectra. While polar excited states of isomeric dyes **JS16-JS19** were confirmed by positive solvatochromism of their emission spectra. Theoretically, it was

established that sufficient overlap of HOMO and LUMO of the dyes **JS18** and **JS19** facilitate the charge transfer propensity form arylamine donor to acceptor and ensure the high molar extinction coefficient for ICT absorption. Among the dyes, the highest power conversion efficiency (η = 7.57%) for the **JS18** is due to its high photocurrent density and open circuit voltage. The superior performance of **JS18** is attributable to the sufficiently low charge transfer resistance revealed by EIS studies. This work suggests that insertion of auxiliary donor is beneficial to attain high electron lifetime and charge collection efficiency; however, further inserting BTD unit between arylamine donor and DTP linker is a suitable strategy to tune photovoltaic properties to achieve high efficiency.

4.4 Experimental

4.4.1 General methods

The general methodology is similar to that described in Chapter 2.

4.4.2 Synthesis

Synthesis of 4-(2-butyl-7-(4-(9,9-dibutyl-9H-fluoren-2-yl)-4H-dithieno[3,2-b:2',3'-d]pyrrol-2-yl)-2H-benzo[d][1,2,3]triazol-4-yl)benzaldehyde ***(14).***

A mixture 4-(7-bromo-2-butyl-2*H*-benzo[*d*][1,2,3]triazol-4-yl)benzaldehyde (**S1**) (0.140 g, 0.40 mmol), **3** (0.80 mmol), $Pd(PPh_3)_2Cl_2$ (0.003 g, 0.04 mmol), and dry DMF (3 mL) was heated at 80 °C under nitrogen atmosphere for 24 h. On the completion of reaction, the reaction mixture was poured into water and organic compound extracted with chloroform. The organic layer was washed with brine solution followed by water and dried over anhydrous Na_2SO_4. The combined organic extracts were concentrated and further purified by column chromatography using alumina as stationary phase and hexanes:chloroform mixture (1:1) as eluent. Red solid; yield 0.205 g (70%); m.p. 105-107 °C; IR (KBr, cm^{-1}) 1697 ($\nu_{C=O}$); ^{1}H NMR (399.78 MHz, $CDCl_3$) δ 0.70-0.76 (m, 10 H), 1.00-1.04 (m, 3 H), 1.09-1.16 (m, 4 H), 1.26-1.32 (m, 2 H), 2.04-2.09 (m, 4 H), 2.19 (t, *J* = 7.2 Hz, 2 H), 4.82-4.85 (m, 2 H), 7.20 (d, *J* = 5.6 Hz, 1 H), 7.28 (d, *J* = 5.6 Hz, 1 H), 7.36-7.42 (m, 3 H), 7.65-7.69 (m, 3 H), 7.75-7.78 (m, 2 H), 7.89 (d, *J* = 8.0 Hz, 1 H), 8.04 (d, *J* = 8.4 Hz, 2 H), 8.27 (d, *J* = 8.4 Hz, 2 H), 8.32 (s, 1 H), 10.08 (s, 1 H); ^{13}C NMR (100.53 MHz, $CDCl_3$) δ 192.1, 152.7, 150.8, 144.7, 143.4, 140.4, 139.3, 138.8, 135.4, 130.2, 129.2, 129.0, 127.7, 127.1, 126.5, 125.6, 124.7, 123.1, 121.9, 121.6, 120.8, 119.8, 117.4, 112.9, 112.4, 56.7, 55.4, 40.3, 32.5, 32.2, 32.0, 29.8, 29.7, 26.2, 23.2, 23.07, 23.0, 22.8, 20.0, 14.2. HRMS calcd for $C_{46}H_{44}N_4OS_2$ $[M+Na]^+$ m/z 755.2848 found 755.2841.

*Synthesis of 4-(2,3-bis(4-(tert-butyl)phenyl)-8-(4-(9,9-dibutyl-9H-fluoren-2-yl)-4H-dithieno[3,2-b:2',3'-d]pyrrol-2-yl)quinoxalin-5-yl)benzaldehyde **(15).***

It was obtained from 4-(8-bromo-2,3-bis(4-(*tert*-butyl)phenyl)quinoxalin-5-yl)benzaldehyde (**S3**) (0.160 g, 0.28 mmol) and **3** (0.56 mmol) by following a procedure same as described above for the synthesis of **14**. Orange solid; yield 0.133 g (50%); m.p. 170-172 °C; IR (KBr, cm^{-1}) 1644 ($\nu_{C=O}$); ^{1}H NMR (399.78 MHz, $CDCl_3$) δ: 0.71-0.74 (m, 10 H), 1.10-1.19 (m, 4 H), 1.25 (s, 9 H), 1.31 (s, 9 H), 2.04 (t, *J* = 8.0 Hz, 4 H), 7.20 (d, *J* = 5.2 Hz, 1 H), 7.28-7.33 (m, 2 H), 7.35-7.41 (m, 5 H), 7.54 (d, *J* = 8.0 Hz, 2 H), 7.64 (s, 1 H), 7.70-7.78 (m, 4 H), 7.82 (d, *J* = 8.0 Hz, 1 H), 7.91 (d, *J* = 8.0 Hz, 1 H), 8.04 (s, 5 H), 8.16 (d, *J* = 7.6 Hz, 1 H), 8.26 (s, 1 H), 10.12 (s, 1 H); ^{13}C NMR (100.53 MHz, $CDCl_3$) δ: 192.5, 152.5, 150.9, 144.1, 138.8, 138.7, 137.3, 137.2, 136.0, 135.8, 135.2, 133.8, 131.6, 130.6, 130.1, 130.0, 129.7, 129.5, 129.2, 127.4, 127.3, 127.1, 126.4, 126.1, 125.9, 125.4, 125.3, 124.5, 123.1, 121.6, 120.8, 119.9, 117.7, 112.6, 55.4, 40.3, 31.3, 29.8, 26.2, 23.2, 14.1, 14.0. HRMS calcd for $C_{64}H_{61}N_3OS_2$ $[M+Na]^+$ m/z 974.4148 found 974.4140.

*Synthesis of 5-(2-butyl-7-(4-(9,9-dibutyl-9H-fluoren-2-yl)-4H-dithieno[3,2-b:2',3'-d]pyrrol-2-yl)-2H-benzo[d][1,2,3]triazol-4-yl)thiophene-2-carbaldehyde **(16).***

It was obtained from 5-(7-bromo-2-butyl-2*H*-benzo[*d*][1,2,3]triazol-4-yl)thiophene-2-carbaldehyde (**S2**) (0.300 g, 0.82 mmol) and **3** (1.64 mmol) by following a procedure similar to that described above for the synthesis of **14**. Red solid; yield (0.351 g, 61%); m.p. 135-137 °C; IR (KBr, cm^{-1}) 1660 ($\nu_{C=O}$); ^{1}H NMR (399.78 MHz, $CDCl_3$) δ 0.68-0.77 (m, 10 H), 1.00-1.04 (m, 3 H), 1.09-1.16 (m, 4 H), 1.46-1.55 (m, 2 H), 2.04-2.08 (m, 4 H), 2.16-2.23 (m, 2 H), 4.84 (t, *J* = 7.2 Hz, 2 H), 7.19 (d, *J* = 5.2 Hz, 1 H), 7.27 (d, *J* = 5.2 Hz, 1 H), 7.34-7.41 (m, 3 H), 7.64-7.69 (m, 3 H), 7.75-7.78 (m, 2 H), 7.82 (d, *J* = 4.4 Hz, 1 H), 7.88 (d, *J* = 8.0 Hz, 1 H), 8.15 (d, *J* = 4.0 Hz, 1 H), 8.31 (s, 1 H), 9.94 (s, 1 H); ^{13}C NMR (100.53 MHz, $CDCl_3$) δ 183.0, 152.6, 150.7, 149.7, 144.8, 144.8, 144.6, 142.3, 142.1, 141.7, 140.2, 139.3, 138.6, 137.3, 137.1, 127.3, 127.1, 127.1, 127.0, 124.9, 124.4, 123.0, 121.5, 121.3, 120.7, 119.7, 118.0, 117.1, 113.0, 112.24, 56.7, 55.3, 40.2, 32.0, 26.1, 23.1, 19.9, 13.9, 13.6. HRMS calcd for $C_{44}H_{42}N_4OS_3$ $[M]^+$ m/z 738.2515 found 738.2520.

*2.1.4 Synthesis of 5-(2,3-bis(4-(tert-butyl)phenyl)-8-(4-(9,9-dibutyl-9H-fluoren-2-yl)-4H-dithieno[3,2-b:2',3'-d]pyrrol-2-yl)quinoxalin-5-yl)thiophene-2-carbaldehyde **(17).***

It was obtained from 5-(8-bromo-2,3-bis(4-(*tert*-butyl)phenyl)quinoxalin-5-yl)thiophene-2-carbaldehyde (**S4**) (0.140 g, 0.24 mmol) and **3** (0.48 mmol) by following a procedure same as described above for the synthesis of **14**. Dark red solid; yield (0.167 g, 73%); m.p. 100-102 °C; IR (KBr, cm^{-1}) 1664 ($\nu_{C=O}$); ^{1}H NMR (399.78 MHz, $CDCl_3$) δ 0.71-0.77 (m, 10 H), 1.12-1.17 (m, 4 H), 1.32 (s, 9 H), 1.36 (s, 9 H), 2.02-2.06 (m, 4 H), 7.19 (d, *J* = 5.2 Hz, 1 H), 7.29 (d, *J* = 6.0 Hz, 1 H), 7.37-7.43 (m, 8 H), 7.63 (d, *J* = 2.0 Hz, 1 H), 7.67-7.73 (m, 4 H), 7.78 (d, *J* = 6.8 Hz, 1 H), 7.81 (d, *J* = 4.0 Hz, 1 H), 7.91 (t, *J* = 4.0 Hz, 2 H), 8.11 (s, 2 H), 8.25 (s, 1 H), 9.98 (s, 1 H); ^{13}C NMR (100.53 MHz, $CDCl_3$) δ 183.5, 152.8, 152.7, 152.6, 150.9, 148.8, 144.9, 144.8, 144.5, 140.3, 139.4, 137.3, 137.1, 135.9, 135.6, 135.6, 134.1, 130.2, 128.9, 128.0, 127.4, 127.9, 127.1, 126.9, 125.8, 125.6, 125.5, 125.4, 125.2, 125.1, 124.8, 123.0, 121.7, 121.0, 120.9, 119.9, 117.7, 117.3, 112.8, 112.2, 55.4, 40.3, 34.9, 31.4, 29.8, 26.2, 23.2, 14.2. HRMS calcd for $C_{62}H_{59}N_3OS_3$ $[M+Na]^+$ m/z 980.3712 found 980.3706.

*Synthesis of 2-(7-bromobenzo[c][1,2,5]thiadiazol-4-yl)-4-(9,9-dibutyl-9H-fluoren-2-yl)-4H-dithieno[3,2-b:2',3'-d]pyrrole (**18**).*

It was prepared from 4,7-dibromobenzo[*c*][1,2,5]thiadiazole (3.270 g, 10.20 mmol), **3** (1.00 mmol) by following a similar procedure described for the synthesis of **14**. Red solid; yield (1.5 g, 48%); m.p. 192-195 °C; ^{1}H NMR (399.78 MHz, $CDCl_3$) δ 0.66-0.76 (m, 10 H), 1.11-1.78 (m, 4 H), 2.01-2.08 (m, 4 H), 7.20 7.22 (m, 1 H), 7.30 (d, *J* = 5.2 Hz, 1 H), 7.35-7.40 (m, 3 H), 7.57 (d, *J* = 8.0 Hz, 1 H), 7.63 (m, 1 H), 7.72 (d, *J* = 8.0 Hz, 1 H), 7.75-7.77 (m, 1 H), 7.83-7.85 (m, 1 H), 7.88 (d, *J* = 8.8 Hz, 1 H), 8.47 (s, 1 H); ^{13}C NMR (100.53 MHz, $CDCl_3$) δ 154.0, 152.8, 151.6, 150.8, 145.1, 144.7, 140.4,139.5, 138.5, 136.5, 132.4, 128.1, 127.2, 125.2, 124.6, 124.0, 123.1, 121.5, 120.9, 119.9, 117.8, 117.5, 114.3, 112.3, 111.5, 108.2, 55.4, 40.4, 40.3, 29.8, , 26.2, 23.3, 14.1. HRMS calcd for $C_{35}H_{30}BrN_3S_3$ $[M+Na]^+$ m/z 690.0683 found 690.0653.

*Synthesis of 4-(7-(4-(9,9-dibutyl-9H-fluoren-2-yl)-4H-dithieno[3,2-b:2',3'-d]pyrrol-2-yl)benzo[c][1,2,5]thiadiazol-4-yl)benzaldehyde (**19**).*

A mixture of **18** (0.400 g, 0.60 mmol), (4-formylphenyl)boronic acid (0.099 g, 0.66 mmol), K_2CO_3 (0.247 g, 1.79 mmol) and $Pd(PPh_3)_4$ (0.036 g, 0.03 mmol) in 24 mL of THF:H_2O (4:1) was heated at 80 °C for 12 h under nitrogen atmosphere. On the

completion of reaction, the reaction mixture was poured into water and extracted with chloroform. The organic layer was washed with brine solution and finally with water, and dried over anhydrous Na_2SO_4. The volatiles were removed to obtain a solid residue. The obtained crude product was further purified by column chromatography using alumina as stationary phase and hexanes: chloroform (2: 3) as eluent. Purple solid; yield (0.160 g, 40%); m.p. 166-168 °C, IR (KBr, cm^{-1}) 1646 ($\nu_{C=O}$); ^{1}H NMR (399.78 MHz, $CDCl_3$) δ 0.67-0.78 (m, 10 H), 1.12-1.21 (m, 4 H), 2.05-2.09 (m, 4 H), 7.22 (d, *J* = 5.2 Hz, 1 H), 7.30 (d, *J* = 5.2 Hz, 1 H), 7.36-7.41 (m, 3 H), 7.64-7.67 (m, 2 H), 7.76-7.80 (m, 1 H), 7.81 (d, *J* = 7.6 Hz, 1 H), 7.89 (d, *J* = 8.4 Hz, 1 H), 7.97 (d, *J* = 7.6 Hz, 1 H), 8.03-8.06 (m, 2 H), 8.16 (d, *J* = 8.0 Hz, 2 H), 10.10 (s, 1 H); ^{13}C NMR (100.53 MHz, $CDCl_3$) δ 192.0, 153.9, 152.8, 152.5, 150.8, 145.2, 144.8, 143.20, 140.4, 139.5, 138.5, 136.9, 135.7, 124.3, 123.1, 121.5, 120.9, 119.9, 118.0, 117.5, 114.4, 112.4, 55. 4, 40.4, 26.3, 23.3, 14.1. HRMS calcd for $C_{42}H_{35}N_3OS_3$ $[M+Na]^+$ m/z 716.1840 found 716.1847.

*Synthesis of 5-(7-(4-(9,9-dibutyl-9H-fluoren-2-yl)-4H-dithieno[3,2-b:2',3'-d]pyrrol-2-yl)benzo[c][1,2,5]thiadiazol-4-yl)thiophene-2-carbaldehyde (**20**).*

A mixture of **18** (0.600 g, 0.90 mmol), (5-(1,3-dioxolan-2-yl)thiophen-2-yl)tributylstannane (0.479 g, 1.08 mmol) , $Pd(PPh_3)_2Cl_2$ (6.3 mg, 0.09 mmol) and 5 mL DMF was heated at 85 °C under nitrogen atmosphere. After 16 h, the mixture was poured into water and extracted with chloroform. The organic layer was washed with brine solution followed by water and dried over anhydrous Na_2SO_4. The volatiles were removed by rotary evaporator to obtain a crude product. Further, crude product was dissolved in glacial acetic acid (5 mL) and heated to 60 °C. After 30 min, it was treated with 10 mL water and the heating was continued for further 6 h. After cooling to room temperature, the reaction mixture was extracted with chloroform. The organic layer was washed with brine solution followed by water and dried over anhydrous Na_2SO_4. The volatiles were removed and the crude product obtained further purified by column chromatography using alumina as stationary phase and hexanes: chloroform (2: 3) as eluent. Indigo solid; yield (0.370g, 59%); m.p. 195-197 °C, IR (KBr, cm^{-1}) 1652 ($\nu_{C=O}$); ^{1}H NMR (399.78 MHz, $CDCl_3$) δ 0.68-0.80 (m, 10 H), 1.16 (m, 4 H), 2.08 (t, *J* = 8.4 Hz, 4 H), 7.19 (d, *J* = 5.6 Hz, 1 H), 7.29 (d, *J* = 5.2 Hz, 1 H), 7.36-7.42 (m, 3 H), 7.62-7.757 (m, 2 H), 7.76-7.78 (m, 1 H), 7.80 (d, *J* = 4.0 Hz, 1 H), 7.84-7.90 (m, 2 H), 7.95 (d, *J* = 7.6 Hz, 1 H), 8.16 (d, *J* = 4.0, 1 H), 8.52 (s, 1H), 9.94 (s, 1 H); ^{13}C NMR (100.53 MHz, $CDCl_3$) δ 183.0, 152.8, 152.6, 152.2, 150.8, 148.8, 145.4, 144.9, 143.2, 140.3, 139.5,

138.4, 136.9, 129.0, 127.7, 127.5, 127.4, 127.1, 126.9, 125.5, 123.9, 123.5, 123.1, 121.5, 120.9, 119.9, 117.5, 117.0, 114.5, 112.4, 65.4, 55.5, 40.4, 26.2, 26.0, 14.09, 13.7. HRMS calcd for $C_{40}H_{33}N_3OS_4$ $[M+H]^+$ m/z 700.1579 found 700.1557.

*Synthesis of 4-(7-(6-bromo-4-(9,9-dibutyl-9H-fluoren-2-yl)-4H-dithieno[3,2-b:2',3'-d]pyrrol-2-yl)benzo[c][1,2,5]thiadiazol-4-yl)benzaldehyde (**21**).*

A mixture of **19** (0.430 g, 0.62 mmol), NBS (0.132 g, 0.74 mmol) and 25 mL of $CHCl_3$ was kept on stirring at RT for overnight. After 12 h, the reaction was quenched by the addition of water. The organic product was extracted with dichloromethane. The collected organic layer was thoroughly washed with brine solution and dried over anhydrous Na_2SO4. Evaporation of the volatiles gave a yellow compound. The crude product obtained further purified by column chromatography using alumina as stationary phase and hexanes: chloroform (2: 3) as eluent. Purple solid; yield (0.230g, 69%); mp 232-234 °C; IR (KBr, cm^{-1}) 1639 ($\nu_{C=O}$); ^{1}H NMR (399.78 MHz, $CDCl_3$) δ; 0.70-0.76 (m, 10 H), 1.14-1.20 (m, 4 H), 2.07 (t, *J* = 8.4 Hz, 4 Hz), 7.25 (s, 1 H), 7.36-7.41 (m, 3H), 7.58-7.60 (m, 2 H), 7.76 (d, *J* = 1.2 Hz, 1 H) 7.78-7.82 (m, 1 H), 7.89 (d, *J* = 7.6 Hz, 1 H), 7.96 (d, *J* = 7.6 Hz, 1 H), 8.04 (d, *J* = 8.4 Hz, 2 H), 8.16 (d, *J* = 8.4 Hz, 2 H), 8.52 (s, 1 H), 10.11 (s, 1 H); ^{13}C NMR (100.53 MHz, $CDCl_3$) δ 192.0,152.9, 152.6, 150.8, 140.2, 139.9, 138.0, 135.8, 130.1, 129.8, 129.1, 127.5, 127.2, 123.1, 121.7, 121.0, 119.9, 117.7, 114.1, 55.5, 40.3, 26.2, 23.3, 14.1. HRMS calcd for $C_{42}H_{34}BrN_3OS_3$ $[M+Na]^+$ m/z 794.0940 found 794.0966.

*Synthesis of 4-(7-(4-(9,9-dibutyl-9H-fluoren-2-yl)-6-(4-(diphenylamino)phenyl)-4H-dithieno[3,2-b:2',3'-d]pyrrol-2-yl)benzo[c][1,2,5]thiadiazol-4-yl)benzaldehyde (**22**).*

It was obtained from **21** (0.200 g, 0.26 mmol) and (4-(diphenylamino)phenyl) boronic acid (0.098 g, 0.34 mmol) by following a procedure described above for **19**. Purple solid; yield (0.183g, 75%); mp 279-281 °C; IR (KBr, cm^{-1}) 1639 ($\nu_{C=O}$); ^{1}H NMR (399.78 MHz, $CDCl_3$) δ; 0.49-0.73 (m, 10 H), 1.00-1.44 (m, 4 H), 2.00 (s, 4 H), 6.57 (d, *J* = 4.8 Hz, 1 H), 6.80-6.84 (m, 1 H), 6.85-6.87 (m, 8 H), 7.03-7.07 (m, 3 H), 7.11 (d, *J* = 8 Hz, 3 H), 7.24 (s, 1 H), 7.28 (s, 1 H), 7.42 (s, 1 H), 7.43-7.44 (m, 4 H), 7.51-7.52 (m, 1 H), 7.61 (d, *J* = 7.2 Hz, 1 H), 7.75-7.78 (m, 1 H), 8.04-8.14 (m, 3 H), 10.11 (s, 1 H); ^{13}C NMR (100.53 MHz, $CDCl_3$) δ 191.9, 151.7, 147.2, 146.6, 140.5, 139.9, 130.03, 129.96, 129.8, 129.4, 129.3, 127.5, 126.3, 124.9, 123.2, 121.4, 120.0, 55.3, 40.3, 26.3, 23.1, 14.0 13.9. HRMS calcd for $C_{60}H_{48}N_4OS_3$ $[M]^+$ m/z 937.3063 found 937.3072.

Synthesis of 4-(7-(6-(9,9-dibutyl-7-(diphenylamino)-9H-fluoren-2-yl)-4-(9,9-dibutyl-9H-fluoren-2-yl)-4H-dithieno[3,2-b:2',3'-d]pyrrol-2-yl)benzo[c][1,2,5]thiadiazol-4-yl)benzaldehyde ***(23).***

It was obtained from 21 (0.150 g, 0.19 mmol) and (9,9-dibutyl-7-(diphenylamino)-9*H*-fluoren-2-yl)boronic acid (0.123 g, 0.25 mmol) by following a procedure described above for **19**. Purple solid; yield (0.180g, 83%); mp 247-249 °C; IR (KBr, cm^{-1}) 1638 ($\nu_{C=O}$); ^{1}H NMR (399.78 MHz, $CDCl_3$) δ 0.68-0.77 (m, 20 H), 1.07-1.12 (m, 4 H), 1.17-1.23 (m, 4 H), 1.89-1.94 (m, 4 H), 2.06-2.12 (m, 4 H), 6.99-7.05 (m, 3 H), 7.08-7.13 (m, 5 H), 7.18-7.25 (m, 1 H), 7.26 (s, 3 H), 7.39-7.43 (m, 4 H), 7.52-7.62 (m, 4 H), 7.71 (d, *J* = 7.2 Hz, 2 H), 7.78-7.80 (m, 2 H), 7.94 (d, *J* = 8.4 Hz, 2 H), 8.04 (d, J = 7.8 Hz, 2 H), 8.15-8.16 (m, 2 H), 8.56 (s, 1 H), 10.11 (s, 1 H) ; ^{13}C NMR (100.53 MHz, $CDCl_3$) δ 191.9, 148.0, 147.5, 138.5, 135.7, 130.0, 129.7, 129.3, 127.5, 127.2, 124.2, 124.6, 124.2, 124.0, 123.5, 123.1, 122.7, 121.8, 120.5, 119.9, 117.7, 107.6, 55.5, 55.2, 40.5, 40.1, 26.24, 26.18, 23.4, 23.1, 14.1, 14.0. HRMS calcd for $C_{75}H_{68}N_4OS_3$ $[M+H]^+$ m/z 1137.4628 found 1137.4654.

Synthesis of 6-(7-bromobenzo[c][1,2,5]thiadiazol-4-yl)-4-(9,9-dibutyl-9H-fluoren-2-yl)-4H-dithieno[3,2-b:2',3'-d]pyrrole-2-carbaldehyde ***(24).***

To the mixture of **18** (0.500 g, 0.75 mmol) and DMF (5 mL) maintained at 0 °C, $POCl_3$ (0.19 mL, 1.5 mmol) was added drop wise. After complete addition, the stirring was continued for further 2 h at room temperature. Then the reaction was quenched by addition of ice-water and neutralized with sodium hydroxide solution. The organic product was extracted into chloroform, washed with brine solution and dried over anhydrous Na_2SO_4. The combined organic extracts were concentrated to obtain a residue. It was purified by column chromatography on alumina using hexane:chloroform (3:2) mixture as eluent. Dark orange solid; yield (0.405 g, 77%); mp 243-245 °C; IR (KBr, cm^{-1}) 1650 (($\nu_{C=O}$); ^{1}H NMR (400 MHz, $CDCl_3$) δ 0.69-0.72 (m, 10 H), 1.03-1.13 (m, 4 H), 2.03-2.11 (m, 4 H), 7.38-7.42 (m, 3 H), 7.61 (d, *J* = 5.6 Hz, 2 H), 7.75-7.81 (m, 3 H), 7.87 (d, *J* = 8.0 Hz, 1 H), 7.92 (d, *J* = 8.4 Hz, 1 H), 8.44 (s, 1 H), 9.90 (s, 1 H); ^{13}C NMR (123.55 MHz, $CDCl_3$) δ 183.0, 154.0, 153.1, 151.4, 150.8, 148.3, 144.2, 141.7, 141.3, 140.4, 140.0, 137.4, 132.2, 127.7, 127.2, 125.6, 124.5, 123.1, 121.8, 121.2, 120.7, 120.0, 117.7, 117.1, 113.7, 113.2, 55.5, 40.5, 40.3, 26.2, 23.3, 14.2, 14.1. HRMS calcd for $C_{36}H_{30}BrN_3OS_3$ $[M+H]^+$ m/z 696.0807 found 696.0799.

Synthesis of 4-(9,9-dibutyl-9H-fluoren-2-yl)-6-(7-(4-(diphenylamino)phenyl)benzo[c][1,2,5]thiadiazol-4-yl)-4H-dithieno[3,2-b:2',3'-d]pyrrole-2-carbaldehyde ***(25).***

It was obtained from **24** (0.200 g, 0.29 mmol) and (4-(diphenylamino)phenyl)boronic acid (0.166 g, 0.57 mmol) by following a procedure described above for **19**. Brown solid; yield (0.200 g, 80%); mp 209-211 °C; IR (KBr, cm^{-1}) 1658 ($\nu_{C=O}$); ^{1}H NMR (399.78 MHz, $CDCl_3$) δ 0.70-0.78 (m, 10 H), 1.13-1.22 (m, 4 H), 2.08 (t, *J* = 8.4 Hz, 4 H), 7.06-7.10 (m, 2 H), 7.18-7.21 (m, 6 H), 7.28-7.32 (m, 4 H), 7.39-7.43 (m, 3 H), 7.62-7.64 (m, 2 H), 7.70 (d, *J* = 7.6 Hz, 1 H), 7.76-7.82 (m, 2 H), 7.87-7.89 (m, 2 H), 7.89 (d, *J* = 7.6 Hz, 1 H), (7.47 (s, 1 H), 7.97 (d, *J* = 8.0 Hz, 1 H), 9.89 (s, 1 H); ^{13}C NMR (100.53 MHz, $CDCl_3$) δ 181.2, 153.0, 152.0, 151.6, 149.8, 147.6, 147.3, 146.3, 143.0, 141.7, 140.2, 139.2, 139.0, 136.5, 132.1, 129.2, 128.9, 128.4, 126.6, 126.2, 126.0, 125.0, 124.7, 124.1, 123.8, 122.5, 122.1, 121.6, 120.8, 120.0, 119.7, 119.0, 116.7, 111.9, 54.5, 39.3, 25.2, 22.2, 130. HRMS calcd for $C_{54}H_{44}N_4OS_3$ $[M+H]^+$ m/z 861.2750 found 861.2765.

Synthesis of 4-(7-(6-(9,9-dibutyl-7-(diphenylamino)-9H-fluoren-2-yl)-4-(9,9-dibutyl-9H-fluoren-2-yl)-4H-dithieno[3,2-b:2',3'-d]pyrrol-2-yl)benzo[c][1,2,5]thiadiazol-4-yl)benzaldehyde ***(26).***

It was obtained from **24** (0.100 g, 0.14 mmol) and (9,9-dibutyl-7-(diphenylamino)-9H-fluoren-2-yl)boronic acid (0.115 g, 0.24 mmol) by following a procedure described above for **19**. Red solid; yield (0.099g, 67%); mp 280-290 °C; IR (KBr, cm^{-1}) 1654 ($\nu_{C=O}$); ^{1}H NMR (399.78 MHz, $CDCl_3$) δ 0.71-0.77 (m, 20 H), 1.07-1.12 (m, 8 H), 1.86-1.92 (m, 2 H), 1.93-2.00 (m, 2 H), 2.01-2.11 (m, 4 H), 7.01-7.06 (m, 3 H), 7.14-7.16 (m, 5 H), 7.25 (s, 1 H), 7.28 (d, *J* = 8.4 Hz, 3 H), 7.38-7.44 (m, 3 H), 7.61-7.66 (m, 3 H), 7.75-7.80 (m, 2 H), 7.82-7.84 (m, 2 H), 7.92-7.99 (m, 2 H), 8.00-8.04 (m, 2 H), 8.52 (s, 1 H), 9.90 (s, 1 H); ^{13}C NMR (100.53 MHz, $CDCl_3$) δ 183.0, 154.3, 153.2, 152.8, 151.2, 150.8, 148.7, 147.6, 144.0, 142.8, 141.6, 141.4, 140.3, 140.1, 137.6, 135.6, 135.0, 134.2, 129.3, 128.3, 127.7, 127.2, 126.1, 124.9, 124.0, 123.7, 123.1, 122.7, 121.9, 121.1, 120.0, 119.3, 119.2, 117.8, 55.5, 55.2, 40.2, 40.1, 29.8, 26.2, 23.3, 23.1. 14.1, 14.0. HRMS calcd for $C_{69}H_{64}N_4OS_3$ $[M+H]^+$ m/z 1061.4315 found 1061.4323.

Synthesis (E)-3-(4-(2-butyl-7-(4-(9,9-dibutyl-9H-fluoren-2-yl)-4H-dithieno[3,2-b:2',3'-d]pyrrol-2-yl)-2H-benzo[d][1,2,3]triazol-4-yl)phenyl)-2-cyanoacrylic acid ***(JS10).***

It was prepared from **14** (0.140 g, 0.20 mmol by following a procedure similar to that described above for the synthesis of **JS1**; yield (0.096 g, 60%); mp 215-217 °C; IR (KBr, cm^{-1}) 2219 ($\nu_{C\equiv N}$); ^{1}H NMR (399.78 MHz, DMSO-d_6) δ 0.53-0.64 (m, 10 H), 0.86-0.92 (m, 3 H), 1.00-1.09 (m, 4 H), 1.31-1.40 (m, 2 H), 2.02-2.17 (m, 6 H), 4.84 (t, *J* = 7.2 Hz, 2 H), 7.25 (d, *J* = 5.6 Hz, 1 H), 7.33-7.39 (m, 2 H), 7.47-7.49 (m, 1 H), 7.58 (d, *J* = 5.2 Hz, 1 H), 7.70 (d, *J* = 8.4 Hz, 1 H), 7.82-7.89 (m, 4 H), 8.03 (d, *J* = 8.0 Hz, 1 H), 8.14 (d, *J* = 8.4 Hz, 2 H), 8.29-8.34 (m, 4 H); ^{13}C NMR (100.53 MHz, DMSO- d_6) δ 163.8, 152.8, 150.8, 144.9, 144.2, 142.9, 141.8, 140.9, 140.3, 139.4, 138.4, 137.1, 131.5, 131.5, 129.0, 127.7, 127.1, 127.0, 125.9, 123.5, 122.4, 121.8, 120.5, 117.9, 117.5, 117.0, 113.0, 112.9, 55.7, 55.4, 32.1, 26.4, 23.0, 22.6, 19.8, 14.3, 13.9. HRMS calcd for $C_{49}H_{45}N_5O_2S_2$ $[M+H]^+$ m/z 800.3087 found 822.3111.

Synthesis of (E)-3-(5-(2-butyl-7-(4-(9,9-dibutyl-9H-fluoren-2-yl)-4H-dithieno[3,2-b:2',3'-d]pyrrol-2-yl)-2H-benzo[d][1,2,3]triazol-4-yl)thiophen-2-yl)-2-cyanoacrylic acid ***(JS11).***

It was prepared from **16** (0.150 g, 0.20 mmol) by following a procedure similar to that described above for the synthesis of **JS1**. Black solid; yield (0.103 g, 64%); m.p. 250-252 °C; IR (KBr, cm^{-1}) 2217 ($\nu_{C\equiv N}$); ^{1}H NMR (399.78 MHz, DMSO-d_6) δ 0.38-0.63 (m, 10 H), 0.89-0.93 (m, 4 H), 1.00-1.07 (m, 3 H), 1.29-1.41 (m, 2 H), 2.02-2.14 (m, 6 H), 4.81-4.83 (d, *J* = 6.4 Hz, 2 H), 7.22-7.38 (m, 4 H), 7.48 (d, *J* = 6.0 Hz, 1 H), 7.54-7.57 (m, 1 H), 7.67-7.88 (m, 4 H), 7.98-8.04 (m, 2 H), 8.15 (t, *J* = 4.0 Hz, 1 H), 8.23-8.26 (m, 1 H), 8.40 (s, 1 H); ^{13}C NMR (100.53 MHz, DMSO-d_6) δ 164.1, 152.8, 155.5, 150.8, 145.7, 145.0, 144.2, 141.7, 141.3, 140.3, 139.3, 138.3, 136.9, 136.3, 127.9, 127.6, 127.2, 126.3, 125.0, 124.0, 123.5, 122.1, 122.0, 121.8, 121.7, 121.0, 120.5, 118.2, 117.6, 117.4, 117.0, 113.2, 112.9, 56.7, 55.3, 31.7, 26.4, 23.0, 19.9, 14.3, 13.9. HRMS calcd for $C_{47}H_{43}N_5O_2S_3$ $[M+Na]^+$ m/z 828.2471 found 828.2491.

Synthesis of (E)-3-(4-(2,3-bis(4-(tert-butyl)phenyl)-8-(4-(9,9-dibutyl-9H-fluoren-2-yl)-4H-dithieno[3,2-b:2',3'-d]pyrrol-2-yl)quinoxalin-5-yl)phenyl)-2-cyanoacrylic acid ***(JS12).***

It was prepared from **15** (0.120 g, 0.13 mmol) by following a procedure similar to that described above for the synthesis of **JS1**. Brown solid; yield (0.095g, 72%); mp 218-220 °C; IR (KBr, cm^{-1}) 2219 ($\nu_{C\equiv N}$); ^{1}H NMR (399.78 MHz, DMSO-d_6) δ 0.54-0.65 (m,

10 H), 0.99-1.08 (m, 4 H), 1.15 (s, 9 H), 1.22 (s, 9 H), 1.95-2.01 (m, 2 H), 2.07-2.14 (m, 2 H), 7.22-7.30 (m, 5 H), 7.33-7.39 (m, 4 H), 7.46-7.48 (m, 1 H), 7.52 (d, *J* = 8.4 Hz, 2 H), 7.59 (d, *J* = 5.2 Hz, 1 H), 7.66 (d, *J* = 7.6 Hz, 1 H), 7.75 (s, 1 H), 7.80 (d, *J* = 7.6 Hz, 1 H), 7.88 (d, *J* = 6.4 Hz, 1 H), 7.94-7.98 (m, 2 H), 8.02 (d, *J* = 8.0 Hz, 1 H), 8.11-8.15 (m, 3 H), 8. 33 (s, 1 H), 8.37 (s, 1 H); ^{13}C NMR (100.53 MHz, DMSO- d_6) δ 163.9, 154.1, 152.8, 152.3, 152.1, 151.4, 151.0, 144.8, 144.1, 142.7, 140.3, 139.3, 138.8, 132.8, 131.8, 131.1, 130.7, 130.2, 129.8, 127.9, 127.6, 126.7, 125.5, 125.4, 123.5, 121.9, 121.7, 120.6, 119.7, 117.7, 117.0, 116.9, 113.8, 112.81, 112.77, 55.5, 34.9, 31.6, 26.4, 23.0, 14.3. HRMS calcd for $C_{67}H_{62}N_4O_2S_2$ $[M+Na]^+$ m/z 1041.4206 found 1041.4214.

Synthesis of (E)-3-(5-(2,3-bis(4-(tert-butyl)phenyl)-8-(4-(9,9-dibutyl-9H-fluoren-2-yl)-4H-dithieno[3,2-b:2',3'-d]pyrrol-2-yl)quinoxalin-5-yl)thiophen-2-yl)-2-cyanoacrylic acid ***(JS13).***

It was prepared from **17** (0.140 g, 0.15 mmol) by following a procedure similar to that described above for the synthesis of **JS1.** Black solid; yield (0.102 g, 66%); mp 232-235 °C; IR (KBr, cm^{-1}) 2224 ($\nu_{C\equiv N}$); ^{1}H NMR (399.78 MHz, $CDCl_3$) δ 0.72-0.74 (m, 10 H), 1.12-1.16 (m, 4 H), 1.37 (d, *J* = 1.6 Hz, 18 H), 2.07-2.15 (m, 4 H), 7.42-7.49 (m, 4 H), 7.57-7.72 (m, 11 H), 7.76-7.82 (m, 1 H), 7.89-8.01 (m, 4 H), 8.35-8.50 (m, 2 H), 8.66 (s, 1 H); ^{13}C NMR (100.53 MHz, $CDCl_3$) δ 153.0, 150.6, 150.3, 150.2, 146.4, 130.1, 129.9, 129.8, 129.6, 129.52, 129.46, 129.3, 127.5, 127.4, 127.1, 127.0, 126.5, 126.4, 122.9, 122.4, 121.6, 120.6, 119.7, 117.6, 114.8, 112.2, 55.2, 39.9, 22.7, 13.43, 13.37. HRMS calcd for $C_{65}H_{60}N_4O_2S_3$ $[M+Na]^+$ m/z 828.2471 found 828.2491.

Synthesis of (E)-2-cyano-3-(4-(7-(4-(9,9-dibutyl-9H-fluoren-2-yl)-4H-dithieno[3,2-b:2',3'-d]pyrrol-2-yl)benzo[c][1,2,5]thiadiazol-4-yl)phenyl)acrylic acid ***(JS14).***

It was prepared from **19** (0.120 g, 0.17 mmol) by following a procedure similar to that described above for **JS1**. Brown solid; yield (0.105 g, 80%); mp 236-238 °C; IR (KBr, cm^{-1}) 2215 ($\nu_{C\equiv N}$); ^{1}H NMR (399.78 MHz, DMSO-d_6) δ 0.54-0.67 (m, 10 H), 1.05-1.12 (m, 4 H), 2.05-2.25 (m, 4 H), 7.27 (d, *J* = 5.6 Hz, 1 H), 7.34-7.40 (m, 2 H), 7.48-7.50 (m, 1 H), 7.58 (d, *J* = 5.2 Hz, 1 H), 7.68 (dd, *J* = 1.2, 7.6 Hz, 1 H), 7.81 (s, 1 H), 7.88 (d, *J* = 6.4 Hz, 1 H), 7.98-8.08 (m, 5 H), 8.06-8.08 (m, 3 H), 1.09 (s, 1 H); ^{13}C NMR (100.53 MHz, DMSO-d_6) δ 158.0, 153.3, 152.3, 150.8, 145.4, 144.8, 143.1, 140.3, 139.8, 138.2, 136.6, 132.0, 130.6, 130.3, 130.1, 130.0, 129.5, 129.2, 129.0, 127.5, 127.2, 124.1, 123.3, 123.1, 121.4, 120.9, 119.9, 118.8, 118.4, 117.5, 116.9, 115.9, 114.6, 113.1, 112.3, 110.3,

55.5, 40.3, 26.2, 23.3, 13.9. HRMS calcd for $C_{45}H_{36}N_4O_2S_3$ $[M]^+$ m/z 760.2000 found 760.1980.

Synthesis of (E)-2-cyano-3-(5-(7-(4-(9,9-dibutyl-9H-fluoren-2-yl)-4H-dithieno[3,2-b:2',3'-d]pyrrol-2-yl)benzo[c][1,2,5]thiadiazol-4-yl)thiophen-2-yl)acrylic acid ***(JS15).***

It was prepared from **20** (0.150 g, 0.22 mmol) by following a procedure similar to that described above for **JS1**. Black solid; yield (0.100 g, 61%); mp 225-228 °C; IR (KBr, cm^{-1}) 2218 ($\nu_{C\equiv N}$). ^1H NMR (399.78 MHz, DMSO- d_6) 0.50-0.71 (m, 10 H), 1.06-1.15 (m, 4 H), 2.05-2.19 (m, 4 H), 7.21 (d, *J* = 5.6 Hz, 1 H), 7.35-7.41 (m, 2 H), 7.50 (d, *J* = 6.4 Hz, 1 H), 7.55 (d, *J* = 5.2 Hz, 1 H), 7.66 (d, *J* = 8.0 Hz, 1 H), 7.81 (s, 1 H), 7.88 (d, *J* = 7.2 Hz, 1 H), 7.93- 7.99 (m, 2 H), 8.03 (d, *J* = 8.0 Hz, 1 H), 8.16-8.19 (m, 2 H), 8.39 (s, 2 H); ^{13}C NMR could not be recorded because of solubility problem. HRMS calcd for $C_{43}H_{34}N_4O_2S_7$ $[M+Na]^+$ m/z 789.1457 found 789.1471.

Synthesis of (E)-2-cyano-3-(4-(7-(4-(9,9-dibutyl-9H-fluoren-2-yl)-6-(4-(diphenylamino)phenyl)-4H-dithieno[3,2-b:2',3'-d]pyrrol-2-yl)benzo[c][1,2,5]thiadiazol-4-yl)phenyl)acrylic acid ***(JS16).***

It was prepared from **22** (0.120 g, 0.13 mmol) by following a procedure similar to that described above for **JS1**. Black solid; yield (0.098 g, 76%); mp = 281-283 °C, IR (KBr, cm^{-1}) 2222 ($\nu_{C\equiv N}$). ^1H NMR (399.78 MHz, $CDCl_3$ δ 0.50-0.67 (m, 10 H), 0.82-1.10 (m, 4 H), 1.89-.19 (m, 4 H), 6.69-6.94 (m, 6 H), 7.02-7.06 (m, 7 H), 7.23-7.48 (m, 9 H), 7.56-7.73 (m, 4 H), 7.90-8.25 (m, 4 H); ^{13}C NMR (100.53 MHz, $CDCl_3$) δ 160.5, 151.5, 147.1, 129.5, 129.3, 124.9, 123.7, 123.3, 123.2, 121.3, 120.0, 119.9, 55.3, 40.3, 26.3, 14.1. HRMS calcd for $C_{63}H_{49}N_5O_2S_3$ $[M+H]^+$ m/z 1004.3121 found 1004.3131.

*Synthesis of (E)-2-cyano-3-(4-(7-(6-(9,9-dibutyl-7-(diphenylamino)-9H-fluoren-2-yl)-4-(9,9-dibutyl-9H-fluoren-2-yl)-4H-dithieno[3,2-b:2',3'-d]pyrrol-2-yl)benzo[c][1,2,5]thiadiazol-4-yl)phenyl)acrylic acid (**JS17**).*

It was prepared from **24** (0.120 g, 0.11 mmol) by following a procedure similar to that described above for **JS1**. Black solid; yield (0.100 g, 79%); mp 342-344 °C, IR (KBr, cm^{-1}) 2228 ($\nu_{C\equiv N}$). ^1H NMR (399.78 MHz, DMSO-d_6 δ 0.70-0.87 (m, 20 H), 1.04-1.12 (m, 4 H), 1.16-1.26 (m, 4 H), 1.85-1.98 (m, 4 H), 2.09-2.20 (m, 4 H), 7.00-7.23 (m, 4 H), 7.37-7.52 (m, 7 H), 7.72 (s, 4 H), 7.80 (d, *J* = 6.8 Hz, 3 H), 7.94 (d, *J* = 8.0 Hz, 4 H), 8.20 (s, 5 H), 8.44-8.58 (5 H); ^{13}C NMR could not be recorded due to poor solubility in solvents. HRMS calcd for $C_{78}H_{69}N_5O_2S_3$ $[M]^+$ m/z 1203.4610 found 1203.4637.

*Synthesis of (E)-2-cyano-3-(4-(9,9-dibutyl-9H-fluoren-2-yl)-6-(7-(4-(diphenylamino)phenyl)benzo[c][1,2,5]thiadiazol-4-yl)-4H-dithieno[3,2-b:2',3'-d]pyrrol-2-yl)acrylic acid (**JS18**).*

It was prepared from 23 (0.150 g, 0.17 mmol) by following a procedure similar to that described above for **JS1**. Black solid; yield (0.115g, 73%); mp 293-295 °C, IR (KBr, cm^{-1}) 2206 ($\nu_{C\equiv N}$). ^1H NMR (399.78 MHz, $CDCl_3$ δ 0.72-0.75 (m, 10 H), 1.15-1.20 (m, 4 H), 2.07-2.11 (m, 4 H), 7.25 (s, 2 H), 7.35 (s. 2 H), 7.41 (d, *J* = 4.4 Hz, 9 H), 7.60-7.63 (m, 5 H), 7.79 (d, J = 5.2 Hz, 3 H), 7.92-7.96 (m, 3 H), 8.35-8.44 (m, 2 H); ^{13}C NMR could not be recorded due to poor solubility in solvents. HRMS calcd for $C_{57}H_{45}N_5O_2S_3$ $[M+H]^+$ m/z 928.2808 found 928.2803.

*Synthesis of (E)-2-cyano-3-(6-(7-(9,9-dibutyl-7-(diphenylamino)-9H-fluoren-2-yl)benzo[c][1,2,5]thiadiazol-4-yl)-4-(9,9-dibutyl-9H-fluoren-2-yl)-4H-dithieno[3,2-b:2',3'-d]pyrrol-2-yl)acrylic acid **(JS19).***

It was prepared from (0.140 g, 0.13 mmol) by following a procedure similar to that described above for **JS1**. Black solid; yield (0.114 g, 77%); mp 354-357 °C, IR (KBr, cm^{-1}) 2216 ($\nu_{C\equiv N}$). ^1H NMR (399.78 MHz, DMSO-d_6 δ 0.70-0.87 (m, 20 H), 1.04-1.12 (m, 4 H), 1.16-1.26 (m, 4 H), 1.85-1.95 (m, 4 H), 2.09-2.20 (m, 4 H), 7.26 (m, 4 H), 7.40-7.52 (m, 9 H), 7.62-7.66 (m, 6 H), 7.79-7.82 (m, 3 H), 7.90-7.99 (m, 4 H), 8.49 (s, 1 H); ^{13}C NMR could not be recorded due to poor solubility in solvents. HRMS calcd for $C_{72}H_{65}N_5O_2S_3$ $[M]^+$ m/z 1127.4295 found 1127.4269.

4.4.3 Computational methods

All the computational methodology used is similar to that described in Chapter 2.

4.4.4 Fabrication and characterization of DSSC

The DSSCs were fabricated and characterized by following the procedures detailed in Chapter 2 for the dyes **JS1-JS5**.

Chapter 5

Dithienopyrrole-based dianchoring H- and λ-shaped dyes: Effect of donors

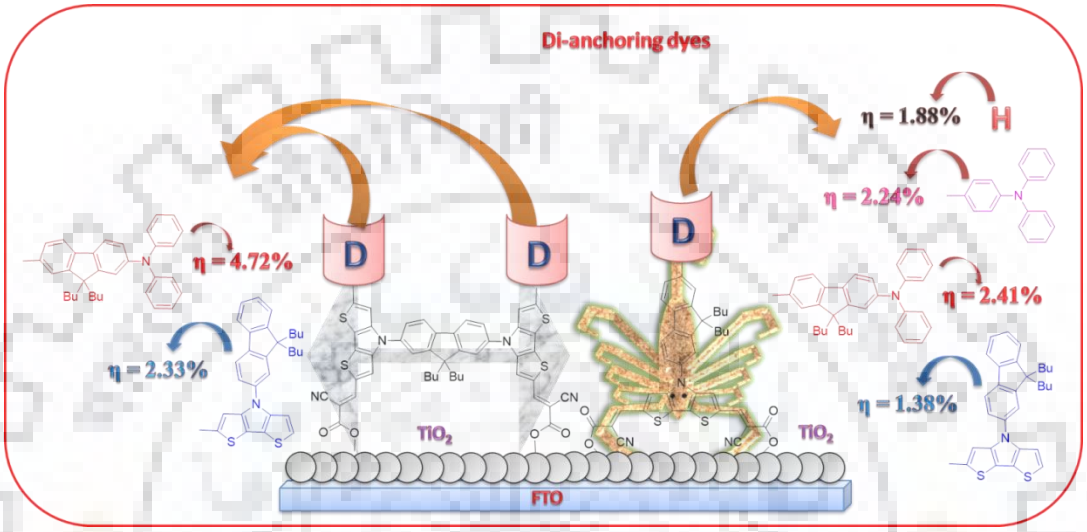

5.1 Introduction

The commonly used motif of the metal free organic dyes is D-π-A, in which D is the donor, π is conjugating spacer and A is the anchoring group [14,18,42,49,217]. During the photoexcitation intramolecular charge transfer (ICT) takes place from D to A and from there electron injected to the conduction band of TiO_2 through anchoring group. Thus the anchoring group determines the binding capacity of the dye on TiO_2 nanoparticles which controls the rate of electron injection from excited dye and the efficiency of the dyes [14,18,42,49,217]. Apart from this, by increasing the number of anchoring groups (multi-anchoring) it is also possible to modulate the position of LUMO energy levels [218,219]. Also in comparison of mono-anchoring dyes, the multi-anchoring dyes possess the advantages such as increase in light harvesting efficiency and long term stability on the surface of TiO_2 [172,218,219]. The different possible architectures of the dyes in which two acceptor/anchoring groups have been inserted so far are (a) A-D-π-D-A (b) D-(π-A)$_2$ (c) (D-π-A)$_2$ (d) D-π-(A)$_2$ shown in Figure 5.1. The cyanoacrylic acid is one of the most commonly used acceptor/anchoring group used for the organic sensitizers as it can efficiently bind on the TiO_2 nanoparticles [13,172].

Therefore cyanoacrylic acid has been used in number of multi-anchoring systems [220-228].

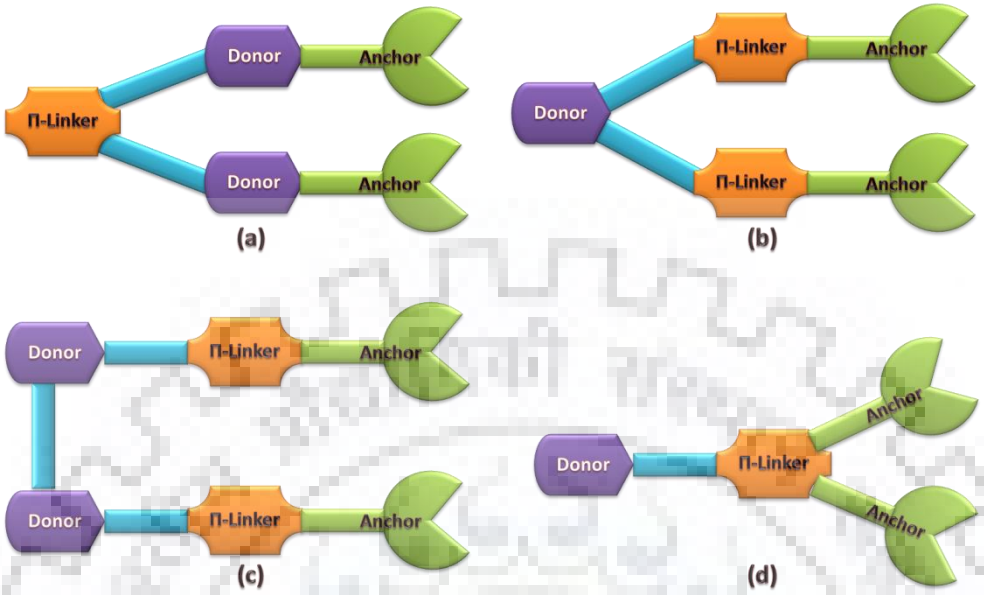

Figure 5.1 Different architectures of metal free organic di-anchoring dyes.

Recently cyanoacrylic acid has been reported in one donor and two acceptors (D-π-A_2) configuration to synthesize di-anchoring dyes **DAZ2** and **DAZ5** constituted by 2,3,5-substituted thiophene [229]. In comparison to the mono-anchoring congener dye **S1,** the di-anchoring dyes showed a high light harvesting efficiency and charge recombination resistance and exhibited PCE 7.02% and 7.28% respectively. Later, imidazole was used to construct the D-π-A_2 motifs, which was further fused to dithienobenzimidazole unit to earn red shifted and enhanced molar extinction coefficient for the longest absorption wavelength [221]. This strategy led to increase in the J_{SC} value. In order to attain the A-D-π-D-A architecture of the dyes, two arylamine donor were connected through π-linker such as biphenyl, fluorene, bithiophene [221,230] etc. these dyes were able to retard the charge recombination and imparted extended electron lifetime as compared to their mono-anchoring counterparts. However, the use of electron deficient moiety (BTD) [222] was found to hamper the photoinduced charge transfer from dye to the CB of TiO_2 in this design.

Lin and co-workers synthesized A-π-D-π-A di-anchoring dyes **S3** and **S4** featuring dithienopyrrole (DTP) donor in conjugation with thiophene and bithiophene conjugating units respectively [139]. These dyes showed broader and extended absorption maxima.

The dye **S3** produced the PCE of 3.70% which was further improved to 4.31% by the use of chenodeoxycholic acid (CDCA) as co-adsorbent.

Later on the use of DTP as a conjugating spacer in A-π-D-π-A configuration showed a high molar extinction coefficient for the dyes **FD1-3** [140]. The use of phenyl unit instead of alkyl chain on nitrogen atom of DTP (the dye **FD2)** found to be beneficial for the retardation of charge recombination, increase in electron life time and exhibited the PCE of 6.32% without the use of co-adsorbent. This discussion showed that conversion of mono-anchoring dye to multi-anchoring system in conjugation with suitable multi-functionalized aromatic moiety can be a promising strategy to improve the efficiency of DSSCs.

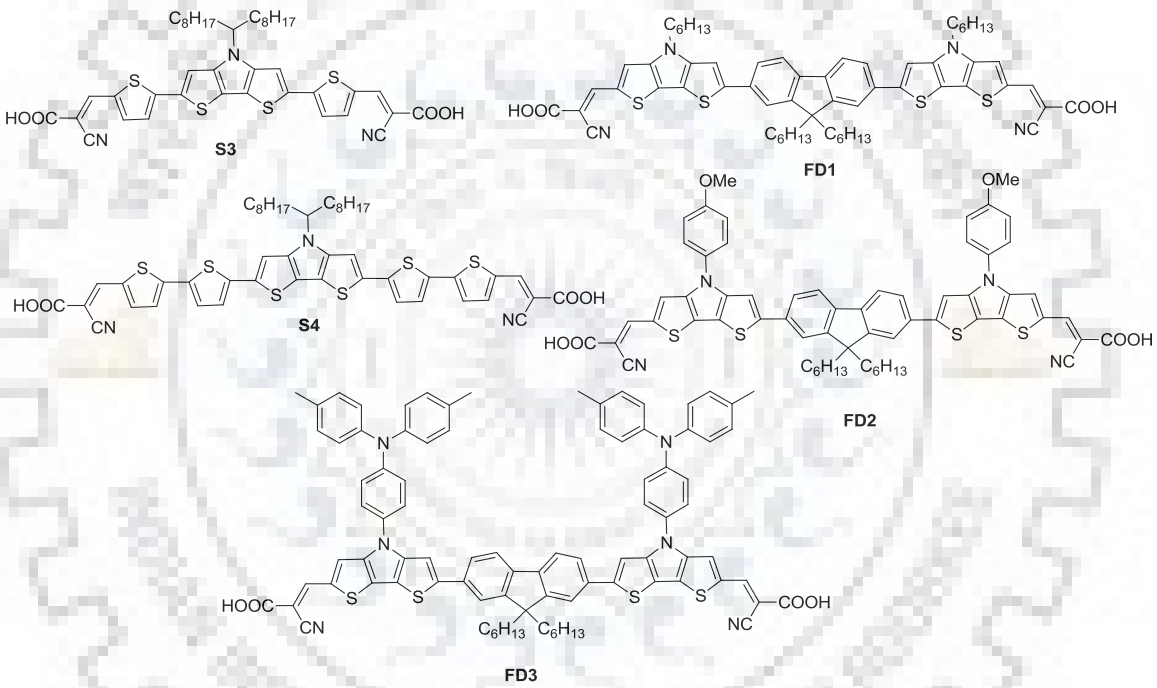

Figure 5.2 Dithienopyrrole based reported di-anchoring dyes [139,140].

In our previous chapters we have used *N*-fluorene appended DTP unit to synthesize the mono-anchoring dyes. Here in this chapter, we explored the fluorene appended DTP through two different design featuring λ- and H-shapes. Where in λ-shaped di-anchoring system, in which DTP has been tri-functionalized with three substituents, one is attached at pyrrole nitrogen atom other two are cyanoacrylic acid at the C2 and C6-positions. On the other hand for H-shaped dyes, fluorene has been used as bridge through the pyrrolic nitrogen of DTPs to connect two monoanchoring dyes **JS4** (chapter 1) and **JS6** (chapter 2). We expected that the di-anchoring dye would be able to bring the structural variety for panchromatic response, extension of π-conjugation and to enhance the binding capacity to

the TiO_2 nanoparticles. We further extended the π-conjugation on *N*-fluorenyl unit by different aromatic chromophores such as triphenylamine (TPA), 9,9-dibutyl-*N*,*N*-diphenyl-9*H*-fluoren-2-amine (DPF) and 4-(9,9-dibutyl-9*H*-fluoren-2-yl)-4*H*-dithieno[3,2-*b*:2',3'-*d*]pyrrole (FDTP) to see their effect on light harvesting efficiency and other photovoltaic parameters. Therefore, in comparison to mono-anchoring dye **JS1**, newly synthesized λ-shaped di-anchoring dyes displayed impressive results and H-shaped dyes were able to increase the light harvesting efficiency almost two-fold in comparison to the mono-anchoring congeners.

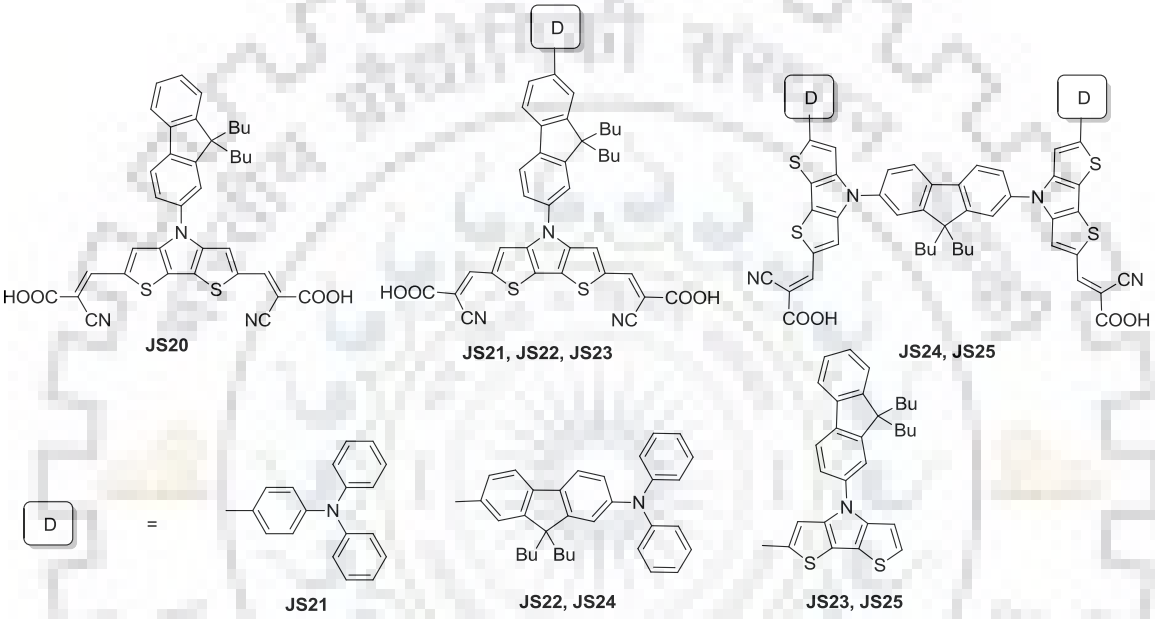

Figure 5.3 Structures of newly synthesized DTP-based λ- and H-shaped di-anchoring dyes.

5.2 Result and discussion

5.2.1 Molecular design and synthesis

The synthetic scheme for the λ-shaped di-anchoring dyes (Figure 5.3) featuring DTP functionalized with different aromatic segments at pyrrolic nitrogen and two cyanoacrylic acid units at C2 and C6-positions of the DTP is depicted in scheme 5.1 whereas, for H-shaped dyes is given in scheme 5.2. A multi-step sequence involving Vilsmeier-Haack formylation, bromination, Suzuki-Miyaura [179]/Stille [158] cross-coupling and Knoevenagel condensation was applied to achieve the target dyes. In the first step for the synthesis of λ-shaped dyes, 4-(9,9-dibutyl-9*H*-fluoren-2-yl)-4*H*-dithieno[3,2-b:2',3'-*d*]pyrrole-2,6-dicarbaldehyde (**27**) was obtained by Vilsmeier-Haack formylation of 4-(9,9-dibutyl-9*H*-fluoren-2-yl)-4*H*-dithieno[3,2-*b*:2',3'-*d*]pyrrole (**1**). Next the bromination

in a stoichiometric controlled reaction yielded the key precursor 4-(7-bromo-9,9-dibutyl-9*H*-fluoren-2-yl)-4*H*-dithieno[3,2-*b*:2',3'-*d*]pyrrole-2,6-dicarbaldehyde (**28**) containing bromine at C7 position of *N*-fluorenyl unit. Subsequently, the aldehydes **29** and **30** were synthesized by performing Suzuki coupling reaction of **28** with (4-(diphenylamino)phenyl)boronic acid and (9,9-dibutyl-7-(diphenylamino)-9*H*-fluoren-2-yl)boronic acid, respectively. However, Stille coupling protocol was employed to obtain the aldehyde **31** from **28** and **3** (chapter 2).

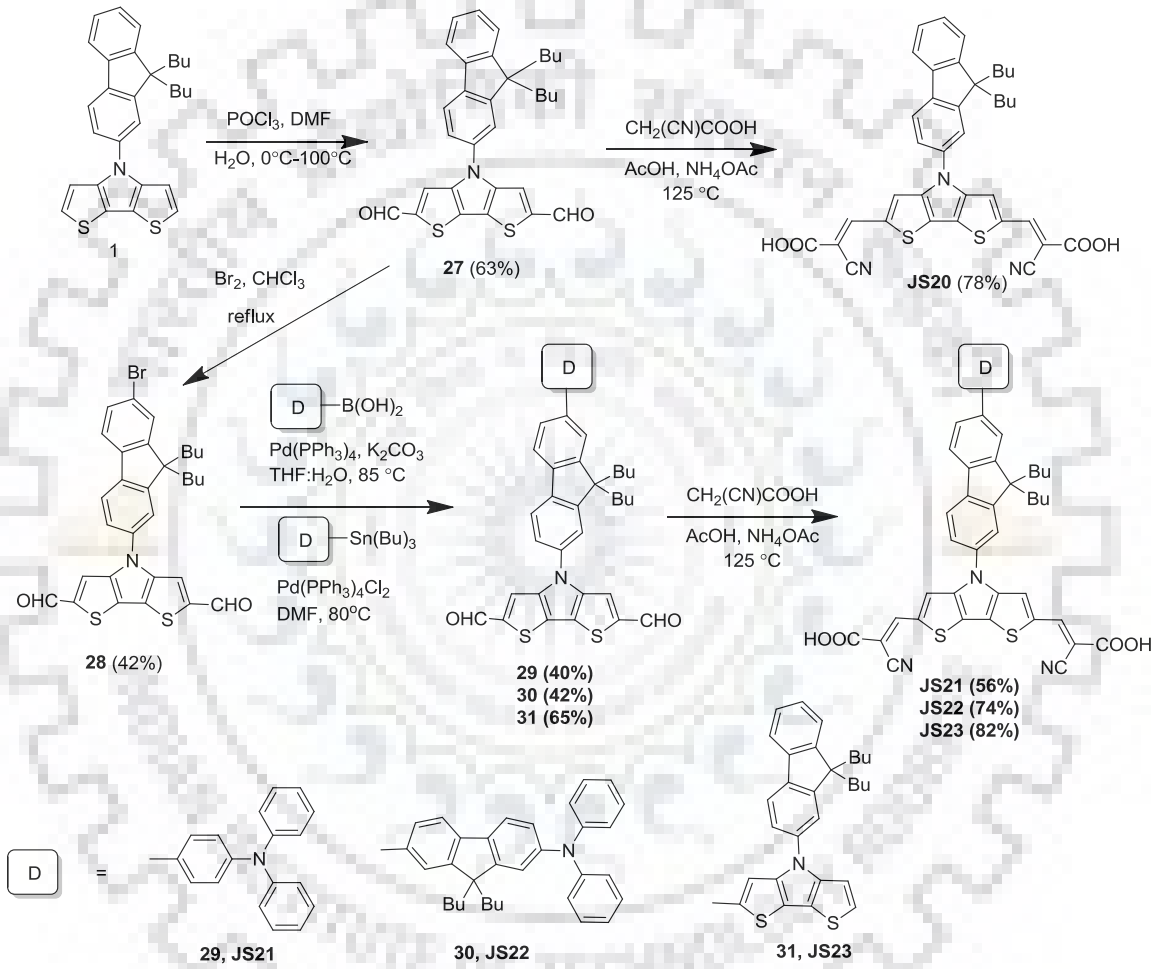

Scheme 5.1 Synthetic scheme for the synthesis of DTP-based λ-shaped di-anchoring dyes **JS20-JS23**.

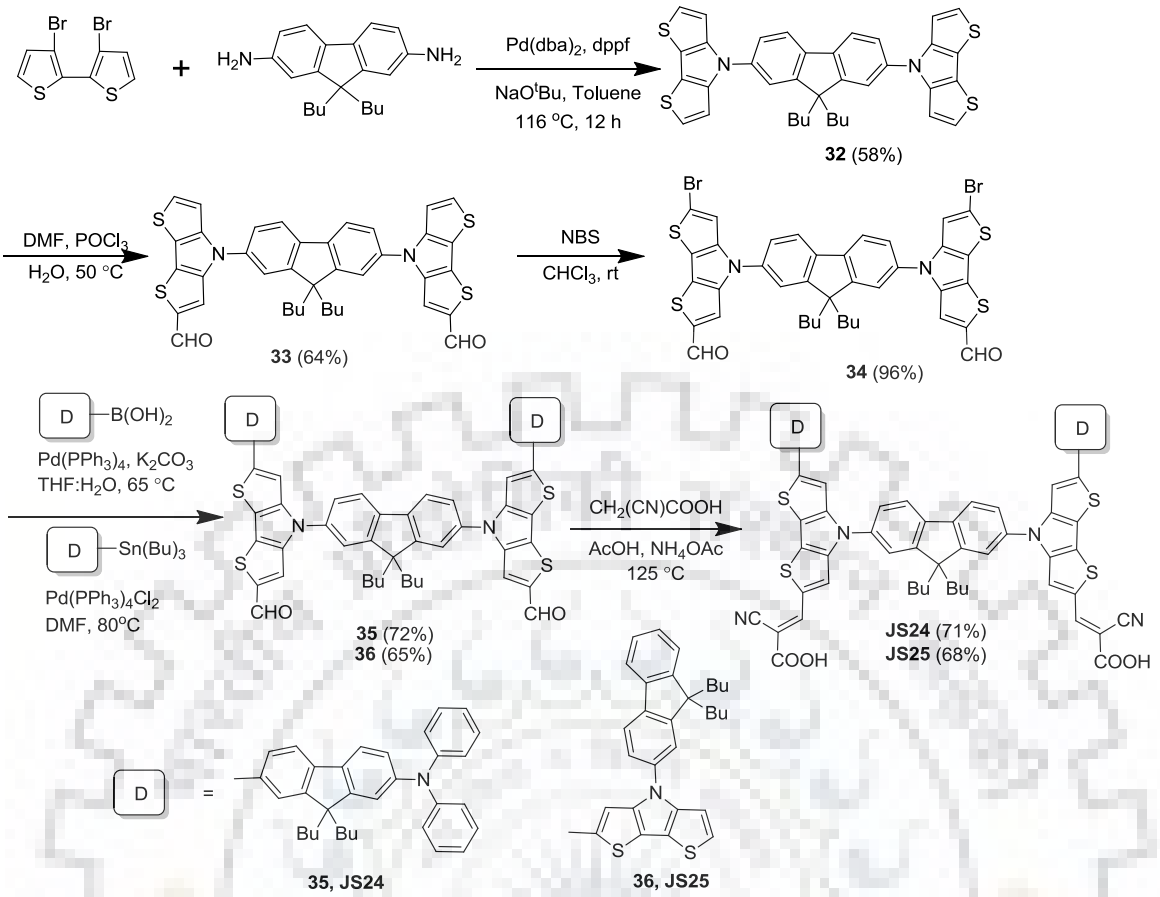

Scheme 5.2 Synthetic scheme for the synthesis of DTP based H-shaped dianchoring dyes **JS24** and **JS25**.

On the other hand, for the synthesis of H-shaped dyes the essential derivative 4,4'-(9,9-dibutyl-9*H*-fluorene-2,7-diyl)bis(4*H*-dithieno[3,2-*b*:2',3'-*d*]pyrrole) **32** was synthesized from 3,3'-dibromo-2,2'-bithiophene and 9,9-dibutyl-9*H*-fluorene-2,7-diamine in reasonable yield by palladium catalyzed Buchwald-Hartwig C-N cross coupling reaction. Next, the stoichiometric controlled formylation of **32** using DMF and $POCl_3$ produced 4,4'-(9,9-dibutyl-9*H*-fluorene-2,7-diyl)bis(4H-dithieno[3,2-b:2',3'-d]pyrrole-2-carbaldehyde) (**33**). Subsequently, 4,4'-(9,9-dibutyl-9*H*-fluorene-2,7-diyl)bis(6-bromo-4*H*-dithieno[3,2-*b*:2',3'-*d*]pyrrole-2-carbaldehyde) (**34**) was obtained by the bromination of **33** using *N*-bromosuccinimide. Further, Suzuki-coupling reaction of **34** with (9,9-dibutyl-7-(diphenylamino)-9*H*-fluoren-2-yl)boronic acid, and Stille coupling reaction with 4-(9,9-dibutyl-9*H*-fluoren-2-yl)-2-(tributylstannyl)-4H-dithieno[3,2-*b*:2',3'-*d*]pyrrole yielded **35** and **36** respectively. Finally, all the aldehydes **27, 29, 30, 31, 35** and **36** were converted into the target dyes **JS20**, **JS21, JS22, JS23, JS24** and **JS25,** respectively by reacting with cyanoacetic acid in the presence of catalytic amount of ammonium acetate.

The new compounds were thoroughly characterized by NMR spectroscopy, FT-IR, and HR mass spectra. The proposed structures of the newly synthesized compounds were found to be consistent with the observed spectral data.

5.2.2 Optical properties

The light harvesting efficiencies of newly synthesized dyes were investigated by recording their absorption spectra in tetrahydrofuran (THF) and displayed in Figure 5.4. Generally, the λ-shaped dyes showed different absorptions owing to the presence of rigid dithienopyrrole (DTP) segment and multiple aromatic chromophores tethered at C7 position of *N*-fluorene unit. The higher energy band occurring at ca. 324 nm for all the dyes can be assigned to the localized π-π* transitions originating from different aromatic segments. It was interesting to note that all the dyes except the dye **JS20** showed additional bands in the region ca. 350-400 nm. These bands can be assigned to delocalized π-π* transitions arising from additional TPA, DPF and FDTP aromatic segments (Figure 5.5a and 5.5b). For these bands higher molar extinction coefficients were observed for the dyes **JS21** and **JS22** when compared to the dye **JS23** ascribed to the extension in the conjugation length by phenyl and fluorene units respectively [163]. Moreover, for the same bands slight bathochromic shift was observed in the order of **JS21** < **JS24** < **JS22** < **JS25** < **JS23**. This is because of the attainment of planarity in the conjugation path in the respective order for the dyes [231].

For λ-shaped dyes, the absorption band appeared at longer wavelength region 400-550 nm can be assigned to the π-π* transitions originating within the conjugation of DTP unit and two cyanoacrylic acid groups (*vide infra*). However, the same absorption band for the H-shaped dyes can be ascribed to the overlapping of ICT band originated from donor to cyanoacrylic acid with delocalized π-π* transitions due to increase in the conjugation length (*vide infra*). Because with extension in conjugation length reduction in π-π* band gap can be expected. The di-anchoring dye **JS20** showed red shifted absorption (λ_{max} = 490 nm) with higher molar extinction coefficient (ε_{max} = 54.4 ×10^3 $M^{-1}cm^{-1}$) when compared to the mono-anchoring congener (λ_{max} = 431 nm and ε_{max} = 35.8 ×10^3 $M^{-1}cm^{-1}$) **JS1**. This may be due to the incorporation of additional cyanoacrylic acids unit which elongated the conjugation length [172]. However, further insertion of TPA, DPF and FDTP units at C7-position of *N*-fluorene of dye **JS20** significantly broadened the absorption profile of the dyes **JS21**, **JS22** and **JS23**. The broadening effect was found to be more pronounced in case of **JS23** due to the presence of more electron rich planar

FDTP unit. This observation suggested that the tethering of aromatic segment to the *N*-fluorene unit is beneficial to increase the light harvesting efficiency of this class of dyes as it extends the conjugation.

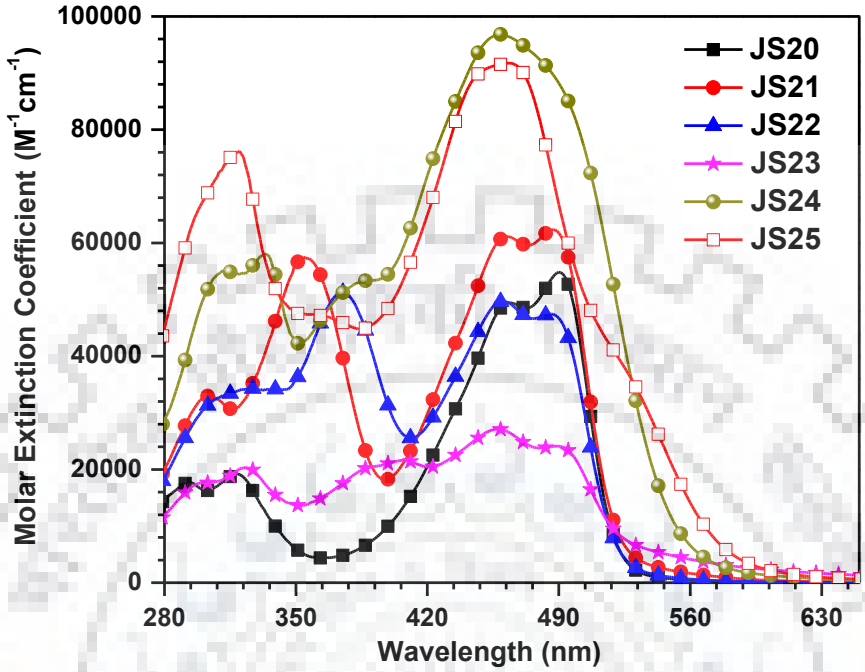

Figure 5.4 Absorption spectra of λ- and H-shaped di-anchoring dyes recorded in THF.

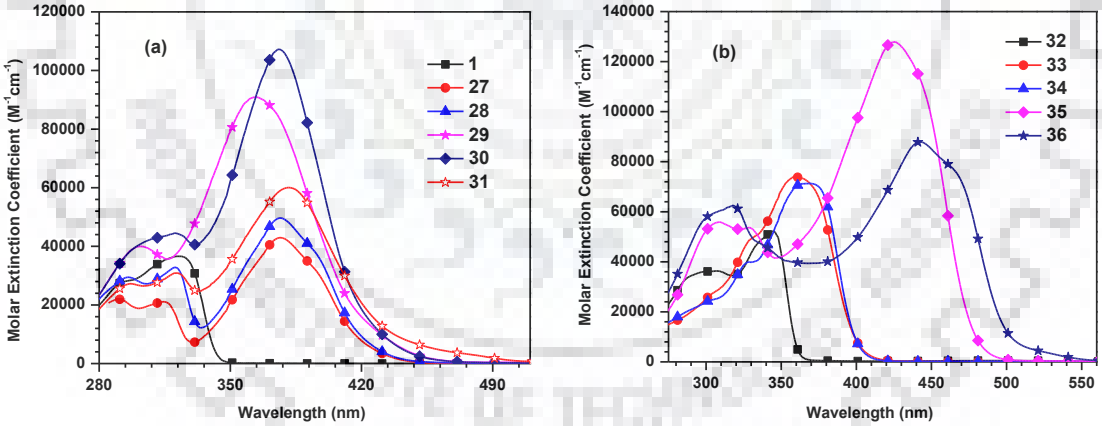

Figure 5.5 Absorption spectra of the derivatives (a) **1, 27, 28** and (b) **29** and **32, 33, 34, 35,** and **36** recorded in THF.

The absorption maxima for dyes **JS24** and **JS25** were observed to be blue shifted as compared to the dyes **JS21**, **JS22**, **JS23** and also from their linear counterparts **JS4** (chapter 1) and **JS6** (chapter 2) respectively. This might be due to the competitive sharing of donating electron from each arylamine donor by two cyanoacrylic acid acceptors in opposite direction, which suppress the charge transfer transitions from donor to acceptor

[231]. However, the similar types of ICT transitions observed from two sides of H-shaped dyes enhanced the higher molar extinction coefficient almost two-fold.

A comparison of the absorption spectra of the λ-shaped dyes with their respective aldehyde precursors confirmed additional π-π* transition band due to elongation of conjugation cyanoacrylic group (Figure 5.5a). On the other hand the comparison of absorption for the H-shaped dyes and their respective aldehyde showed the presence of charge transfer character of the absorption maxima (Figure 5.5b). This observation further supported by measuring the acid/base equilibria for the H-shaped dyes. There was significant blue/red shift observed only for longer wavelength shoulders on addition of TEA/TFA (Figure 5.6). Also, the addition of TEA resulted in blue shift, while the addition of TFA showed no significant shift for the absorption maxima for the λ-shaped dyes (**JS20**-**JS23**) (Figure 5.6). This observation suggested that these dyes were partially in deprotonate state in THF. The solvatochromism studies were carried out by recording the absorption spectra for the dyes in the solvents of different polarities (Figure 5.7). The absorption spectra for the dyes recorded in polar solvents such as DMF and MeOH exhibited blue shift. The blue shift was found to be more pronounced in DMF solvent. This might be due to the more basic nature of DMF which leads to the deprotonation of cyanoacrylic acid and hence decrease in donor-acceptor interactions. This behavior confirmed the polar ground state of the dyes being more stabilized by the polar solvents [159].

The absorption spectra of the dyes adsorbed on the mesoporous thin film of nanocrystalline TiO_2 was recorded and displayed in Figures 5.8 and 5.9. It was observed that as compared to the solution, the absorption maxima on TiO_2 for the λ-shaped dyes were blue shifted (Figure 5.4). This was due to either deprotonation of the dyes or H-type of self-aggregate formation [161]. However, for the H-shaped dyes the absorption maxima on TiO_2 red shifted as compared to the solution due to the formation of J-type aggregates on the TiO_2 surface (Figure 5.9) [161]. The absorption spectra of the dyes on TiO_2 tailed upto 600 nm for λ-shaped dyes and for the H-shaped dyes extended upto 700 nm. This might be attributed to the stronger interaction between the dye molecules and TiO_2 [139,140].

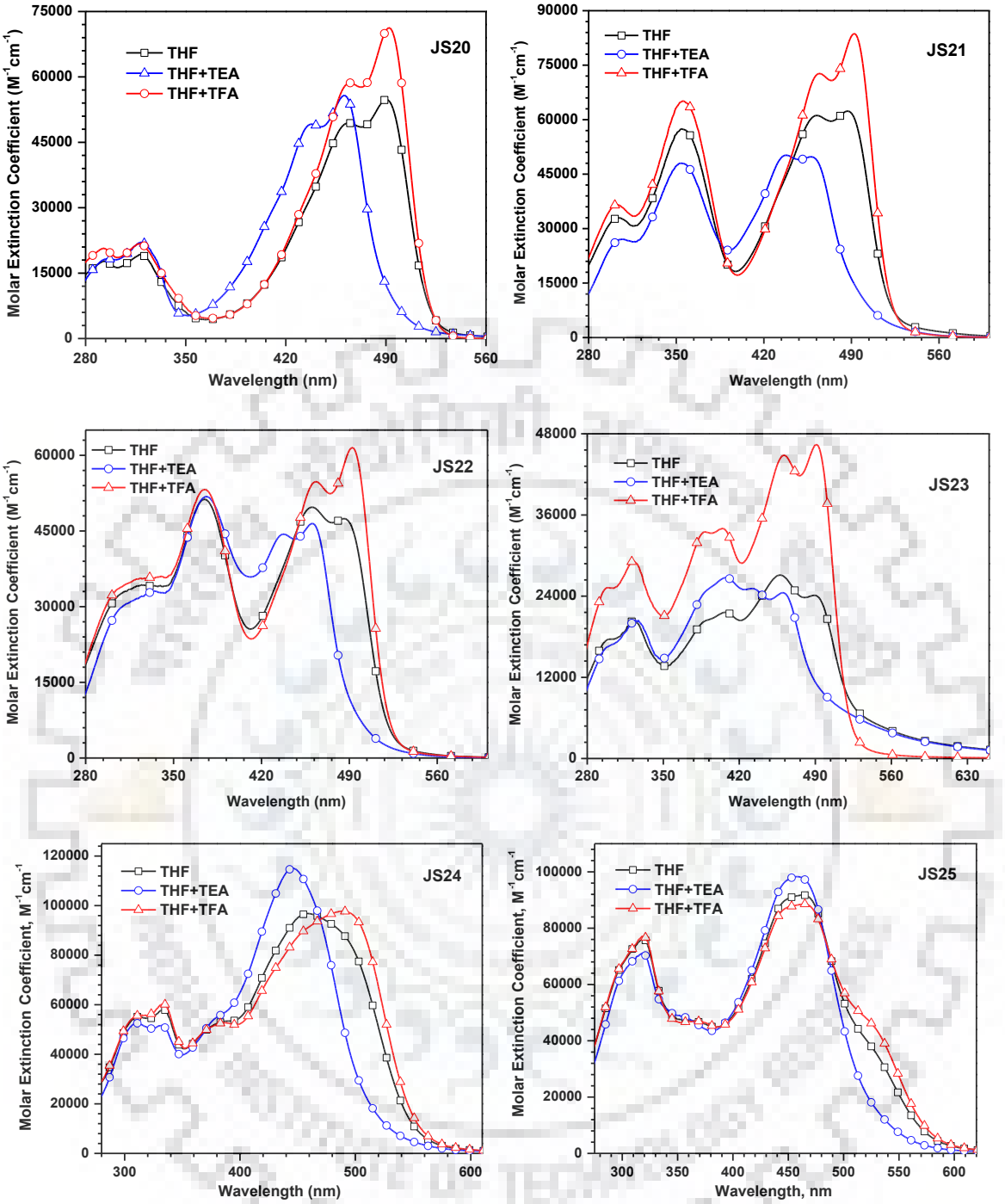

Figure 5.6 Absorption spectra of the dyes **JS20**-**JS25** recorded in THF before and after the addition of TEA/TFA.

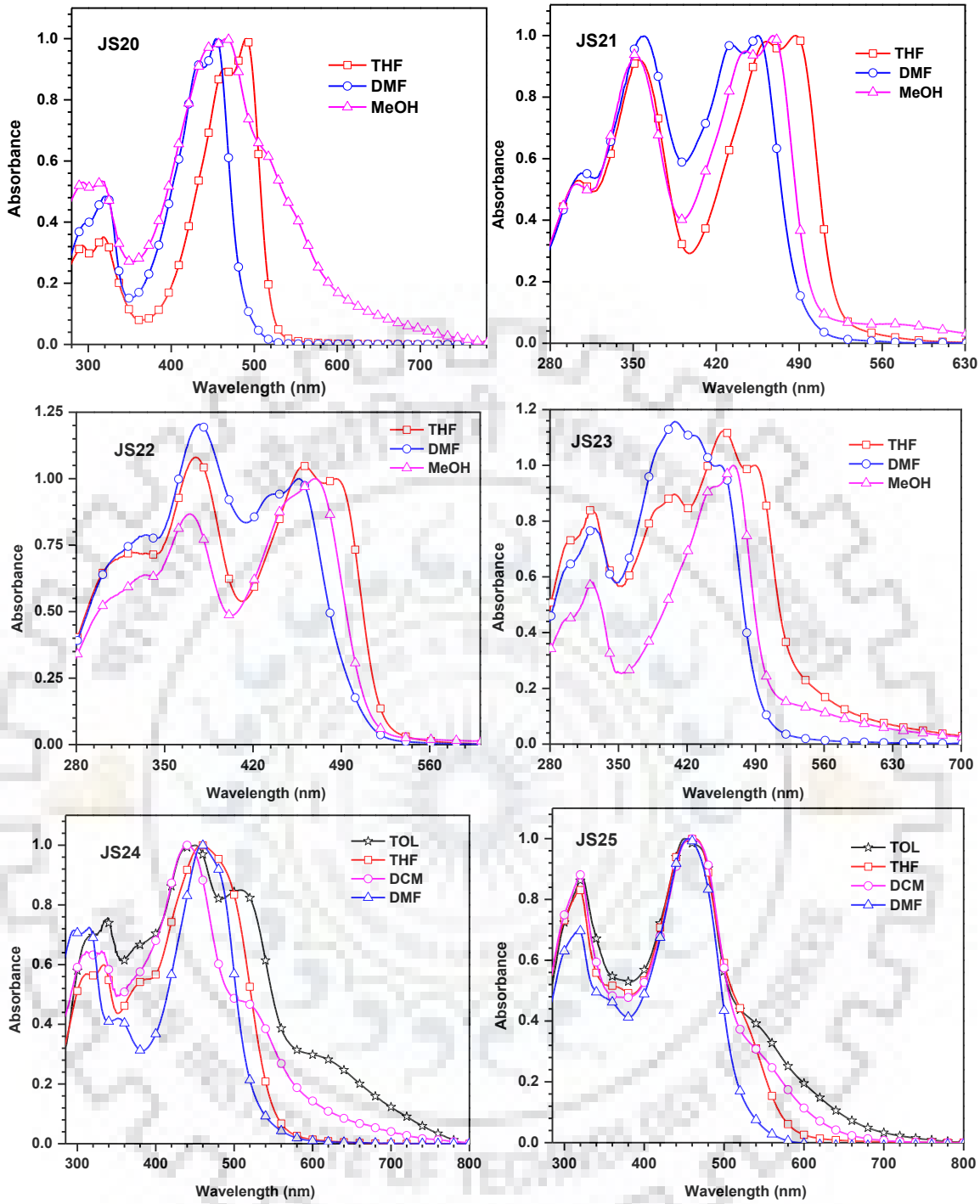

Figure 5.7 Absorption spectra of the dyes **JS20-JS25** recorded in different solvents.

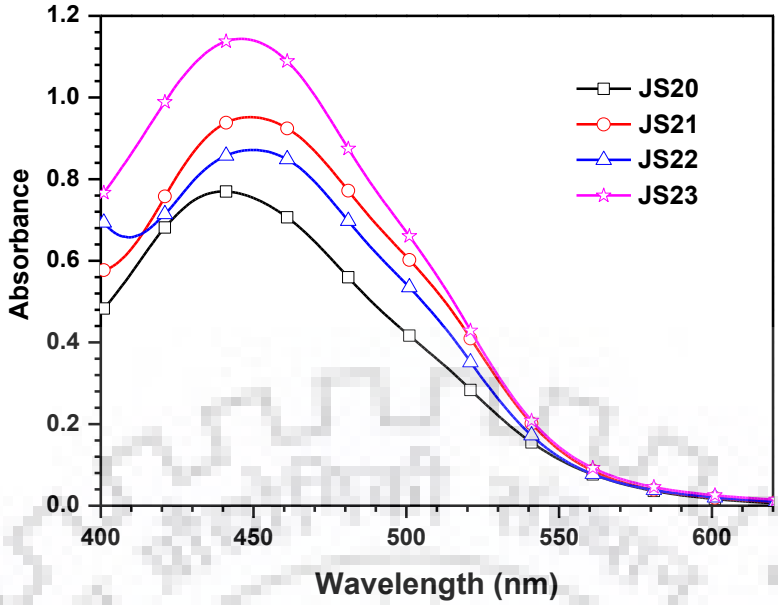

Figure 5.8 Absorption spectra of λ- shaped di-anchoring dyes **JS20-JS23** anchored on TiO_2.

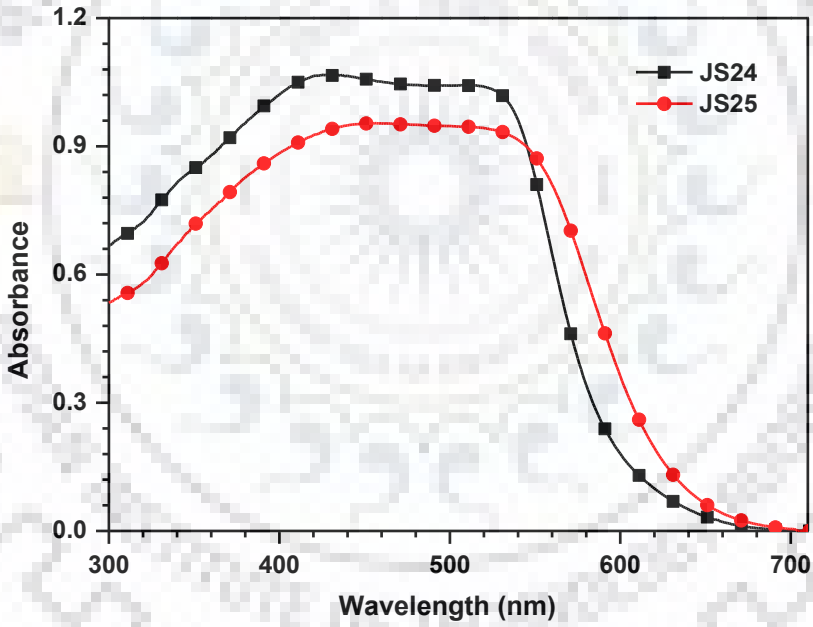

Figure 5.9 Absorption spectra of H-shaped di-anchoring dyes **JS24** and **JS25** anchored on TiO_2.

Table 5.1 Optical and electrochemical data of the **JS20-JS25** dyes recorded in THF.

Dyes	$\lambda_{abs.}$ (nm (ε_{max} ×10^3 $M^{-1}cm^{-1}$))	λ_{max}^{TiO2} (nm)	E_{OX} (mV (ΔE_p, mV)) [a]	E_{OX} (eV) (Vs NHE)	HOMO (eV)[b]	LUMO (eV)[c]	$E_{0\text{-}0}$ (eV)[d]	E_{OX}* (eV)[e]
JS20	490 (54.8), 464 (49.4), 318 (19.3), 293 (17.8)	440	980 [f]	1.750	-5.780 [f]	-3.358[f]	2.422[d, f]	-0.672[f]
JS21	487 (62.3), 462 (61.2), 354 (57.5), 304 (33.0)	449	531 (113)	1.301	-5.331	-2.909	2.422	-1.121
JS22	486 (47.5), 460 (49.7), 375 (51.3), 315 (33.4)	449	465 (105)	1.235	-5.265	-2.814	2.451	-1.216
JS23	489 (24.1), 458 (27.1), 407 (21.6), 323 (20.4)	446	462 (90)	1.232	-5.262	-2.802	2.460	-1.228
JS24	495 (sh), 459 (96.8), 334 (58.1), 314 (55.0)	514	458 (113), 533 (160)	1.228	-5.258	-2.855	2.403	-1.175
JS25	528 (sh), 462 (91.8), 320 (76.2)	509	289 (213)	1.059	-5.089	-2.624	2.465	-1.406

[a] Oxidation potentials are reported with reference to the ferrocene internal standard.

[b] Deduced from the oxidation potential using the formula HOMO = -(4.8 + E_{OX})

[c] Deduced using the formula LUMO = HOMO + $E_{0\text{-}0}$.

[d] Calculated from intersection of absorption & emission spectra.

[e] Calculated from E_{OX}* = E_{OX} - $E_{0\text{-}0}$ (Vs. NHE).

[f] Recorded in ACN solutions.

5.2.3 Electrochemical properties

In order to examine the susceptibility of the dyes to inject the electrons into the CB of TiO_2 and regeneration by electrolyte, the electrochemical properties were measured. The oxidation potential corresponds to the HOMO and reduction potential to the LUMO of the dyes. To find out these parameters we carried CV and DPV studies for the dyes. The cyclic voltammograms of the dyes **JS21-JS25** are displayed in Figure 5.10 and the relevant parameters listed in Table 5.1. Except the dye **JS20**, all other dyes exhibited quasi-reversible oxidation. The oxidation potential of the λ- shaped dyes are found to be highly dependent on the electronic richness of the unit attached to the fluorene and followed the trend as **JS20** > **JS21** > **JS22** > **JS23**. This trend indicates that more electronic richness of the auxiliary segments make the removal of electron facile from the dye and lifting the HOMO energy levels in upward direction. However, the low oxidation potential for H-shaped dyes observed as compare to λ-shaped dyes is attributable to the fact that in former dyes, two donors being shared by two acceptors which promote the extraction of electron in comparison to the later dyes in which only one donor being shared by two acceptors. The two oxidation potentials observed for the dye **JS24,** first by removal of electron from donor and the second oxidation potential is due to removal of electron from the DTP unit present as π-linker. The high value of second oxidation potentials may be due to the direct attachment of DTP-linker to the cyanoacrylic acids acceptor that makes the removal of electron little difficult.

The excited state oxidation potential of the dyes followed the reverse trend of the oxidation potential i.e. **JS20** < **JS21** < **JS24** < **JS22** < **JS23** < **JS25**. This shows that electron richness of the tethering units not only facilitate the uplifting of HOMO but also raise the LUMO energy levels significantly which maintain the energy band gaps nearly similar for all the dyes. This observation is consistent with the recorded absorption maxima for the dyes in THF. The sufficiently more positive oxidation potentials (1.23-1.75 V *vs.* NHE) for the dyes than I^-/I^{3-}electrolyte redox potential (0.4 V *vs.* NHE) [162], these are conducive for the regeneration of oxidized dyes thermodynamically feasible. Moreover, the excited state oxidation potentials (-0.67 to -1.23 V *vs.* NHE) are sufficiently more negative than that of CB (-0.5 V *vs.* NHE) [163] of TiO_2, which ensure the energetically facile electron injection from the dye at excited state to CB of TiO_2.

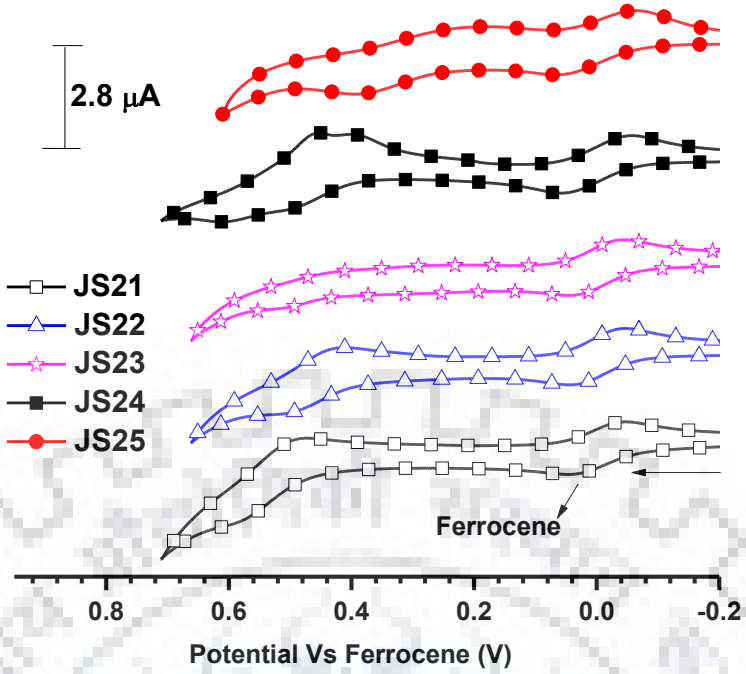

Figure 5.10 Cyclic voltammograms of the dyes **JS21-JS25** recorded in THF.

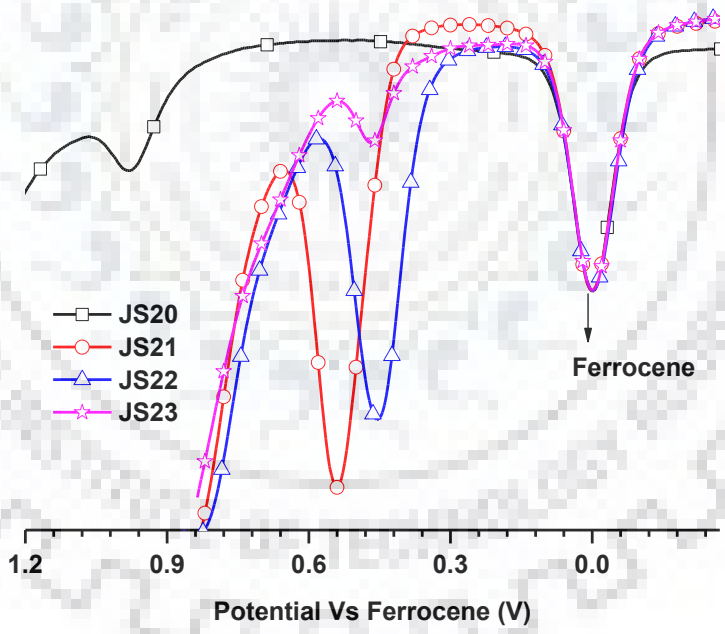

Figure 5.11 Differential pulse voltammograms of the dyes **JS20-JS23** recorded in THF.

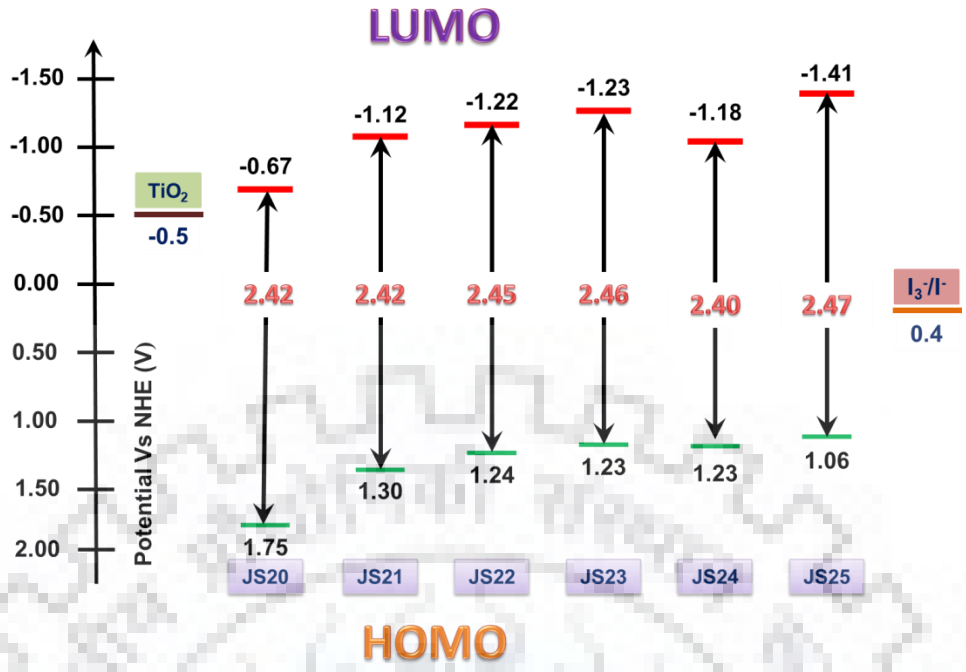

Figure 5.12 Energy level diagram for the dyes **JS20-JS25**.

5.2.4 Theoretical calculations

Further to gain more insight on the oxidation and photophysical properties of the dyes density functional theory (DFT) [164,165] calculations for λ-shaped dyes were carried out at B3LYP/6-31g(d,p) level (DFT calculations were not carried out for H-shaped dyes due to giant size). The optimized geometries of the dyes showed significant non-coplanarity between the *N*-fluorene unit and C7-substituted aromatic segments (Figure 5.14). The dyes **JS21** and **JS22** showed inter-planar angle (ca. 36°) while the **JS23** moderate inter-planar angle (ca. 26°) with the *N*-fluorene unit (Figure 5.13). Due to the non-coplanarity the HOMOs for the dyes **JS21**, **JS22** and **JS23** were mainly constituted by the TPA, DPF and FDTP aromatic fragments but for the dye **JS20** it was localized on DTP unit itself. The LUMO and LUMO + 1 for all the dyes were delocalized over two cyanoacrylic acids through DTP unit. The HOMO-1 for the dyes **JS20**, **JS21** and **JS22** were delocalized over the *N*-fluorene and tethered segments except for the dye **JS23** constituted by only tethered FDTP unit.

To elucidate the lowest energy transitions and absorption wavelengths the time-dependent density functional theory (TD-DFT) was employed to compute the electronic excitation parameters by using BMK functional and DGDZVP basis set. The calculated excitation energies, their oscillator strength (*f*) and molecular orbital contributions are

listed in Table 5.2. It has been observed that longer wavelength absorption (~460 nm) obtained from HOMO to LUMO transition for the dye **JS20** and HOMO-2 to LUMO transitions for the dyes **JS21-JS23** which are originated from DTP to cyanoacrylic acids. These transitions possessed reasonably high oscillator strength for the dyes. The transitions at ~320 nm due to HOMO-2 to LUMO+1 for the dyes **JS21-JS23** arise from DTP to cyanoacrylic acid and from HOMO to LUMO+1 for the dye **JS20**. In case of the dyes **JS21-JS23** the absorption at 340-370 nm by HOMO to LUMO+2 transitions are from aromatic segments. These theoretical calculations were found to be well supporting with the experimental results and indicate the major absorption originate from π-π* transition of the DTP-cyanoacrylic and chromophore.

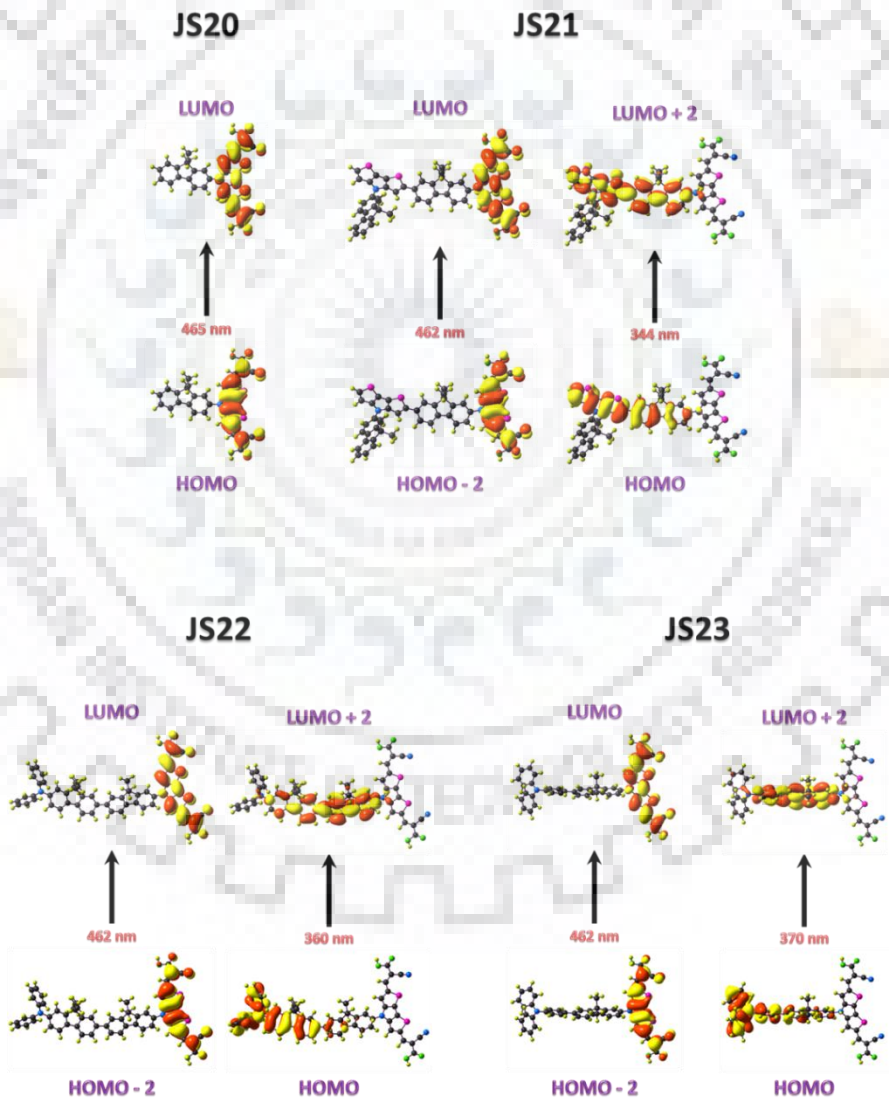

Figure 5.13 Electronic transitions involved in the dyes **JS20-JS23** and their molecular orbitals of the.

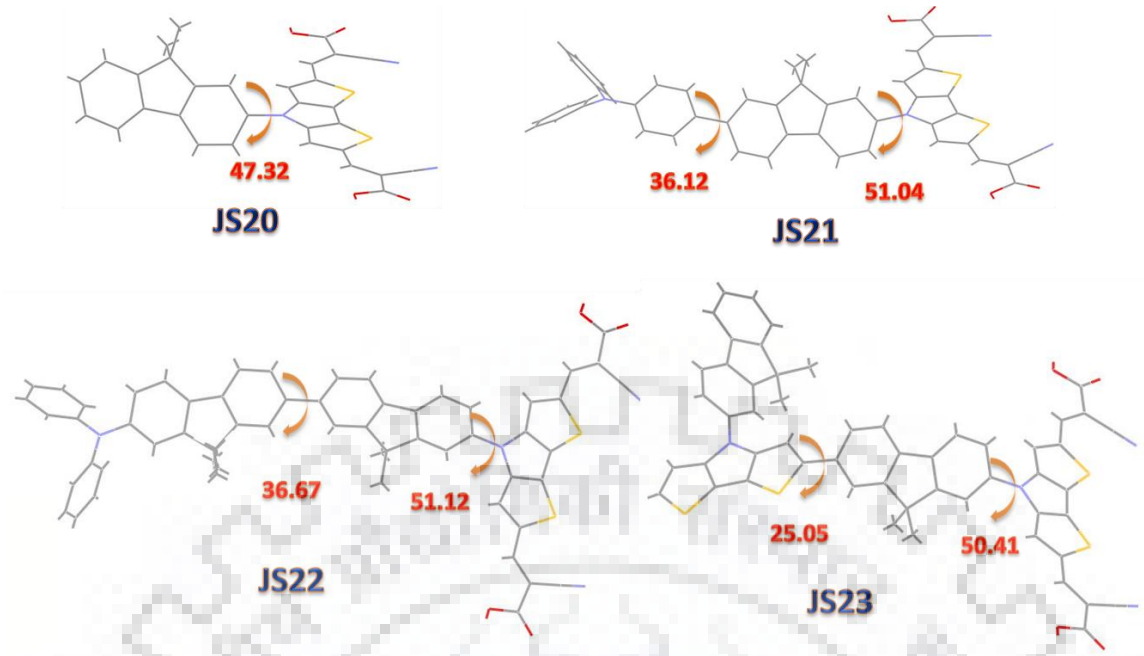

Figure 5.14 Computed inter-planar angles between the different aromatic segments of the dyes **JS20-JS23**.

Table 5.2 Computed vertical transition energies and their oscillator strengths and configurations for the dyes **JS20-JS23**.

Dye	λ_{max}^{abs}(nm)	*f*	Configuration	HOMO (eV)	LUMO (eV)	Band gap (eV)
JS20	465	1.63	HOMO→LUMO (98%)	-6.72	-2.92	3.81
	322	0.37	HOMO→LUMO+1 (90%)			
JS21	461.9	1.61	HOMO-2→ LUMO (97%)	-5.86	-2.89	2.97
	343.6	1.63	HOMO→ LUMO+2 (75%)			
	320.7	0.10	HOMO-2→ LUMO +1 (89%)			
JS22	462.0	1.60	HOMO-2→ LUMO (98%)	-5.74	-2.89	2.84
	359.7	1.90	HOMO→ LUMO+2 (72%)			
	323.1	0.31	HOMO-2→LUMO +1 (85%)			
JS23	461.8	1.61	HOMO-2→ LUMO (98%)	-5.95	-2.90	3.05
	370.2	1.90	HOMO→ LUMO+2 (92%)			
	318.5	0.12	HOMO-2→ LUMO+1 (65%)			

5.2.5 Photovoltaic properties

We employed the newly synthesized dyes as sensitizers to fabricate DSSCs and elucidated their photovoltaic properties. The incident photon-to-current conversion efficiencies (IPCE) of the DSSCs against different irradiation wavelengths are plotted in Figure 5.15. The IPCE spectrum of a dye depends upon its light harvesting efficiency and

the λ-shaped dyes showed IPCE spectra extended up to 600 nm and for the H-shaped dyes tailed upto 650 nm consistent with the absorption spectra of respective photoanodes. Thus, the superior IPCE spectra of the **JS24** can be attributed to their high molar extinction coefficients. The dyes **JS23** and **JS25** showed lowest IPCE value attributable to the poor electron injection from excited dye to CB of TiO_2 might be due to the quenching of excited electrons by the oxidized half of the electrolyte due the presence of thiophene fused ring on donor DTPs [66,232] or aggregation of the dye on TiO_2 surface [233]. Under the simulated solar conditions the current-voltage (I-V) characteristics were measured and presented in Figure 5.16. The photocurrent density (J_{SC}) of the dyes followed the order of **JS24 > JS25** > **JS22** > **JS21** > **JS20** > **JS23**. The highest J_{SC} for **JS24** is credited to its broad and intense absorption profile. While, the lowest J_{SC} value for the dye **JS23** may be due to the presence of high lying HOMO which slow down the regeneration of oxidized dye and probably led to facile recombination of photo-injected electrons [234]. The trend for the open circuit voltage (V_{OC}) of the dyes is **JS24** > **JS22** > **JS21~JS25** > **JS23** > **JS20** largely attributable to the bulkiness of the attached donor segment. Bulkier group probably retard the approach of electrolyte and dye aggregation on the TiO_2 surface, and improve the open circuit voltage. In case of λ-shaped dyes, the presence of hydrophobic DPF unit on **JS22** in place of phenyl of the **JS23** is more beneficial for the inhibition of charge recombination which led to high V_{OC}. However, the H-shaped dyes showed lowest J_{SC} and V_{OC} values as compared to their linear congeners **JS4** and **JS6** despite the two-fold light harvesting propensity. This may be due the two-fold size of H-shaped dyes made the dye loading on the TiO_2 surface to less extent as compared to linear congeners and eventually led to decrement in the power conversion efficiency. It is noteworthy to mention here that the V_{OC} (0.61-0.67 V) of these dyes are sufficiently higher than that of previously reported DTP based di-anchoring dyes (0.58 and 0.50 V respectively) [139]. This observation suggests that the presence of bulky aromatic chromophores at *N*-position of DTP can retard the charge recombination more efficiently and beneficial to increase the V_{OC} of di-anchoring dyes. The efficiency of dyes follow the order **JS24 > JS22** > **JS25** > **JS21** > **JS20** > **JS23**, which is similar to the order of J_{SC} values. In the present work H-shaped dye **JS24** showed highest efficiency of 4.72% can be attributed to the high J_{SC} and V_{OC} values. This study suggests that increase in conjugation by suitable bulky and electron rich units at *N*-atom of DTP is beneficial to increase both J_{SC} and V_{OC} for the present λ- shaped design of the dyes.

Table 5.3 Performance parameters of the DSSCs fabricated using o the dyes **JS20-JS25.**

Dye	η (%)	V_{OC} (V)	J_{SC} (mA cm^{-2})	*FF*	R_{ct2} (ohm)	τ_e (ms)	R_{rec} (ohm)
JS20	1.88	0.61	4.53	0.68	40.32	1.45	12.25
JS21	2.24	0.63	5.29	0.67	39.76	1.71	25.54
JS22	2.41	0.66	5.47	0.67	31.26	2.01	27.91
JS23	1.38	0.62	3.30	0.67	50.66	1.45	15.27
JS24	4.72	0.67	11.19	0.63	25.53	2.01	35.56
JS25	2.33	0.63	5.83	0.63	38.14	1.45	23.44

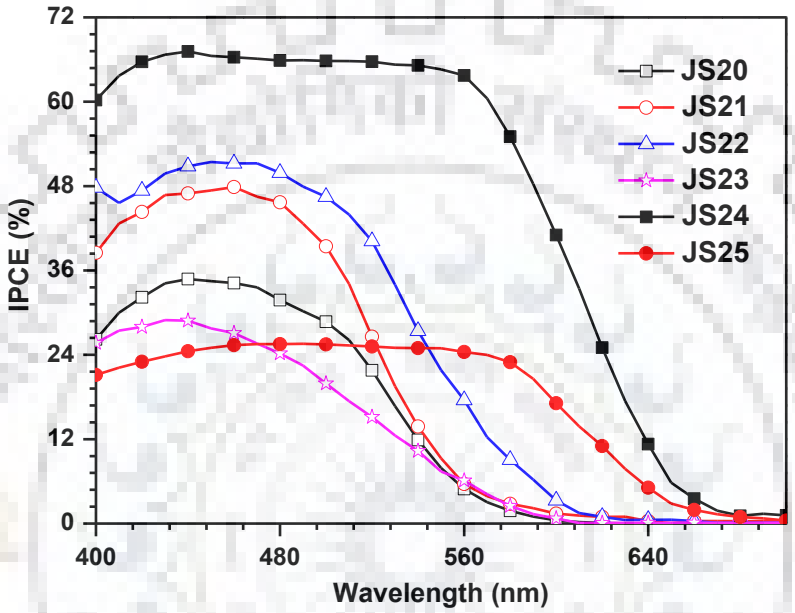

Figure 5.15 IPCE spectra of the DSSCs fabricated using the dyes **JS20-JS25**.

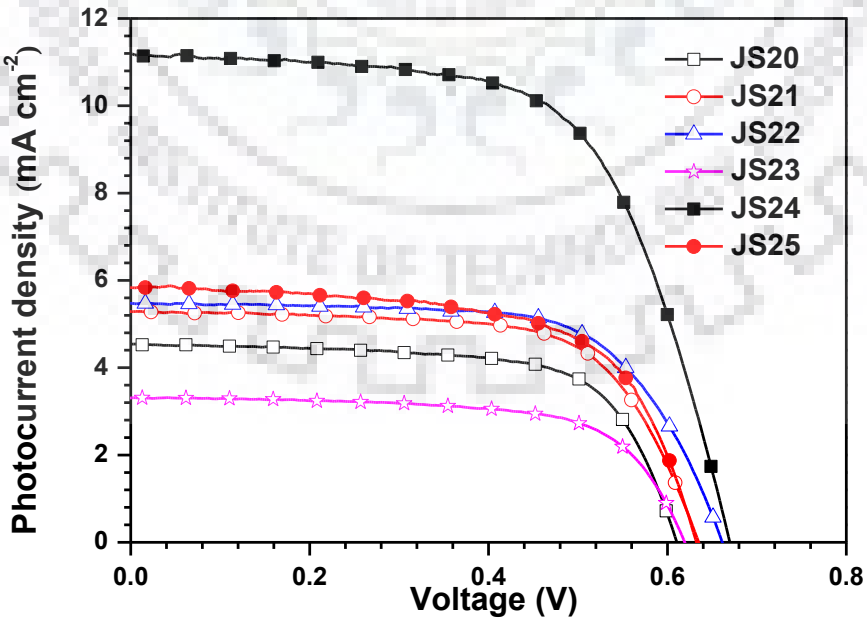

Figure 5.16 *J-V* characteristics of the DSSCs fabricated with dyes **JS20-JS25**.

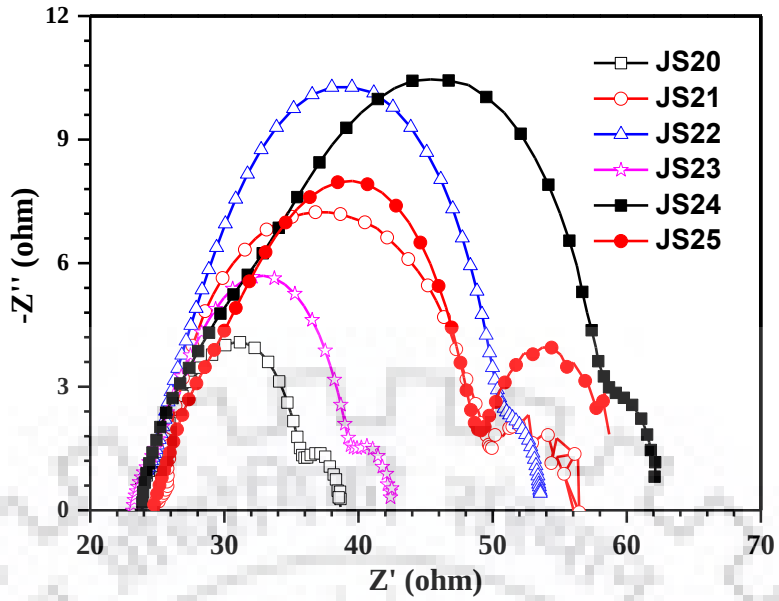

Figure 5.17 Nyquist plots observed for the DSSCs fabricated with dyes **JS20-JS25** under dark condition.

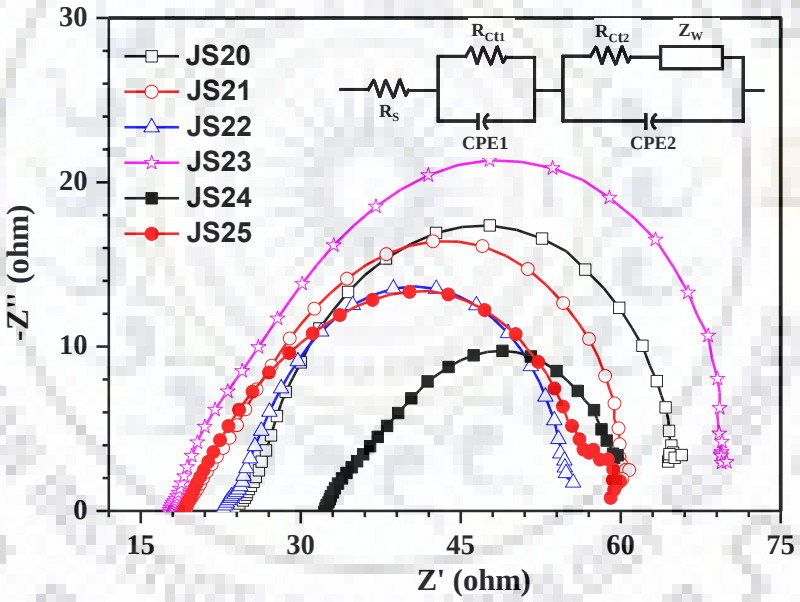

Figure 5.18 Nyquist plots observed for the DSSCs fabricated with dyes **JS20-JS25** under illumination.

5.2.6 Electrochemical impedance spectroscopy

To further understand the fate of electrons at the interfaces of the DSSCs due to structural change by different tethering substituents, we performed the electrochemical impedance (EIS) measurements under dark and one sun illumination conditions. The Nyquist plots obtained in dark and illumination conditions are displayed in Figures 5.17 and 5.18, respectively. The second semicircle of Nyquist plots in Figure 5.17 showed the

charge recombination resistance (R_{rec}) at the interfaces of TiO_2/dye/electrolyte. Thus, the order of R_{rec} is **JS24** > **JS22** > **JS21** > **JS25** > **JS23** > **JS20**. The order of R_{rec} was found to be consistent with the trend of V_{OC} recorded for the dyes. The highest R_{rec} value recorded for the dyes **JS24** and **JS22** suggested that the presence DPF aromatic segment was more effective to suppress the recombination of photo-injected electrons with the oxidized dye and the oxidized half of the electrolyte. Also, the high light harvesting abilities of the dyes **JS24** and **JS22** were beneficial to populate electrons in the CB of TiO_2 and shifted the Fermi energy level upwardly and thus displayed better charge collection efficiency and longer electron lifetime [167,168]. Further, the charge-transport resistance (R_{ct2}) estimated from the large semicircle of the Nyquist plots in Figure 5.18 recorded under the one sun illumination conditions. The R_{ct2} of the dyes followed the order of **JS23** > **JS20** > **JS21** > **JS25** > **JS22** > **JS24** which showed the large charge collection efficiency for the dye **JS24**. The larger R_{ct2} value for the dye **JS23** originated from the unfavorable interactions of the electrolytes with the condensed thiophene units of DTP ring [169,170]. The electron life time (τ_e) for the devices can be measured from the equation $\tau_e = 1/\omega_{min}$ by the mid-frequency peaks of the Bode phase plot (Figure 5.19) where ω_{min} is the angular frequency of low frequency peak [44,45]. The effective suppression of the back electron transfer for the dye **JS24** showed highest τ_e when compared to the other dyes. Also, the effective electronic coupling with TiO_2 nanoparticles and aggressive reduction of charge recombination render in the elevation of photovoltaic properties for the dye **JS24**.

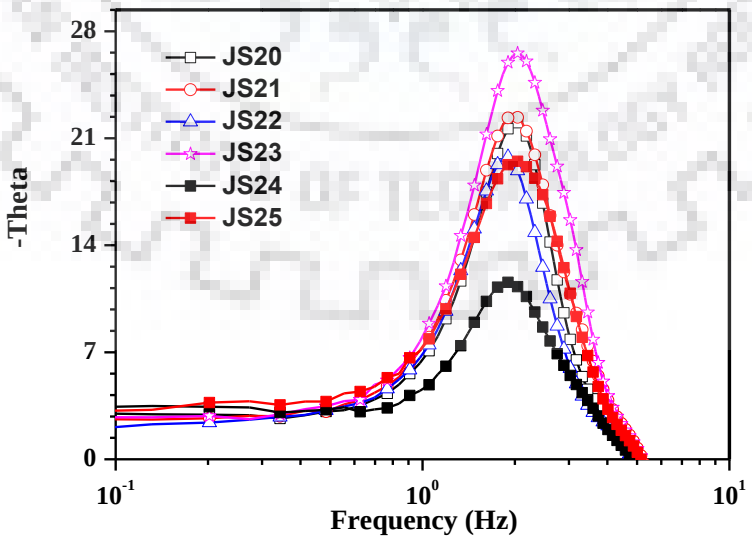

Figure 5.19 Bode phase plots for the DSSCs fabricated using dyes **JS20-JS25 and** measured under illumination.

5.3 Conclusions

In summary, we demonstrated two new strategies to developed λ- and H-shaped dianchoring dyes by tri-functionalization of dithienopyrrole and bridging of two DTPs by fluorene respectively. The λ- and H-shaped shaped dyes showed red shifted absorption maxima in comparison to previously mono-anchoring congeners **JS1, JS4**, and **JS6** respectively. Further, in case of λ-shaped dyes, decoration of conjugated electronic rich units at C7 position of fluorene was found to be beneficial for broadening the absorption spectra. Also the insertion of different aromatic chromophores exerted similar effect on raising the HOMO and LUMO energy levels as a result of which energy band gap remain almost constant for all the dyes except for dye **JS24**. Theoretical calculation established that the HOMOs for λ-shaped dye remained spread over the electron rich aromatic segments while LUMOs are delocalized between two cyanoacrylic acids through DTP segments. The absorption maxima for the dye **JS20** realized from HOMO to LUMO transitions while for the dyes **JS21-JS23** originated from HOMO-2 to LUMO transitions. Among the dyes, **JS24** displayed highest power conversion efficiency due to high photocurrent density and open circuit voltage. The EIS studies infer the superior performance of **JS24** originating from large recombination resistance and small charge transfer resistance. This work suggests that the strategy of synthesizing multi-anchoring dyes with the choice suitable aromatic system can be promising work to improve the efficiency of DSSCs.

5.4 Experimental

5.4.1 General methods

The general methodology is similar to that described in Chapter 2.

5.4.2 Synthesis

*Synthesis of 4-(9,9-dibutyl-9H-fluoren-2-yl)-4H-dithieno[3,2-b:2',3'-d]pyrrole-2,6-dicarbaldehyde **(27)**.*

To the mixture of 4-(9,9-dibutyl-9*H*-fluoren-2-yl)-4*H*-dithieno[3,2-b:2',3'-*d*]pyrrole (1.00 g, 2.19 mmol) and DMF (8 mL) at 0 °C temperature, $POCl_3$ (0.69 mL, 7.00 mmol) was added drop wise. After complete addition, temperature of the reaction was maintained at 100 °C for 8 h. On completion, the reaction was quenched with addition of ice-water and mixture was neutralized with sodium hydroxide solution. The organic product was extracted three times with chloroform, washed with brine solution and dried

over anhydrous Na_2SO_4. The combined organic extracts were concentrated and further purified by alumina column chromatography using a hexane: chloroform (3:2) as eluent. Greenish-yellow solid; yield (0.708 g, 63%); mp 204-205°C; IR (KBr, cm^{-1}) 1659 ($\nu_{C=O}$); ^{1}H NMR (500 MHz, $CDCl_3$) δ 0.72 (quin, *J* = 7.5 Hz, 10 H), 1.11-1.17 (m, 4 H), 2.03-2.06 (m, 4 H), 7.40 (d, *J* = 4.5 Hz, 3 H), 7.53-7.55 (m, 2 H), 7.79-7.80 (m, 3 H), 7.90 (d, *J* = 8.0 Hz, 1 H), 7.94 (s, 1 H), 9.94 (s, 2 H); ^{13}C NMR (123.55 MHz, $CDCl_3$) δ; 183.15, 153.21, 150.77, 146.54, 144.51, 140.90, 39.63, 136.63, 127.85, 127.22, 123.37, 123.07, 121..91, 121.16, 120.09, 120.04, 117.85, 55.45, 40.02, 26.14, 23.00. 13.91. HRMS calcd for $C_{31}H_{29}NO_2S_2$ $[M]^+$ m/z 511.1634 found 511.1622.

*Synthesis of 4-(7-bromo-9,9-dibutyl-9H-fluoren-2-yl)-4H-dithieno[3,2-b:2',3'-d]pyrrole-2,6-dicarbaldehyde (**28**)*

A mixture of **27** (1.9 g, 3.7 mmol), bromine (0.220 mL, 4.1 mmol) and Chloroform (7 mL) was heated at 65 °C for 12 h. On completion, the reaction was quenched with the addition of aq. $NaHCO_3$. The organic product was extracted with chloroform. The collected organic layer was thoroughly washed with brine solution and dried over anhydrous Na_2SO_4. Evaporation of the volatiles gave a greenish yellow residue. The obtained crude product was further purified by column chromatography using hexane: chloroform (1:4) as eluent. Pale yellow solid; yield (0.900 g, 42%). mp 265-267 °C; IR (KBr, cm^{-1}) 1652 ($\nu_{C=O}$); ^{1}H NMR (399.78 MHz $CDCl_3$) δ 0.65-0.771 (m, 10 H), 1.14 (sex, *J* = 6.8 Hz, 4 H), 1.98-2.03 (m, 4 H), 7.51-7.56 (m, 4 H), 7.63 (d, *J* = 8.4 Hz, 1 H), 7.79 (s, 2 H), 7.87 (d, *J* = 8.0 Hz, 1 H), 9.94 (s, 2 H); ^{13}C NMR (100.53 MHz, $CDCl_3$) δ; 183.3, 153.0, 152.9, 146.5, 144.6, 139.8, 138.7, 137.1, 130.6, 126.4, 123.6, 122.2, 122.0, 121.53, 121.47, 120.1, 117.8, 55.8, 40.0, 26.1, 26.2, 23.2, 23.0, 14.0. HRMS calcd for $C_{31}H_{28}BrNO_2S_2$ $[M+Na]^+$ m/z 612.0637 found 612.0650.

*Synthesis of 4-(9,9-dibutyl-7-(4-(diphenylamino)phenyl)-9H-fluoren-2-yl)-4H-dithieno[3,2-b:2',3'-d]pyrrole-2,6-dicarbaldehyde (**29**)*

A mixture of **28** (0.150 g, 0.25 mmol), (4-(diphenylamino)phenyl)boronic acid (0.95 g, 0.33 mmol), K_2CO_3 (0.104, 0.10 mmol), $Pd(PPh_3)_4$ (0.020 g, 0.02 mmol) and 20 mL of THF/H_2O (4/1) was heated at 80 °C under nitrogen atmosphere. After 16 h, the reaction was quenched by the addition of water. The organic product was extracted with chloroform. The collected organic layer was thoroughly washed with brine solution and dried over anhydrous Na_2SO_4. Evaporation of the volatiles gave a residue. It was purified

column chromatography using neutral alumina as static phase and hexane: chloroform (1:4) as eluent. Orange solid; yield (0.080 g, 41%); mp 268 - 270 °C; IR (KBr, cm^{-1}) 1653 ($\nu_{C=O}$); ^{1}H NMR (399.78 MHz, $CDCl_3$) δ 0.73-0.86 (m, 10 H),1.11-1.18 (m, 4 H), 2.06-2.13 (m, 4 H), 7.05 (t, *J* = 6.8 Hz, 2 H), 7.15-7.20 (m, 6 H), 7.27-7.31 (m, 4 H), 7.53 -7.65 (m, 6 H), 7.79-7.83 (m, 3 H), 7.89-7.92 (m, 1 H), 9.95 (s, 2 H); ^{13}C NMR (100.53 MHz, $CDCl_3$) δ 183.4, 153.5, 151.6, 151.1, 147.7, 147.5, 147.3, 146.6, 140.7, 140.5, 138.5, 136.6, 135.1, 129.4, 127.9, 126.0, 124.9, 124.6, 123.9, 123.4, 123.2, 122.1, 121.1, 120.7, 120.4, 120.3, 118.0, 117.9, 117.8, 255.6, 55.5, 40.2, 26.3, 23.1, 14.1. HRMS calcd for $C_{49}H_{42}N_2O_2S_2$ $[M+Na]^+$ m/z 777.2580 found 777.2585.

*Synthesis of 4-(9',9'-dibromo-9,9-dibutyl-7'-(diphenylamino)-9H,9'H-[2,2'-bifluoren]-7-yl)-4H-dithieno[3,2-b:2',3'-d]pyrrole-2,6-dicarbaldehyde (**30**)*

It was prepared from **28** (0.150 g, 0.25 mmol) and (9,9-dibutyl-7-(diphenylamino)-9*H*-fluoren-2-yl)boronic acid (0.177 g, 0.33 mmol) by following a procedure similar to that described above for **29**. Orange microcrystalline solid; yield (0.105 g, 42%); mp 261-263 °C; IR (KBr, cm^{-1}) 1626 ($\nu_{C=O}$); ^{1}H NMR (399.78 MHz, $CDCl_3$) δ 0.69-0.89 (m, 20 H), 1.06-1.22 (m, 8 H), 1.87-2.13 (m, 8 H), 7.00-7.06 (m, 3 H), 7.14 (d, *J* = 7.6 Hz, 5 H), 7.25 (s, 1 H), 7.28 (s, 1 H), 7.51- 7.62 (m, 6 H), 7.66-7.73(m, 3 H), 7.79 (d, *J* = 7.6 Hz, 1 H), 7.83 (d, *J* = 3.6 Hz, 2 H), 7.87 (d, *J* = 10.0 Hz, 1 H), 7.91-7.94 (m, 1 H), 9.95 (s, 2 H); ^{13}C NMR (100.53 MHz, $CDCl_3$) δ 183.4, 153.5, 153.0, 152.5, 151.6, 148.0, 147.4, 146.6, 146.5, 144.6, 141.4, 140.6, 139.2, 138.7, 136.6, 135.8, 130.6, 129.3, 126.51, 126.46, 126.2, 124.0, 123.6, 123.5, 122.7, 122.1, 121.5, 121.3, 120.8, 120.5, 120.4, 120.3, 120.2, 119.7, 119.4, 118.0, 55.7, 55.2, 40.1, 40.0, 26.3, 26.1, 23.13, 23.05, 14.2, 14.0. HRMS calcd for $C_{64}H_{62}N_2O_2S_2$ $[M]^+$ m/z 954.4272 found 954.4262.

*Synthesis of 4-(9,9-dibutyl-7-(4-(9,9-dibutyl-9H-fluoren-2-yl)-4H-dithieno[3,2-b:2',3'-d]pyrrol-2-yl)-9H-fluoren-2-yl)-4H-dithieno[3,2-b:2',3'-d]pyrrole-2,6-dicarbaldehyde (**31**)*

A mixture of **28** (0.200 g, 0.34 mmol), 4-(9,9-dibutyl-9*H*-fluoren-2-yl)-2-(tributylstannyl)-4*H*-dithieno[3,2-b:2',3'-d]pyrrole (0.51 mmol), $Pd(PPh_3)_2Cl_2$ (0.004 g, 0.05 mmol) and 5 mL of DMF was heated at 85 °C under nitrogen atmosphere. After 16 h, the reaction was quenched by the addition of water. The organic product was extracted with chloroform. The collected organic layer was thoroughly washed with brine solution and dried over anhydrous Na_2SO_4. Evaporation of the volatiles gave a residue. The

obtained crude product was further purified by column chromatography using neutral alumina as static phase and hexane: chloroform (1:4) as eluent. Yellow solid; yield (0.250 g, 65%); mp 193-195 °C; IR (KBr, cm^{-1}) 1627 ($\nu_{C=O}$); 0.65-0.81 (m, 20 H), 1.13-1.17 (m, 8 H), 2.00-2.10 (m, 8 H), 7.19-7.20 (m, 1 H), 7.25 (s, 1 H), 7.36-7.42 (m, 2 H), 7.52-7.57 (m, 4 H), 7.61-7.65 (m, 3 H), 7.69-7.71 (m, 1 H), 7.55-7.81 (m, 4 H), 7.86-7.90 (t, *J* = 8.0 Hz, 2 H), 9.94 (s, 2 H); ^{13}C NMR (100.53 MHz, $CDCl_3$) δ 183.3, 153.4, 153.0, 152.8, 151.8, 150.8, 146.5, 144.62, 144.6, 144.5, 144.1, 142.5, 140.3, 140.1, 140.0, 139.3, 139.5, 139.1, 138.6, 137.1, 136.7, 135.1, 130.6, 127.4, 127.2, 126.5, 124.8, 124.2, 123.6, 123.5, 123.1, 120.9, 120.7, 120.3, 120.1, 119.8, 119.5, 117.9, 117.6, 117.1,116.3, 112.3,108.3, 55.7, 40.2, 40.0, 26.3, 23.1, 14.1. HRMS calcd for $C_{60}H_{56}N_2O_2S_4$ $[M]^+$ m/z 964.3219 found 964.3237.

*4,4'-(9,9-dibutyl-9H-fluorene-2,7-diyl)bis(4H-dithieno[3,2-b:2',3'-d]pyrrole) (**32**)*

A mixture of 9,9-dibutyl-9*H*-fluorene-2,7-diamine (1.00 g, 3.26 mmol), 3,3'-dibromo-2,2'-bithiophene (2.12 g, 6.5 mmol), Na^{t}OBu (1.876 g, 19.5 mmol), $Pd(dba)_2$ (190 mg, 0.32 mmol), dppf (544 mg, 0.98 mmol) and 80 mL toluene was heated at 120 °C under nitrogen atmosphere. After 20 h, the reaction was quenched by the addition water. The organic product was extracted with dichloromethane. The collected organic layer was thoroughly washed with brine solution and dried over anhydrous Na_2SO_4. Evaporation of the volatiles gave a light yellow residue. It was purified by column chromatography using hexane: chloroform (4:1) as eluent. Green yellow solid; yield (1.2 g, 58%); mp 240-242 °C; ^{1}H NMR (399.78 MHz, DMSO-d_6) δ 0.74 – 0.83 (m, 10 H), 1.126 – 1.20 (m, 4 H), 2.05 – 2.09 (m, 4 H), 7.19 – 7.24 (m, 8 H), 7.59 – 7.62 (m, 4 H), 7.86 (m, *J* = 8.0 Hz, 2 H); ^{13}C NMR (100.53 MHz, DMSO-d_6) δ 152.7, 144.1, 139.0, 138.3, 124.23, 124.19, 123.2, 121.6, 120.8, 117.4, 117.1, 112.8, 55.6, 40.3, 26.3, 23.2, 14.0. HRMS calcd for $C_{37}H_{32}N_2S_4$ $[M+H]^+$ m/z 632.1442 found 632.1459.

*Synthesis of 4,4'-(9,9-dibutyl-9H-fluorene-2,7-diyl)bis(4H-dithieno[3,2-b:2',3'-d]pyrrole-2-carbaldehyde)**(33)***

To a mixture of **32** (0.500 g, 0.74 mmol) and DMF (5 mL), $POCl_3$ (0.2 mL, 2.6 mmol) was added at 0 °C and then the reaction mixture was allowed to stir at 0 °C for 45 min, at RT for 15 min, and finally at 50 °C for 3 hrs. The reaction was quenched by the addition of ice-water and a saturated solution of NaOH was added to neutralize the reaction. The organic product was extracted with dichloromethane. The collected organic

layer was thoroughly washed with brine solution and dried over anhydrous Na_2SO_4. Evaporation of the volatiles gave a light yellow residue. It was purified by column chromatography using neutral alumina as static phase and dichloromethane/hexane (4:1) as eluent. Pale yellow microcrystalline solid; yield (0.350 g, 64%); mp 298-300 °C; IR (KBr, cm^{-1}) 1647 ($\upsilon_{C=O}$); ^{1}H NMR (399.78 MHz, $CDCl_3$) δ 0.77-0.84 (m, 10 H), 1.19 (q, *J* = 7.2 Hz, 4 H), 2.08-2.12 (m, 4 H), 7.20 (d, *J* = 5.2Hz, 2 H), 7.48 (d, *J* = 5.6 Hz, 2 H), 7.59-7.63 (m, 4 H), 7.83 (s, 2 H), 7.92 (d, *J* = 8.0 Hz, 2 H), 9.90 (s, 2 H); ^{13}C NMR could not be recorded due to poor solubility. HRMS calcd for $C_{39}H_{32}N_2O_2S_4$ $[M+H]^+$ m/z 689.1419 found 689.1407.

*Synthesis of 4,4'-(9,9-dibutyl-9H-fluorene-2,7-diyl)bis(6-bromo-4H-dithieno[3,2-b:2',3'-d]pyrrole-2-carbaldehyde) (**34**)*

A mixture of **33** (0.300 g, 0.44 mmol), NBS (0.233 g, 1.3 mmol) and 25 mL of $CHCl_3$ was kept on stirring at RT for overnight. After 12 h, the reaction was quenched by the addition of water. The organic product was extracted with dichloromethane. The collected organic layer was thoroughly washed with brine solution and dried over anhydrous NaSO4. Evaporation of the volatiles gave a yellow compound. Yellow microcrystalline solid; yield (0.366 g, 96%); mp 295-297 °C; IR (KBr, cm^{-1}) 1650 ($\upsilon_{C=O}$); ^{1}H NMR (399.78 MHz, $CDCl_3$) δ 0.75-0.90 (m, 10 H), 1.14-1.25 (m, 4 H), 2.08-2.13 (m, 4 H), 7.24 (s, 2 H), 7.54-7.59 (m, 4 H), 7.78 (s, 2 H), 7.92 (d, *J* = 8.0 Hz, 2 H), 9.89 (s, 2 H); ^{13}C NMR (100.53 MHz, $CDCl_3$) δ 183.0, 153.2, 145.7, 142.6, 141.2, 139.1, 137.8, 124.7, 124.2, 121.5, 120.5, 117.8, 117.0, 116.2, 115.5, 55.9, 40.0, 26.4, 23.1, 14.1. HRMS calcd for $C_{39}H_{30}Br_2N_2O_2S_4$ $[M]^+$ m/z 843.9551 found 843.9538.

*Synthesis of 4,4'-(9,9-dibutyl-9H-fluorene-2,7-diyl)bis(6-(9,9-dibutyl-7-(diphenylamino)-9H-fluoren-2-yl)-4H-dithieno[3,2-b:2',3'-d]pyrrole-2-carbaldehyde) (**35**)*

It was prepared yield from **34** (0.250 g, 0.30 mmol) and (9,9-dibutyl-7-(diphenylamino)-9*H*-fluoren-2-yl)boronic acid (0.363 g, 0.68 mmol) by following a procedure similar to that described above for **29**. Yellow microcrystalline solid; yield (0.360 g, 72%); mp 213-215 °C; IR (KBr, cm^{-1}) 1652 ($\upsilon_{C=O}$); ^{1}H NMR (399.78 MHz, $CDCl_3$) δ 0.70-0.73 (m, 18 H), 0.82-0.92 (m, 10 H), 1.05-1.12 (m, 8 H), 1.12-1.35 (m, 6 H), 1.84-1.98 (m, 8 H), 2.14-2.18 (m, 4 H), 7.01-7.05 (m, 7 H), 7.03 (d, J = 8.4 Hz, 11 H), 7.24 (s, 3 H), 7.28 (s, 2 H), 7.46 (s, 2 H), 7.57 (s, 3 H), 7.28 (s, 2 H), 7.46 (s, 2 H), 7.57 (d, J = 8.4 Hz, 4 H), 7.63 (s, 4 H), 7.66-7.70 (m, 5 H), 7.81 (s, 2 H), 7.99 (d, J = 8.4 Hz, 2

H), 9.90 (s, 2 H); ^{13}C NMR (100.53 MHz, $CDCl_3$) δ 182.9, 153.1, 154.4, 151.6, 149.1, 148.6, 147.9, 147.8, 143.2, 141.8, 140.6, 139.0, 138.2, 135.3, 132.5, 129.3, 125.5, 124.9, 123.4, 122.5, 122.3, 121.5, 120.7, 120.5, 119.7, 119.0, 117.9, 115.8, 107.1, 55.9, 55.2, 40.2, 40.1, 26.1, 23.1, 14.0. HRMS calcd for $C_{105}H_{98}N_4O_2S_4$ $[M+H]^+$ m/z 1575.6645 found 1575.6674.

*Synthesis of 4,4''-(9,9-dibutyl-9H-fluorene-2,7-diyl)bis(4'-(9,9-dibutyl-9H-fluoren-2-yl)-4H,4'H-[2,2'-bidithieno[3,2-b:2',3'-d]pyrrole]-6-carbaldehyde) (**36**)*

It was prepared from **34** (0.200 g, 0.24 mmol) and 4-(9,9-dibutyl-9*H*-fluoren-2-yl)-2-(tributylstannyl)-4*H*-dithieno[3,2-b:2',3'-d]pyrrole (0.60 mmol) by following a procedure similar to that described above for **29**. Red solid; yield (0.250 g, 65%); mp 251-253 °C; IR (KBr, cm^{-1}) 1650 ($\upsilon_{C=O}$); ^{1}H NMR (399.78 MHz, $CDCl_3$) δ 0.72-0.77 (m, 20 H), 0.81-0.90 (m, 10 H), 1.13-1.23 (m, 8 H), 1.25-1.33 (m, 4 H), 2.05-2.08 (m, 8 H), 2.18 (d, *J* = 8.0 Hz, 4 H), 7.14-7.17 (m, 2 H), 7.23-7.25 (m, 1 H), 7.28 (s, 1 H), 7.35-7.43 (m, 9 H), 7.55-7.59 (m, 5 H), 7.62-7.66 (m, 4 H), 7.62-7.66 (m, 4 H), 7.85-7.89 (m, 2 H), 7.92-7.96 (m, 2 H), 9.84 (s, 2 H); ^{13}C NMR could not be recorded due to poor solubility. HRMS calcd for $C_{97}H_{86}N_4O_2S_8$ $[M]^+$ m/z 1594.4511 found 1594.4495.

*Synthesis of (2E,2'E)-3,3'-(4-(9,9-dibutyl-9H-fluoren-2-yl)-4H-dithieno[3,2-b:2',3'-d]pyrrole-2,6-diyl)bis(2-cyanoacrylic acid) **(JS20)***.

A mixture of **27** (0.150 g, 0.29 mmol), cyanoacetic acid (0.069 g, 0.82 mmol), acetic acid (5 mL) and ammonium acetate (10 mg) was heated at 125 °C for 12 h. The reaction was quenched by the addition of water. The organic dye was collected after filtration. The collected organic dye was recrystallized with MeOH and hexane mixture to get pure dye. Red solid; yield (0.149 g, 78%); mp 268-270 °C; IR (KBr, cm^{-1}) 2210 ($\nu_{C\equiv N}$); ^{1}H NMR (500 MHz, DMSO-d_6) δ 0.49-0.66 (m, 10 H), 1.06 (sept, *J* = 7.0, 4 H), 1.99-2.05 (m, 2 H), 2.12-2.18 (m, 2 H), 7.37-7.38 (m, 2 H), 7.48-7.49 (m, 1 H), 7.68 (d, *J* = 1.5 Hz, 1 H), 7.68 (d, *J* = 8.0 Hz, 1 H), 7.92 (d, J = 6.0 Hz, 1 H), 8.05 (d, *J* = 8.0 Hz, 1 H), 8.14 (s, 2 H), 8.48 (s, 2 H); ^{13}C NMR (100.53 MHz, DMSO-d_6) δ; 163.94, 152.59, 150.55, 145.54, 139.71, 139.55, 138.01, 136.76, 127.63, 127.23, 127.15, 123.28, 123.00, 121.60, 121.41, 120.94, 120.23, 117.77, 117.16, 101.68, 101.50, 55.24, 25.96, 22.46, 13.93. HRMS calcd for $C_{37}H_{31}N_3O_4S_2$ $[M]^+$ m/z 645.1750 found 645.1720.

*Synthesis of (2E,2'E)-3,3'-(4-(9,9-dibutyl-7-(4-(diphenylamino)phenyl)-9H-fluoren-2-yl)-4H-dithieno[3,2-b:2',3'-d]pyrrole-2,6-diyl)bis(2-cyanoacrylic acid) (**JS21**)*

It was prepared from **29** (0.080 g, 0.11 mmol) by following a procedure similar to that described above for **JS20**. Brown solid; yield (0.055 g, 56%); mp 313-315 °C; IR (KBr, cm^{-1}) 2216 ($\nu_{C\equiv N}$); ^{1}H NMR (399.78 MHz, DMSO-d_6) δ 0.58-0.66 (m, 10 H), 1.03-1.09 (m, 4 H), 2.09-2.19 (m, 4 H), 7.04-7.07 (m, 8 H), 7.30-7.33 (m, 4 H), 7.65 (d, *J* = 6.4 Hz, 2 H), 7.69 (d, *J* = 6.8 Hz, 2 H), 7.76 (s, 1 H), 7.81 (s, 1 H), 7.93 (d, *J* = 6.0 Hz, 1 H), 8.02 (d, *J* = 6.8 Hz, 1 H), 8.14 (s, 2 H), 8.50 (s, 2 H); ^{13}C NMR (100.53 MHz, $CDCl_3$) δ 163.9, 151.4, 147.1, 146.6, 145.9, 139.4, 138.6, 137.9, 136.4, 134.4, 129.6, 127.8, 124.3, 124.1, 124.0, 123.9, 123.6, 123.2, 116.9, 55.4, 22.9, 22.4, 13.8; HRMS calcd for $C_{55}H_{44}N_4O_4S_2$ $[M+H]^+$ m/z 889.2877 found 889.2852.

*Synthesis of (2E,2'E)-3,3'-(4-(9',9'-dibromo-9,9-dibutyl-7'-(diphenylamino)-9H,9'H-[2,2'-bifluoren]-7-yl)-4H-dithieno[3,2-b:2',3'-d]pyrrole-2,6-diyl)bis(2-cyanoacrylic acid) (**JS22**)*

It was prepared from **30** (0.090 g, 0.09 mmol) by following a procedure similar to that described above for **JS20**. Brown solid; yield (0.075 g, 74%); mp 280-283 °C; IR (KBr, cm^{-1}) 2215 ($\nu_{C\equiv N}$); ^{1}H NMR (399.78 MHz, DMSO-d_6) δ 0.56-0.67 (m, 20 H), 0.99-1.13 (m, 8 H), 1.86-1.89 (m, 2 H), 2.01-2.07 (m, 2 H), 2.12-2.19 (m, 4 H), 6.95 (d,d, *J* = 3.6, 1.6 Hz, 1 H), 7.01-7.04 (m, 5 H), 7.10 (d, *J* = 1.2 Hz, 1 H), 7.25-7.31 (m, 4 H), 7.54-7.56 (m, 1 H), 7.68-7.82 (m, 7 H), 7.87 (d, *J* = 8.0 Hz, 1 H), 7.98 (d, *J* = 8.0 Hz, 1 H), 8.06-8.08 (m, 1 H), 8.13 (d, *J* = 8.0 Hz, 2 H), 8.4 (d, *J* = 4.8 Hz, 2 H); ^{13}C NMR could not be recorded because of poor solubility of the compound; HRMS calcd for $C_{70}H_{64}N_4O_4S_2$ $[M]^+$ m/z 1088.4363 found 1088.4345.

*Synthesis of (2E,2'E)-3,3'-(4-(9,9-dibutyl-7-(4-(9,9-dibutyl-9H-fluoren-2-yl)-4H-dithieno[3,2-b:2',3'-d]pyrrol-2-yl)-9H-fluoren-2-yl)-4H-dithieno[3,2-b:2',3'-d]pyrrole-2,6-diyl)bis(2-cyanoacrylic acid) (**JS23**)*

It was prepared from **31** (0.120 g, 0.12 mmol) by following a procedure similar to that described above for **JS20**. Brown solid; yield (0.108 g, 82%); mp 265-267 °C; IR (KBr, cm^{-1}) 2212 ($\nu_{C\equiv N}$); ^{1}H NMR (399.78 MHz, DMSO-d_6) δ 0.39-0.80 (m, 20 H), 0.96-1.17 (m, 8 H), 1.95-2.21 (m, 8 H), 7.23-7.43 (m, 3 H), 7.49-7.56 (m, 2 H), 7.63-7.76 (m, 5 H), 7.81-791 (m, 4 H), 8.04 (s, 4 H), 8.34 (s, 2 H); ^{13}C NMR could not be recorded

because of poor solubility of the compound. HRMS calcd for $C_{66}H_{58}N_4O_4S_4$ $[M]^+$ m/z 1098.3335 found 1098.3345.

*Synthesis of (2E,2'E)-3,3'-(4,4'-(9,9-dibutyl-9H-fluorene-2,7-diyl)bis(6-(9,9-dibutyl-7-(diphenylamino)-9H-fluoren-2-yl)-4H-dithieno[3,2-b:2',3'-d]pyrrole-4,2-diyl))bis(2-cyanoacrylic acid) (**JS24**)*

It was prepared from **35** (0.150 g, 0.09 mmol) by following a procedure similar to that described above for **JS20**. Brown solid; yield (0.115 g, 71%); mp 268-270 °C; IR (KBr, cm^{-1}) 2207 ($\upsilon_{C\equiv N}$); ^{1}H NMR (399.78 MHz, DMSO-d_6) δ 0.50-0.73 (m, 20 H), 0.81-0.82 (m, 8 H), 0.98-1.06 (m, 8 H), 1.44-1.51 (m, 4 H), 1.83-1.99 (m, 8 H), 2.24-2.30 (m, 6 H), 6.92-7.03 (m, 13) 7.08 (d, *J* = 8 Hz, 2 H), 7.25-7.28 (m, 11), 7.67 (d, *J* = 7.6 Hz, 2 H), 7.72-7.80 (m, 12 H), 7.98 (d, *J* = 8.8 Hz, 1 H), 8.12 (d, *J* = 8.4 Hz, 1 H), 8.20 (d, *J* = 6.4 Hz, 2 H); ^{13}C NMR could not be recorded because of poor solubility of the compound. HRMS calcd for $C_{111}H_{100}N_6O_4S_4$ $[M+H]^+$ m/z 1709.6762 found 17096752.

*Synthesis of (2E,2'E)-3,3'-(4,4''-(9,9-dibutyl-9H-fluorene-2,7-diyl)bis(4'-(9,9-dibutyl-9H-fluoren-2-yl)-4H,4'H-[2,2'-bidithieno[3,2-b:2',3'-d]pyrrole]-6,4-diyl))bis(2-cyanoacrylic acid) (**JS25**)*

It was prepared from **36** (0.120 g, 0.08 mmol) by following a procedure similar to that described above for **JS20**. Brown solid; yield (0.094 g, 68%); mp 318-320 °C; IR (KBr, cm^{-1}) 2208 ($\upsilon_{C\equiv N}$); ^{1}H and ^{13}C NMR could not be recorded because of poor solubility of the compound HRMS calcd for $C_{103}H_{88}N_6O_4S_8$ $[M]^+$ m/z 1728.4627 found 1728.4649.

5.4.3 Computational methods

All the computational methodology used is similar to that described in Chapter 2.

5.4.4 Fabrication and characterization of DSSC

The DSSCs were fabricated and characterized by following the procedures detailed in Chapter 2 for the dyes **JS1-JS5**.

Chapter 6

Conclusions and outlook

In realizing the goals outlined in first chapter, we have first attempted to synthesize DTP-based dyes containing different π-spacers, additional donors/acceptors and dianchoring sites with cyanoacrylic acid acceptor. We recorded the absorption and emission spectra of newly synthesized dyes in THF/DCM solution. Optical properties of the synthesized dyes were also elucidated by the addition of TFA/TEA and in different solvents by UV-visible and fluorescence spectroscopic methods. The electrochemical characteristics of the dyes were investigated by using cyclic voltammetry (CV) and differential pulse voltammetry (DPV) methods. To gain further insight in the correlation between structure and the physical properties as well as the device performance, quantum chemistry computations were conducted. The photovoltaic performances of the dyes were evaluated using the Grätzel photoelectrochemical cells. The effects of structural elements of the different dyes on the electron transport at the interfaces in the DSSCs were estimated with the aid of electrochemical impedance spectroscopy (EIS) measurements.

Chapter 2

- In chapter 2, we demonstrated the use of dithienopyrrole as a donor in organic dyes featuring thienyl/DTPs as π-linkers and cyanoacrylic acid acceptor.
- In comparison to thienyl, DTP-linkers showed remarkably improved light harvesting efficiency and reduced oxidation potentials for the dyes. The sufficient spatial separation between HOMO and LUMO orbitals establishes the presence of charge transfer on electronic excitation in the visible region for the DTP-linked dyes.
- The presence of bulky and electron rich DTP units in conjugating bridge for DTP donor dyes is found to be beneficial to retard the charge recombination processes. Therefore, the dye containing one DTP-linker showed the highest efficiency of 5.94% in the series attributable to its high J_{SC} and V_{OC} values.
- Irrespective of intense absorption, low efficiency was observed for the dye containing two DTP-linkers owing to its low charge collection efficiency and reduced electron lifetime.

Chapter 3

- In chapter 3, we have synthesized new organic dyes containing DTP as a linker in conjugation with different donors (triphenylamine, fluorenyldiphenylamine, carbazole and phenothiazine).
- The dyes showed red shifted absorption and high molar extinction coefficients when compared to the control dye lacking donor. Electron richness of the fluorene appended DTP considerably influenced the optical and electrochemical properties of the dyes.
- From theoretical calculations, the absorption in the visible region is presumed to result in migration of charge from the arylamine/heterocyclic donor to cyanoacrylic acid acceptor.
- Non-planar fluorene moiety on the DTP unit proved to be beneficial for retarding the aggregation of the dyes and impeding the electron recombination.
- The DSSC fabricated using fluorenyldiphenylamine donor-based sensitizer showed promising power conversion efficiency (6.81 %) in the series attributable to the high charge recombination resistance (R_{rec}) and low charge transfer resistance (R_{ct2}).

Chapter 4

- In chapter 4, we demonstrated the use of dithienopyrrole as a donor in organic dyes featuring D-A-π-A structural organization by employing different electron-demanding linkers such as BTZ, Qx and BTD along phenyl/thienyl π-spacer with cyanoacrylic acid acceptor.
- We further incorporated TPA and DPF auxiliary donor on BTD dye with phenyl-linker to extend the conjugation length and to improve the spectral response for the dyes. Moreover, variation of position of BTD unit from D-D-A-π-A to D-A-D-A architecture adequately improved the absorption and electrochemical characteristics.
- The dyes, which possess BTD after DTP show negative solvatochromism in the absorption spectra, while the dyes containing BTD before DTP exhibit positive solvatochromism in the emission spectra. This clearly indicates that the former dyes are polar in ground state while the later are polarized only on electronic excitation.
- Theoretically, it was established that sufficient overlap of HOMO and LUMO of the dyes featuring BTD between donor and DTP units facilitate the charge transfer propensity form arylamine donor to acceptor and ensure high molar extinction coefficients in absorption.

- ❖ Among the dyes, the highest power conversion efficiency (η = 7.57%) observed for one of the dye is owed to its high photocurrent density and open circuit voltage. The superior performance of most efficient dye is attested to the sufficiently low charge transfer resistance by EIS studies.
- ❖ This work suggests that insertion of auxiliary donor is beneficial to attain high electron lifetime and charge collection efficiency; however, further inserting BTD unit amidst of arylamine donor and DTP linker is a suitable strategy to tune photovoltaic properties to achieve high efficiency.

Chapter 5

- ❖ In chapter 5, we demonstrated the two new sets of λ- and H-shaped dianchoring dyes obtained by tri-functionalization of dithienopyrrole and bridging of two DTPs trough fluorene, respectively. The λ- and H-shaped shaped dyes showed red shifted absorption maxima in comparison to previously known mono-anchoring congeners.
- ❖ Further, in case of λ-shaped dyes, decoration of conjugated electron rich units at C7 position of fluorene was found to be beneficial for broadening the absorption.
- ❖ Also, the insertion of different aromatic chromophores exerted similar effect on raising the HOMO and LUMO energy levels as a result of which energy band gap remained almost constant for all the dyes except for one dye.
- ❖ Theoretical calculation established that the HOMOs for λ-shaped dye remained spread over the electron rich aromatic segments while LUMOs are delocalized between two cyanoacrylic acids through DTP segments. The absorption maxima for the dye lacking auxiliary donor realized from HOMO to LUMO transitions while for λ-shaped dyes originated from HOMO-2 to LUMO transitions.
- ❖ Among the dyes, a fluorene containing H-shaped dye displayed highest power conversion efficiency due to high photocurrent density and open circuit voltage. The EIS studies revealed the large recombination resistance and small charge transfer resistance is responsible for the relatively superior performance.
- ❖ This work suggests that the strategy of synthesizing multi-anchoring dyes with the choice of suitable aromatic system can be promising method to improve the efficiency of DSSCs.

On the basis of above results it is supposed that DTP chromophore afford a great prospect to create essential functional materials for photovoltaic applications. Also, thiophene-based DTP represents a promising class of semiconducting materials

because of their fused-rigid backbone and good molecular planarity. In which S-S interactions enhance the electronic transport between molecules. Thus, a strategy can be made to design heteroacenes containing increasing S:N ratio, which may further enhance intermolecular interactions due to S-S contact.

Future prospects

The building block developed in the work can be utilized to develop non-fullerene acceptors for solar cells (Figure 6.1).

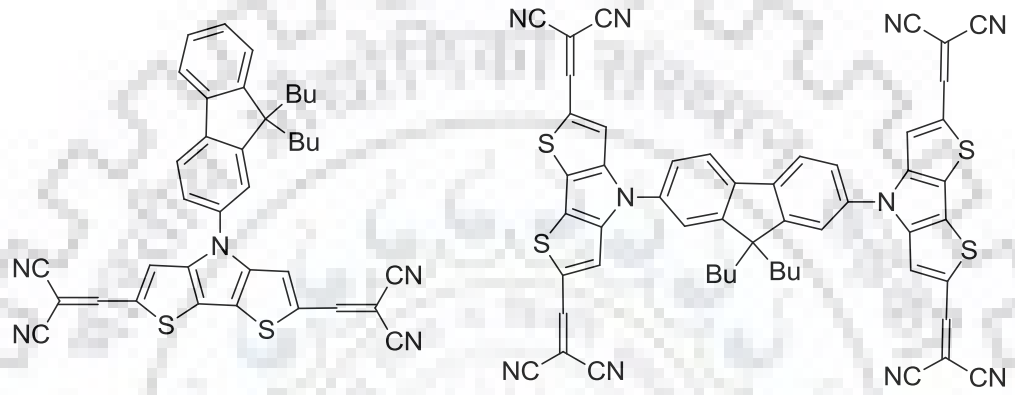

Figure 6.1 Proposed structures of DTP-based acceptors for solar cells.

Since the studies revealed that the DTP donor is electronically isolated from *N*-fluorene, this motif may be used to develop TADF emitters for OLED (Figure 6.2).

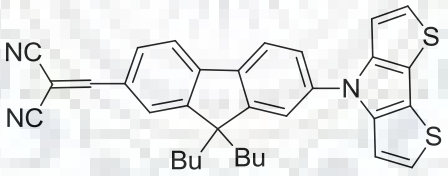

Figure 6.2 Proposed structures of DTP-based TADF emitter for OLED.

References

[1] O'Regan B.; Grätzel M. A low-cost, high-efficiency solar cell based on dye-sensitized colloidal TiO_2 films. *Nature*, **1991**, *353*, 737.

[2] Yu G.; Gao, J.; Hummelen J.C.; Wudl, F.; Heeger A.J. Polymer photovoltaic cells: Enhanced via a network of internal donor-acceptor heterojunctions. *Science*, **1995**, *270*, 1789-1791.

[3] Halls J.J.M.; Walsh C.A.; Greenham N.C.; Marseglia E.A.; Friend R.H.; Moratti S.C.; Holmes A.B. Efficient photodiodes from interpenetrating polymer networks. *Nature*, **1995**, *376*, 498.

[4] Grätzel M. 2003. Dye-sensitized solar cells. *J. Photochem. Photobiol. C* **2003**, *4*, 145-153.

[5] Ning Z.; Fu Y.; Tian H. Improvement of dye-sensitized solar cells: What we know and what we need to know. *Energy. Environ. Sci.* **2010**, *3*, 1170-1181.

[6] Grätzel C.; Zakeeruddin S.M. Recent trends in mesoscopic solar cells based on molecular and nano pigment light harvesters. *Mater. Today* **2013**, *16*, 11-18.

[7] Nazeeruddin M.K.; De Angelis F.; Fantacci S.; Selloni A.; Viscardi G.; Liska P.; Ito S.; Takeru B.; Grätzel M. Combined experimental and DFT-TDDFT computational study of photoelectrochemical cell ruthenium sensitizers. *J. Am. Chem. Soc.* **2005**, *127*, 16835- 16847.

[8] Jiang J.Q.; Sun C.L.; Shi Z.F.; Zhang H.L. Squaraines as light-capturing materials in photovoltaic cells. *RSC Adv.* **2014**, *4*, 32987-32996.

[9] Lee C.P.; Lin R.Y.Y.; Lin L.Y.; Li C.T.; Chu T.C.; Sun S.S.; Lin J.T.; Ho K.C. Recent progress in organic sensitizers for dye-sensitized solar cells. *RSC Adv.* **2015**, *5*, 23810-23825.

[10] Chen G.; Sasabe H.; Igarashi T.; Hong Z.; Kido J. Squaraine dyes for organic photovoltaic cells. *J. Mater. Chem. A* **2015**, *3*, 14517-1453.

[11] Mathew S.; Yella A.; Gao P.; Humphry-Baker R.; Curchod B.F.; Ashari-Astani N.; Tavernelli I.; Rothlisberger U.; Nazeeruddin M.K.; Grätzel M. Dye-sensitized solar cells with 13% efficiency achieved through the molecular engineering of porphyrin sensitizers. *Nat. Chem.* **2014**, *6*, 242-247.

[12] Chen C.Y.; Wang M.; Li J.Y.; Pootrakulchote N.; Alibabaei L.; Ngoc-le C.H.; Decoppet J.D.; Tsai, J.H.; Grätzel C.; Wu C.G.; Zakeeruddin S.M. Highly efficient

light-harvesting ruthenium sensitizer for thin-film dye-sensitized solar cells. *ACS Nano* **2009**, *3*, 3103-3109.

[13] Hagfeldt A.; Boschloo G.; Sun L.; Kloo L.; Pettersson H. Dye-sensitized solar cells. *Chem. Rev.* **2010**, *110*, 6595-6663.

[14] Mishra A.; Fischer M.K.; Bäuerle P. Metal-free organic dyes for dye-sensitized solar cells: From structure: Property relationships to design rules. *Angew. Chem. Int. Ed.* **2009**, *48*, 2474-2499.

[15] Li X.; Zheng Z.; Jiang W.; Wu W.; Wang Z.; Tian H. New D-A-π-A organic sensitizers for efficient dye-sensitized solar cells. *Chem. Commun.* **2015**, *51*, 3590-3592.

[16] Chen W.C.; Nachimuthu S.; Jiang J.C. Revealing the influence of cyano in anchoring groups of organic dyes on adsorption stability and photovoltaic properties for dye-sensitized solar cells. *Sci. Rep.* **2017**, *7*, 4979.

[17] Zhang S.; Yang X.; Numata Y.; Han L. Highly efficient dye-sensitized solar cells: progress and future challenges. *Energy Environ. Sci.*, **2013**, *6*, 1443-1464.

[18] Wu Y.; Zhu W. Organic sensitizers from D-π-A to D-A-π-A: effect of the internal electron-withdrawing units on molecular absorption, energy levels and photovoltaic performances. *Chem. Soc. Rev.*, **2013**, *42*, 2039-2058.

[19] Yao Z.; Zhang M.; Wu H.; Yang L.; Li R.; Wang P. Donor/acceptor indenoperylene dye for highly efficient organic dye-sensitized solar cells. *J. Am. Chem. Soc.* **2015**, *137*, 3799-3802.

[20] Liu J.; Li R.; Si X.; Zhou D.; Shi Y.; Wang Y.; Jing X.; Wang P. Oligothiophene dye-sensitized solar cells. *Energy Environ. Sci.* **2010**, *3*, 1924-1928.

[21] Zhang M.; Liu J.; Wang Y.; Zhou D.; Wang P. Redox couple related influences of π-conjugation extension in organic dye-sensitized mesoscopic solar cells. *Chem. Sci.* **2011**, *2*, 1401-1406.

[22] Pei K.; Wu Y.; Islam A.; Zhu S.; Han L.; Geng Z.; Zhu W. Dye-sensitized solar cells based on quinoxaline dyes: Effect of π-linker on absorption, energy levels, and photovoltaic performances. *J. Phys. Chem. C* **2014**, *118*, 16552-16561.

[23] Yao Z.; Zhang M.; Li R.; Yang L.; Qiao Y.; Wang P. A metal-free *N*-annulated thienocyclopentaperylene dye: Power conversion efficiency of 12% for dye-sensitized solar cells. *Angew. Chem. Int. Ed.* **2015**, *54*, 5994-5998.

[24] Hagberg D.P.; Marinado T.; Karlsson K.M.; Nonomura K.; Qin P.; Boschloo G.; Brinck T.; Hagfeldt A.; Sun L. Tuning the HOMO and LUMO energy levels of

organic chromophores for dye sensitized solar cells. *J. Org. Chem.* **2007**, *72*, 9550-9556.

[25] Yao Z.; Yang L.; Cai Y.; Yan C.; Zhang M.; Cai N.; Dong X.; Wang P. Rigidifying the π-linker to enhance light absorption of organic dye-sensitized solar cells and influences on charge transfer dynamics. *J. Phys. Chem. C.* **2014**, *118*, 2977-2986.

[26] Zhang G.; Bala H.; Cheng Y.; Shi D.; Lv X.; Yu Q.; Wang P. High efficiency and stable dye-sensitized solar cells with an organic chromophore featuring a binary π-conjugated spacer. *Chem. Commun.* **2009**, 2198-2200.

[27] Xu M.; Zhou D.; Cai N.; Liu J.; Li R.; Wang P. Electrical and photophysical analyses on the impacts of arylamine electron donors in cyclopentadithiophene dye-sensitized solar cells. *Energy Environ. Sci.* **2011**, *4*, 4735-4742.

[28] Cao Y.; Cai N.; Wang Y.; Li R.; Yuan Y.; Wang P. Modulating the assembly of organic dye molecules on titania nanocrystals via alkyl chain elongation for efficient mesoscopic cobalt solar cells. *Phys. Chem. Chem. Phys.* **2012**, *14*, 8282-8286.

[29] Jiang S.; Lu X.; Zhou G.; Wang Z.-S. Charge transfer in cross conjugated 4,8-dithienylbenzo[1,2-*b*:4,5-*b*′]dithiophene based organic sensitizers. *Chem. Commun.* **2013**, *49*, 3899-3901.

[30] Yen Y.S.; Chen Y.C.; Chou H.H.; Huang S.T.; Lin J.T. Novel organic sensitizers containing 2,6-difunctionalized anthracene unit for dye sensitized solar cells. *Polymers* **2012**, *4*, 1443-1461.

[31] Setayesh S.; Marsitzky D.; Müllen K. Bridging the gap between polyfluorene and ladder-poly-π-phenylene: Synthesis and characterization of poly-2,8-indenofluorene. *Macromolecules* **2000**, *33*, 2016-2020.

[32] Jacob J.; Zhang J.; Grimsdale A.C.; Müllen K.; Gaal M.; List E.J.W. Poly(tetraarylindenofluorene)s: New stable blue-emitting polymers. *Macromolecules* **2003**, *36*, 8240-8245.

[33] Hertel D.; Scherf U.; Bässler H. Charge carrier mobility in a ladder-type conjugated polymer. *Adv. Mater.* **1998**, *10*, 1119‑1122.

[34] Ye L.; Zhang S.; Zhao W.; Yao H.; Hou J. Highly efficient 2D-conjugated benzodithiophene-based photovoltaic polymer with linear alkylthio side chain. *Chem. Mater.* **2014**, *26*, 3603- 605.

[35] Venkateswararao A.; Thomas K.R.J.; In Solar Cell Nanotechnology: Tiwari A.; Boukherroub R.; Sharon M.,;Eds., Wiley-Scrivener: Beverly, MA, **2014**, Chapter 2, pp 41.

[36] Horie M.; Kettle J.; Yu C.Y.; Majewski L.A.; Chang S.W.; Kirkpatrick J.; Tuladhar S.M.; Nelson J.; Saunders B.R.; Turner M.L. Cyclopentadithiophene-benzothiadiazole oligomers and polymers; synthesis, characterisation, field-effect transistor and photovoltaic characteristics. *J. Mater. Chem.* **2012**, *22*, 381-389.

[37] Rasmussen S.C.; Evenson S.J. Dithieno[3,2-*b*:2′,3′-*d*]pyrrole-based materials: Synthesis and application to organic electronics. *Prog. Polym. Sci.* **2013**, *38*, 1773-1804.

[38] Wu W.; Liu Y.; Zhu D. π-Conjugated molecules with fused rings for organic field-effect transistors: design, synthesis and applications. *Chem. Soc. Rev.* **2010**, *39*, 1489-1502.

[39] Longhi E.; Bossi A.; Di Carlo G.; Maiorana S.; De Angelis F.; Salvatori P.; Petrozza A.; Binda M.; Roiati V.; Mussini P.R.; Baldoli C. Metal-free benzodithiophene-containing organic dyes for dye-sensitized solar cells. *Eur. J. Org. Chem.* **2013**, 84-94.

[40] Mahmood A. Triphenylamine based dyes for dye sensitized solar cells: A review. *Sol. Energy* **2016**,*123*, 127-144.

[41] Chaurasia S.; Liang C. J.; Yen Y.S.; Lin J.T. Sensitizers with rigidified-aromatics as the conjugated spacers for dye-sensitized solar cells. *J. Mater. Chem. C* **2015**, *3*, 9765-9780.

[42] Liang M.; Chen J. Arylamine organic dyes for dye-sensitized solar cells. *Chem. Soc. Rev.* **2013**, *42*, 3453-3488.

[43] Kim S.; Lee J.K.; Kang S.O.; Ko J.; Yum J.H.; Fantacci S.; De Angelis F.; Di Censo D.; Nazeeruddin M.K.; Grätzel, M. Molecular engineering of organic sensitizers for solar cell applications. *J. Am. Chem. Soc.*, **2006**, *128*, 16701-16707.

[44] Wang S.; Guo J.; He L.; Wang H.; Zhao J.; Lu C. Influence of thiophene and benzene unit in triphenylamine dyes on the performance of dye-sensitized solar cells. *Synth. Met.* **2013**, *168*, 1-8.

[45] Wang C.; Liang M.; Huang J.; Cheng F.; Wang H.; Guo Y.; Xue, S. Redox couple related influences of bulky electron donor as well as spacer in organic dye-sensitized mesoscopic solar cells. *Tetrahedron* **2014**, *70*, 6203-6210.

[46] Ko S.; Choi H.; Kang M.S.; Wang H.H.; Ji H.; Kim J.; Ko J.; Kang Y.J. Silole-spaced triarylamine derivatives as highly efficient organic sensitizers in dye-sensitized solar cells (DSSCs). *J. Mater. Chem.* **2010**, *20*, 2391-2399.

[47] Choi H.; Raabe I.; Kim D.; Teocoli F.; Kim C.; Song K.; Yum J.H.; Ko J.; Nazeeruddin M.K.; Grätzel M. High molar extinction coefficient organic sensitizers for efficient dye-sensitized solar cells. *Chem. Eur. J.* **2010**, *16*, 1193-1201.

[48] Baheti A.; Gajjela S.R.; Balaya P.; Thomas K.R.J. Synthesis, optical, electrochemical and photovoltaic properties of organic dyes containing trifluorenylamine donors. *Dyes Pigm.* **2015**, *113*, 78-86.

[49] Teng C.; Yang X.; Li S.; Cheng M.; Hagfeldt A.; Wu L.Z.; Sun L. Tuning the HOMO energy levels of organic dyes for dye-sensitized solar cells based on Br^- /Br^{3-} electrolytes. *Chem. -Eur. J.* **2010**, *16*, 13127-13138.

[50] Tan H.; Cai D.; Liu Z.; Zhong F.; Lv H.; Zhang X.; Yang S.; Pan C. Effects of 2-hexylthiophene on the performance of triphenylamine based organic dye for dye-sensitized solar cells. *Synth. Met.* **2016**, *214*, 56-61.

[51] Barea E.M.; Zafer C.; Gultekin B.; Aydin B.; Koyuncu S.; Icli S.; Santiago F.F.; Bisquert J. Quantification of the effects of recombination and injection in the performance of dye-sensitized solar cells based on *N*-substituted carbazole dyes. *J. Phys. Chem. C* **2010**, *114*, 19840-19848.

[52] Venkateswararao A.; Thomas K.R.J.; Lee C.P.; Ho K.C. Synthesis and characterization of organic dyes containing 2,7-disubstituted carbazole π-linker. *Tetrahedron Lett.* **2013**, *54*, 3985-3989.

[53] Kotchapradist P.; Prachumrak N.; Tarsang R.; Jungsuttiwong S.; Keawin T.; Sudyoadsuk T.; Promarak V. Pyrene-functionalized carbazole derivatives as non-doped blue emitters for highly efficient blue organic light-emitting diodes. *J. Mater. Chem. C* **2013**, *1*, 4916-4924.

[54] Cui L.-S.; Dong S.-C.; Liu Y.; Li, Q.; Jiang Z.-Q.; Liao L.-Z. A simple systematic design of phenylcarbazole derivatives for host materials to high-efficiency phosphorescent organic light-emitting diodes. *J. Mater. Chem. C* **2013**, *1*, 3967-3975.

[55] Thomas K.R.J.; Lin, J.T.; Tao, Y.T.; Ko, C.W. Light-emitting carbazole derivatives: potential electroluminescent materials. *J. Am. Chem. Soc.* **2001**, *123*, 9404-9411.

[56] Wang H.Y.; Liu F.; Xie L.H.; Tang C.; Peng B.; Huang W.; Wei W. Topological arrangement of fluorenyl-substituted carbazole triads and starbursts: Synthesis and optoelectronic properties. *J. Phys. Chem. C* **2011**, *115*, 6961-6967.

[57] Ooyama Y.; Inoue S.; Nagano T.; Kushimoto K.; Ohshita J.; Imae I.; Komaguchi K.; Harima Y. Dye-sensitized solar cells based on donor-acceptor π-conjugated fluorescent dyes with a pyridine ring as an electron-withdrawing anchoring group. *Angew. Chem., Int. Ed.* **2011**, *50*, 7429-7433.

[58] Huang H.; Fu Q.; Pan B.; Zhuang S.; Wang L.; Chen J.; Ma D.; Yang C. Butterfly-shaped tetrasubstituted carbazole derivatives as a new class of hosts for highly efficient solution processable green phosphorescent organic light-emitting diodes. *Org. Lett.* **2012**, *14*, 4786-4789.

[59] Murakami T.N.; Koumura N.; Uchiyama T.; Uemura Y.; Obuchi K.; Masaki N.; Kimura M.; Mori S. Recombination inhibitive structure of organic dyes for cobalt complex redox electrolytes in dye-sensitised solar cells. *J. Mater. Chem. A* **2013**, *1*, 792-798.

[60] Kakiage K.; Aoyama Y.; Yano T.; Otsuka T.; Kyomen T.; Unnoand M.; Hanaya M. An achievement of over 12 percent efficiency in an organic dye-sensitized solar cell. *Chem. Commun.* **2014**, *50*, 6379-6381.

[61] Soni S.S.; Fadadu K.B.; Vaghasiya J.V.; Solanki B.G.; Sonigara K.K.; Singh A.; Das D.; Iyer P.K. Improved molecular architecture of D-π-A carbazole dyes: 9% PCE with a cobalt redox shuttle in dye sensitized solar cells. *J. Mater. Chem. A* **2015**, *3*, 21664-21671.

[62] Liu B.; Wang B.; Wang R.; Gao L.; Huo S.; Liu Q.; Lia X.; Zhu W. Influence of conjugated π-linker in D-D-π-A indoline dyes: towards long-term stable and efficient dye-sensitized solar cells with high photovoltage. *J. Mater. Chem. A* **2014**, *2*, 804-812.

[63] Baheti A.; Thomas K.R.J.; Lee C.P.; Li C.T.; Ho K.C. Organic dyes containing fluoren-9-ylidene chromophores for efficient dye-sensitized solar cells. *J. Mater. Chem. A* **2014**, *2*, 5766-5779.

[64] Ci Z.; Yu X.; Bao M.; Wang C.; Ma, T. Influence of the benzo[*d*]thiazole-derived π-bridges on the optical and photovoltaic performance of D-π-A dyes. *Dyes Pigm.* **2013**, *96*, 619-625.

[65] Thomas K.R.J.; Venkateswararao A.; Lee C.P.; Ho K.C. Organic dyes containing fluoreneamine donor and carbazole π-linker for dye-sensitized solar cells. *Dyes Pigm.* **2015**, *123*,154-165.

[66] Aghazada S.; Gao P.; Yella A.; Moehl T.; Teuscher J.; Moser J.E.; Grätzel M.; Nazeeruddin M.K. Unraveling the dual character of sulfur atoms on sensitizers in dye sensitized solar cells. *ACS Appl. Mater. Interfaces* **2016**, *8*, 26827-26833.

[67] Cai S.; Tian G.; Li X.; Su J.; Tian H. Efficient and stable DSSC sensitizers based on substituted dihydroindolo[2,3-*b*]carbazole donors with high molar extinction coefficients. *J. Mater. Chem. A* **2013**, *1*, 11295-11305.

[68] Huang Z.S.; Feng H.L.; Zang X.F.; Iqbal Z.; Zeng H.; Kuang D.B.; Wang L.; Meier H.; Cao D. Dithienopyrrolobenzothiadiazole-based organic dyes for efficient dye-sensitized solar cells. *J. Mater. Chem. A* **2014**, *2*, 15365-15376.

[69] Zhang M.; Wang Y.; Xu M.; Ma W.; Li R.; Wang P. Design of high-efficiency organic dyes for titania solar cells based on the chromophoric core of cyclopentadithiophene-benzothiadiazole. *Energy Environ. Sci.* **2013**, *6*, 2944-2949.

[70] Zhou N.; Prabakaran K.; Lee B.; Chang S.H.; Harutyunyan B.; Guo P.; Butler M.R.; Timalsina A.; Bedzyk M.J.; Ratner M.A.; Vegiraju S. Metal-free tetrathienoacene sensitizers for high-performance dye-sensitized solar cells. *J. Am. Chem. Soc.* **2015**, *137*, 4414-4423.

[71] Shim J.Y.; Baek J.; Kim J.; Park S.Y.; Kim J.; Kim I.; Chun H.H.; Kim J.Y.; Suh H. Synthesis and properties of low band gap polymers based on thienyl thienoindole as a new electron-rich unit for organic photovoltaics. *Polym. Chem.* **2015**, *6*, 6011-6020.

[72] Lo C.; Doucoure B.I.; Aaron J.-J.; Svoboda J.; Kozmik V.; Brochon J.-C.; Henry E.; Maurel F.; Capochichi M. Synthesis and spectral properties of new fluorescent alkoxy-substituted thieno[3,2-*b*]indole derivatives. *Spectrochim. Acta, Part A* **2014**, *120*, 47-54.

[73] Baert F.; Cabanetos C.; Allain M.; Silvestre V.; Leriche P.; Blanchard P. Thieno[2,3-*b*]indole-based small push-pull chromophores: Synthesis, structure, and electronic properties. *Org. Lett.* **2016**, *18*, 1582-1585.

[74] Zhang X.-H.; Cui Y.; Katoh R.; Koumura N.; Hara K. Organic Dyes containing thieno[3,2-*b*]indole donor for efficient dye-sensitized solar cells. *J.Phys. Chem. C* **2010**, *114*, 18283-18290.

[75] Ni J.-S.; Yen Y.-C.; Lin J.T. Organic sensitizers with a rigid dithienobenzotriazole-based spacer for high performance dye-sensitized solar cells. *J. Mater. Chem. A* **2016**, *4*, 6553-6560.

[76] Eom Y.K.; Kang S.H.; Choi I.T.; Yoo Y.; Kim J.; Kim H.K. Significant light absorption enhancement by a single heterocyclic unit change in the π-bridge moiety from thieno[3,2-*b*]benzothiophene to thieno[3,2-*b*]indole for high performance dye sensitized and tandem solar cells. *J. Mater. Chem. A* **2017**, *5*, 2297-2308.

[77] Ogawa K.; Rasmussen S.C. A Simple and efficient route to *N*-functionalized dithieno[3,2-*b*:2',3'-*d*]pyrroles: Fused-ring building blocks for new conjugated polymeric systems. *J. Org. Chem.* **2003**, *68*, 2921-2928.

[78] Koeckelberghs G.; De Cremer L.; Vanormelingen W.; Dehaen W.; Verbiest T.; Persoons A.; Samyn C. Improved synthesis of *N*-alkyl substituted dithieno[3,2-*b*:2',3'-*d*]pyrroles. *Tetrahedron* **2005**, *61*, 687-691.

[79] Förtsch S.; Bäuerle P. Synthesis and characterization of two isomeric dithienopyrrole series and the corresponding electropolymers. *Polym. Chem.* **2017**, *8*, 3586-3595.

[80] Wu J.; Ma Y.; Wu N.; Lin Y.; Lin J.; Wang L.; Ma C.-Q. 2,2-Dicyanovinyl-end-capped oligothiophenes as electron acceptor in solution processed bulk-heterojunction organic solar cells. *Org. Electron.* **2015**, *23*, 28-38.

[81] Schulz G. L.; Kar P.; Weidelener M.; Vogt A.; Urdanpilleta M.; Linden M.; Mena-Osteritz E.; Mishra A.; Bäuerle P. The influence of alkyl side chains on molecular packing and solar cell performance of dithienopyrrole-based oligothiophenes. *J. Mater. Chem. A* **2016**, *4*, 10514-10523.

[82] Wessendorf C. D.; Schulz G.L.; Mishra A.; Kar P.; Ata I.; Weidelener M.; Urdanpilleta M.; Hanisch J.; Mena-Osteritz E.; Linden M.; Ahlswede E.; Bäuerle P. Efficiency improvement of solution-processed dithienopyrrole-based A-D-A oligothiophene bulk-heterojunction solar cells by solvent vapor annealing. *Adv. Energy Mater.* **2014**, *4*, 1400266.

[83] Marco A.B.; Martínez de Baroja N.; Franco S.; Garín J.; Orduna J.; Villacampa B.; Andreu R. Dithienopyrrole as a rigid alternative to the bithiophene π relay in chromophores with second-order nonlinear optical properties. *Chem. Asian J.* **2015**, *10*, 188-197.

[84] Mo H.; Radke K.R.; Ogawa K.; Heth C.L.; Erpelding B.T.; Rasmussen S.C. Solution and solid-state properties of highly fluorescent dithieno[3,2-*b*:2′,3′-*d*]pyrrole-based oligothiophenes. *Phys. Chem. Chem. Phys.* **2010**, **12**, 14585-14595.

[85] Evenson S.J.; Pappenfus T.M.; Delgado M.C.R.; Radke-Wohlers K.R.; Navarretec J.T.L.; Rasmussen S.C. Molecular tuning in highly fluorescent dithieno[3,2-*b*:2',3'-*d*]pyrrole-based oligomers: effects of *N*-functionalization and terminal aryl unit. *Phys. Chem. Chem. Phys.* **2012**, *14*, 6101-6111.

[86] Tiwari S.P.; Kim J.; Knauer K.A.; Hwang D.K.; Polander L.E.; Barlow S.; Marder S.R.; Kippelen B. Complementary-like inverters based on an ambipolar solution-processed molecular bis(naphthalene diimide)-dithienopyrrole derivative, *Org. Electron.* **2012**, *13*, 1166-1170.

[87] Polander L.E.; Pandey L.; Barlow S.; Tiwari S. P.; Risko C.; Kippelen B.; Brêdas J.-L.; Marder S.R. Benzothiadiazole-dithienopyrrole donor-acceptor-donor and acceptor-donor-acceptor triads: synthesis and optical, electrochemical, and charge-transport properties. *J. Phys. Chem. C* **2011**, *115*, 23149-23163.

[88] Zhan X.; Tan Z.A.; Zhou E.; Li Y.; Misra R.; Grant; A.; Domercq B.; Zhang X.H.; An Z.; Zhang X.; Barlow S. Copolymers of perylene diimide with dithienothiophene and dithienopyrrole as electron-transport materials for all-polymer solar cells and field-effect transistors. *J. Mater. Chem.* **2009**, *19*, 5794-5803.

[89] Zhang X.; Steckler T.T.; Dasari R.R.; Ohira S.; Potscavage W.J.; Tiwari S.P.; Coppée S.; Ellinger S.; Barlow S.; Brédas J.L.; Kippelen B. Dithienopyrrole-based donor-acceptor copolymers: low band-gap materials for charge transport, photovoltaics and electrochromism. *J. Mater. Chem.* **2010**, *20*, 123-134.

[90] Zhang X.; Shim J.W.; Tiwari S.P.; Zhang Q.; Norton J.E.; Wu P.T.; Barlow S.; Jenekhe S.A.; Kippelen B.; Brédas J.L.; Marder S.R. Dithienopyrrole-quinoxaline/pyridopyrazine donor-acceptor polymers: synthesis and electrochemical, optical, charge-transport, and photovoltaic properties. *J. Mater. Chem.* **2011**, *21*, 4971-4982.

[91] Nelson T.L.; Young T.M.; Liu J.; Mishra S.P.; Belot J.A.; Balliet C.L.; Javier A.E.; Kowalewski T.; McCullough R.D. Transistor paint: high mobilities in small bandgap polymer semiconductor based on the strong acceptor, diketopyrrolopyrrole and strong donor, dithienopyrrole. *Adv. Mater.* **2010**, *22*, 4617-4621.

[92] Zhang S.; Wen Y.; Zhou W.; Guo Y.; Ma L.; Zhao X.; Zhao Z.; Barlow S.; Marder S.R.; Liu Y.; Zhan X. Perylene diimide copolymers with dithienothiophene and dithienopyrrole: Use in n-channel and ambipolar field-effect transistors. *J. Polym. Sci., Part A: Polym. Chem.* **2013**, *51*, 1550-1558.

[93] Parameswaran M.; Balaji G.; Jin T.M.; Vijila C.; Vadukumpully S.; Furong Z.; Valiyaveettil S. Charge transport studies in fluorene-dithieno[3,2-*b*:2′,3′-*d*]pyrrole oligomer using time-of-flight photoconductivity method. *Org. Electron.* **2009**, *10*, 1534-1540.

[94] Colbert A.E.; Janke E.M.; Hsieh S.T.; Subramaniyan S.; Schlenker C.W.; Jenekhe S.A.; Ginger D.S. Hole transfer from low band gap quantum dots to conjugated polymers in organic/inorganic hybrid photovoltaics. *J. Phys. Chem. Lett.* **2013**, *4*, 280-284.

[95] Choa M.J.; Seob J.; Yoona S.H.; Choia D.H.; Prasadc P.N. Effects of side chains on physical and photovoltaic properties of methyl thiophene-3-carboxylate containing dithienopyrrole-based copolymers. *Synth. Met.* **2013**, *182*, 22-27.

[96] Wang C.; Liu G.; Chen Y.; Liu S.; Chen Q.; Li R.; Zhang B. Dithienopyrrole-/benzodithiophene-based donor–acceptor polymers for memristor. *Chem Plus Chem* **2014**, *79*, 1263-1270.

[97] Geng Y.; Cong J.; Tajima K.; Zeng Q.; Zhou E. Synthesis and properties of D-A copolymers based on dithienopyrrole and benzothiadiazole with various numbers of thienyl units as spacers. *Polym. Chem.* **2014**, *5*, 6797-6803.

[98] Kesters J.; Verstappen P.; Vanormelingen W.; Drijkoningen J.; Vangerven T.; Devisscher D.; Marin L.; Champagne B.; Manca J.; Lutsen L.; Vanderzande D. *N*-acyl-dithieno[3,2-*b*:2’,3’-*d*]pyrrole-based low bandgap copolymers affording improved open-circuit voltages and efficiencies in polymer solar cells. *Sol. Energy Mater. Sol. Cells* **2015**, *136*, 70-77.

[99] Yue W.; Larsen-Olsen T.T.; Hu X.; Shi M.; Chen H.; Hinge M.; Fojan P.; Krebs F.C.; Yu D. Synthesis and photovoltaic properties from inverted geometry cells and roll-to-roll coated large area cells from dithienopyrrole-based donor-acceptor polymers. *J. Mater. Chem. A* **2013**, *1*, 1785-1793.

[100] Yue W.; Huang X.; Yuan J.; Ma W.; Krebs F.C.; Yu D. A novel benzodipyrrolidone-based low band gap polymer for organic solar cells. *J. Mater. Chem. A* **2013**, *1*, 10116-10119.

[101] Vanormelingen W.; Kesters J.; Verstappen P.; Drijkoningen J.; Kudrjasova J.; Koudjina S.; Liégeois V.; Champagne B.; Manca J.; Lutsen L.; Vanderzande D. Enhanced open-circuit voltage in polymer solar cells by dithieno[3,2-*b*:2′,3′-*d*]pyrrole *N*-acylation. *J. Mater. Chem. A* **2014**, *2*, 7535-7545.

[102] Li W.; An Y.; Wienk M.M.; Janssen R.A. Polymer-polymer solar cells with a near-infrared spectral response. *J. Mater. Chem. A* **2015**, *3*, 6756-6760.

[103] Wunsch B.H.; Rumi M.; Tummala N.R.; Risko C.; Kang D.Y.; Steirer K.X.; Gantz, J.; Said M.; Armstrong,N.R.; Brédas J.L.; Bucknall D. Structure-processing-property correlations in solution-processed, small-molecule, organic solar cells. *J. Mater. Chem. C* **2013**, *1*, 5250-5260.

[104] Lee W.; Kim G.H.; Jeong E.; Wang X.; Yum S.; Ko S.J.; Hwang S.; Kim J.Y.; Woo H.Y. Dithieno[3,2-b:2′,3′-d]pyrrole and benzothiadiazole-based semicrystalline copolymer for photovoltaic devices with indene-C_{60} bisadduct. *Macromol. Chem. Phys.* **2013**, *214*, 2083-2090.

[105] Zhou E.; Cong J.; Tajima K.; Yang C.; Hashimoto K. Conjugated polymers based on 1, 3-dithien-2-yl-thieno[3,4-*c*]pyrrole-4,6-dione: synthesis, characterization, and solvent effects on photovoltaic performance. *J. Phys. Chem. C* **2012**, *116*, 2608-2614.

[106] Song H.; Tong H.; Xie Z.; Wang L.; Wang F. Synthesis and photovoltaic properties of a donor-acceptor polymer containing both dithieno[3,2-*b*:2′,3′-*d*] pyrrole and fluorene as donor units. *Polymer* **2012**, *53*, 5103-5108.

[107] Yassin A.; Savitha G.; Leriche P.; Frere P.; Roncali J. A donor-acceptor-donor (D-A-D) molecule based on 3-alkoxy-4-cyanothiophene and dithienopyrrole units as active material for organic solar cells. *New J. Chem.* **2012**, *36*, 2412-2416.

[108] Kast H.; Mishra A.; Schulz G.L.; Urdanpilleta M.; Mena-Osteritz E.; Bäuerle P. Acceptor-substituted *S,N*-heteropentacenes of different conjugation length: Structure-property relationships and solar cell performance. *Adv. Funct. Mater.* **2015**, *25*, 3414-3424.

[109] Weidelener M.; Wessendorf C.D.; Hanisch J.; Ahlswede E.; Götz G.; Lindén M.; Schulz G.; Mena-Osteritz E.; Mishra A.; Bäuerle P. Dithienopyrrole-based oligothiophenes for solution-processed organic solar cells. *Chem. Commun.* **2013**, *49*, 10865-10867.

[110] Lu H.I.; Lu C.W.; Lee Y.C.; Lin H.W.; Lin L.Y.; Lin F.; Chang J.H.; Wu C.I.; Wong K.T. New molecular donors with dithienopyrrole as the electron-donating

group for efficient small-molecule organic solar cells. *Chem. Mater.* **2014**, *26*, 4361-4367.

[111] Gupta A.; Ali A.; Gao M.; Singh T.B.; Bilic A.; Watkins S.E.; Bach U.; Evans R.A. Small molecules containing rigidified thiophenes and a cyanopyridone acceptor unit for solution-processable bulk-heterojunction solar cells. *Dyes Pigm.* **2015**, *119*, 122-132.

[112] Schulz G.L.; Löbert M.; Ata I.; Urdanpilleta M.; Lindén M.; Mishra A.; Bäuerle P. Functional tuning of A-D-A oligothiophenes: the effect of solvent vapor annealing on blend morphology and solar cell performance. *J. Mater. Chem. A* **2015**, *3*, 13738-13748.

[113] Mishra A.; Keshtov M.L.; Looser A.; Singhal R.; Stolte M.; Würthner F.; Bäuerle P.; Sharma G.D. Unprecedented low energy losses in organic solar cells with high external quantum efficiencies by employing non-fullerene electron acceptors. *J. Mater. Chem. A* **2017**, *5*, 14887-14897.

[114] Balaji G.; Parameswaran M.; Jin T.M.; Vijila C.; Furong Z.; Valiyaveettil S. Synthesis and hole-transporting properties of highly fluorescent *N*-aryl dithieno[3,2-*b*:2′,3′-*d*]pyrrole-based oligomers. *J. Phys. Chem. C* **2010**, *114*, 4628-4635.

[115] Yassin A.; Leriche P.; Allain M.; Roncali J. Donor-acceptor-donor (D-A-D) molecules based on isoindigo as active material for organic solar cells. *New J. Chem.* **2013**, *37*, 502-507.

[116] Busireddy M.R.; Mantena V.N.R.; Chereddy N.R.; Shanigaram B.; Kotamarthi B.; Biswas S.; Sharma G.D.; Vaidya J.R. Dithienopyrrole-benzodithiophene based donor materials for small molecular BHJSCs: Impact of side chain and annealing treatment on their photovoltaic properties. *Org. Electron.* **2016**, *37*, 312-325.

[117] Yassin A.; Rousseau T.; Leriche P.; Cravino A.; Roncali J. Evaluation of bis-dicyanovinyl short-chain conjugated systems as donor materials for organic solar cells. *Sol. Energy Mater. Sol. Cells* **2011**, *95*, 462-468.

[118] Xu M.; Zhang M.; Pastore M.; Li R.; De Angelis F.; Wang P. Joint electrical, photophysical and computational studies on D-π-A dye sensitized solar cells: the impacts of dithiophene rigidification. *Chem. Sci.* **2012**, *3*, 976-983.

[119] Polander L.E.; Yella A.; Teuscher J.; Humphry-Baker R.; Curchod B.F.; Ashari Astani, N.; Gao P.; Moser J.E.; Tavernelli I.; Rothlisberger U.; Grätzel, M. Unravelling the potential for dithienopyrrole sensitizers in dye-sensitized solar cells. *Chem. Mater.* **2013**, *25*, 2642-2648.

[120] Lim K.; Ju M.J.; Song J.; Choi I.T.; Do K.; Choi H.; Song K.; Kim H.K.; Ko J. Organic sensitizers featuring a planar indeno[1,2-*b*]-thiophene for efficient dye-sensitized solar cells. *ChemSusChem* **2013**, *6*, 1425-1431.

[121] Yella, A.; Humphry-Baker, R.; Curchod, B. F. E.; Astani, N. A.; Teuscher, J.; Polander, L. E.; Mathew, S.; Tavernelli, I.; Rothlisberger, U.; Moser, J.-E.; Grätzel, M.; Nazeeruddin, M. K.; Frey, J. Molecular engineering of a fluorene donor for dye-sensitized solar cells. *Chem. Mater.* **2013**, *25*, 2733-2739.

[122] Jradi F.M.; Kang X.; O'Neil D.; Pajares G.; Getmanenko Y.A.; Szymanski P.; Parker T.C.; El-Sayed M.A.; Marder S.R. Near-infrared asymmetrical squaraine sensitizers for highly efficient dye sensitized solar cells: the effect of π-bridges and anchoring groups on solar cell performance. *Chem. Mater.* **2015**, *27*, 2480-2487.

[123] Delcamp J.H.; Shi Y.; Yum J.H.; Sajoto T.; Dell'Orto E.; Barlow S.; Nazeeruddin M.K.; Marder S.R.; Grätzel M. The role of π bridges in high-efficiency DSCs based on unsymmetrical squaraines. *Chem. Eur. J.* **2013**, *19*, 1819-1827.

[124] Wang Z.; Liang M.; Wang H.; Wang P.; Cheng F.; Sun Z.; Song X. Joint electrical, photophysical, and photovoltaic studies on truxene dye-sensitized solar cells: impact of arylamine electron donors. *ChemSusChem* **2014**, *7*, 795-803.

[125] Xia Q.; Liang M.; Tan Y.; Gao W.; Ouyang L.; Ge G.; Sun Z.; Xue S. Engineering of the electron donor of triarylamine sensitizers for high-performance dye-sensitized solar cells. *Org. Electron.* **2015**, *17*, 285-294.

[126] Dong H.; Liang M.; Zhang C.; Wu Y.; Sun Z.; Xue S. Twisted fused-ring thiophene organic dye-sensitized solar cells. *J. Phys. Chem. C* **2016**, *120*, 22822-22830.

[127] Lu Z.; Dai P.; Wang C.; Liang M.; Zong X.; Sun Z.; Xue S. Synthesis of new dithieno[3,2-*b*:2′,3′-*d*]pyrrole (DTP) dyes for dye-sensitized solar cells: Effect of substituent on photovoltaic properties. *Tetrahedron* **2016**, *72*, 3204-3212.

[128] Ge G.; Dai P.; Lu Z.; Liang M.; Dong H.; Sun Z.; Xue S. Synthesis of new dithieno[3,2-*b*:2′,3′-*d*]pyrrole (DTP) units for photovoltaic cells. *Dyes Pigm.* **2016**, *128*, 8-18.

[129] Cai N.; Zhang J.; Xu M.; Zhang M.; Wang P. Improving the photovoltage of dithienopyrrole dye-sensitized solar cells via attaching the bulky bis(octyloxy) biphenyl moiety to the conjugated π-linker. *Adv. Funct. Mater.* **2013**, *23*, 3539-3547.

[130] Zhang J.; Yao Z.; Cai Y.; Yang L.; Xu M.; Li R.; Zhang M.; Dong X.; Wang P. Conjugated linker correlated energetics and kinetics in dithienopyrrole dye-sensitized solar cells. *Energy Environ. Sci.* **2013**, *6*, 1604-1614.

[131] Wang Z.; Liang M.; Wang L.; Hao Y.; Wang C.; Sun Z.; Xue S. New triphenylamine organic dyes containing dithieno [3,2-*b*:2′,3′-*d*] pyrrole (DTP) units for iodine-free dye-sensitized solar cells. *Chem. Commun.* **2013**, *49*, 5748-5750.

[132] Wang Z.; Liang M.; Hao Y.; Zhang Y.; Wang L.; Sun Z.; Xue S. Influence of the *N*-heterocycle substituent of the dithieno[3,2-*b*:2′,3′-*d*]pyrrole (DTP) spacer as well as sensitizer adsorption time on the photovoltaic properties of arylamine organic dyes. *J. Mater. Chem. A* **2013**, *1*, 11809-11819.

[133] Wang Z.; Wang H.; Liang M.; Tan Y.; Cheng F.; Sun Z.; Xue, S. Judicious design of indoline chromophores for high-efficiency iodine-free dye-sensitized solar cells. *ACS Appl. Mater. Interfaces* **2014**, *6*, 5768-5778.

[134] Miao K.; Liang M.; Wang Z.; Zhang C.; Sun Z.; Xue S. Organic sensitizers featuring thiophene derivative based donors with improved stability and photovoltaic performance. *Phys. Chem. Chem. Phys.* **2017**, *19*, 1927-1936.

[135] Zhang H.; Iqbal Z.; Chen Z.E.; Hong Y.P. Effect of structural optimization on the photovoltaic performance of dithieno[3,2-*b*:2′,3′-*d*]pyrrole-based dye-sensitized solar cells. *RSC Adv.* **2017**, *7*, 35598-35607.

[136] Xie Y.; Wu W.; Zhu H.; Liu J.; Zhang W.; Tian H.; Zhu W.H. Unprecedentedly targeted customization of molecular energy levels with auxiliary-groups in organic solar cell sensitizers. *Chem. Sci.* **2016**, *7*, 544-549.

[137] Li F.; Chen Y.; Zong X.; Qiao W.; Fan H.; Liang M.; Xue S. New benzothiadiazole-based dyes incorporating dithieno[3,2-*b*:2′,3′-*d*]pyrrole (DTP) π-linker for dye-sensitized solar cells with different electrolytes. *J. Power Sources* **2016**, *332*, 345-354.

[138] Dai P.; Yang L.; Liang M.; Dong H.; Wang P.; Zhan C.; Sun, Z.; Xue S. Influence of the terminal electron donor in D-D-π-A organic dye-sensitized solar cells: dithieno[3,2-*b*:2′,3′-*d*]pyrrole versus bis(amine). *ACS Appl. Mater. Interfaces* **2015**, 7, 22436-22447.

[139] Sahu D.; Padhy H.; Patra D.; Yin J.F.; Hsu Y.C.; Lu K.L.; Wei K.H.; Lin H.C. Synthesis and applications of novel acceptor-donor-acceptor organic dyes with dithienopyrrole- and fluorene-cores for dye-sensitized solar cells. *Tetrahedron* **2011**, *67*, 303-311.

[140] Zhang H.; Fan J.; Iqbal Z.; Kuang D.B.; Wang L.; Meier H.; Cao D. Novel dithieno[3,2-*b*:2',3'-*d*]pyrrole-based organic dyes with high molar extinction coefficient for dye-sensitized solar cells. *Org. Electron.* **2013**, *14*, 2071-2081.

[141] Zhao J.; Yang X.; Hao Y.; Cheng M.; Tian J.; Sun L. Effect of different numbers of -CH_2- units on the performance of isoquinolinium dyes. *ACS Appl. Mater. Interfaces* **2014**, *6*, 3907-3914.

[142] Ooyama Y.; Harima Y. Molecular designs and syntheses of organic dyes for dye-sensitized solar cells. *Eur. J. Org. Chem.* **2009**, *2009*, 2903-2934.

[143] Baheti A.; Singh P.; Lee C.P.; Thomas K.R.J.; Ho K.C. 2, 7-Diaminofluorene-based organic dyes for dye-sensitized solar cells: effect of auxiliary donor on optical and electrochemical properties. *J. Org. Chem.* **2011**, *76*, 4910-4920.

[144] Velusamy M.; Thomas, K.R.J.; Lin J.T.; Hsu Y.C.; Ho K.C. Organic dyes incorporating low-band-gap chromophores for dye-sensitized solar cells. *Org. Lett.* **2005**, *7*, 1899-1902.

[145] Zhao J.; Oniwa K.; Islam A.; Qin C.; Asao N.; Han L.; Yamamoto Y.; Jin T. Thieno[2,3,*a*]carbazole donor-based organic dyes for high efficiency dye-sensitized solar cells. *Org. Chem. Front.* **2015**, *2*, 253-258.

[146] Huang J.H.; Jiang K.J.; Yu C.C.; Li S.G.; Li G.; Yang L.M.; Song Y.L. A tetrahydropyrene-based organic dye for solar cell application. *RSC Adv.* **2014**, *4*, 22181-22185.

[147] Hua Y.; Chang S.; Huang D.; Zhou X.; Zhu X.; Zhao J.; Chen T.; Wong W.Y.; Wong W.K. Significant improvement of dye-sensitized solar cell performance using simple phenothiazine-based dyes. *Chem. Mater.* **2013**, *25*, 2146-2153.

[148] Song J.L.; Amaladass P.; Wen S.H.; Pasunooti K.K.; Li A.; Yu Y.L.; Wang X.; Deng W.Q.; Liu X.W. Aryl/hetero-arylethyne bridged dyes: The effect of planar π-bridge on the performance of dye-sensitized solar cells. *New J. Chem.* **2011**, *35*, 127-136.

[149] Kakiage K.; Aoyama Y.; Yano T.; Oya K.; Kyomen T.; Hanaya M. Fabrication of a high-performance dye-sensitized solar cell with 12.8% conversion efficiency using organic silyl-anchor dyes. *Chem. Commun.* **2015**, *51*, 6315-6317.

[150] Tan L.L.; Xie L.J.; Shen,Y.; Liu J.M.; Xiao L.M.; Kuang D.B.; Su C.Y. Novel organic dyes incorporating a carbazole or dendritic 3,6-diiodocarbazole unit for efficient dye-sensitized solar cells. *Dyes Pigm.* **2014**, *100*, 269-277.

[151] Thongkasee P.; Thangthong A.; Janthasing N.; Sudyoadsuk T.; Namuangruk S.; Keawin T.; Jungsuttiwong S.; Promarak V. Carbazole-dendrimer-based donor-π-acceptor type organic dyes for dye-sensitized solar cells: Effect of the size of the carbazole dendritic donor. *ACS Appl. Mater. Interfaces* **2014**, *6*, 8212-8222.

[152] Qian X.; Zhu Y.Z.; Chang W.Y.; Song J.; Pan B.; Lu L.; Gao H.H.; Zheng J.Y. Benzo[*a*]carbazole-based Donor-π-Acceptor type organic dyes for highly efficient dye-sensitized solar cells. *ACS Appl. Mater. Interfaces* **2015**, *7*, 9015-9022.

[153] Cao W.; Fang M.; Chai Z.; Xu H.; Duan T.; Li Z.; Chen X.; Qin J.; Han H. New D-π-A organic dyes containing a *tert*-butyl-capped indolo[3,2,1-*jk*]carbazole donor with bithiophene unit as π-linker for dye-sensitized solar cells. *RSC Adv.* **2015**, *5*, 32967-32975.

[154] Gupta A.; Kelson M.M.; Armel V.; Bilic A.; Bhosale S.V. *N*-Alkyl- and *N*-aryl-dithieno[3,2-*b*:2′,3′-*d*]pyrrole-containing organic dyes for efficient dye-sensitized solar cells. *Tetrahedron* **2014,** *70*, 2141-2150.

[155] Wang Z.; Liang M.; Tan Y.; Ouyang L.; Sun Z.; Xue S. Organic dyes containing dithieno[2,3-*d*:2′,3′-*d*′]thieno[3,2-*b*:3′,2′-*b*′]dipyrrole core for efficient dye-sensitized solar cells. *J. Mater. Chem. A* **2015**, *3*, 4865-4874.

[156] Hartwig J.F. Transition metal catalyzed synthesis of arylamines and aryl ethers from aryl halides and triflates: Scope and mechanism. *Angew. Chem. Int. Ed.* **1998**, *37*, 2046-2067.

[157] Liu J.; Zhang R.; Sauvé G.; Kowalewski T.; McCullough R.D. Highly disordered polymer field effect transistors: *N*-alkyl dithieno[3,2-*b*:2′,3′-*d*]pyrrole-based copolymers with surprisingly high charge carrier mobilities. *J. Am. Chem. Soc.* **2008**, *130*, 13167-13176.

[158] Stille J.K. The palladium-catalyzed cross-coupling reactions of organotin reagents with organic electrophiles [new synthetic methods (58)]. *Angew. Chem. Int. Ed.* **1986**, *25*, 508-524.

[159] Reichardt C. Solvatochromic dyes as solvent polarity indicators. *Chem. Rev.* **1994**, *94*, 2319-2358.

[160] Granzhan A.; Ihmels H.; Viola G. 9-Donor-substituted acridizinium salts: Versatile environment-sensitive fluorophores for the detection of biomacromolecules. *J. Am. Chem. Soc.* **2007**, *129*, 1254-1267.

[161] Sayama K.; Tsukagoshi S.; Hara K.; Ohga Y.; Shinpou A.; Abe Y.; Suga S.; Arakawa H. Photoelectrochemical properties of *J*-aggregates of benzothiazole

merocyanine dyes on a nanostructured TiO_2 film. *J. Phys. Chem. B* **2002**, *106*, 1363-1371.

[162] Grätzel M. Photoelectrochemical cells. *Nature* **2001**, *414*, 338-344.

[163] Green A.N.; Palomares E.; Haque S.A.; Kroon J.M.; Durrant J.R. Charge transport versus recombination in dye-sensitized solar cells employing nanocrystalline TiO_2 and SnO_2 films. *J. Phys. Chem. B* **2005**, *109*, 12525-12533.

[164] Sholl D.; Steckel J.A. Density functional theory: A practical introduction, Wiley-VCH, **2009**.

[165] Koch W.; Holthausen M.C. A Chemist's guide to density functional theory, Wiley-VCH, **2000**.

[166] Zhang H.; Iqbal Z.; Chen Z.E.; Hong Y.P. Effect of structural optimization on the photovoltaic performance of dithieno[3,2-*b*:2′,3′-*d*]pyrrole-based dye-sensitized solar cells. *RSC Adv.* **2017**, *7*, 35598-35607.

[167] Ying W.; Guo F.; Li J.; Zhang Q.; Wu W.; Tian H.; Hua J. Series of new D-A-π-A organic broadly absorbing sensitizers containing isoindigo unit for highly efficient dye-sensitized solar cells. *ACS Appl. Mater. Interfaces* **2012**, *4*, 4215-4224.

[168] Qu S.; Wang B.; Guo F.; Li J.; Wu W.; Kong C.; Long Y.; Hua J. New diketo-pyrrolo-pyrrole (DPP) sensitizer containing a furan moiety for efficient and stable dye-sensitized solar cells. *Dyes Pigm.* **2012**, *92*, 1384-1393.

[169] Mora-Sero I.; Gimenez S.; Fabregat-Santiago F.; Gomez R.; Shen Q.; Toyoda T.; Bisquert J. Recombination in quantum dot sensitized solar cells. *Acc. Chem. Res.* **2009**, *42*, 1848-1857.

[170] Van de Lagemaat J.; Park N.G.; Frank A.J. Influence of electrical potential distribution, charge transport, and recombination on the photopotential and photocurrent conversion efficiency of dye-sensitized nanocrystalline TiO_2 solar cells: A study by electrical impedance and optical modulation techniques. *J. Phys. Chem. B* **2000**, *104*, 2044-2052.

[171] Chang Y.J.; Chou P.T.; Lin S.Y.; Watanabe M.; Liu Z.Q.; Lin J.L.; Chen K.Y.; Sun S.S.; Liu C.Y.; Chow T.J. High-performance organic materials for dye-sensitized solar cells: Triarylene-linked dyads with a 4-*tert*-butylphenylamine donor. *Chem. Asian J.* **2013**, *7*, 572-581.

[172] Zhang L.; Cole J.M. Anchoring groups for dye-sensitized solar cells. *ACS Appl. Mater. Interfaces* **2015**, *7*, 3427-3455.

[173] Hua Y.; Lee L.T.L.; Zhang C.; Zhao J.; Chen T.; Wong W.Y.; Wong W.K.; Zhu X. Co-sensitization of 3D bulky phenothiazine-cored photosensitizers with planar squaraine dyes for efficient dye-sensitized solar cells. *J. Mater. Chem. A* **2015**, *3*, 13848-13855.

[174] Yang L.; Zheng Z.; Li Y.; Wu W.; Tian H.; Wang Z. *N*-Annulated perylene-based metal-free organic sensitizers for dye-sensitized solar cells. *Chem. Commun.* **2015**, *51*, 4842-4845.

[175] Singh P.; Baheti A.; Thomas K.R.J.; Lee C.P.; Ho K.C. Fluorene-based organic dyes containing acetylene linkage for dye-sensitized solar cells. *Dyes Pigm.* **2012**, *95*, 523-533.

[176] Liu X.; Long J.; Wang G.; Pei Y.; Zhao B.; Tan S. Effect of structural modification on the performances of phenothiazine-dye sensitized solar cells. *Dyes Pigm.* **2015**, *121*, 118-127.

[177] Yang X.; Zhao J.; Wang L.; Tian J.; Sun L. Phenothiazine derivatives-based D-π-A and D-A-π-A organic dyes for dye-sensitized solar cells. *RSC Adv.* **2014**, *4*, 24377-24383.

[178] Iqbal Z.; Wu W.Q.; Huang Z.S.; Wang L.; Kuang D.B.; Meier H.; Cao D. Trilateral π-conjugation extensions of phenothiazine-based dyes enhance the photovoltaic performance of the dye-sensitized solar cells. *Dyes Pigm.* **2016**, *124*, 63-71.

[179] Miyaura N.; Suzuki A. Palladium-catalyzed cross-coupling reactions of organoboron compounds. *Chem. Rev.* **1995**, *95*, 2457-2483.

[180] Wan Z.; Jia C.; Duan Y.; Zhou L.; Zhang J.; Lin Y.; Shi Y. Influence of the antennas in starburst triphenylamine-based organic dye-sensitized solar cells: Phenothiazine versus carbazole. *RSC Adv.* **2012**, *2*, 4507-4514.

[181] Zhang F.; Luo Y.H.; Song J.S.; Guo X.Z.; Liu W.L.; Ma C.P.; Huang Y.; Ge M.F.; Bo Z.; Meng Q.B. Triphenylamine-based dyes for dye-sensitized solar cells. *Dyes Pigm.* **2009**, *81*, 224-230.

[182] Koumura N.; Wang Z.S.; Mori S.; Miyashita M.; Suzuki E.; Hara K. Alkyl-functionalized organic dyes for efficient molecular photovoltaics. *J. Am. Chem. Soc.* **2006**, *128*, 14256-14257.

[183] Chou H.H.; Chen Y.C.; Huang H.J.; Lee T.H.; Lin J.T.; Tsai C.; Chen K. High-performance dye-sensitized solar cells based on 5,6-bis-hexyloxy-benzo[2,1,3]thiadiazole. *J. Mater. Chem.* **2012**, *22*, 10929-10938.

[184] Correa N.M.; Levinger N.E. What can you learn from a molecular probe? New insights on the behavior of C343 in homogeneous solutions and AOT reverse micelles. *J. Phys. Chem. B* **2006**, *110*, 13050-13061.

[185] Cheng H.M.; Hsieh W.F. High-efficiency metal-free organic-dye-sensitized solar cells with hierarchical ZnO photoelectrode. *Energy Environ. Sci.* **2010**, *3*, 442-447.

[186] Raghuraman H.; Kelkar D.A.; Chattopadhyay A. In Reviews in fluorescence **2005**; Geddes C.D.; Lakowicz J. R.; Eds. Springer: New York, **2005**, pp 199.

[187] Kantchev E.A.B.; Norsten T.B.; Sullivan M.B. Time-dependent density functional theory (TDDFT) modelling of Pechmann dyes: From accurate absorption maximum prediction to virtual dye screening. *Org. Biomol. Chem.* **2012**, *10*, 6682-6692.

[188] Yum J.H.; Holcombe T.W.; Kim Y.; Rakstys K.; Moehl T.; Teuscher J.; Delcamp J.H.; Nazeeruddin M.K.; Grätzel M. Blue-coloured highly efficient dye-sensitized solar cells by implementing the diketopyrrolopyrrole chromophore. *Sci. Rep.* **2013**, *3*, 2446.

[189] Seo K.D.; You B.S.; Choi I.T.; Ju M.J.; You M.; Kang H.S.; Kim H.K. Dual-channel anchorable organic dyes with well-defined structures for highly efficient dye-sensitized solar cells. *J. Mater. Chem. A* **2013**, *1*, 9947-9953.

[190] Nguyen W.H.; Bailie C.D.; Burschka J.; Moehl T.; Grätzel M.; McGehee M.D.; Sellinger A. Molecular engineering of organic dyes for improved recombination lifetime in solid-state dye-sensitized solar cells. *Chem. Mater.* **2013**, *25*, 1519-1525.

[191] Wielopolski M.; Kim J.H.; Jung Y.S.; Yu Y.J.; Kay K.Y.; Holcombe T.W.; Zakeeruddin S.M.; Grätzel M.; Moser J.E. Position-dependent extension of π-conjugation in D-π-A dye sensitizers and the impact on the charge-transfer properties. *J. Phys. Chem. C* **2013**, *117*, 13805-13815.

[192] Zhu W.H.; Wu Y.Z.; Wang S.T.; Li W.Q.; Li X.; Chen J.; Wang Z. S.; Tian H. Organic D-A-π-A solar cell sensitizers with improved stability and spectral response. *Adv. Funct. Mater.* **2011**, *21*, 756-763.

[193] Wu Y.; Zhu W.H.; Zakeeruddin S.M.; Grätzel M. Insight into D-A-π-A structured sensitizers: a promising route to highly efficient and stable dye-sensitized solar cells. *ACS Appl. Mater. Interfaces* **2015**, *7*, 9307-9318.

[194] Wu Y.; Marszalek M.; Zakeeruddin S.M.; Zhang Q.; Tian H.; Grätzel M.; Zhu W. High-conversion-efficiency organic dye-sensitized solar cells: Molecular engineering on D-A-π-A featured organic indoline dyes. *Energy Environ. Sci.* **2012**, *5*, 8261-8272.

[195] Zhu H.; Li W.; Wu Y.; Liu B.; Zhu S.; Li X.; Ågren H.; Zhu W. Insight into benzothiadiazole acceptor in D-A- π-A configuration on photovoltaic performances of dye-sensitized solar cells. *ACS Sustainable Chem. Eng.* **2014**, *2*, 1026-1034.

[196] Mao J.; Guo F.; Ying W.; Wu W.; Li J.; Hua J. Benzotriazole-bridged sensitizers containing a furan moiety for dye-sensitized solar cells with high open-circuit voltage performance. *Chem. Asian J.* **2012**, *7*, 982-991.

[197] Yen Y.S.; Lee C.T.; Hsu C.Y.; Chou H.H.; Chen Y.C.; Lin J.T. Benzotriazole-containing D-π-A conjugated organic dyes for dye-sensitized solar cells. *Chem. Asian J.* **2013**, *8*, 809-816.

[198] Ni J.S.; Yen Y.C.; Lin J.T. Organic dyes with a fused segment comprising benzotriazole and thieno[3,2-*b*]pyrrole entities as the conjugated spacer for high performance dye-sensitized solar cells. *Chem. Commun.* **2015**, *51*, 17080-17083.

[199] Yang J.; Ganesan P.; Teuscher J.; Moehl T.; Kim Y.J.; Yi C.; Comte P.; Pei K.; Holcombe T.W.; Nazeeruddin M.K.; Hua J. Influence of the donor size in D-π-A organic dyes for dye-sensitized solar cells. *J. Am. Chem. Soc.* **2014**, *136*, 5722-5730.

[200] Li X.; Hu Y.; Sanchez-Molina I.; Zhou Y.; Yu F.; Haque S.A.; Wu W.; Hua J.; Tian H.; Robertson N. Insight into quinoxaline containing D-π-A dyes for dye-sensitized solar cells with cobalt and iodine based electrolytes: The effect of π-bridge on the HOMO energy level and photovoltaic performance. *J. Mater. Chem. A* **2015**, *3*, 21733-21743.

[201] Qu S.; Qin C.; Islam A.; Wu Y.; Zhu W.; Hua J.; Tian H.; Han L. A novel D-A-π-A organic sensitizer containing a diketopyrrolopyrrole unit with a branched alkyl chain for highly efficient and stable dye-sensitized solar cells. *Chem. Commun.* **2012**, *48*, 6972-6974.

[202] Li S.S.; Jiang K.J.; Zhang F.; Huang J.H.; Li S.G.; Chen M.G.; Yang L.M.; Song Y.L. New diketopyrrolopyrrole-based organic dyes for highly efficient dye-sensitized solar cells. *Org. Electron.* **2014**, *15*, 1579-1585.

[203] Li H.; Wu Y.; Geng Z.; Liu J.; Xu D.; Zhu W. Co-sensitization of benzoxadiazole based D-A-π-A featured sensitizers: compensating light-harvesting and retarding charge recombination. *J. Mater. Chem. A* **2014**, *2*, 14649-14657.

[204] Zhu H.; Wu Y.; Liu J.; Zhang W.; Wu W.; Zhu W.H. D-A-π-A featured sensitizers containing an auxiliary acceptor of benzoxadiazole: Molecular engineering and co-sensitization. *J. Mater. Chem. A* **2015**, *3*, 10603-10609.

[205] Patel D.G.D.; Feng F.; Ohnishi Y.; Abboud K.A.; Hirata S.; Schanze K.S.; Reynolds J.R. It takes more than an imine: The role of the central atom on the electron-accepting ability of benzotriazole and benzothiadiazole oligomers. *J. Am. Chem. Soc.* **2012**, *134*, 2599-2612.

[206] Blouin N.; Michaud A.; Gendron D.; Wakim S.; Blair E.; Neagu-Plesu R.; Belletete M.; Durocher G.; Tao Y.; Leclerc M. Toward a rational design of poly(2,7-carbazole) derivatives for solar cells. *J. Am. Chem. Soc.* **2007**, *130*, 732-742.

[207] Qu S.Y.; Wu W.J.; Hua J.L.; Kong C.; Long Y.T.; Tian, H. New diketopyrrolopyrrole (DPP) dyes for efficient dye-sensitized solar cells. *J. Phys. Chem. C* **2010**, *114*, 1343-1349.

[208] Holcombe T.W.; Yum J.; Yoon J.; Gao P.; Marszalek M.; Censo D.D.; Rakstys K.; Nazeeruddin M.K.; Grätzel M. A structural study of DPP-based sensitizers for DSC applications. *Chem. Commun.* **2012**, *48*, 10724-10726.

[209] Yum J.; Holcombe T. W.; Kim Y.; Yoon J.; Rakstys K.; Nazeeruddin M.K.; Grätzel, M. Towards high-performance DPP based sensitizers for DSC applications. *Chem. Commun.* **2012**, *48*, 10727-10729.

[210] Wang C.; Wang J.; Bai F.; Chen J.; Zhang H. Molecular design of organic dyes with diketopyrrolopyrrole for dye-sensitized solar cell: A theoretical approach. *Int. J. Quantum Chem.* **2014**, *114*, 560-567.

[211] Zhang F.; Jiang K.; Huang J.; Yu C.; Li S.; Chen M.; Yang L.; Song Y. A novel compact DPP dye with enhanced light harvesting and charge transfer properties for highly efficient DSCs. *J. Mater. Chem. A* **2013**, *1*, 4858-4863.

[212] Haid S.; Marszalek M.; Mishra A.; Wielopolski M.; Teuscher J.; Moser J.; Humphry-Baker R.; Zakeeruddin S. M.; Grätzel M.; Bäuerle P. Significant improvement of dye-sensitized solar cell performance by small structural modification in π-conjugated donor-acceptor dyes. *Adv. Funct. Mater.* **2012**, *22*, 1291-1302.

[213] Yella A.; Mai C.; Zakeeruddin S.M.; Chang S.; Hsieh C.; Yeh C.; Grätzel M. Molecular engineering of push-pull porphyrin dyes for highly efficient dye-sensitized solar cells: The role of benzene spacers. *Angew. Chem., In. Ed.* **2014**, *53*, 2973-2977.

[214] Joly D.; Pellejá L.; Narbey S.; Oswald F.; Chiron J.; Clifford J.N.; Palomares E.; Demadrille R. A robust organic dye for dye sensitized solar cells based on

iodine/iodide electrolytes combining high efficiency and outstanding stability. *Sci. Rep.* **2014**, *4*, 4033.

[215] Wu Y.; Zhu W.H.; Zakeeruddin S.M.; Grätzel M. Insight into D-A-π-A structured sensitizers: A promising route to highly efficient and stable dye-sensitized solar cells. *ACS Appl. Mater. Interfaces* **2015**, *7*, 9307-9318.

[216] Fan S.Q.; Geng Y.; Kim C.; Paik S.; Ko J. Correlating the photovoltaic performance of alumina modified dye-sensitized solar cells with the properties of metal-free organic sensitizers. *Mater. Chem. Phys.* **2012**, *132*, 943-949.

[217] Kanaparthi R.K.; Kandhadi J.; Giribabu L. Metal-free organic dyes for dye-sensitized solar cells: recent advances. *Tetrehadron* **2012**, 68, 8383-8393.

[218] Abbotto A.; Manfred N.; Marinzi C.; De Angelis F.; Mosconi E.; Yum J.H.; Xianxi Z.; Nazeeruddin M.K.; Grätzel M. Di-branched di-anchoring organic dyes for dye-sensitized solar cells. *Energy Environ Sci*. **2009**, *2*, 1094-1101.

[219] Chen Y.C.; Lin J.T. Multi-anchored sensitizers for dye-sensitized solar cells. *Sustainable Energy Fuels* **2017**, *1*, 969-985.

[220] Bodedla G.B.; Thomas K.R.J; Fan M.S.; Ho K.C. Di-anchoring organic dyes containing benzimidazole branch for dye-sensitized solar cells: Effect of π-spacer and peripheral donor on functional properties. *Chem. Asian J.* **2016**, *11*, 2564-2577.

[221] Siu C.H.; Lee L.T.L; Ho P.Y.; Majumdar P.; Ho C.L.; Chen T.; Zhao J.; Li H.; Wong W.Y. Fluorene-bridged organic dyes with di-anchoring groups for efficient co-adsorbent-free dye sensitized solar cells. *J. Mater. Chem. C* **2014**, *2*, 7086-7095.

[222] Shang H.; Li Q.; Jiang K.; Zhan X. Organic dyes based on triphenylamine for dye-sensitized solar cells. *J. Energy. Chem.* **2016**, *25*, 615-620.

[223] Chen Y.F.; Liu J.M.; Huang J.F.; Tan L.L.; Shen Y.; Xiao L.M. Kuang D.B.; Su C.Y. Stable organic dyes based on the benzo[1,2-*b*:4,5-*b*']-dithiophene donor for efficient dye- sensitized solar cells. *J. Mater. Chem. A* **2015**, *3*, 8083-8090.

[224] Dai X.X.; Feng H.L.; Huang Z.S.; Wang M.J.; Wang L.; Kuang D.B.; Meier H.; Cao D. Synthesis of phenothiazine-based di-anchoring dyes containing fluorene linker and their photovoltaic performance. *Dyes Pigm.* **2015**, *114*, 47-54.

[225] Mao M.; Zhang X.L.; Fang X.Q.; Wu G.H.; Dai S.Y.; Song Q.H.; Zhang X.X. Highly efficient light-harvesting boradiazaindacene sensitizers for dye-sensitized solar cells featuring phenothiazine donor antenna. *J. Power Sources* **2014**, *268*, 965-976.

[226] Jiang S.; Fan S.; Lu X.; Zhou G.; Wang Z.S. Double D-π-A branched organic dye isomers for dye-sensitized solar cells. *J. Mater. Chem. A* **2014**, *2*, 17153-17164.

[227] Huang Z.S.; Cai C.; Zang X.F.; Iqbal Z.; Zeng H.; Kuang D.B.; Wang L.; Meier H.; Cao D. Effect of the linkage location in double branched organic dyes on the photovoltaic performance of DSSCs. *J. Mater. Chem. A* **2015**, *3*, 1333-1344.

[228] Zhang F.; Fan J.; Yu H.; Ke Z.; Nie C.; Kuang D.; Shao G.; Su C. Nonplanar organic sensitizers featuring a tetraphenylethene structure and double electron-withdrawing anchoring groups. *J. Org. Chem.* **2015**, *80*, 9034-9040.

[229] Bodedla G.B.; Thomas K.R.J.; Fan M.S.; Ho K.C. Di-anchoring organic dyes containing benzimidazole branch for dye-sensitized solar cells: Effect of π-spacer and peripheral donor on functional properties. *Chem Asian J* **2016**, *11*, 2564-2577.

[230] Ahn H.J.; Thogiti S.; Cho J.M.; Jang B.Y.; Kim J.H. Comparison of triphenylamine based single and double branched organic dyes in dye-sensitized solar cells. *Electron. Mater. Lett.* **2015**, *11*, 822-827..

[231] Thomas K.R.J.; Kapoor N.; Lee C.P.; Ho K.C. Organic dyes containing pyrenylamine-based cascade donor systems with different aromatic π-linkers for dye-sensitized solar cells: Optical, electrochemical, and device characteristics. *Chem. Asian J.* **2012**, *7*, 738-750.

[232] Arrechea S.; Clifford J.N.; Pellejà L.; Aljarilla A.; de la Cruz P.; Palomares E.; Langa F. Charge recombination losses in thiophene-substituted porphyrin dyesensitized solar cells. *Dyes Pigm.* **2016**, *126*, 147-153.

[233] Li G.; Jiang K.J.; Bao P.; Li Y.F.; Li S.L.; Yang L.M. Molecular design of triarylamine-based organic dyes for efficient dye-sensitized solar cells. *New J. Chem.* **2009**, *33*, 868-876.

[234] Goncalves A.D. Davolos M.R.; Masaki N.; Yanagida S.; Mori S.; Nogueira A.F. Stepped light-induced transient measurements of photocurrent and voltage in dye-sensitized solar cells based on ZnO and ZnO:Ga. *J. Appl. Phys.* **2009**, *106*, 064316.

Supplementary Information

^{1}H & ^{13}C NMR for unpublished work

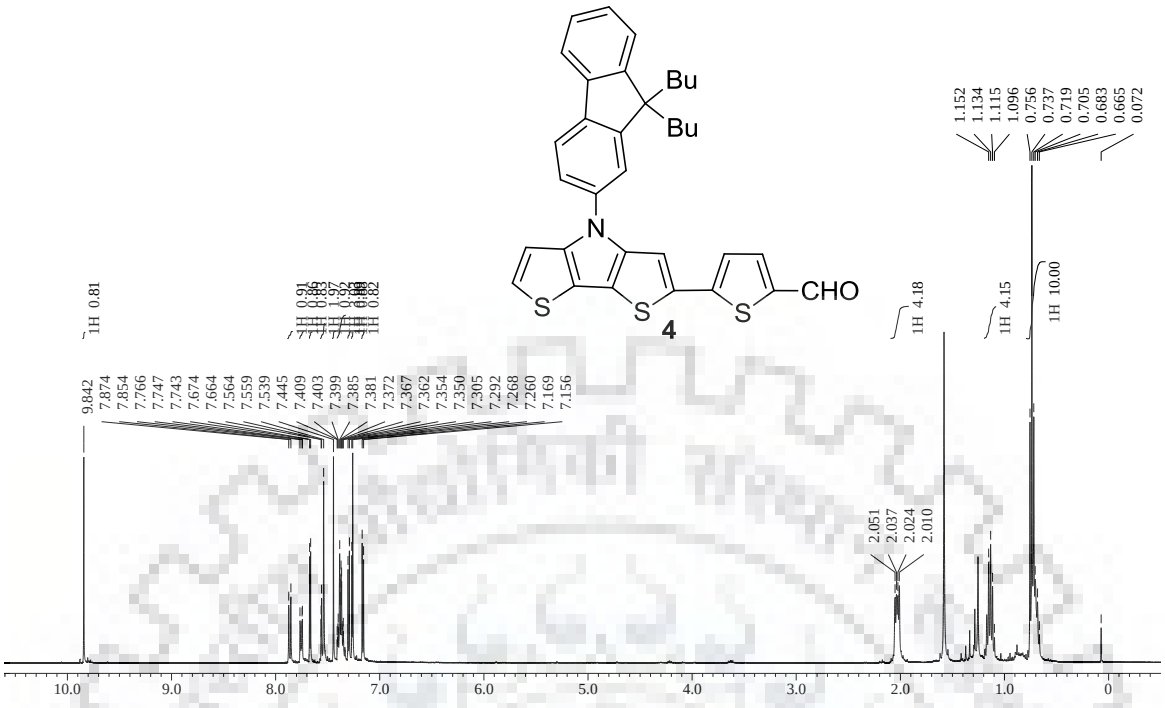

Figure S1 ^{1}H NMR spectra of **4** recorded in $CDCl_3$.

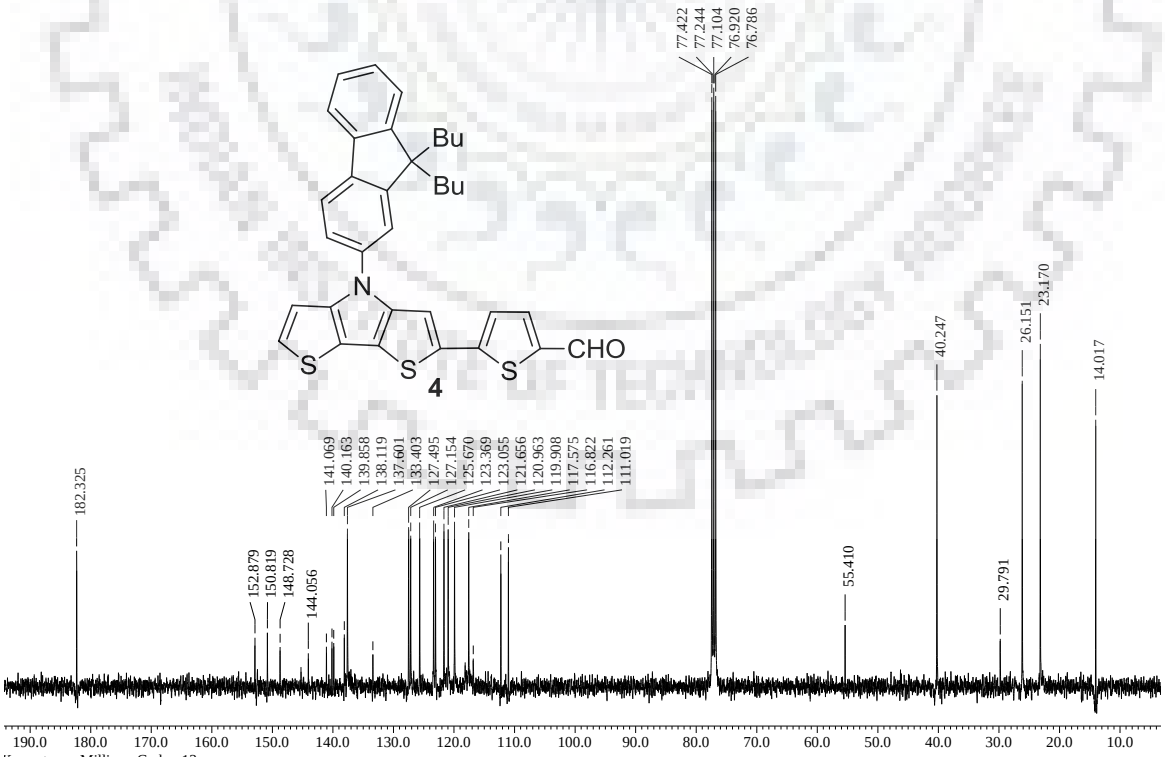

Figure S2 ^{13}C NMR spectra of **4** recorded in $CDCl_3$.

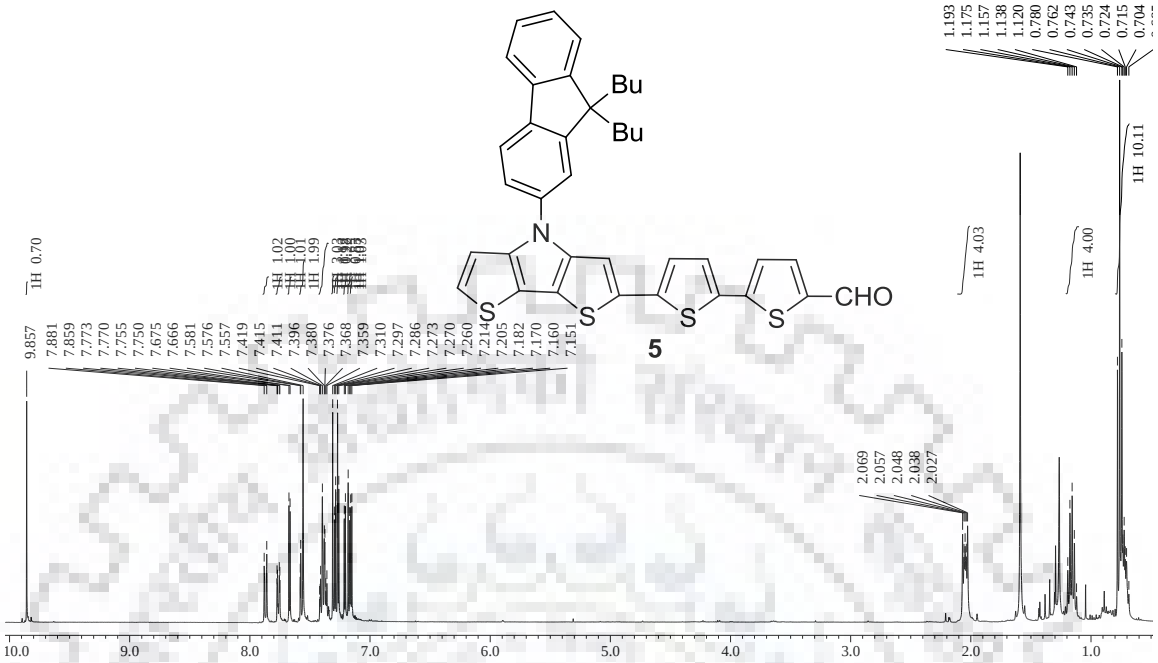

Figure S3 ^{1}H NMR spectra of **5** recorded in $CDCl_3$.

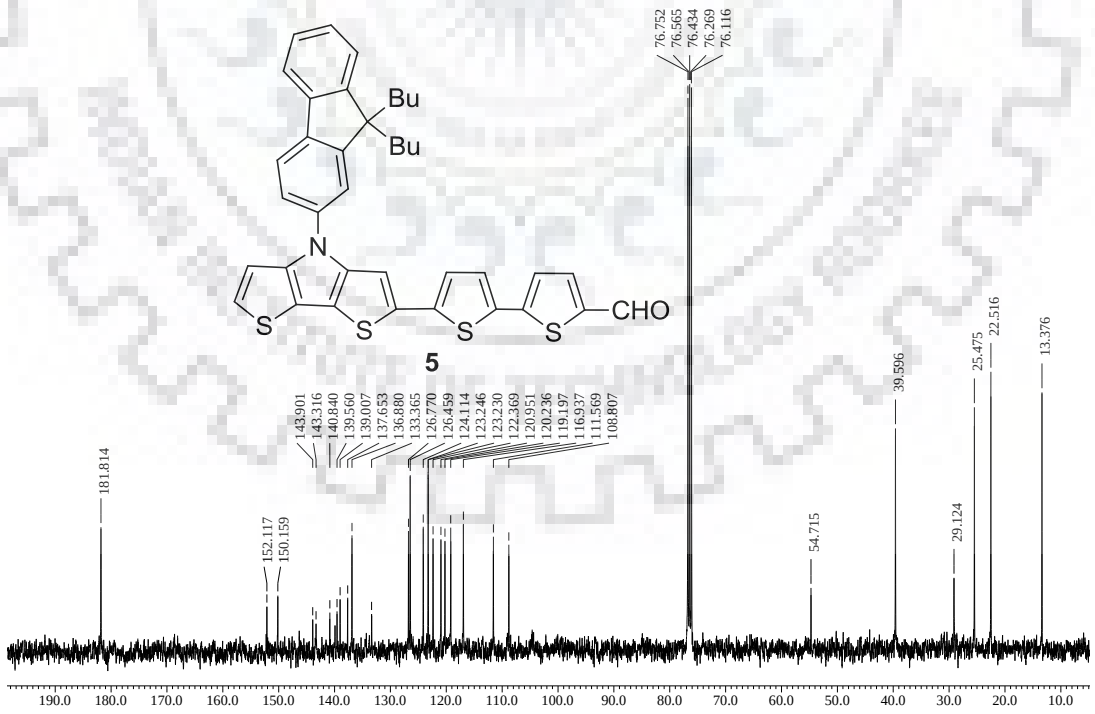

Figure S4 ^{13}C NMR spectra of **5** recorded in $CDCl_3$.

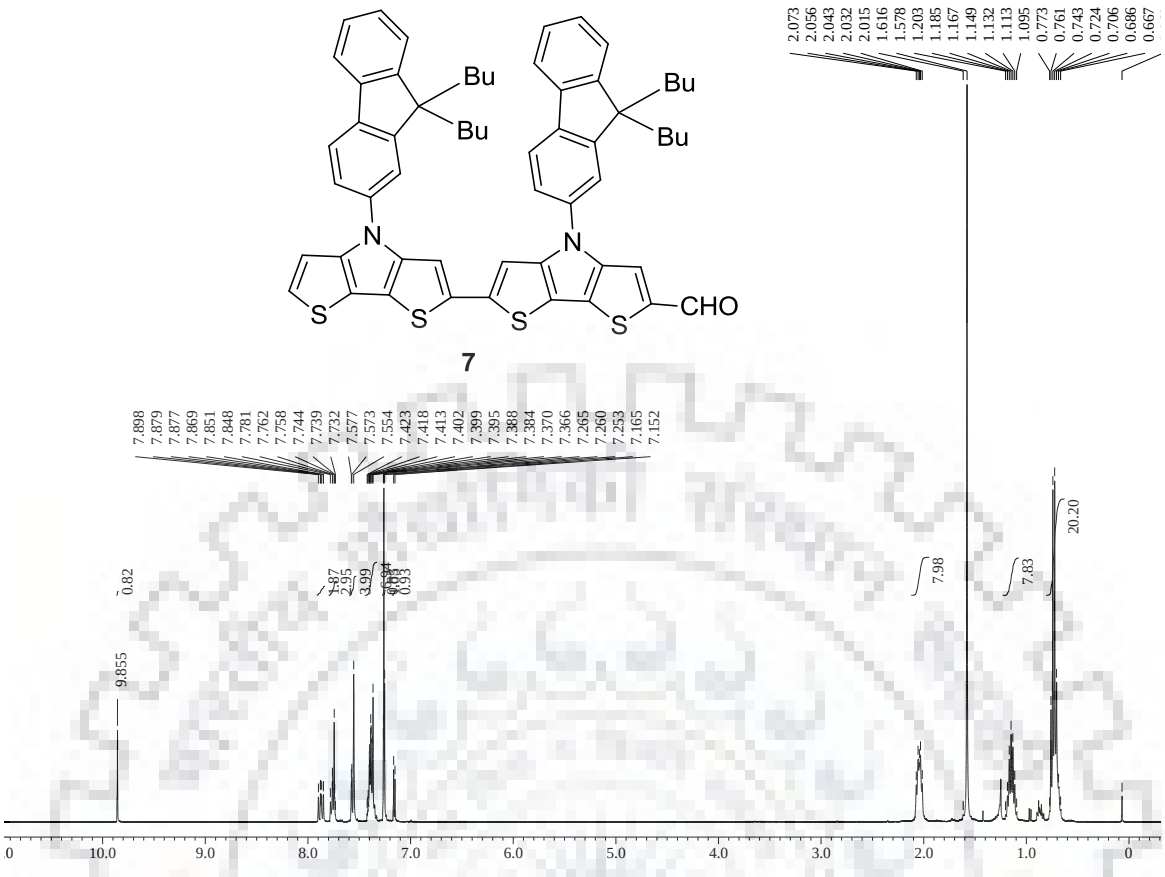

Figure S5 ^{1}H NMR spectra of **7** recorded in $CDCl_3$.

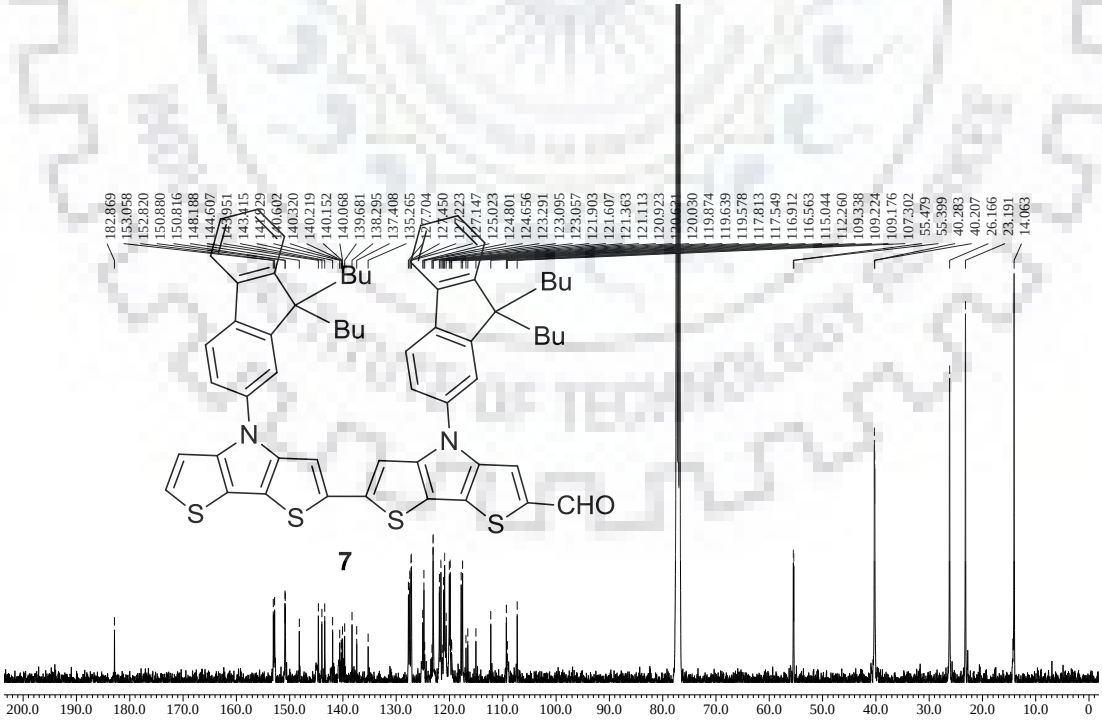

Figure S6 ^{13}C NMR spectra of **7** recorded in $CDCl_3$.

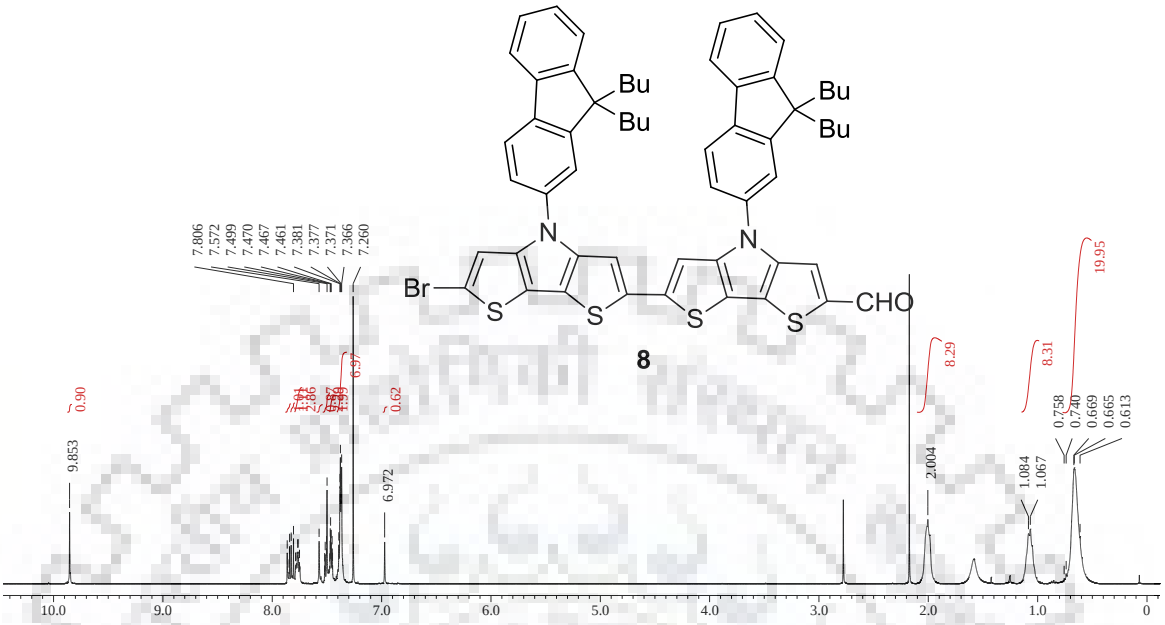

Figure S7 ^{1}H NMR spectra of **8** recorded in $CDCl_3$.

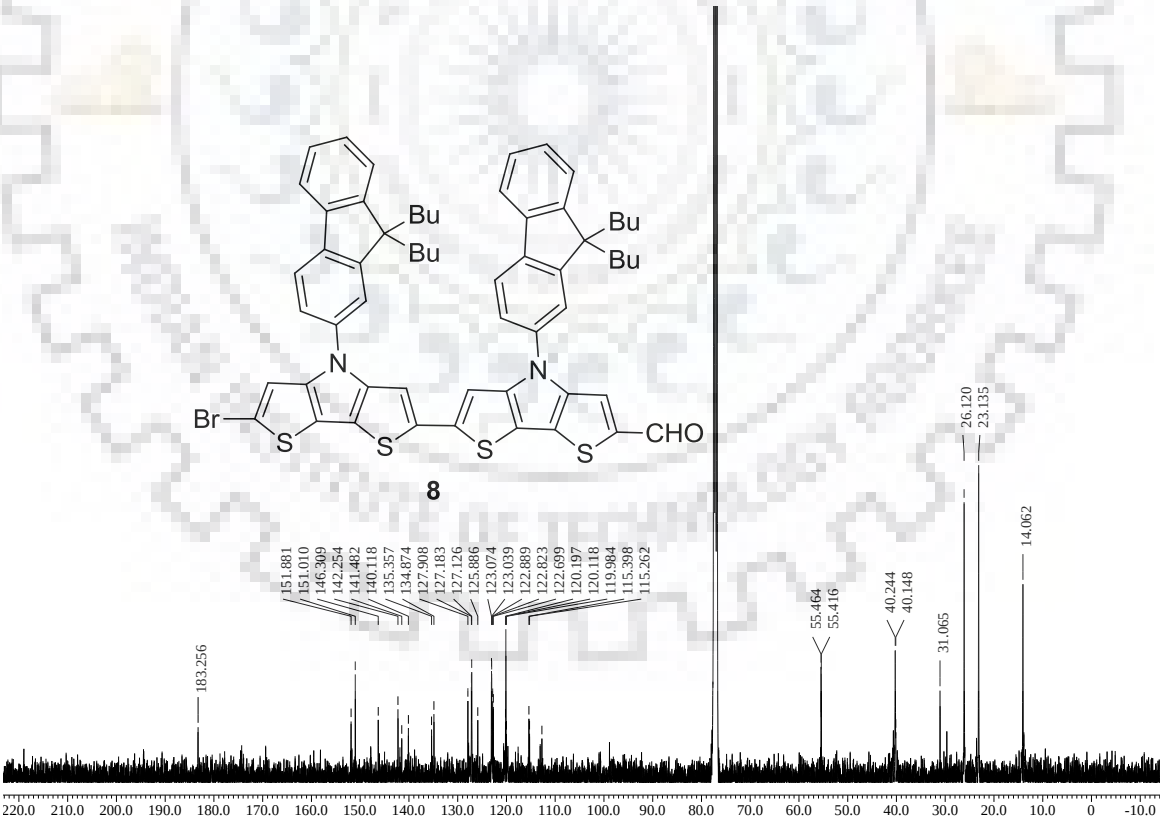

Figure S8 ^{13}C NMR spectra of **8** recorded in $CDCl_3$.

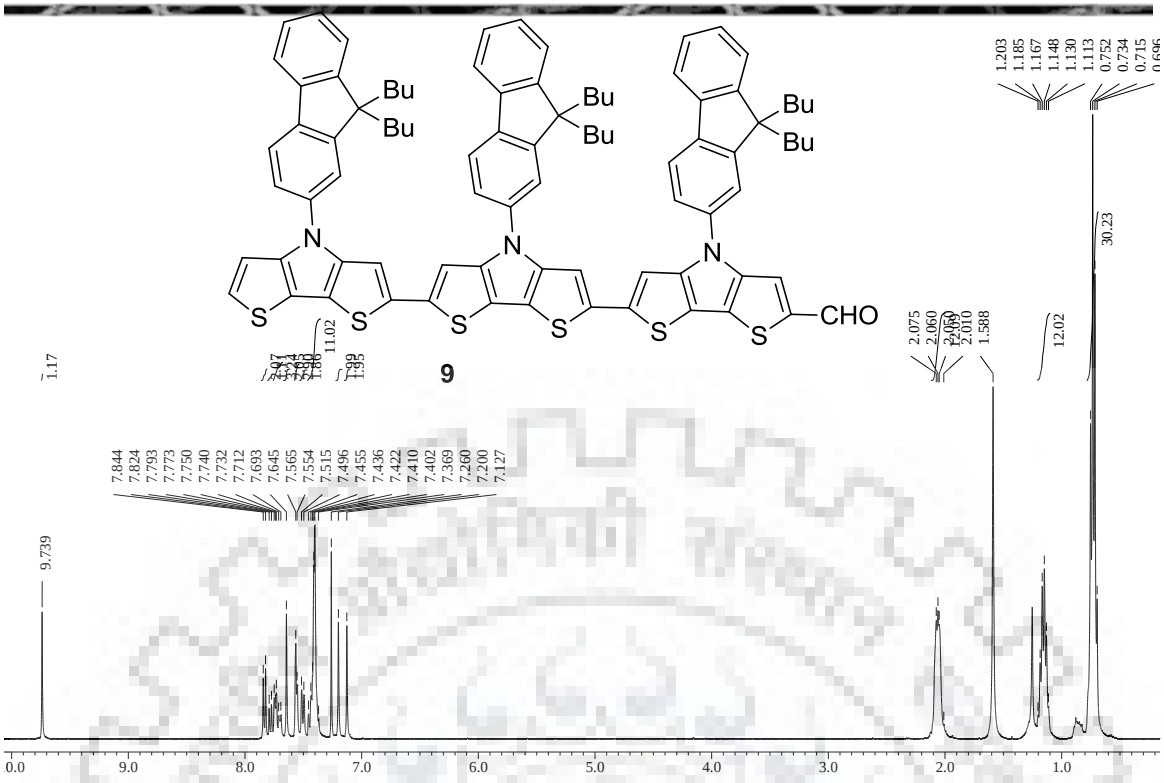

Figure S9 ^{1}H NMR spectra of **9** recorded in $CDCl_3$.

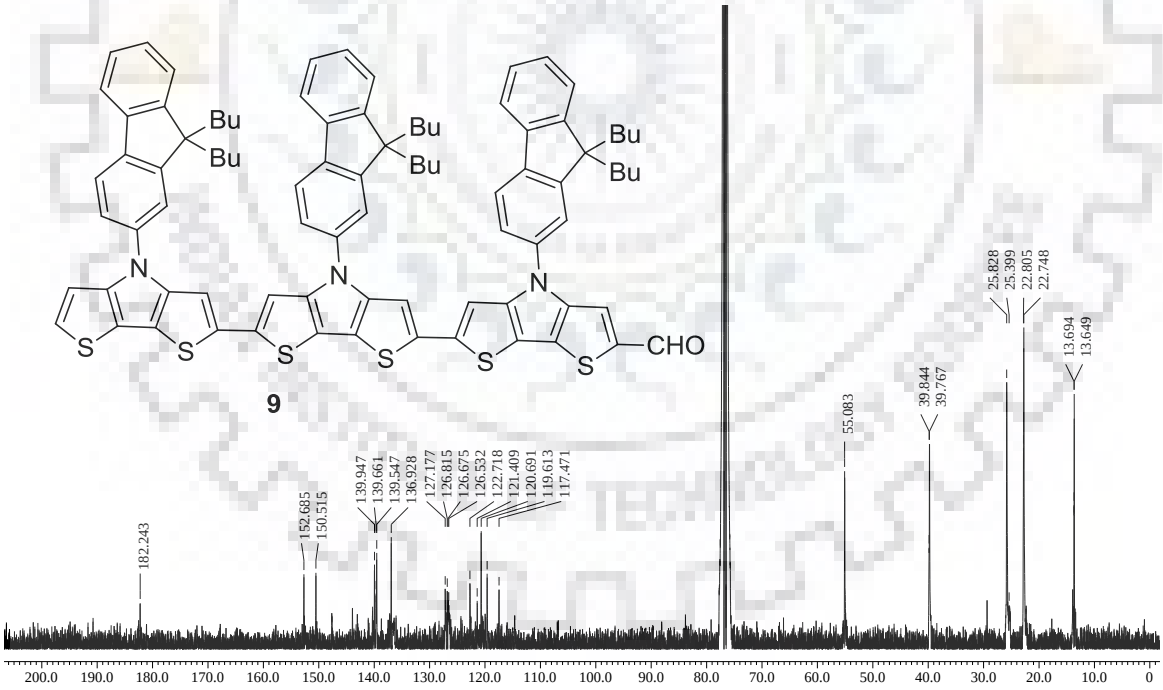

Figure S10 ^{13}C NMR spectra of **9** recorded in $CDCl_3$.

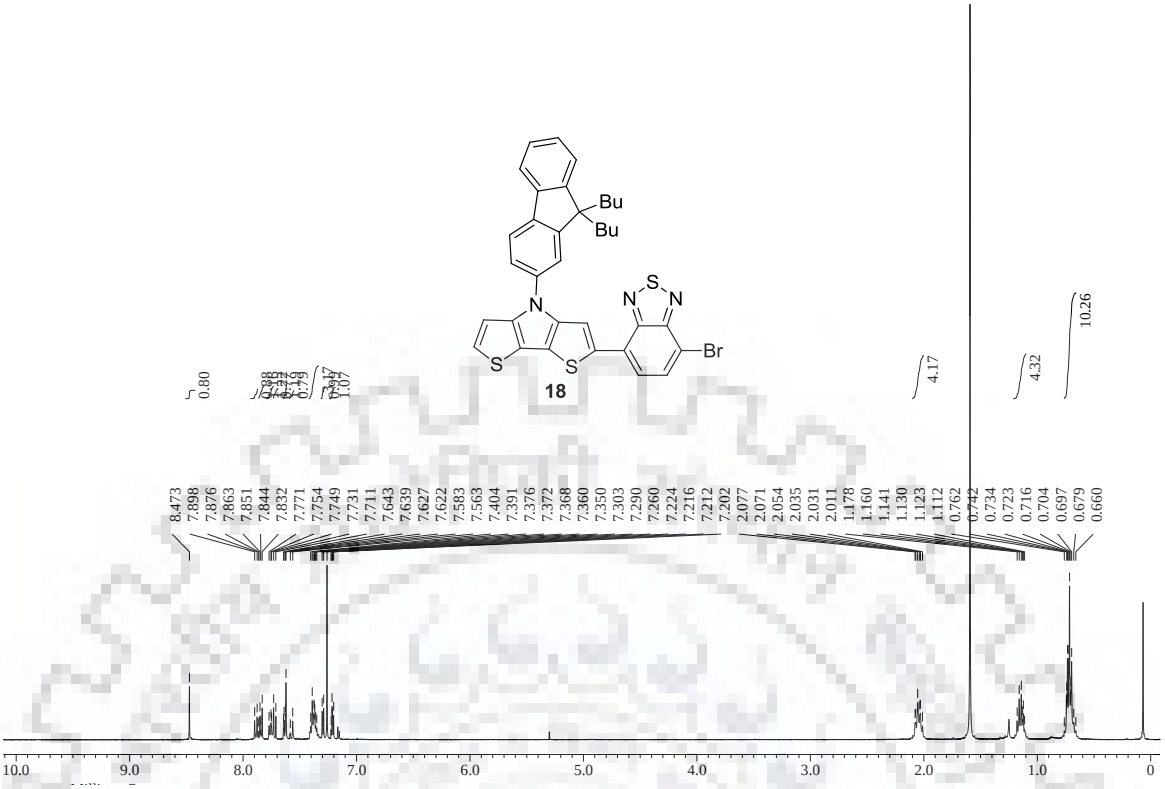

Figure S11 ^{1}H NMR spectra of **18** recorded in $CDCl_3$.

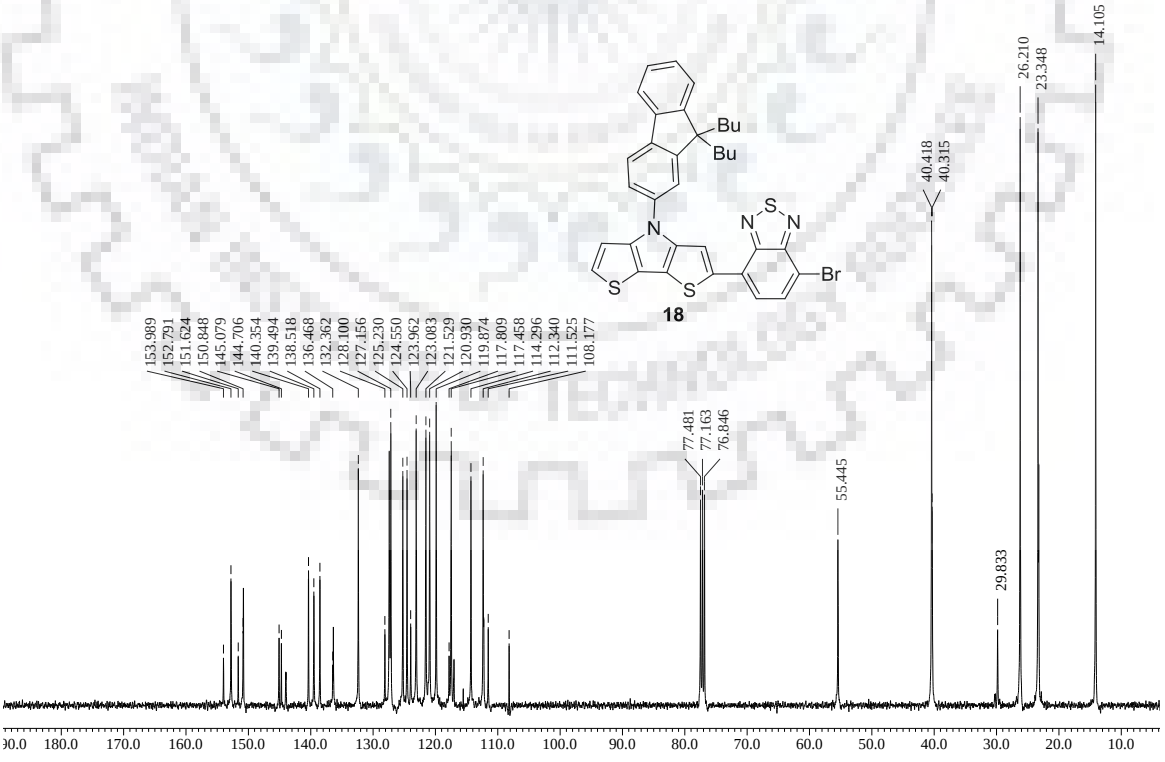

Figure S12 ^{13}C NMR spectra of **18** recorded in $CDCl_3$.

Figure S13 ^{1}H NMR spectra of **19** recorded in $CDCl_3$.

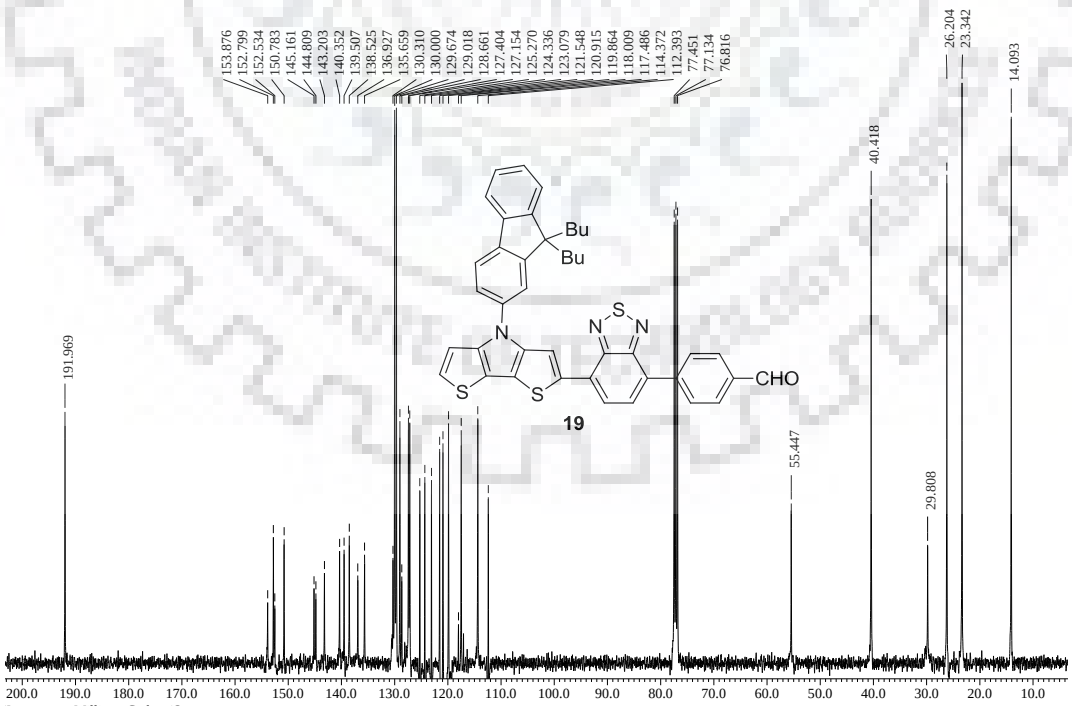

Figure S14 ^{13}C NMR spectra of **19** recorded in $CDCl_3$.

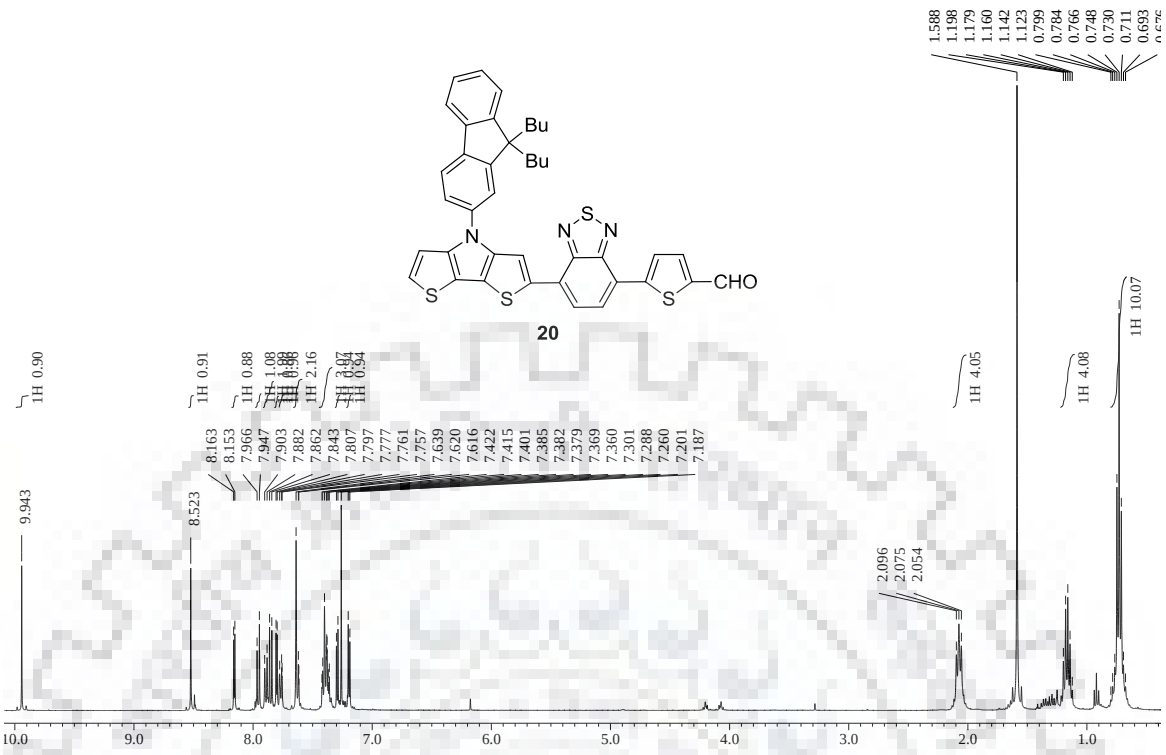

Figure S15 ^{1}H NMR spectra of **20** recorded in $CDCl_3$.

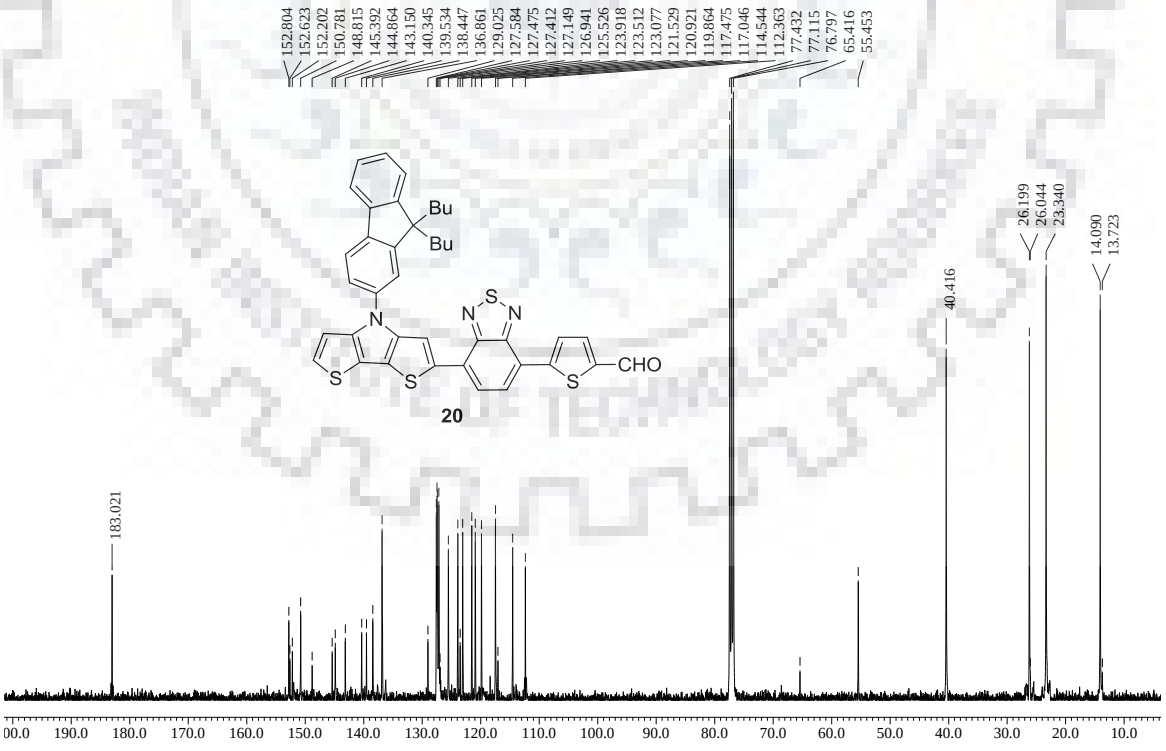

Figure S16 ^{13}C NMR spectra of **20** recorded in $CDCl_3$.

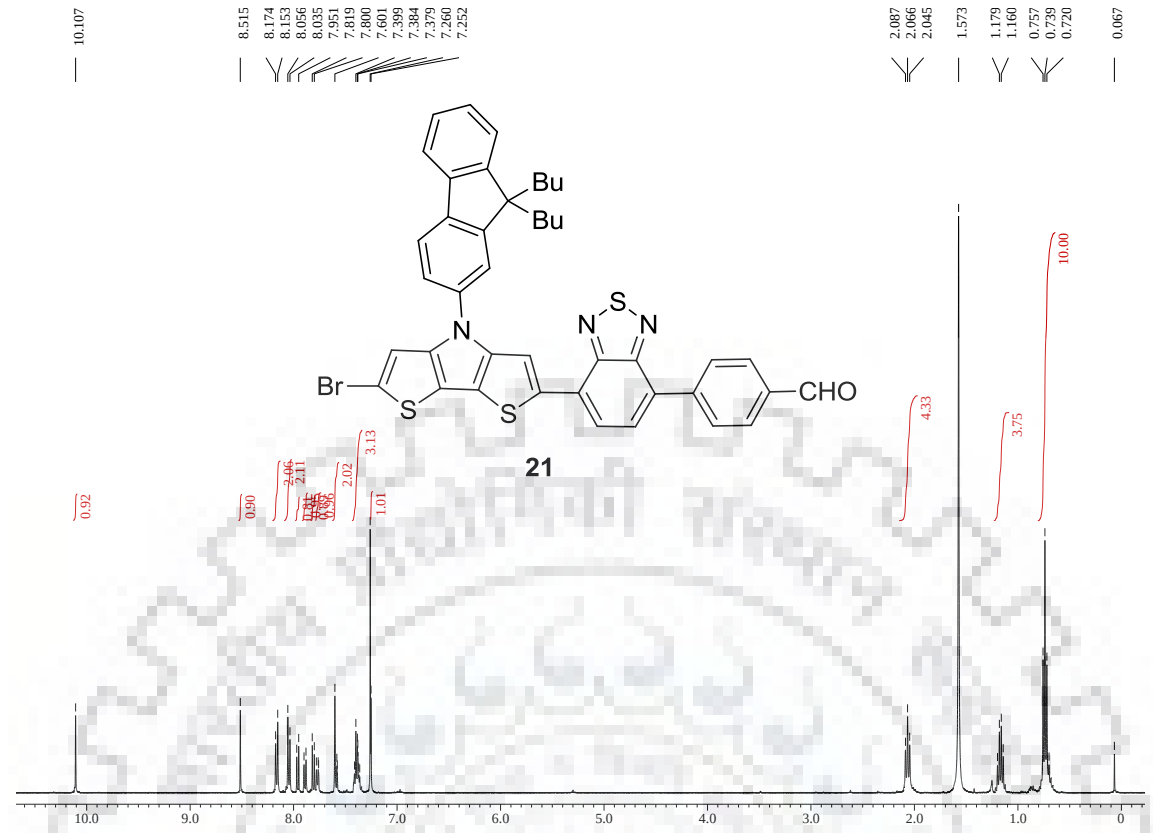

Figure S17 ^{1}H NMR spectra of **21** recorded in $CDCl_3$.

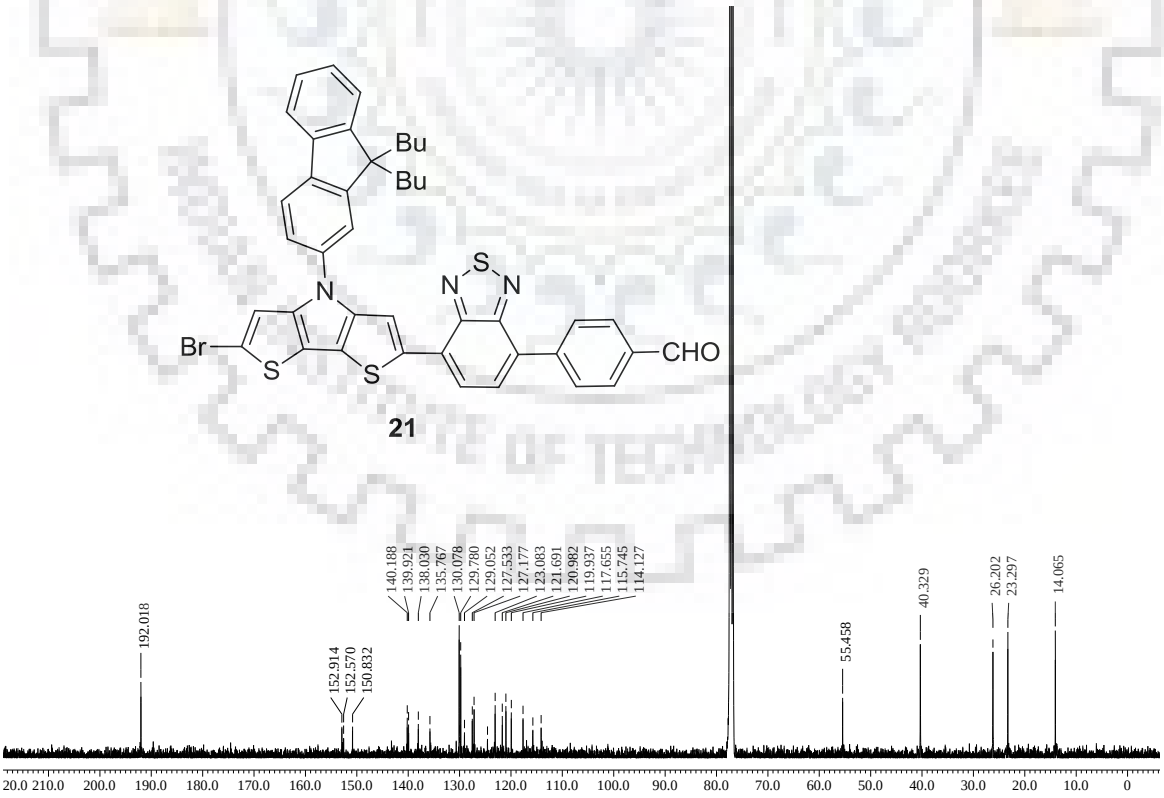

Figure S18 ^{13}C NMR spectra of **21** recorded in $CDCl_3$.

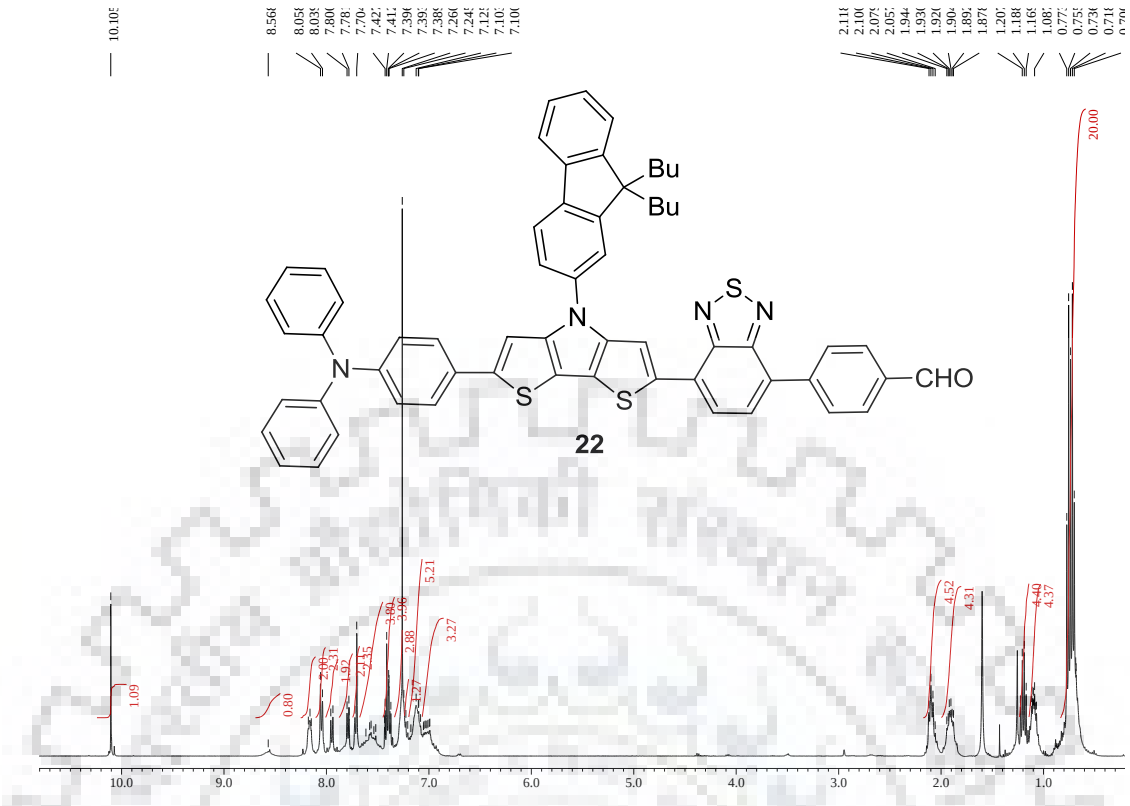

Figure S19 ^{1}H NMR spectra of **22** recorded in $CDCl_3$.

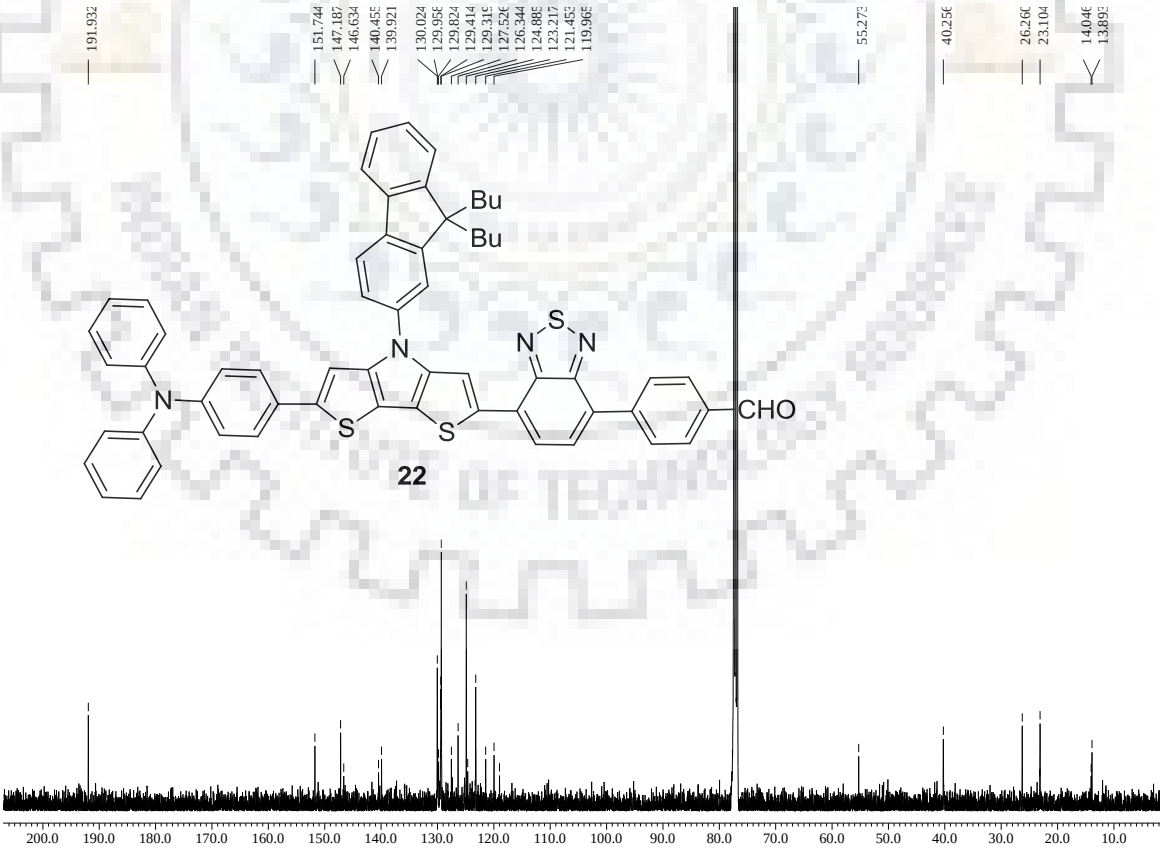

Figure S20 ^{13}C NMR spectra of **22** recorded in $CDCl_3$.

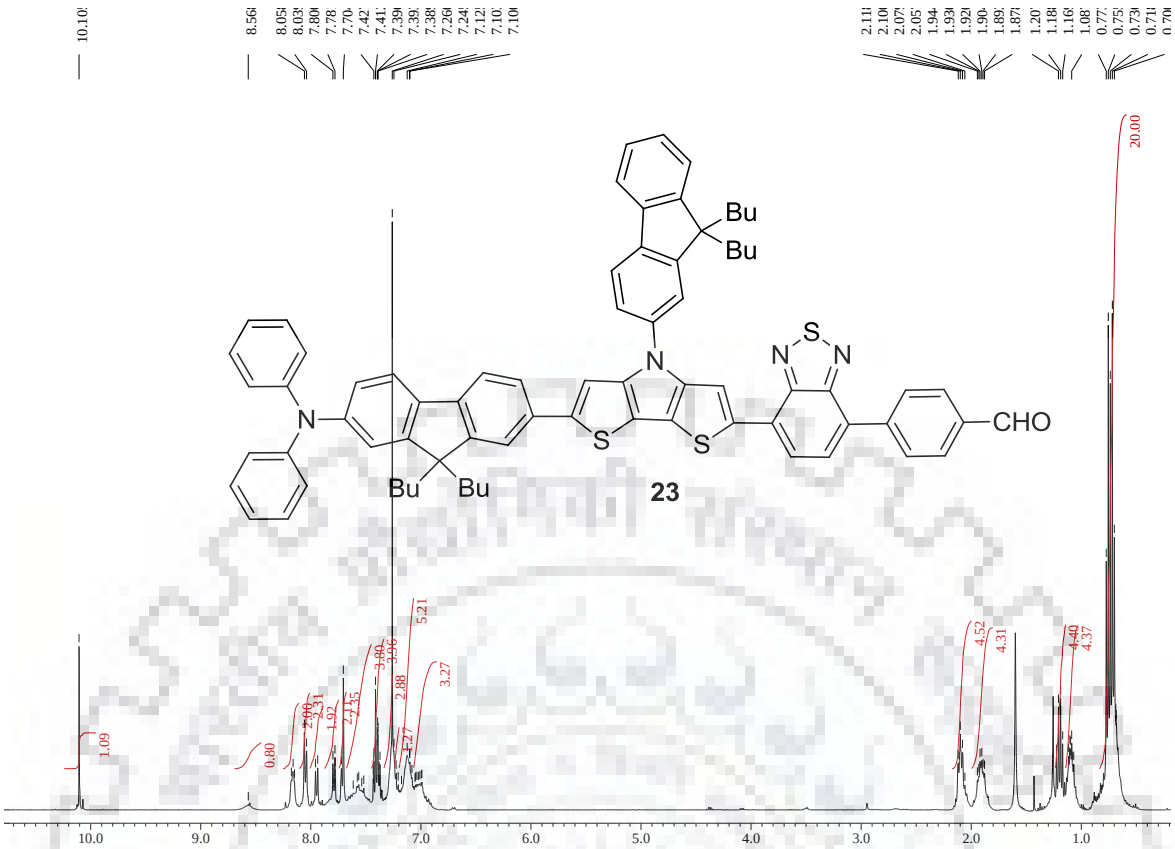

Figure S21 ^{1}H NMR spectra of **23** recorded in $CDCl_3$.

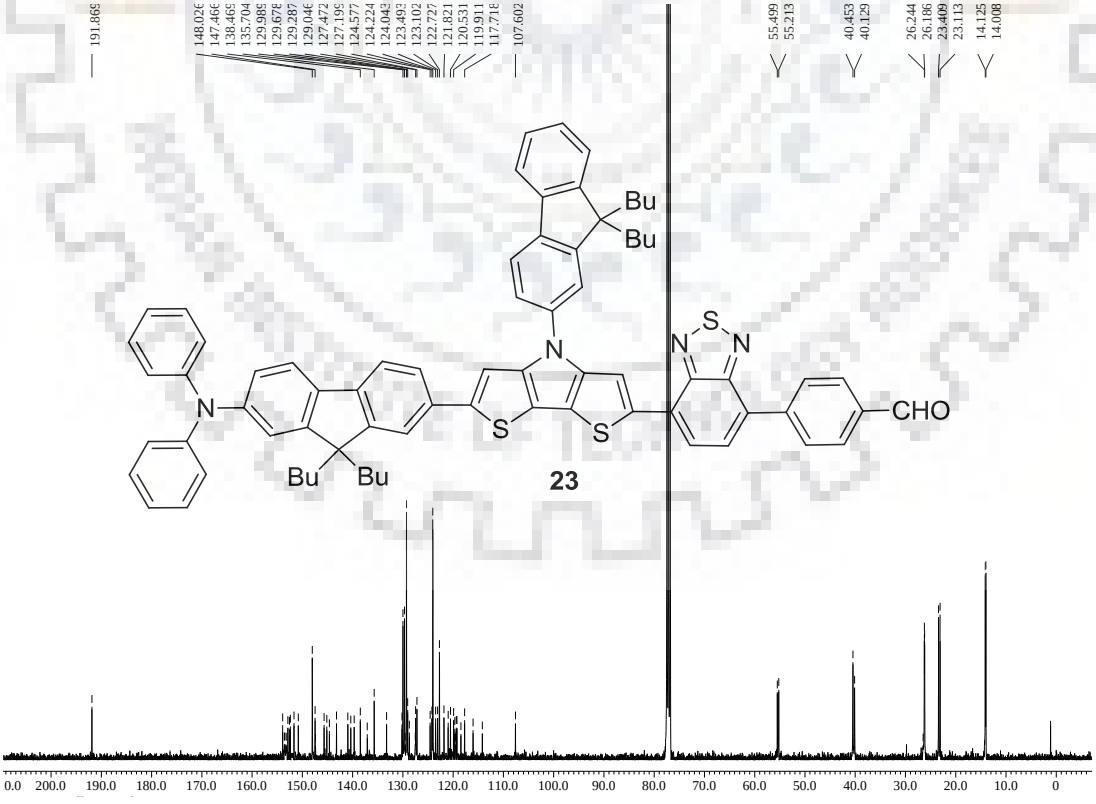

Figure S22 ^{13}C NMR spectra of **23** recorded in $CDCl_3$.

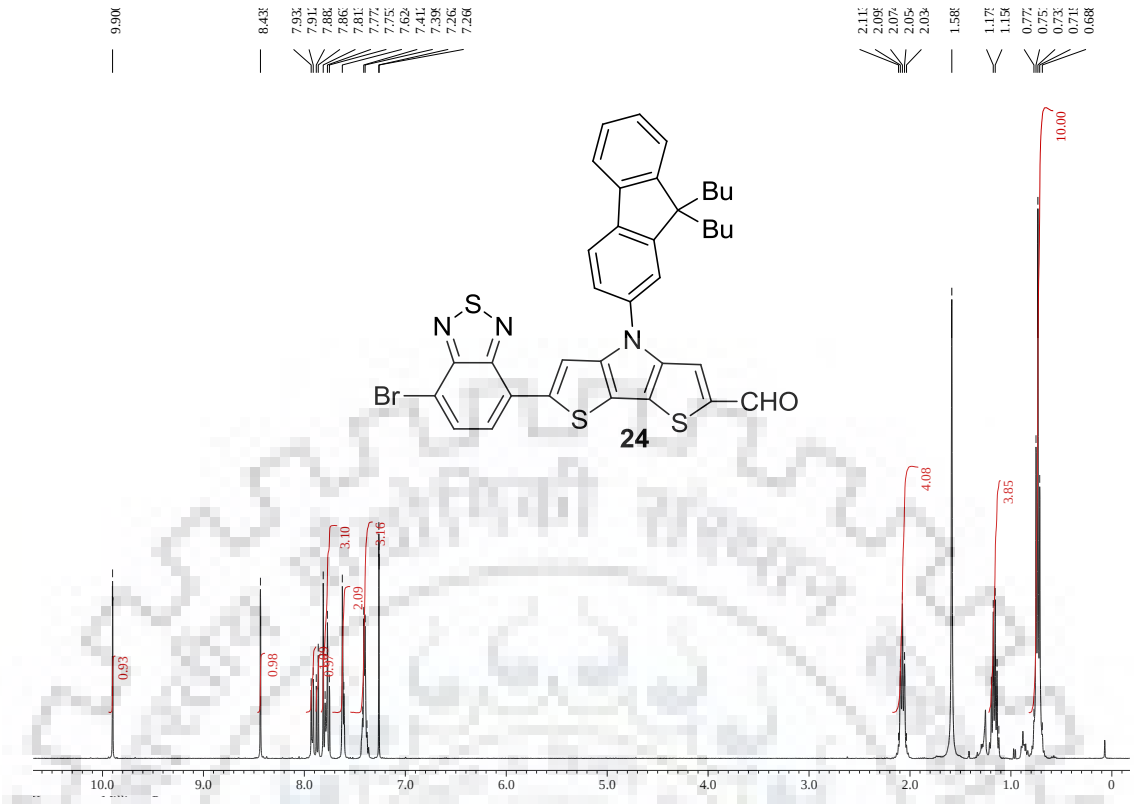

Figure S23 ^{1}H NMR spectra of **24** recorded in $CDCl_3$.

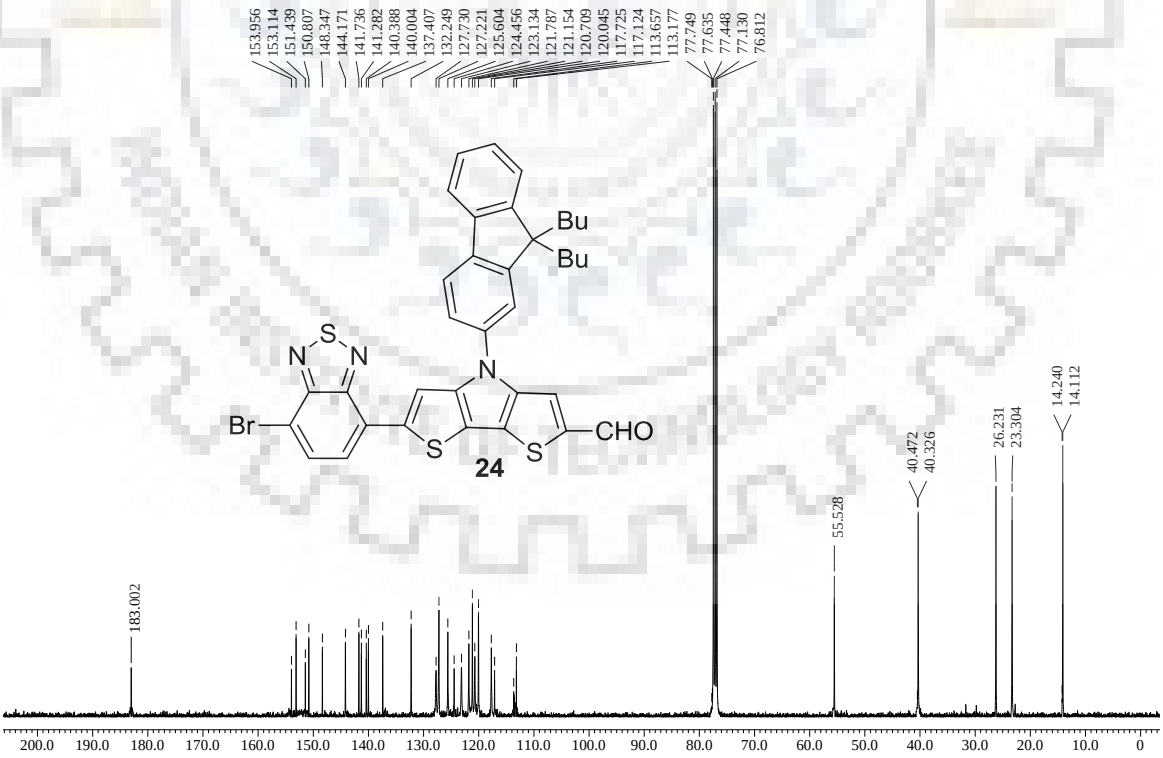

Figure S24 ^{13}C NMR spectra of **24** recorded in $CDCl_3$.

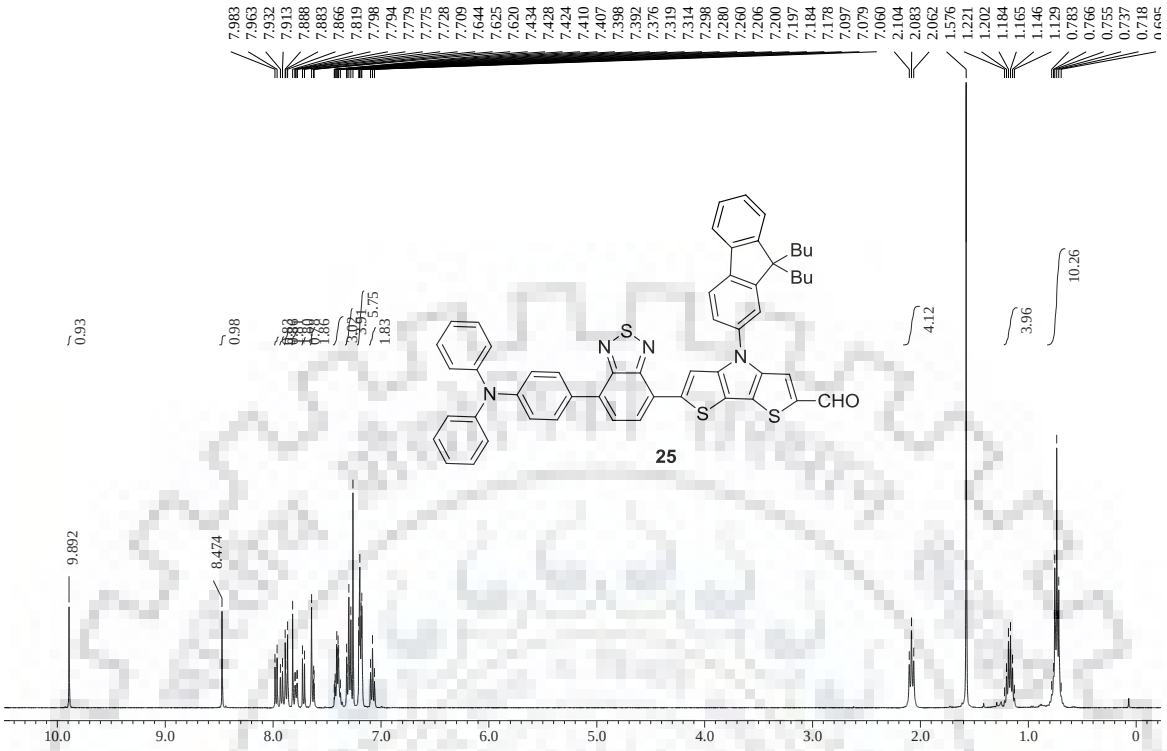

Figure S25 ^{1}H NMR spectra of **25** recorded in $CDCl_3$.

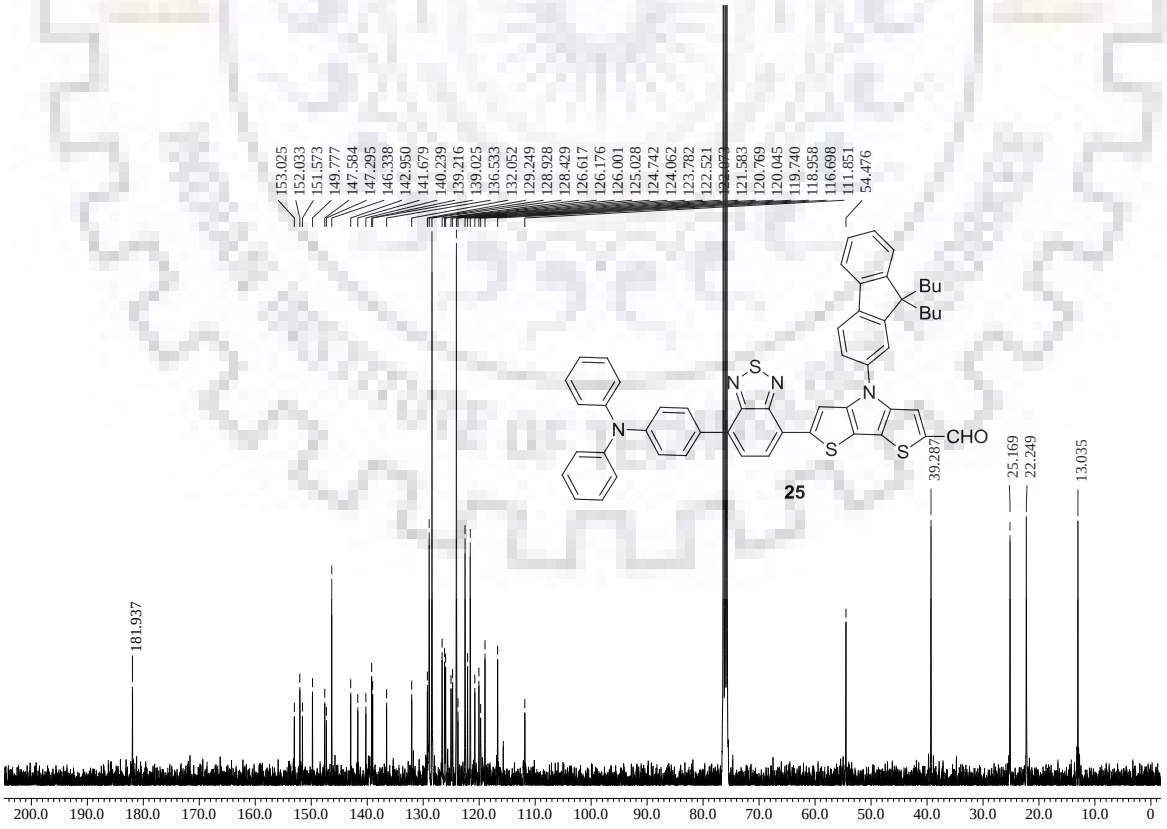

Figure S26 ^{13}C NMR spectra of **25** recorded in $CDCl_3$.

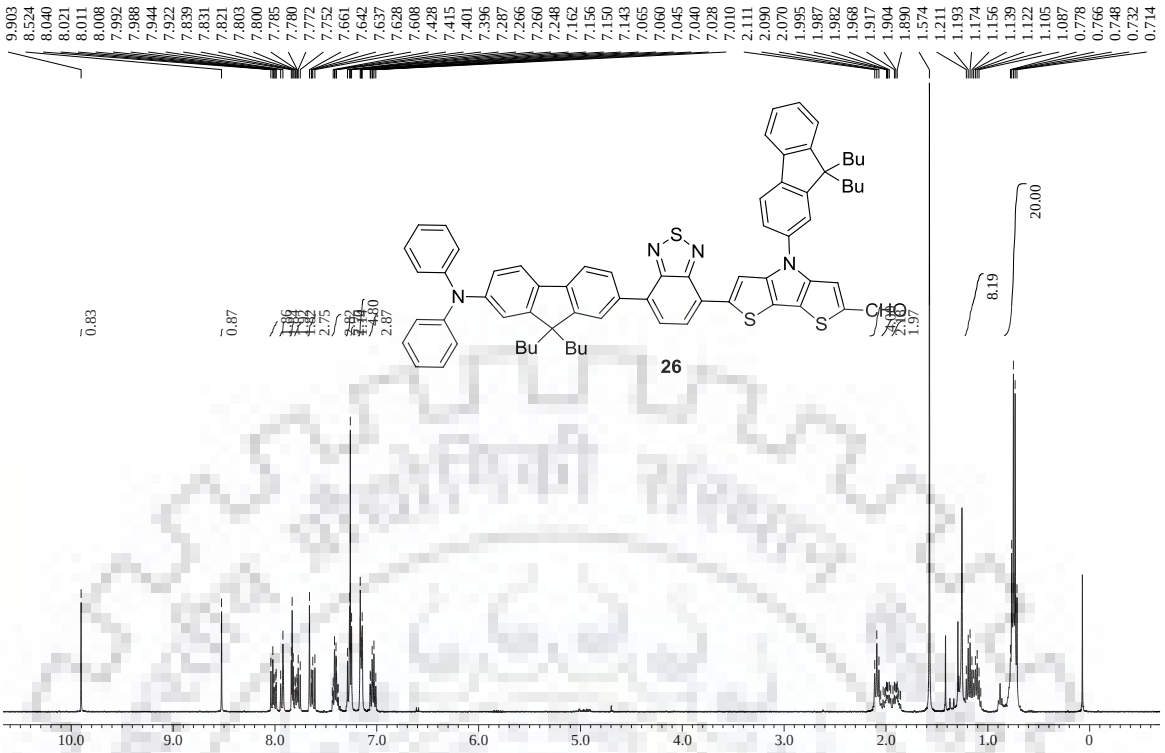

Figure S27 ^{1}H NMR spectra of **26** recorded in $CDCl_3$.

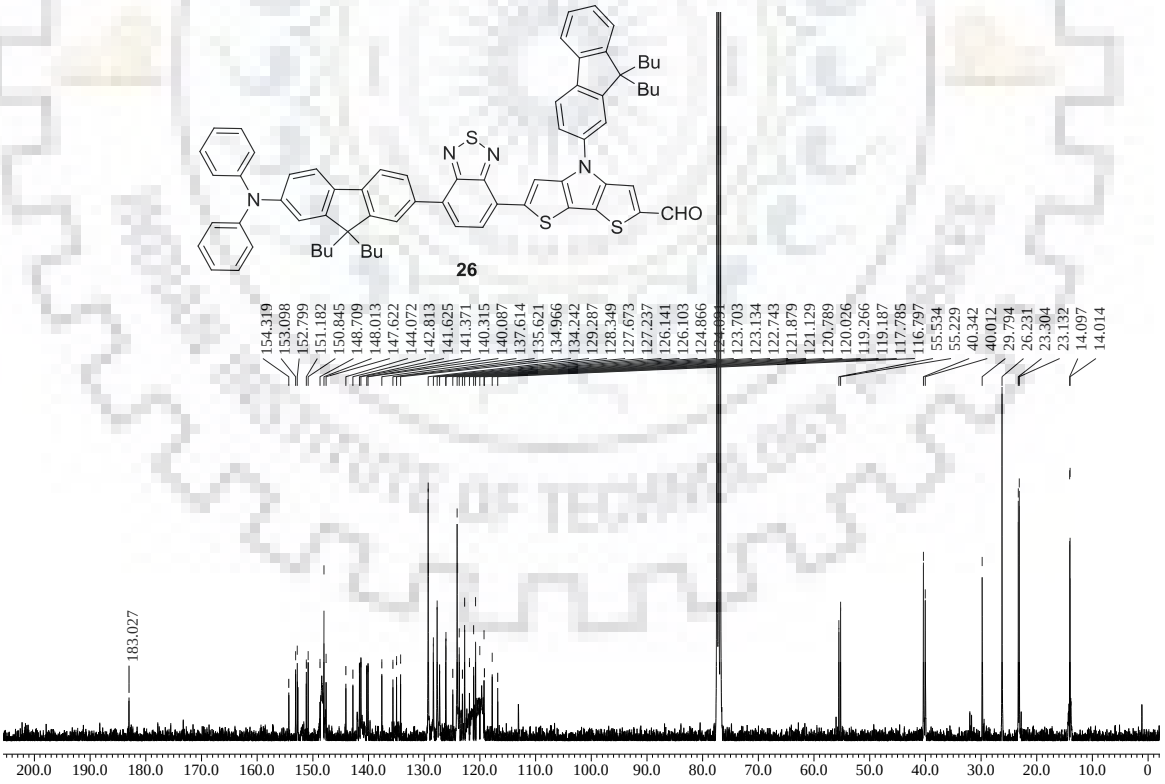

Figure S28 ^{13}C NMR spectra of **26** recorded in $CDCl_3$.

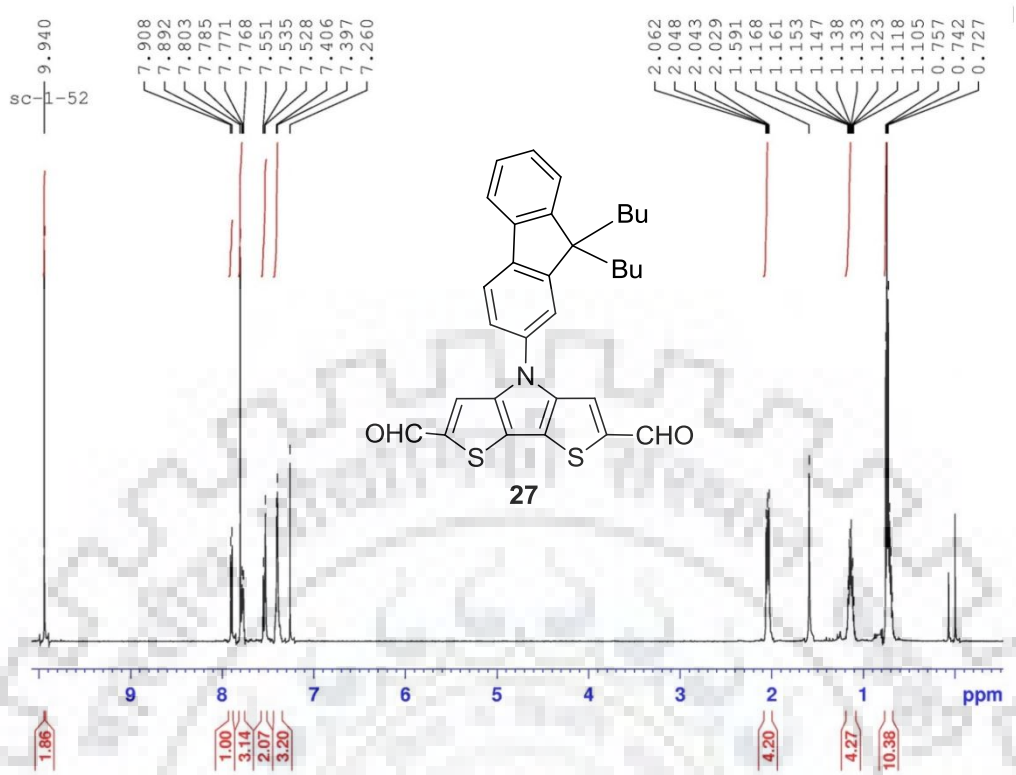

Figure S29 ^{1}H NMR spectra of **27** recorded in $CDCl_3$.

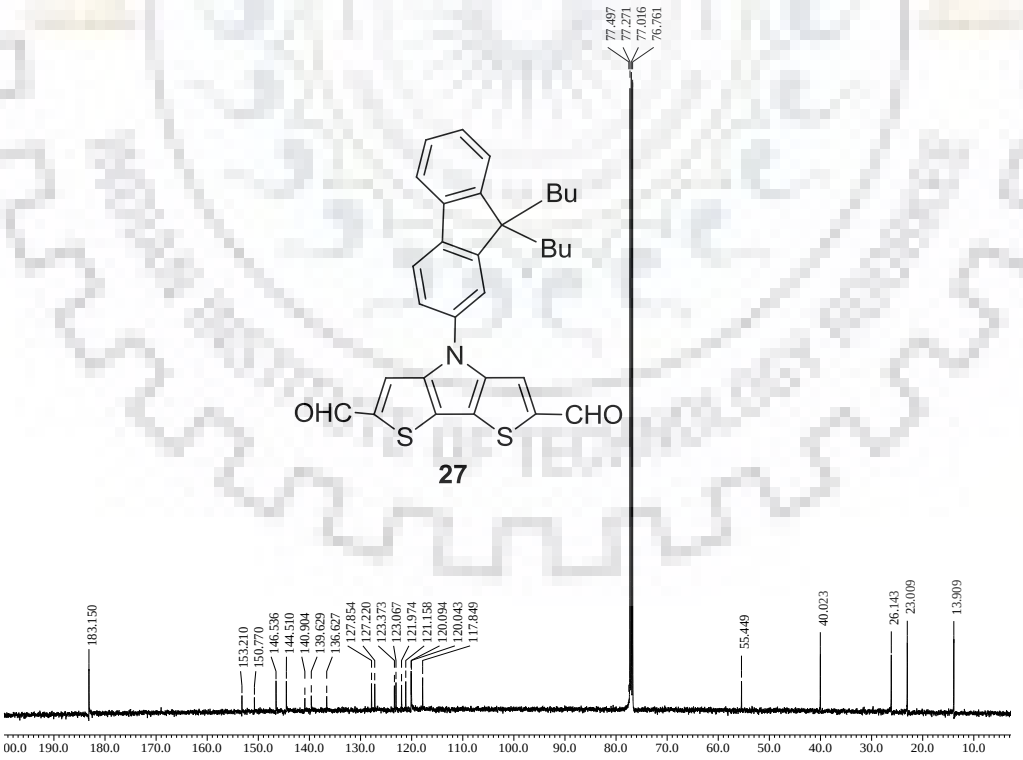

Figure S30 ^{13}C NMR spectra of **27** recorded in $CDCl_3$.

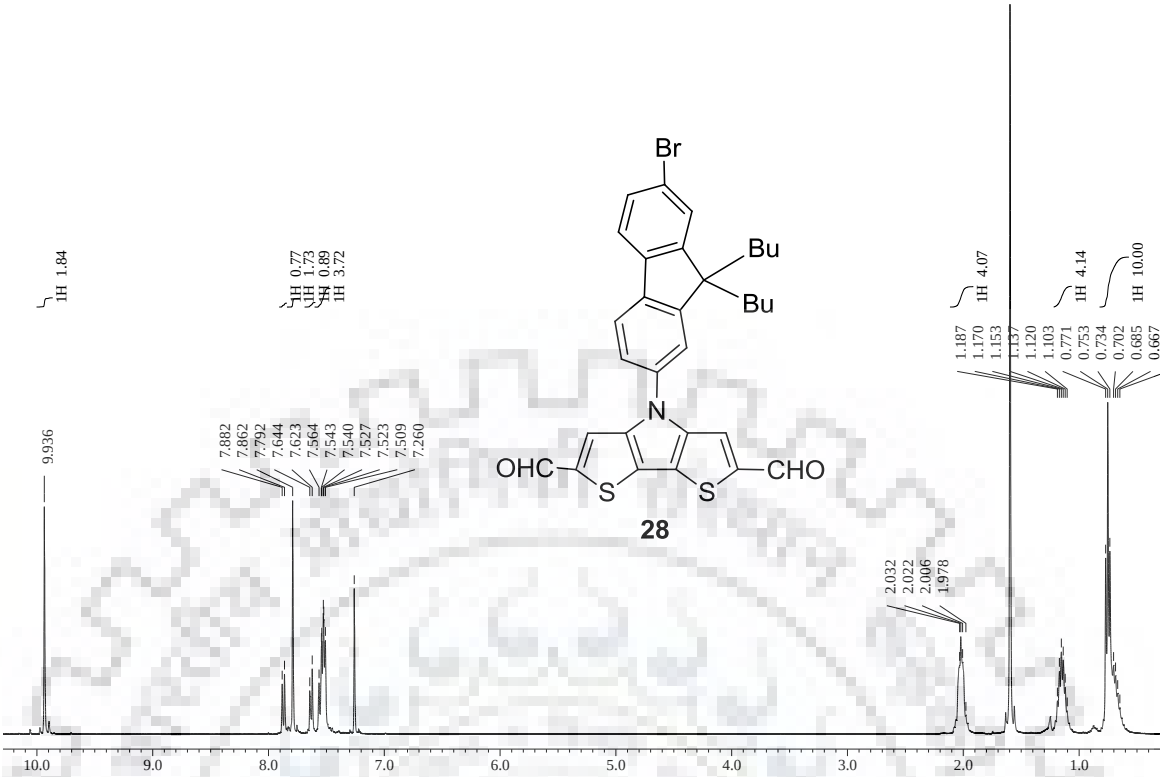

Figure S31 ^{13}C NMR spectra of **28** recorded in $CDCl_3$.

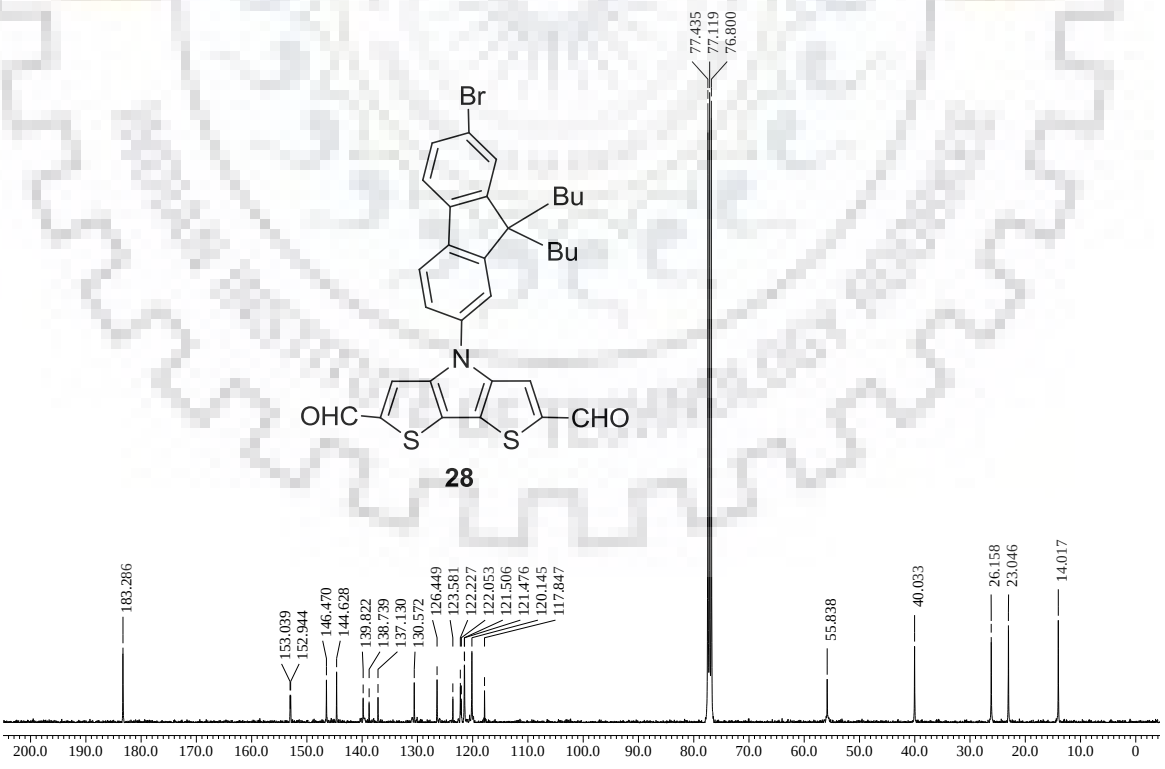

Figure S32 ^{13}C NMR spectra of **28** recorded in $CDCl_3$.

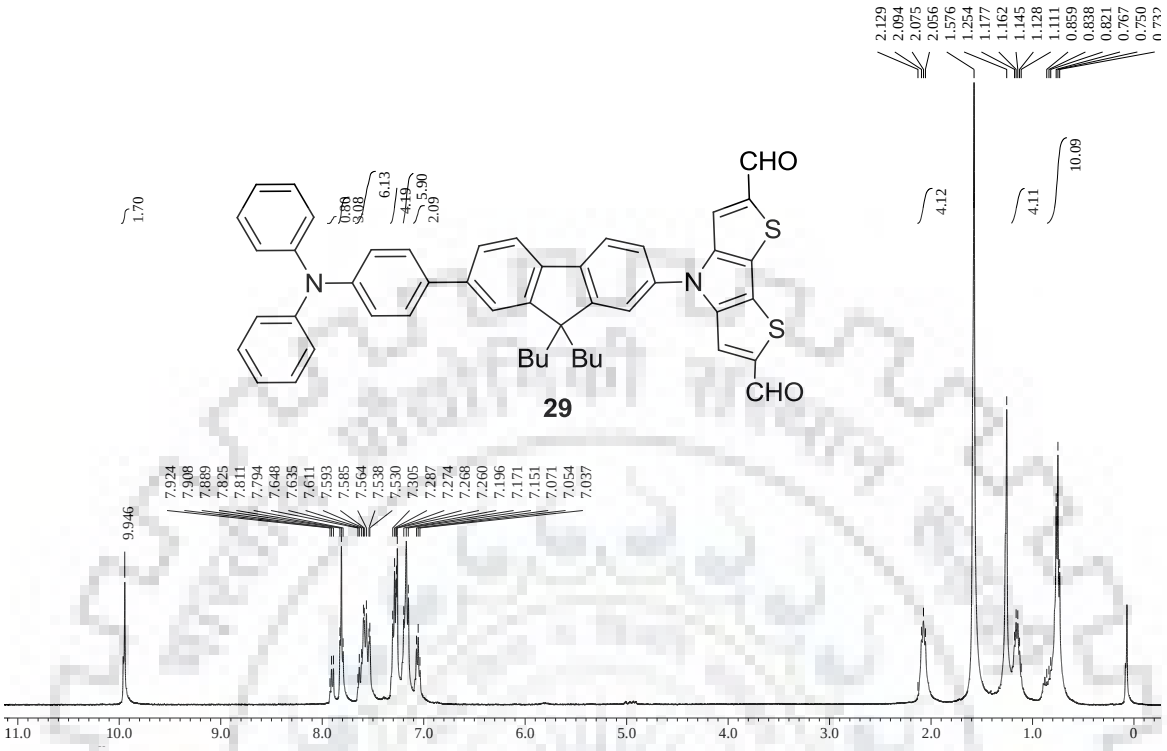

Figure S33 ^{1}H NMR spectra of **29** recorded in $CDCl_3$.

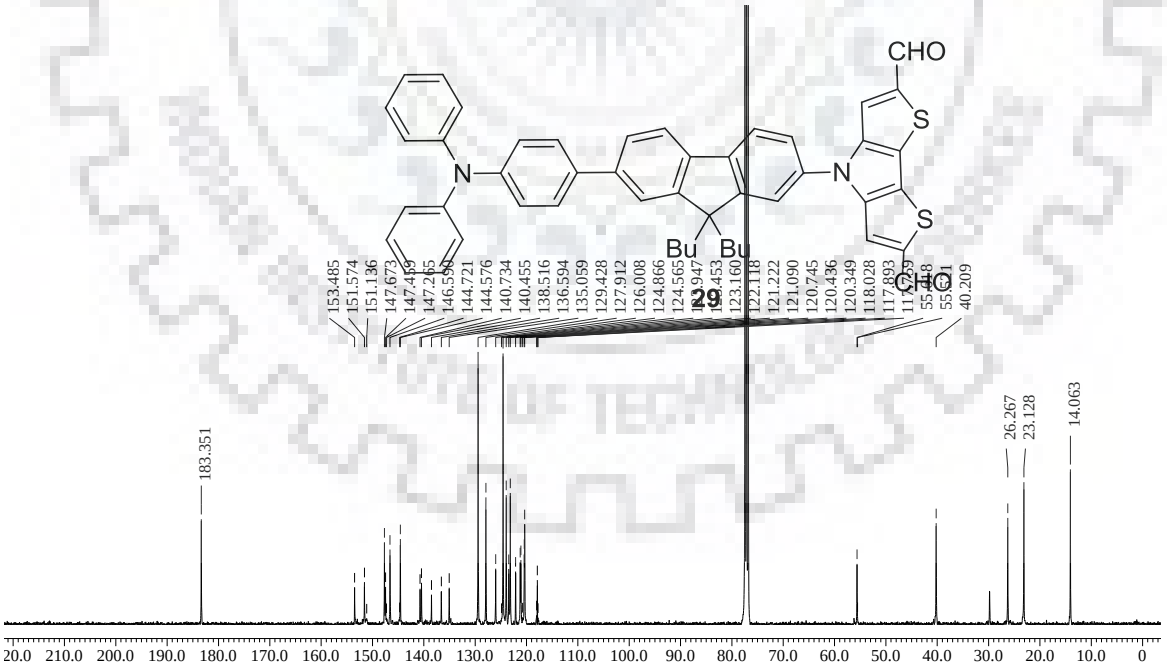

Figure S34 ^{13}C NMR spectra of **29** recorded in $CDCl_3$.

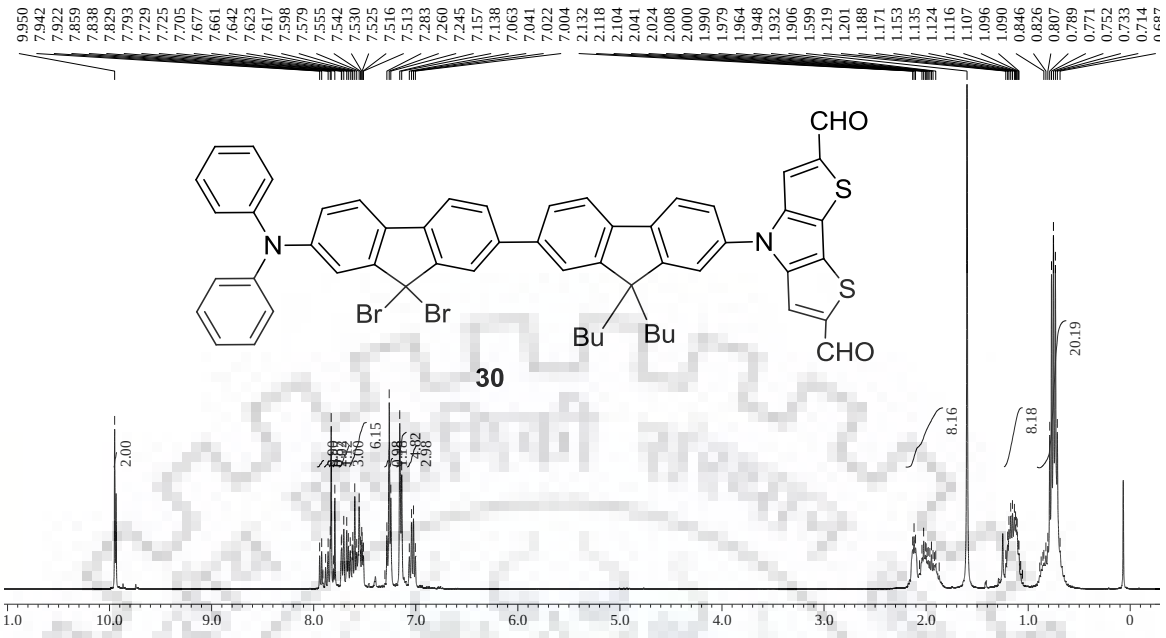

Figure S35 ^{1}H NMR spectra of **30** recorded in $CDCl_3$.

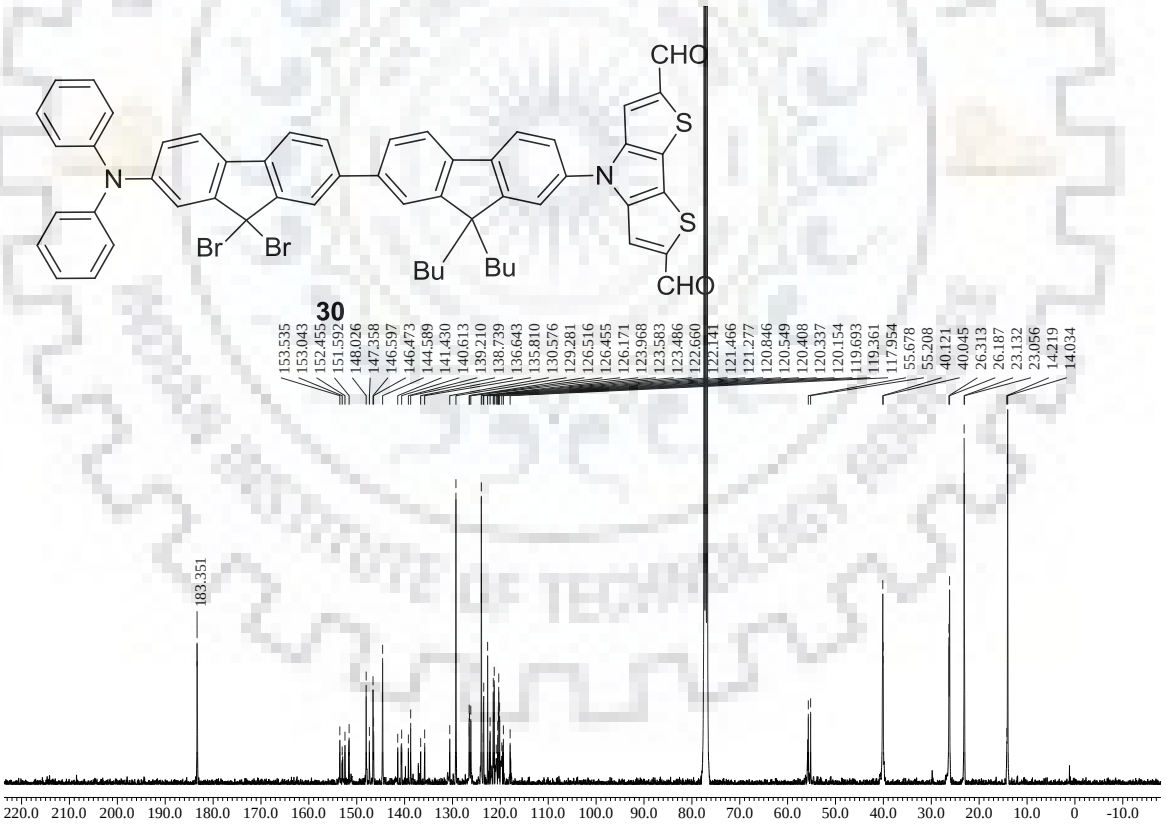

Figure S36 ^{13}C NMR spectra of **30** recorded in $CDCl_3$.

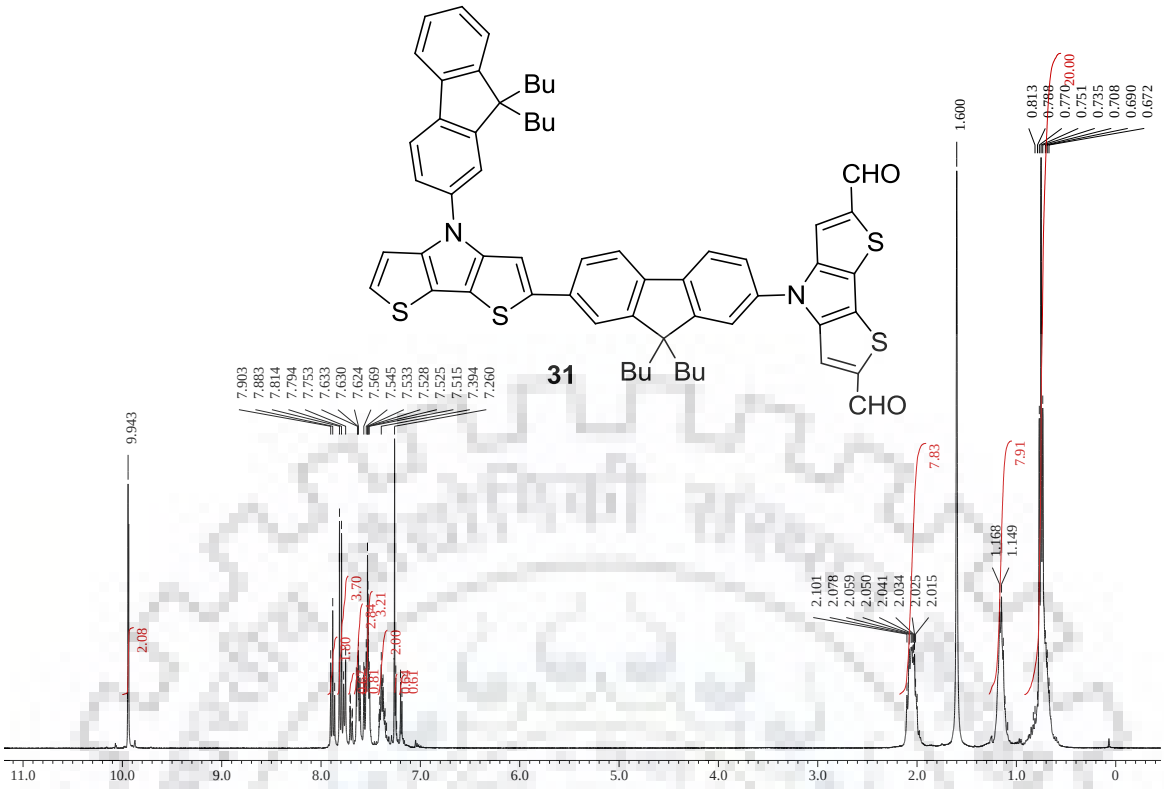

Figure S37 ^{1}H NMR spectra of **31** recorded in $CDCl_3$.

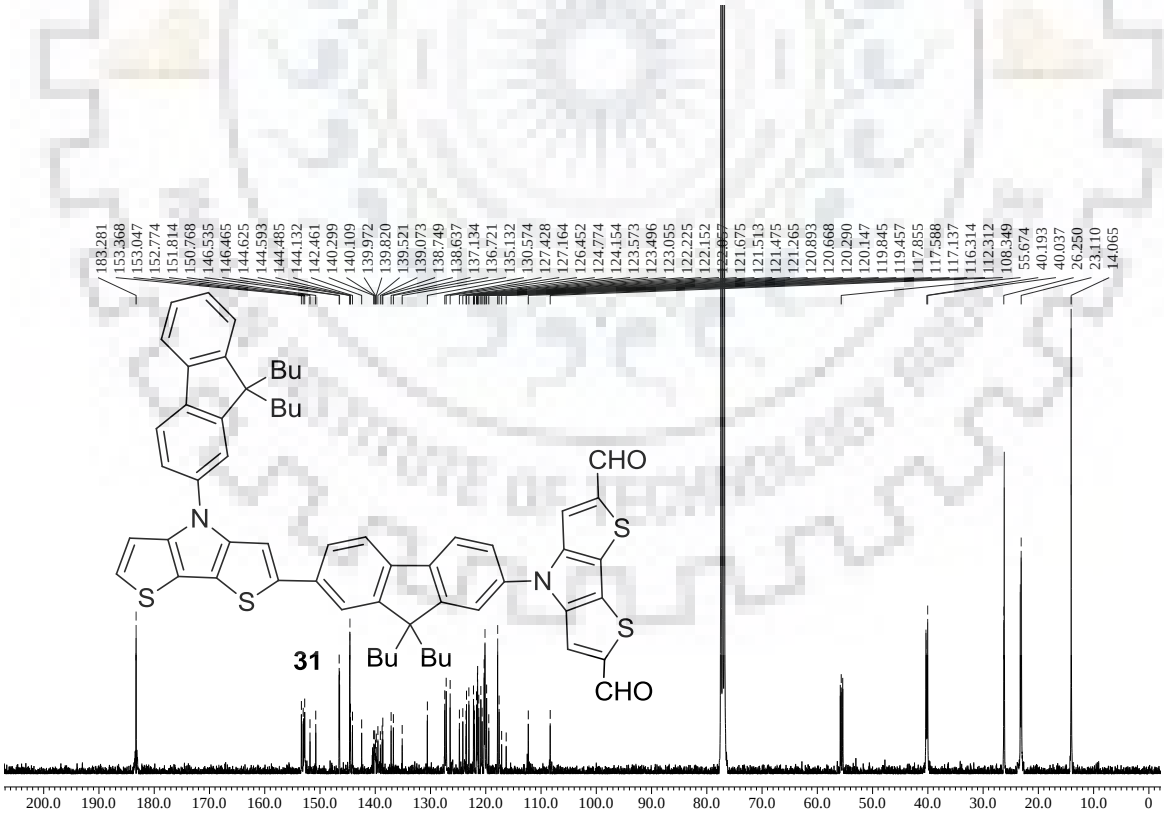

Figure S38 ^{13}C NMR spectra of **31** recorded in $CDCl_3$.

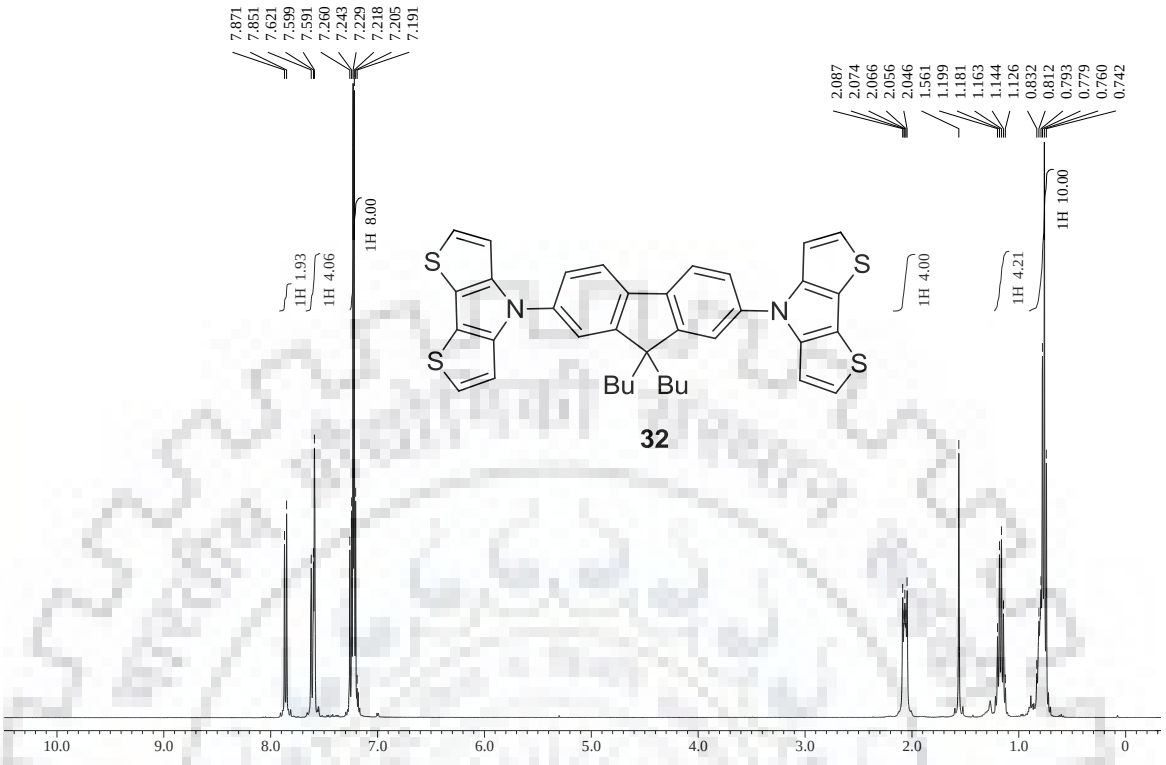

Figure S39 ^{1}H NMR spectra of **32** recorded in $CDCl_3$.

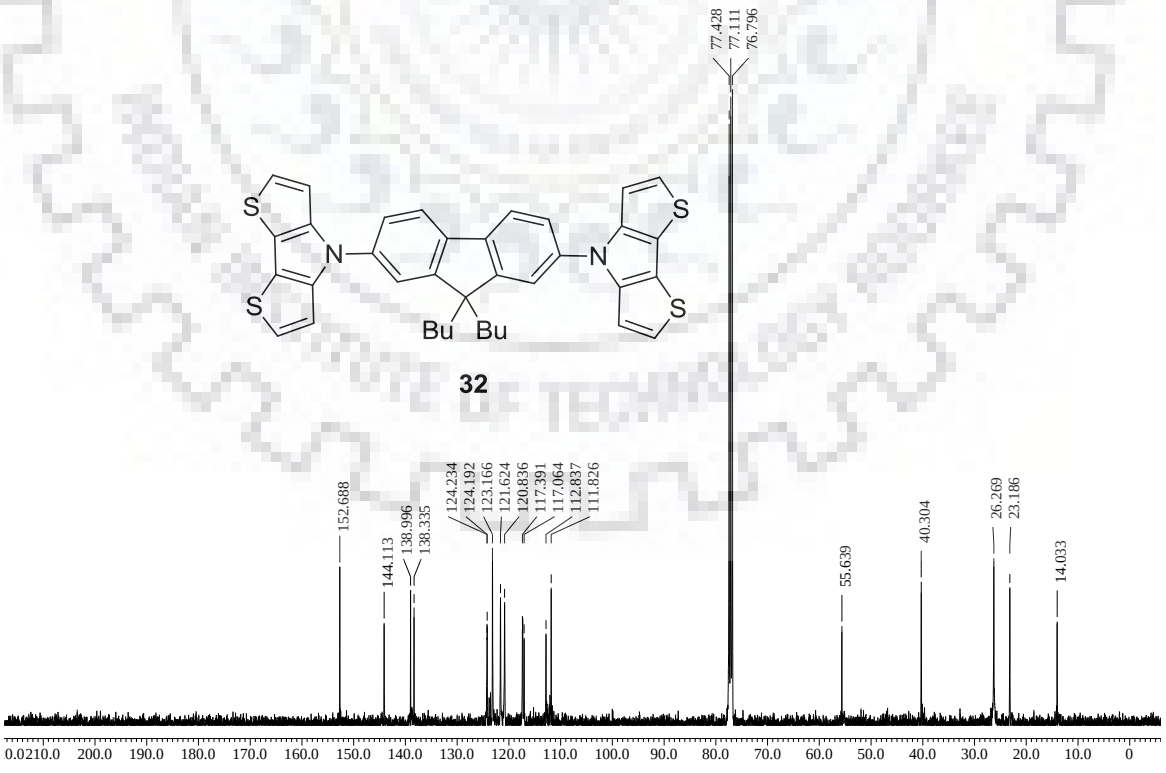

Figure S40 ^{13}C NMR spectra of **32** recorded in $CDCl_3$.

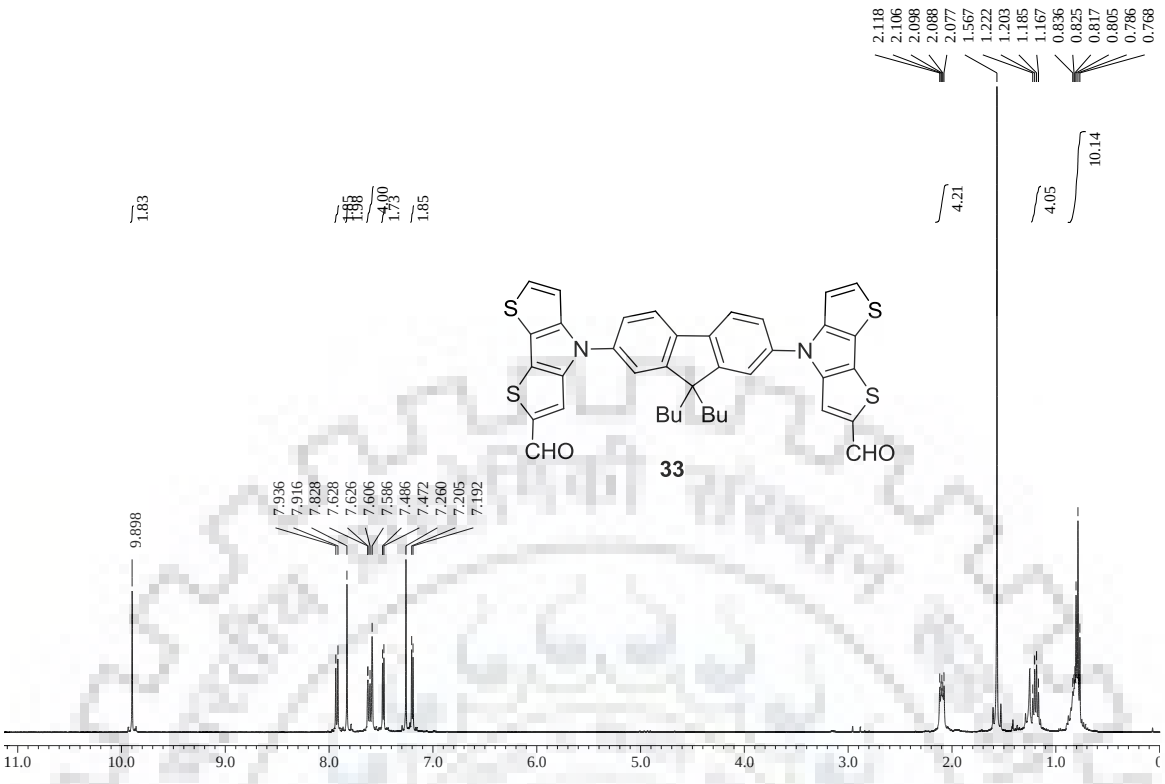

Figure S41 ^{1}H NMR spectra of **33** recorded in $CDCl_3$.

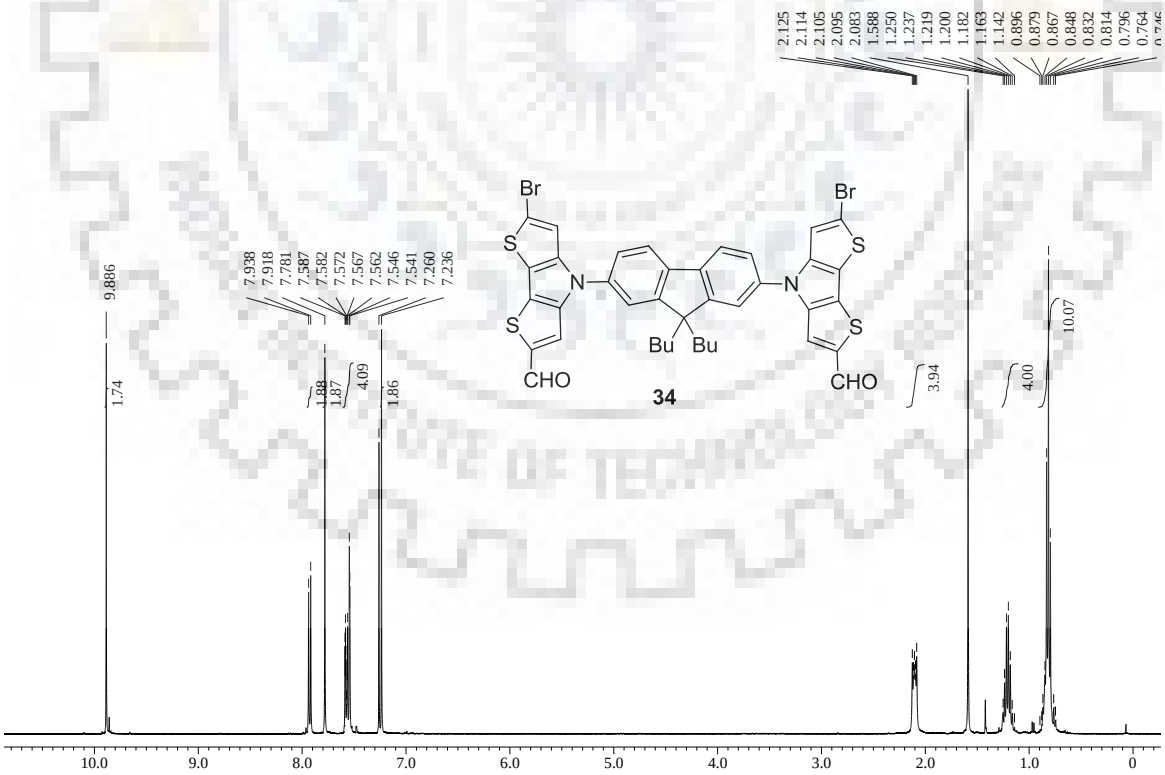

Figure S42 ^{1}H NMR spectra of **34** recorded in $CDCl_3$.

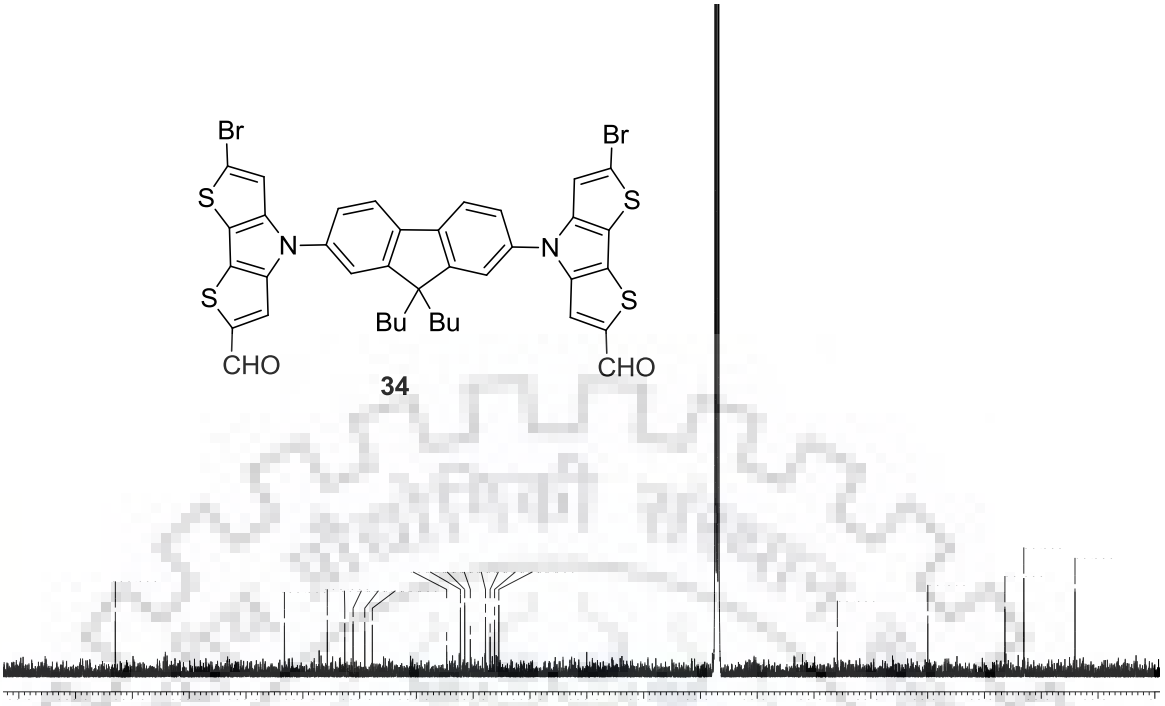

Figure S43 ^{13}C NMR spectra of **34** recorded in $CDCl_3$.

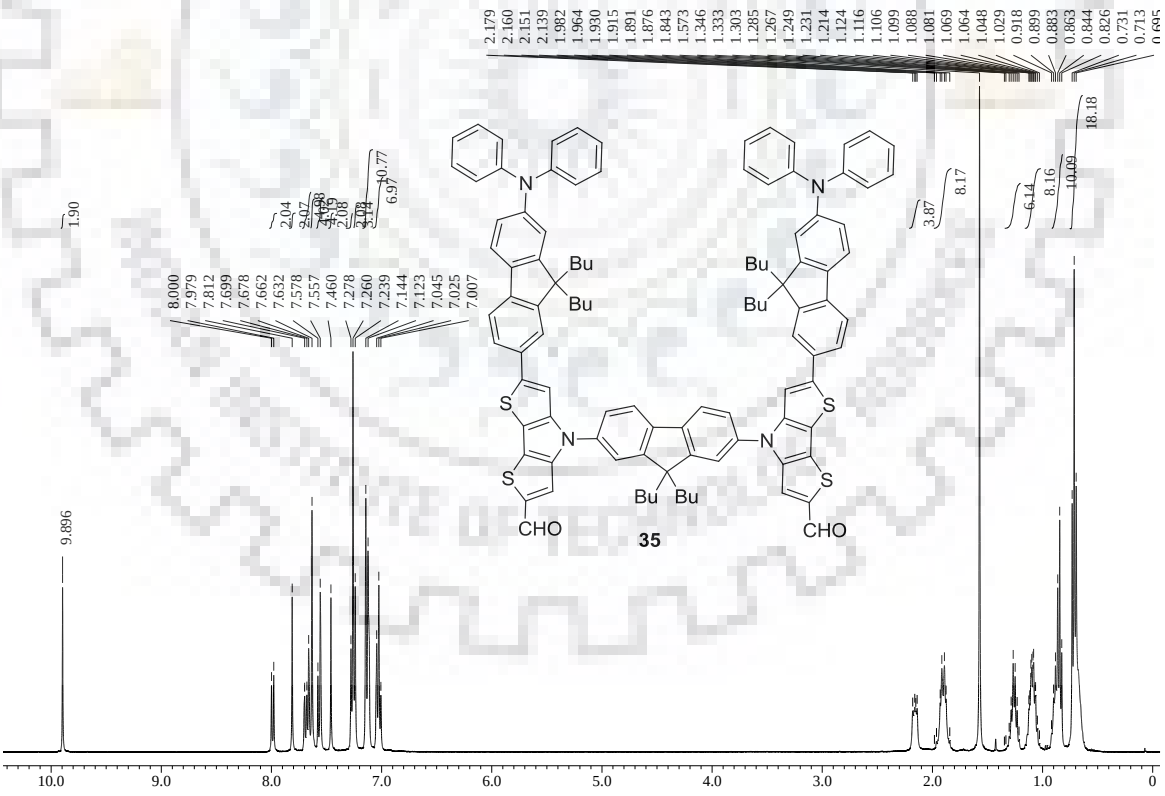

Figure S44 ^{1}H NMR spectra of **35** recorded in $CDCl_3$.

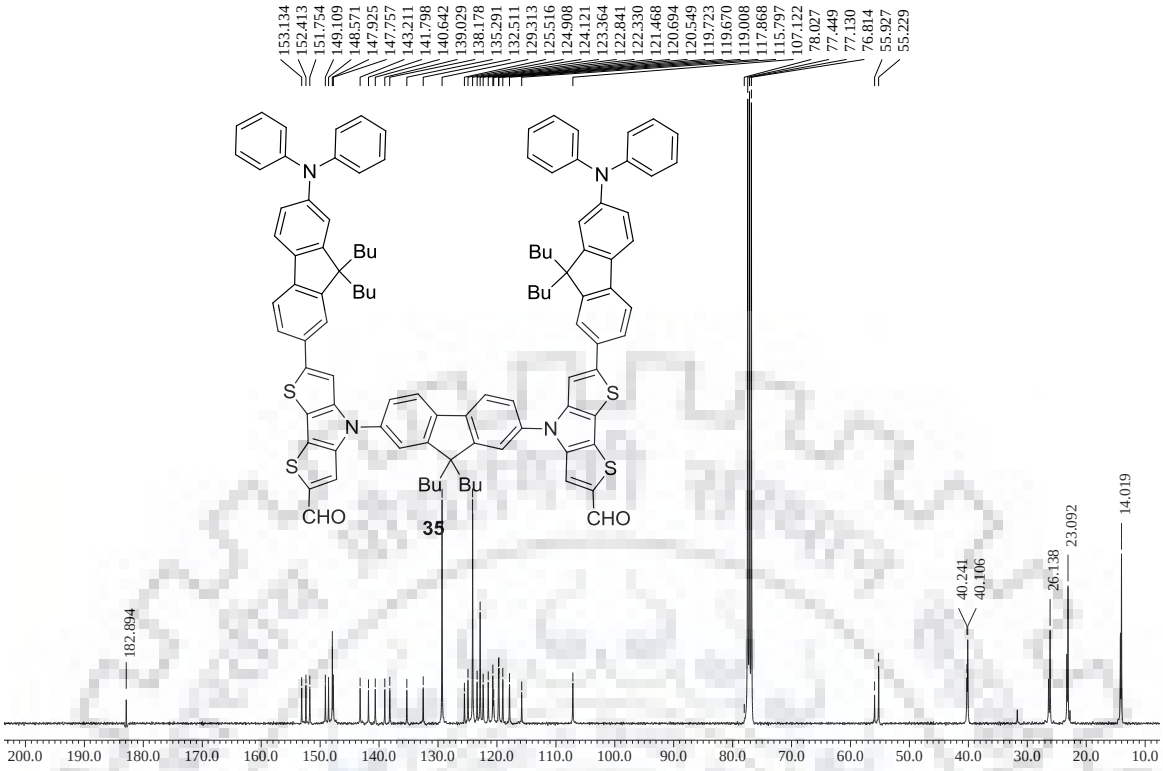

Figure S45 ^{13}C NMR spectra of **35** recorded in $CDCl_3$.

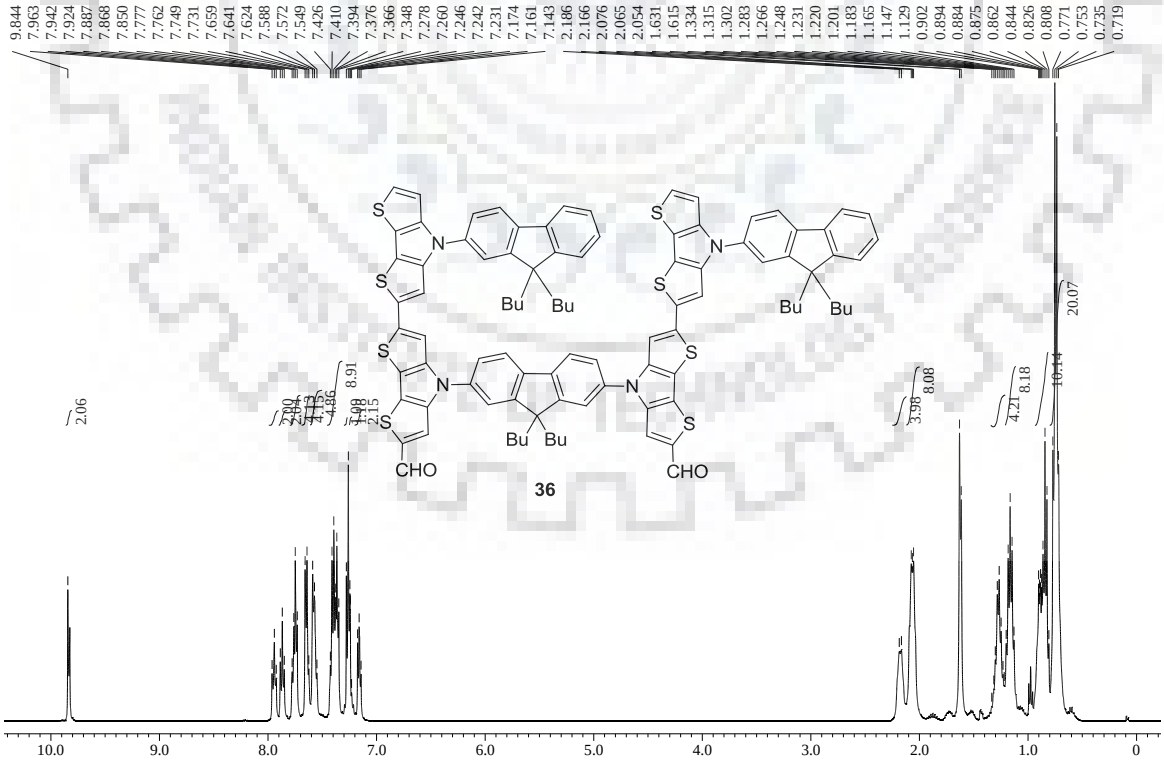

Figure S46 ^{1}H NMR spectra of **36** recorded in $CDCl_3$.

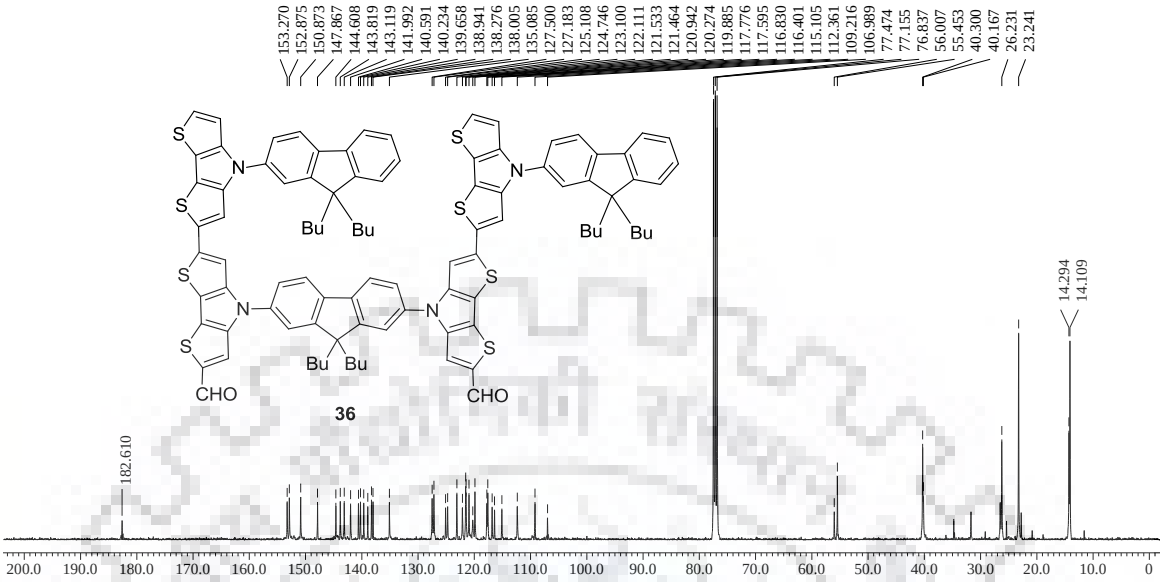

Figure S47 ^{13}C NMR spectra of **36** recorded in $CDCl_3$.

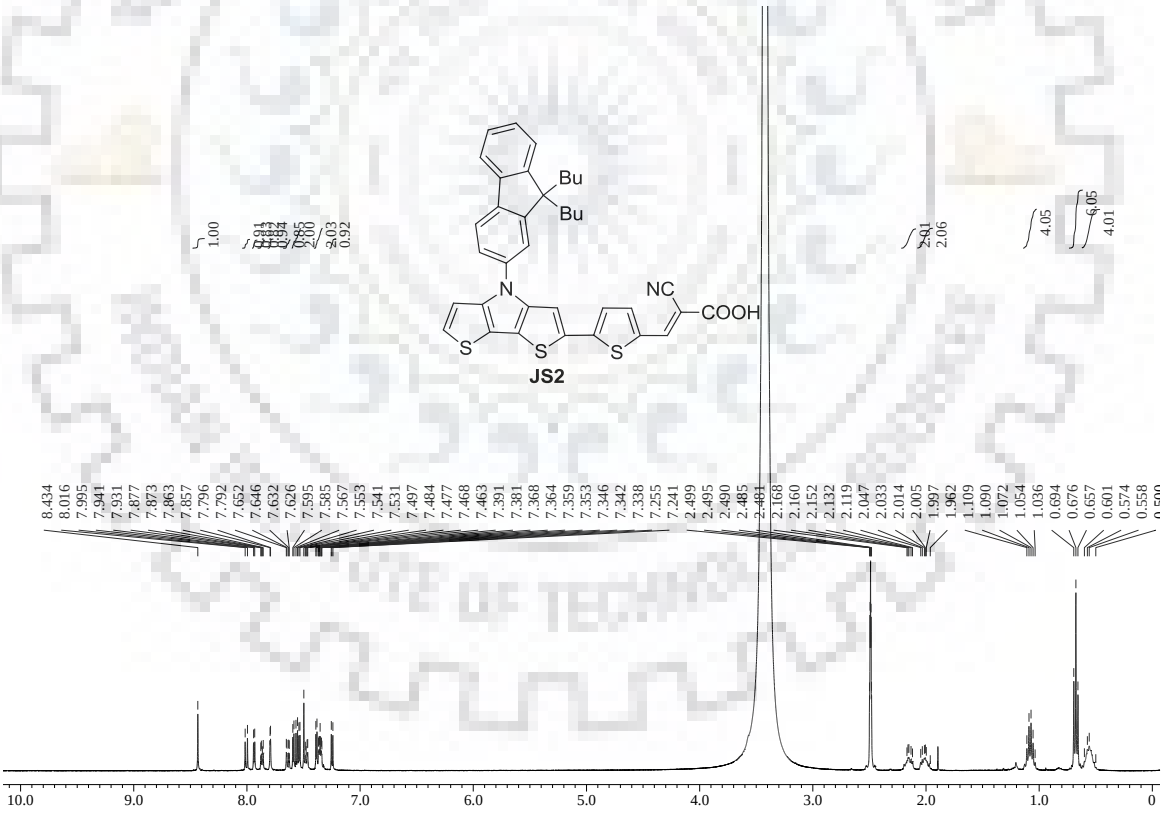

Figure S48 ^{1}H NMR spectra of **JS2** recorded in DMSO-d_6.

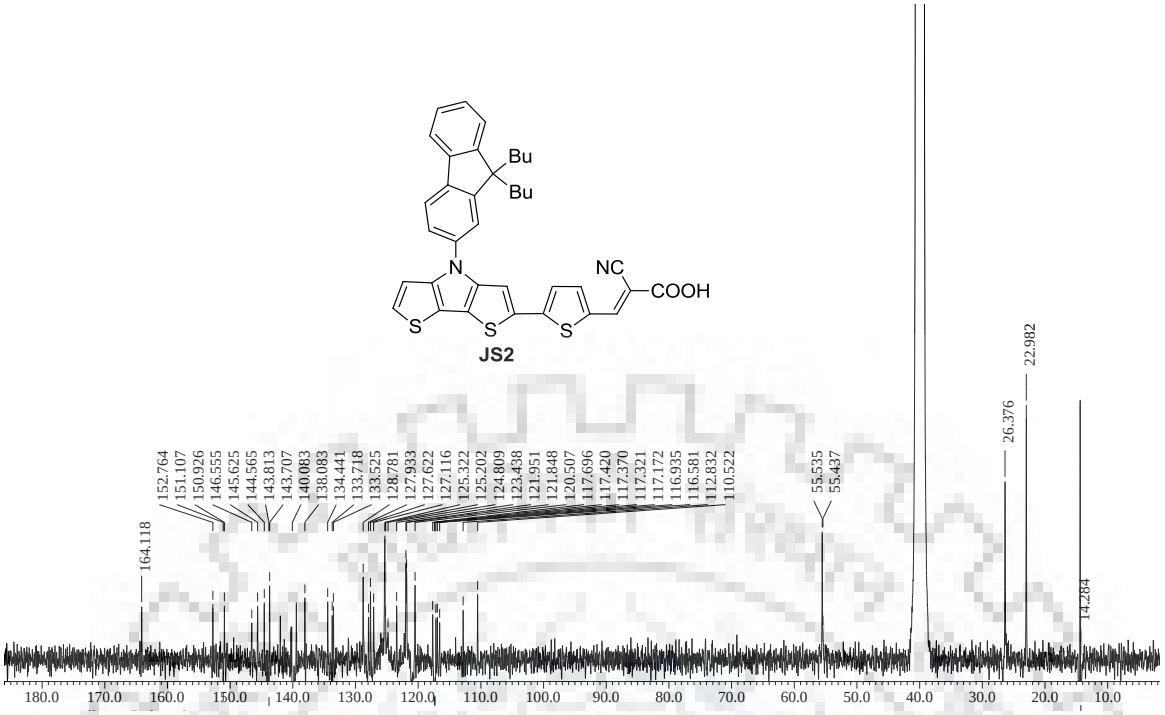

Figure S49 ^{13}C NMR spectra of **JS2** recorded in DMSO-d_6.

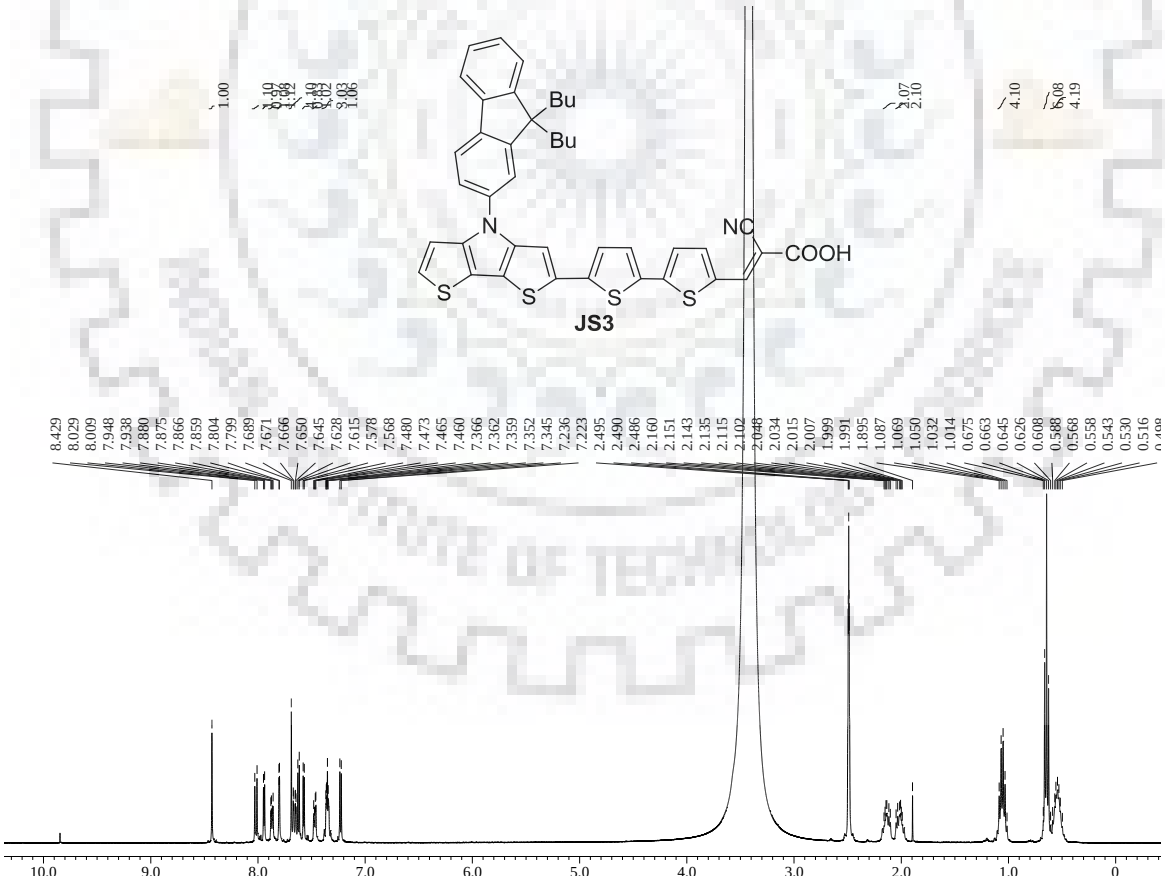

Figure S50 ^{1}H NMR spectra of **JS3** recorded in DMSO-d_6.

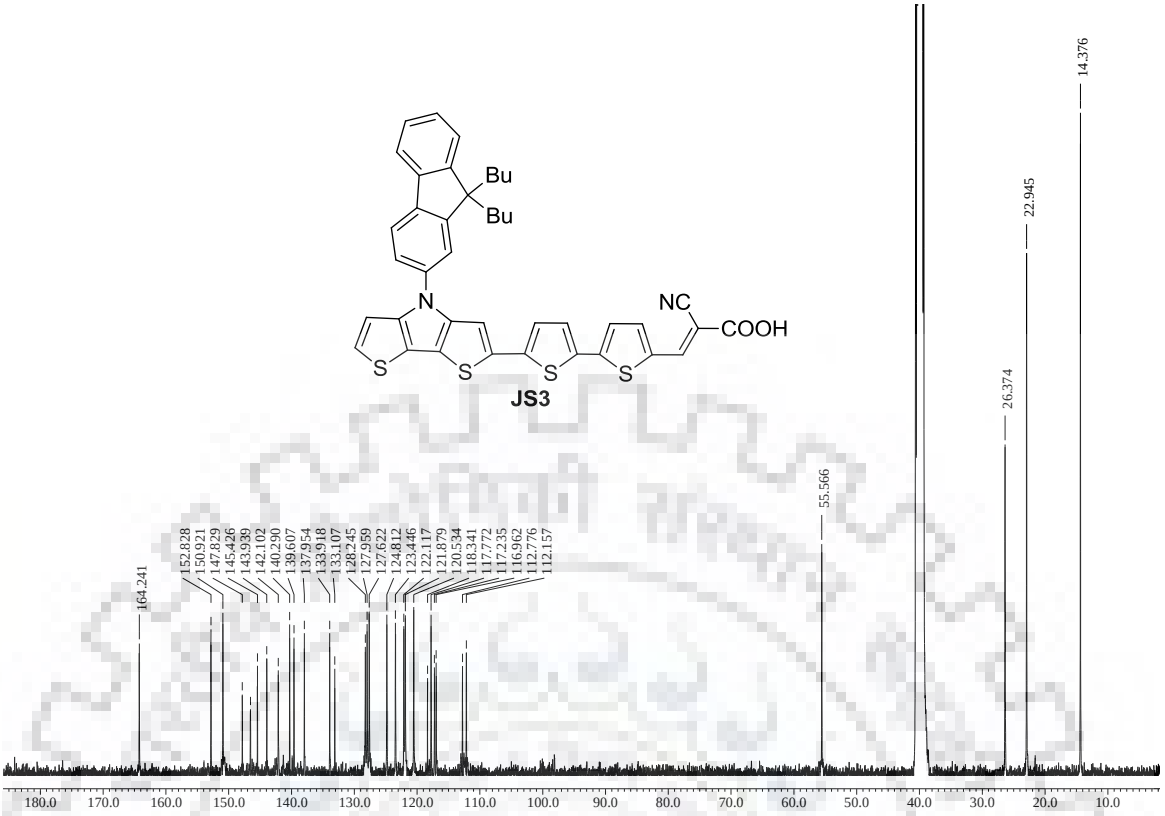

Figure S51 ^{13}C NMR spectra of **JS3** recorded in DMSO-d_6.

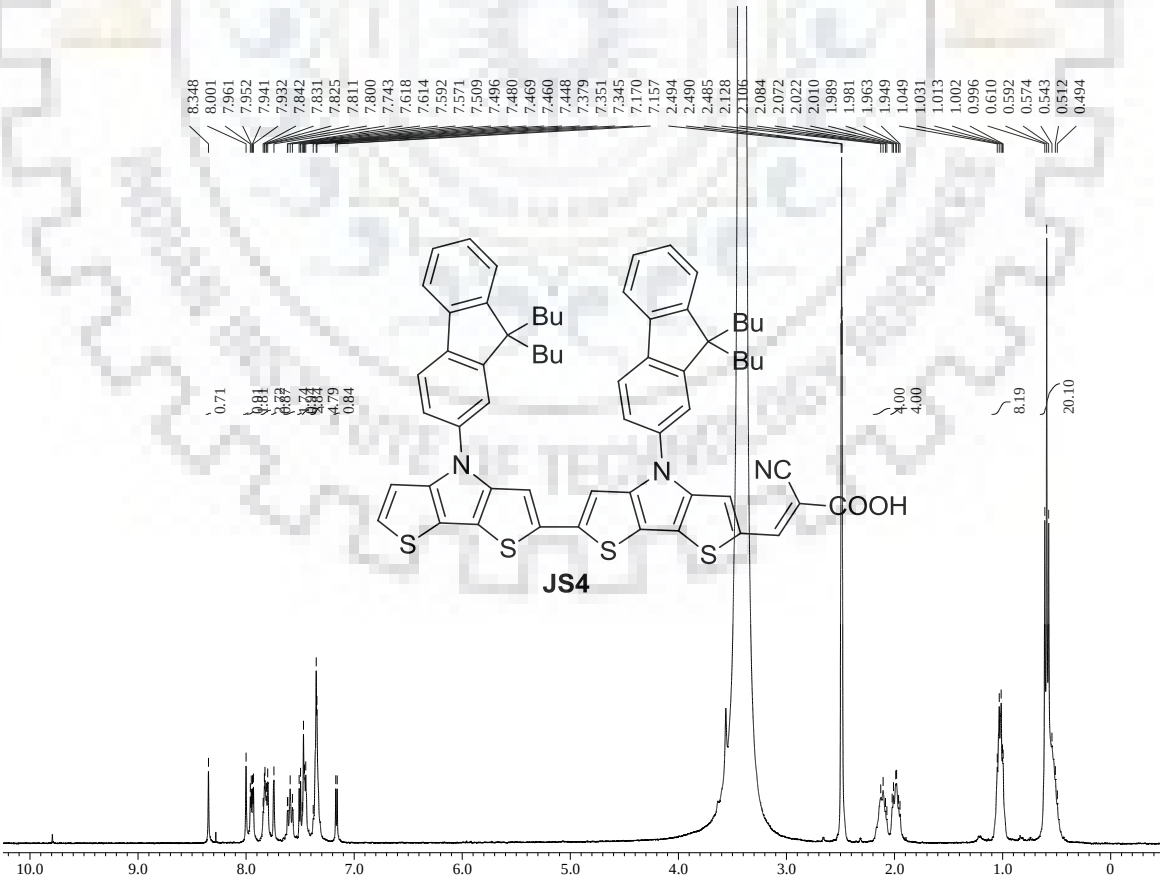

Figure S52 ^{1}H NMR spectra of **JS4** recorded in DMSO-d_6.

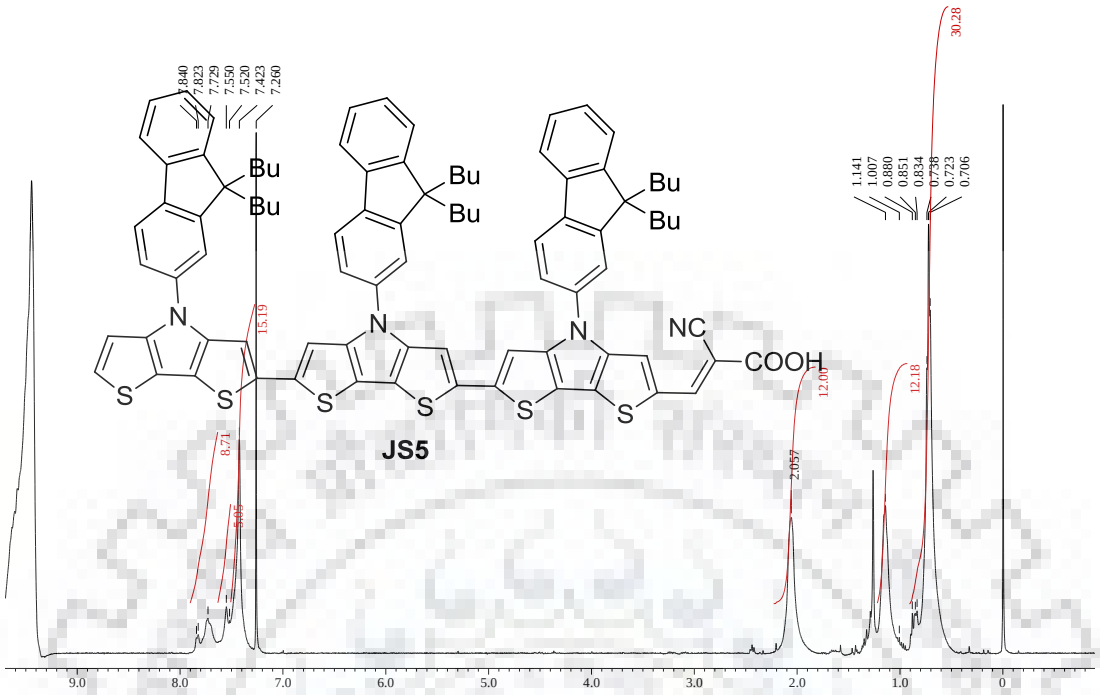

Figure S53 ^{1}H NMR spectra of **JS5** recorded in $CDCl_3$ with small amount of TFA.

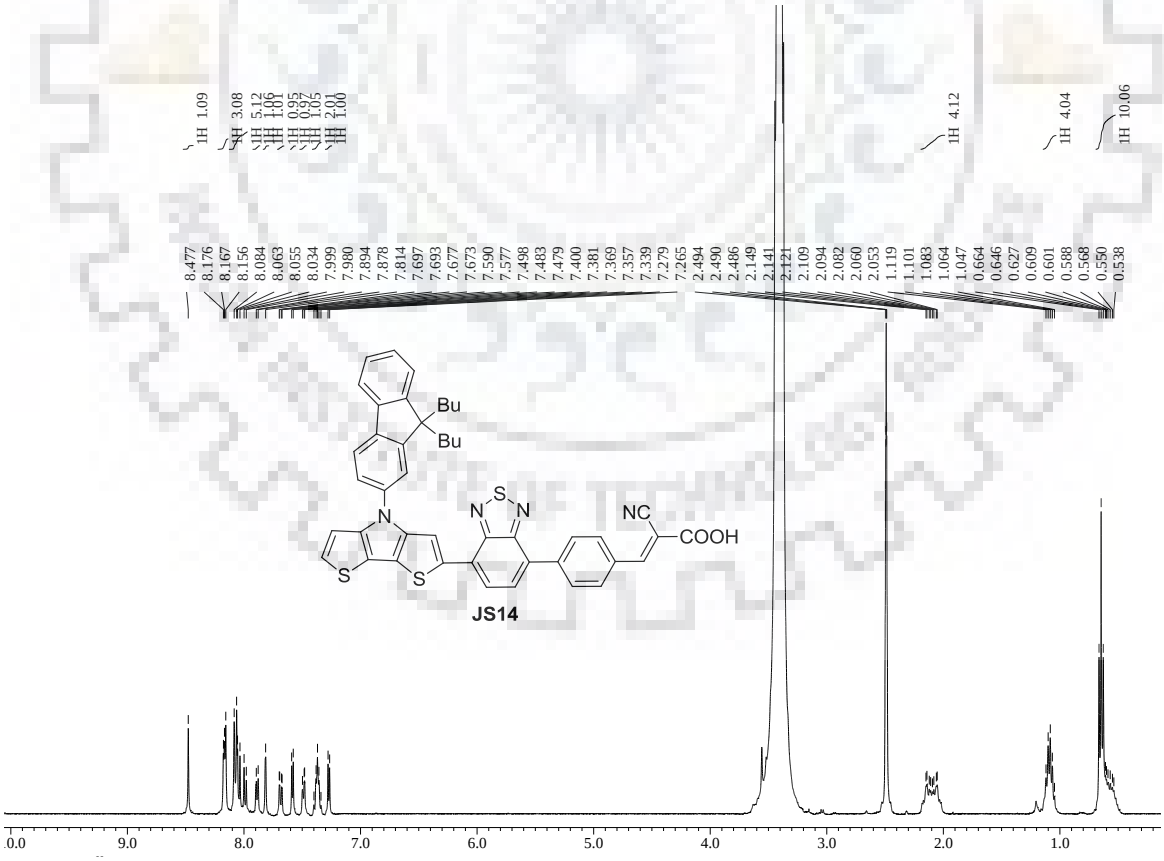

Figure S54 ^{1}H NMR spectra of **JS14** recorded in DMSO-d_6.

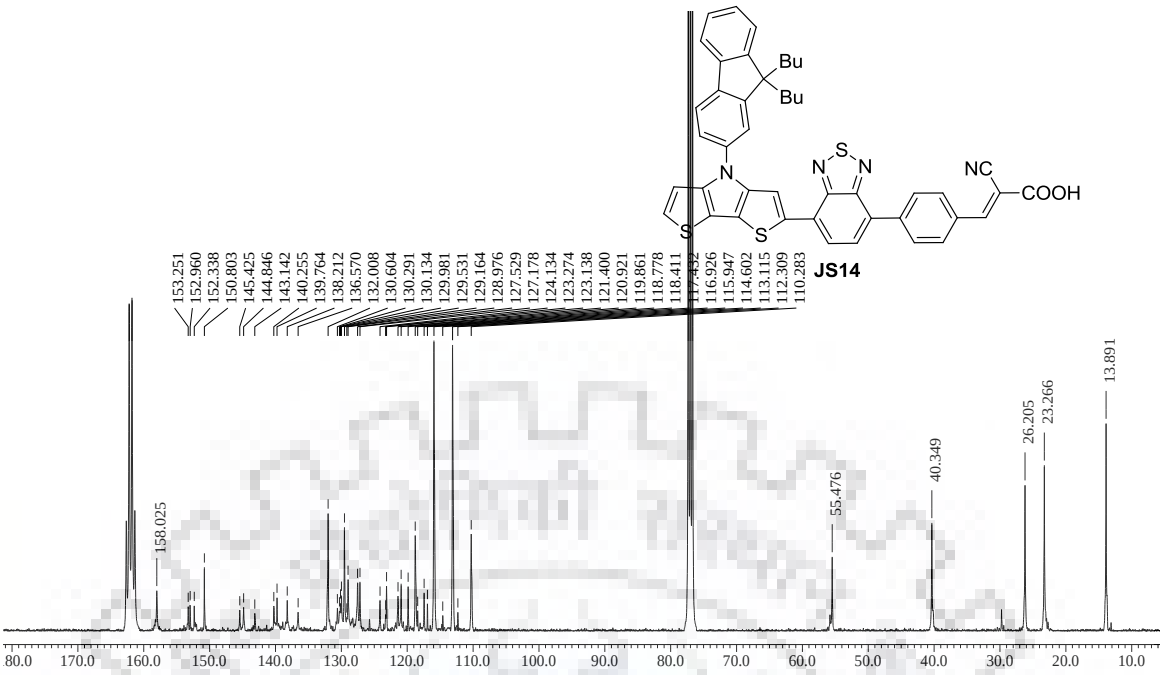

Figure S55 ^{13}C NMR spectra of **JS14** recorded in $CDCl_3$ with small amount of TFA.

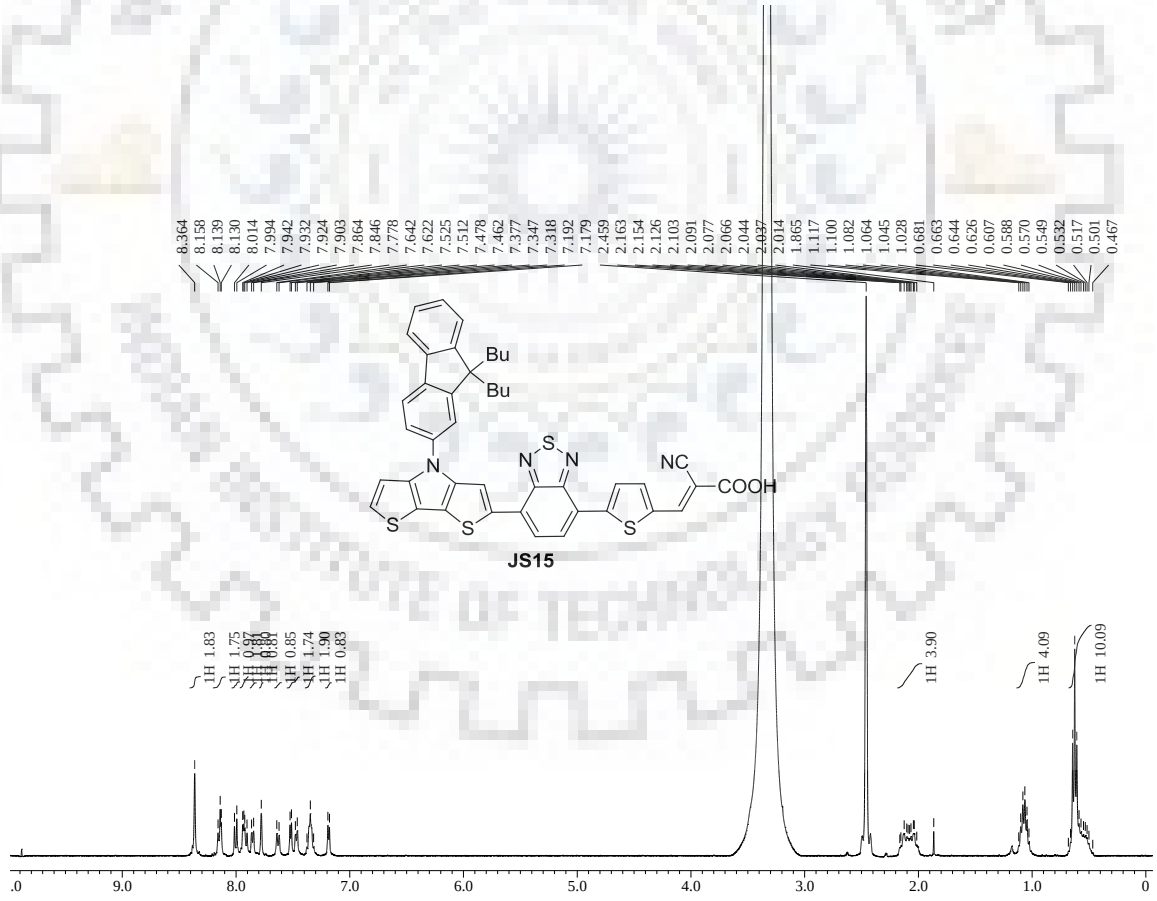

Figure S56 ^{1}H NMR spectra of **JS15** recorded in DMSO-d_6.

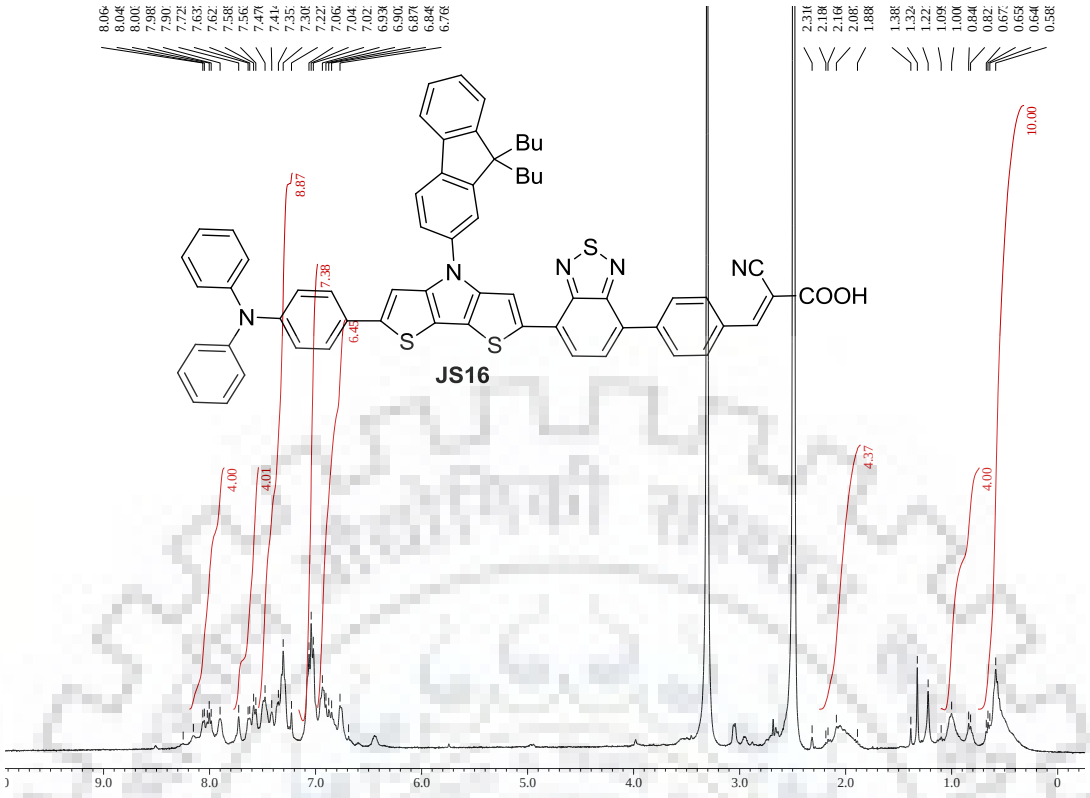

Figure S57 ^{1}H NMR spectra of **JS16** recorded in DMSO-d_6.

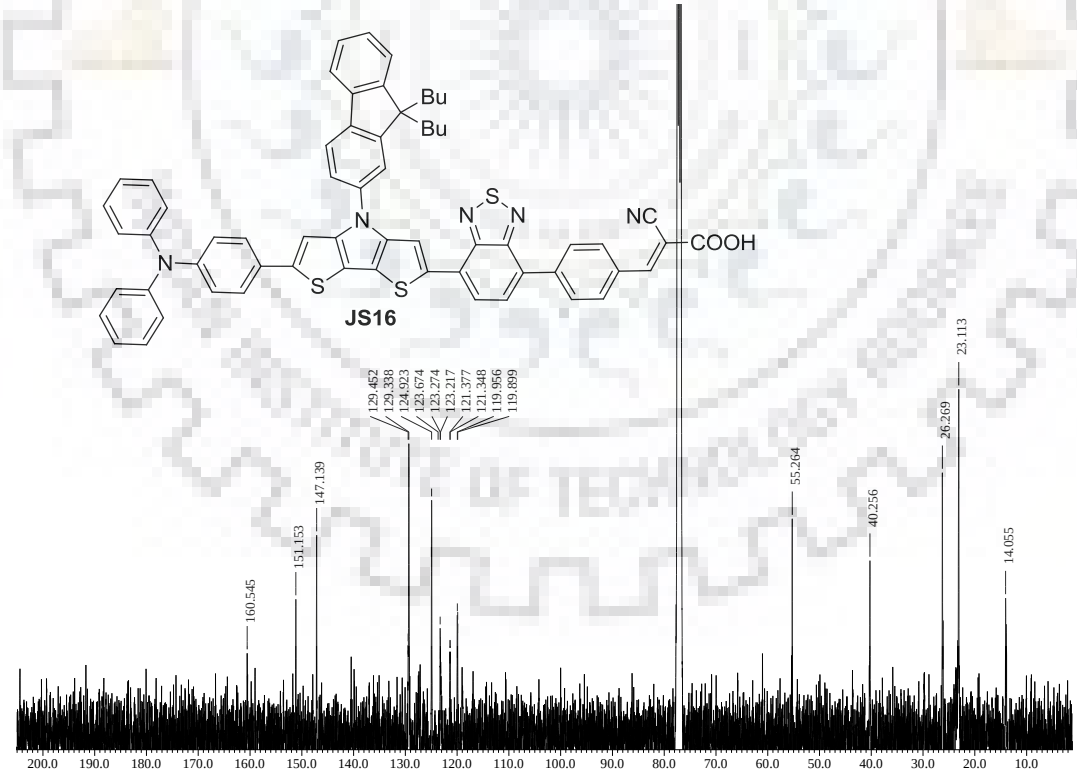

Figure S58 ^{13}C NMR spectra of **JS16** recorded in $CDCl_3$ with small amount of TFA.

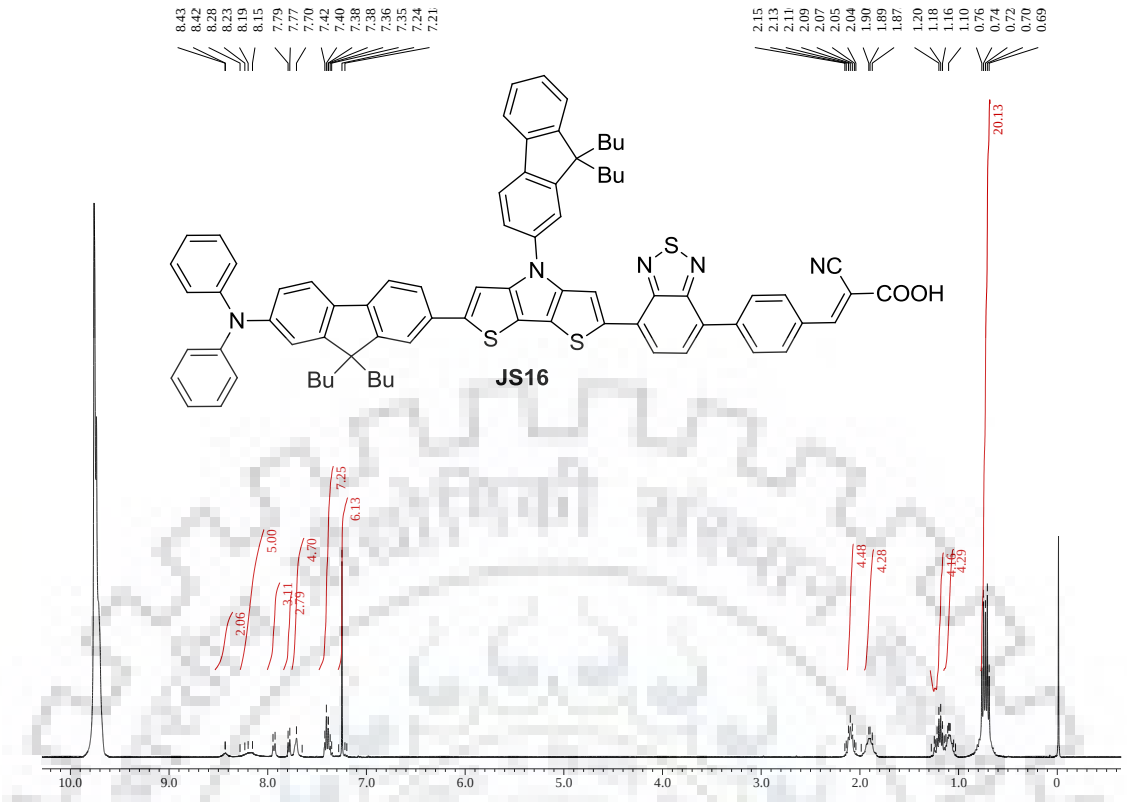

Figure S59 ^{1}H NMR spectra of **JS16** recorded in $CDCl_3$ with small amount of TFA.

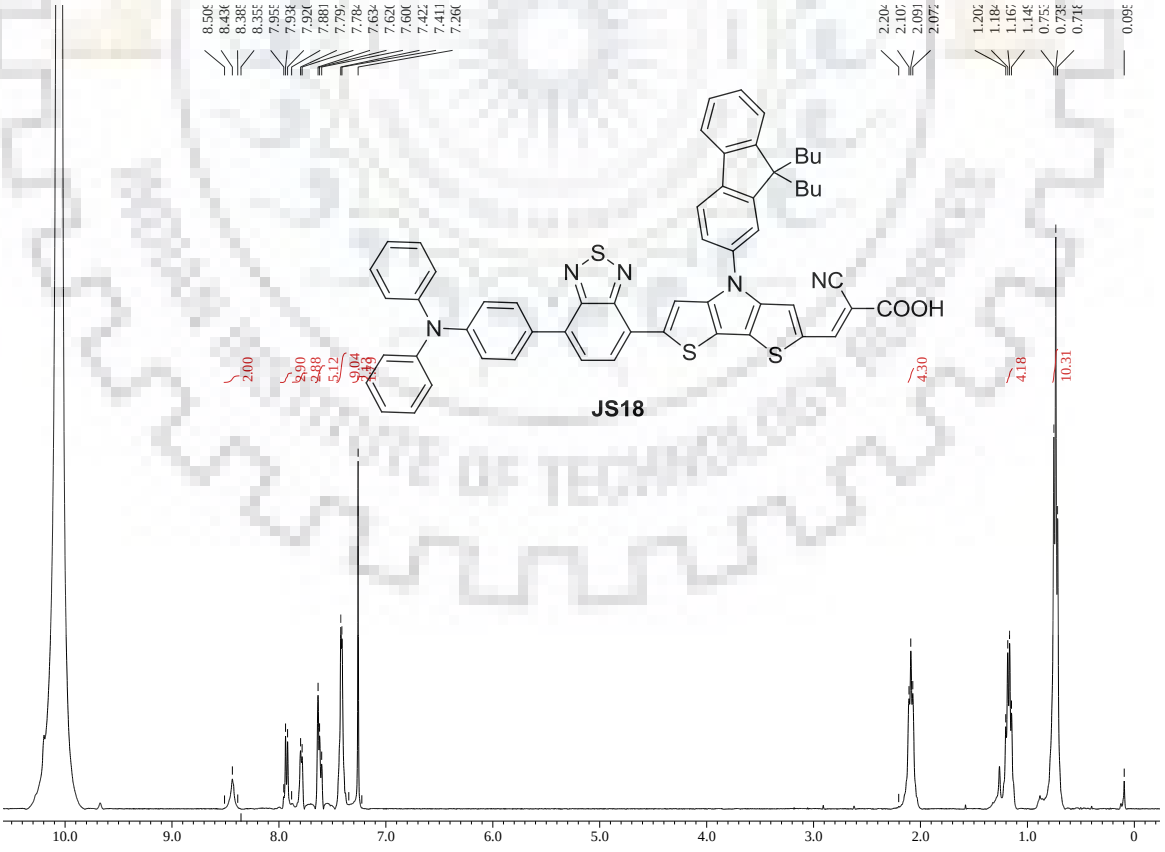

Figure S60 ^{1}H NMR spectra of **JS18** recorded in $CDCl_3$ with small amount of TFA.

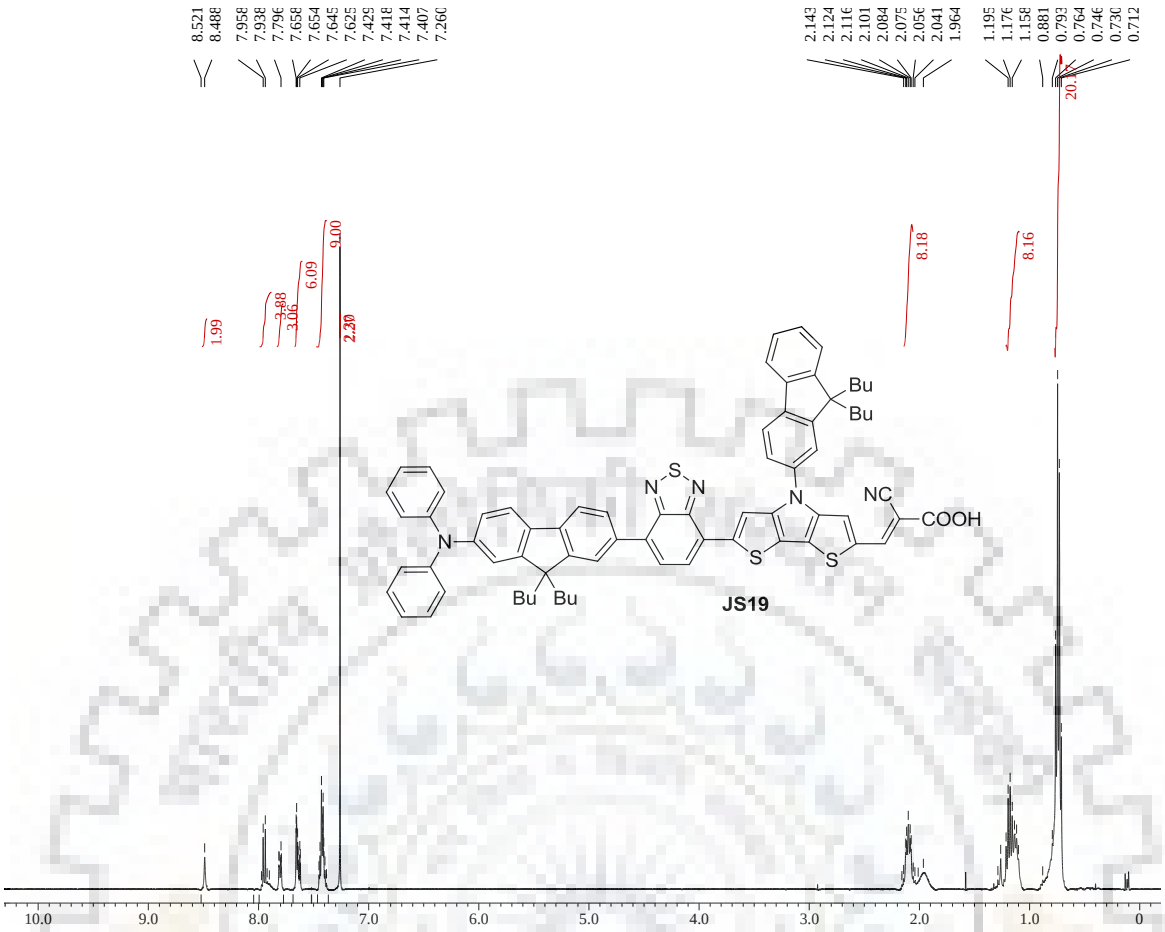

Figure S61 ^{1}H NMR spectra of **JS19** recorded in $CDCl_3$ with small amount of TFA.

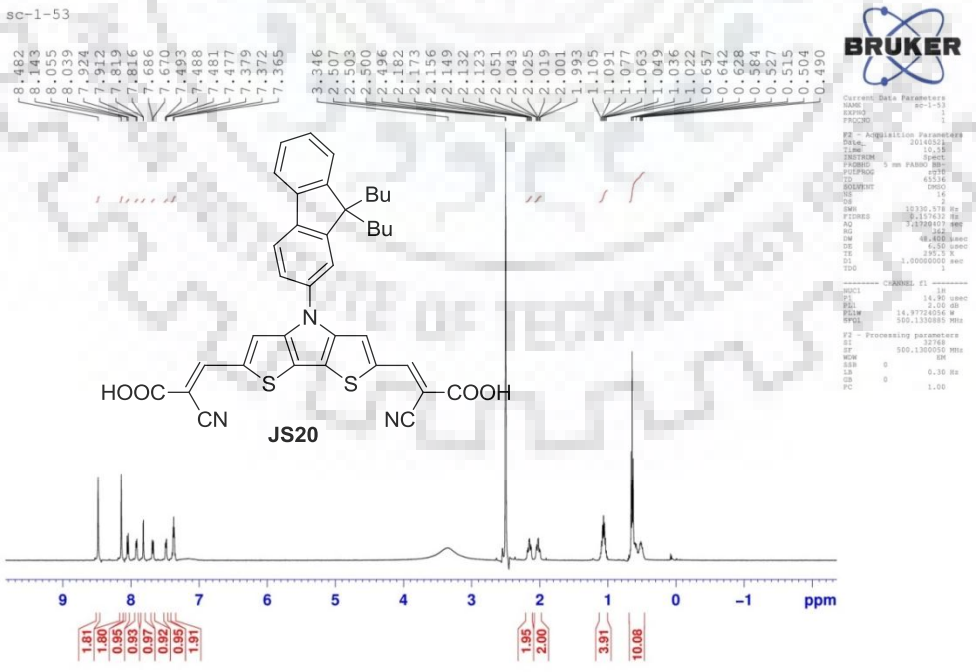

Figure S62 ^{1}H NMR spectra of **JS20** recorded in DMSO-d_6.

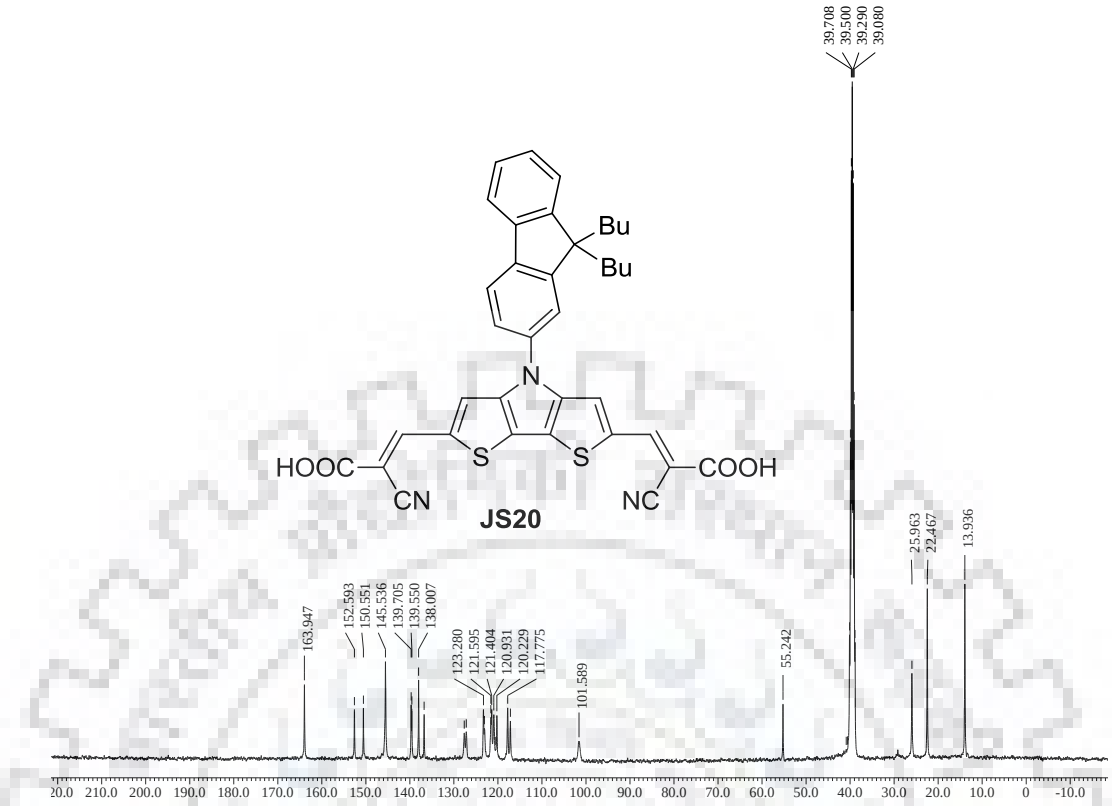

Figure S63 ^{13}C NMR spectra of **JS20** recorded in DMSO-d_6.

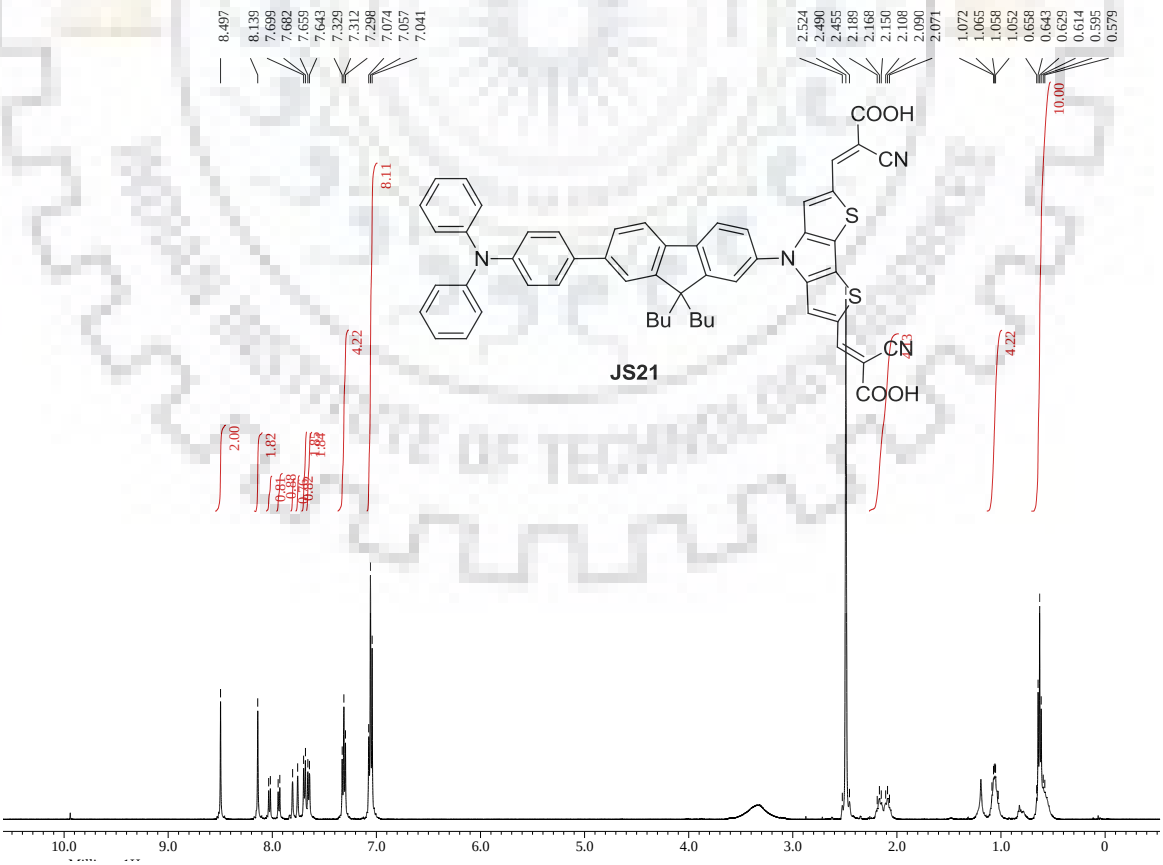

Figure S64 ^{1}H NMR spectra of **JS21** recorded in DMSO-d_6.

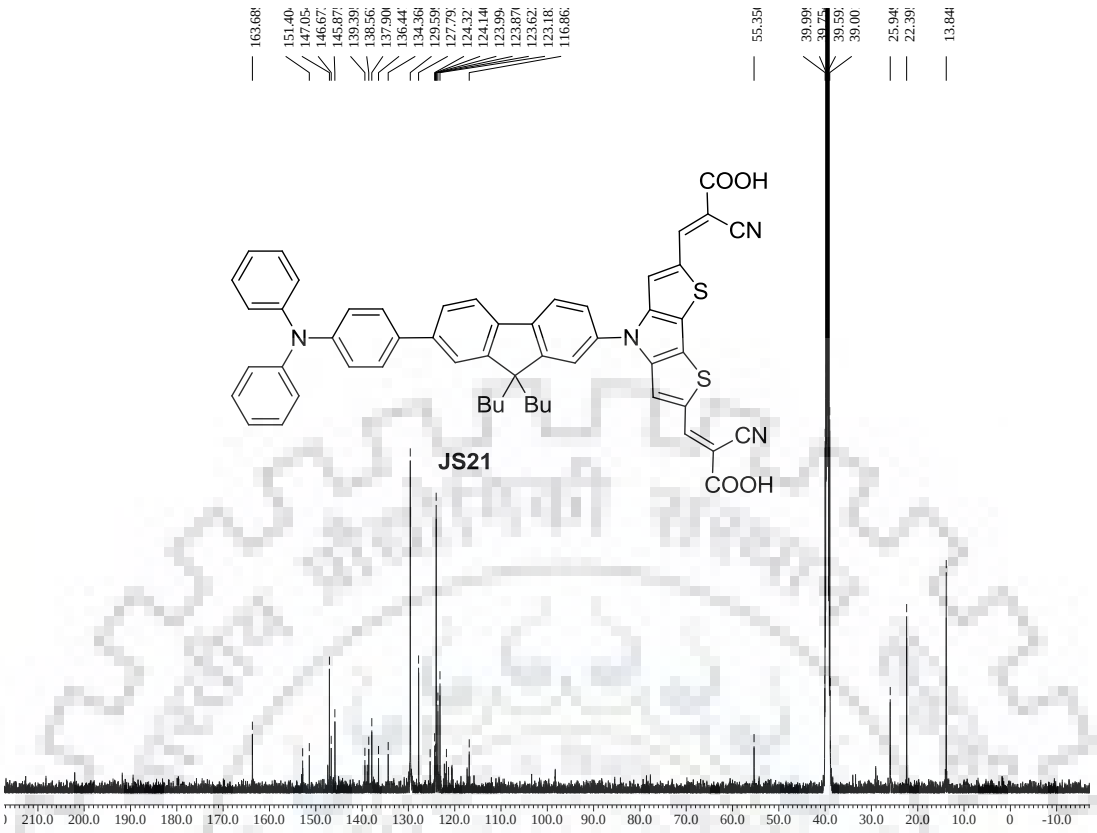

Figure S65 ^{13}C NMR spectra of **JS21** recorded in DMSO-d_6.

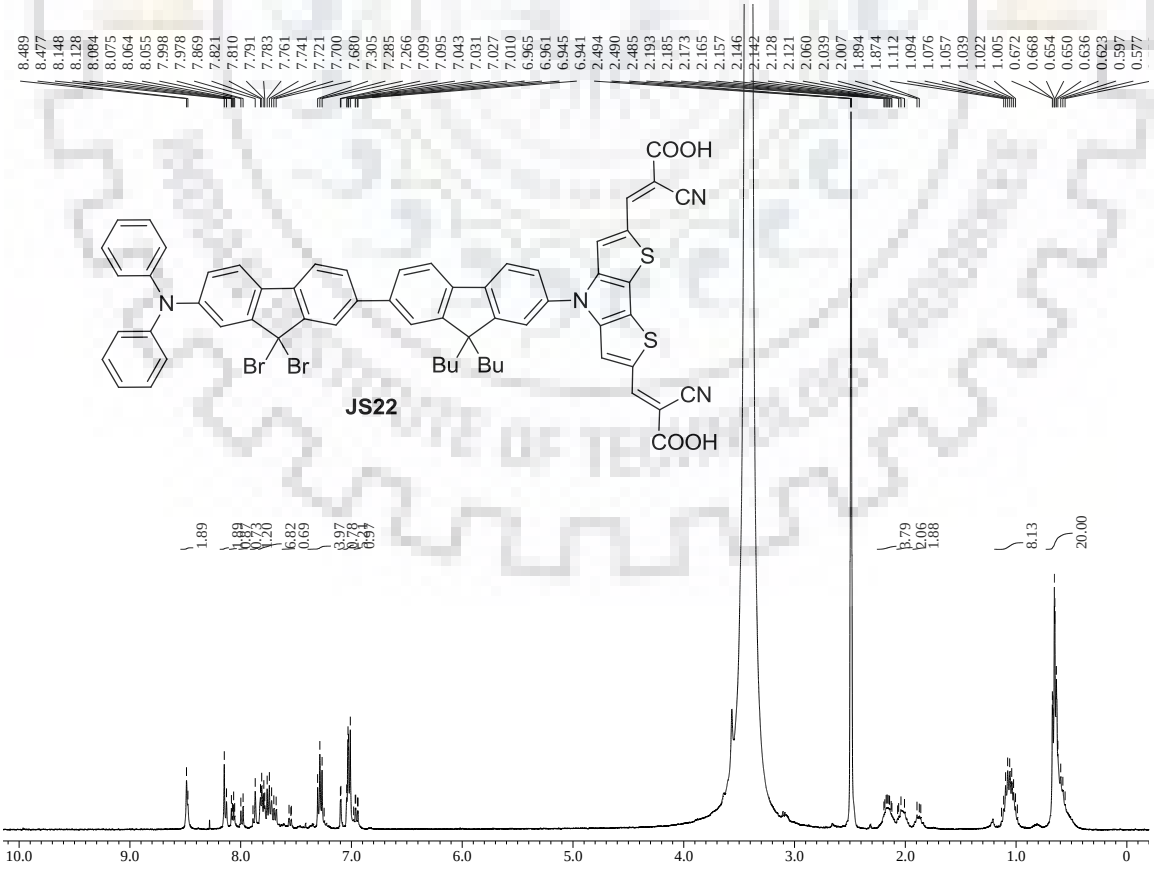

Figure S66 ^{1}H NMR spectra of **JS22** recorded in DMSO-d_6.

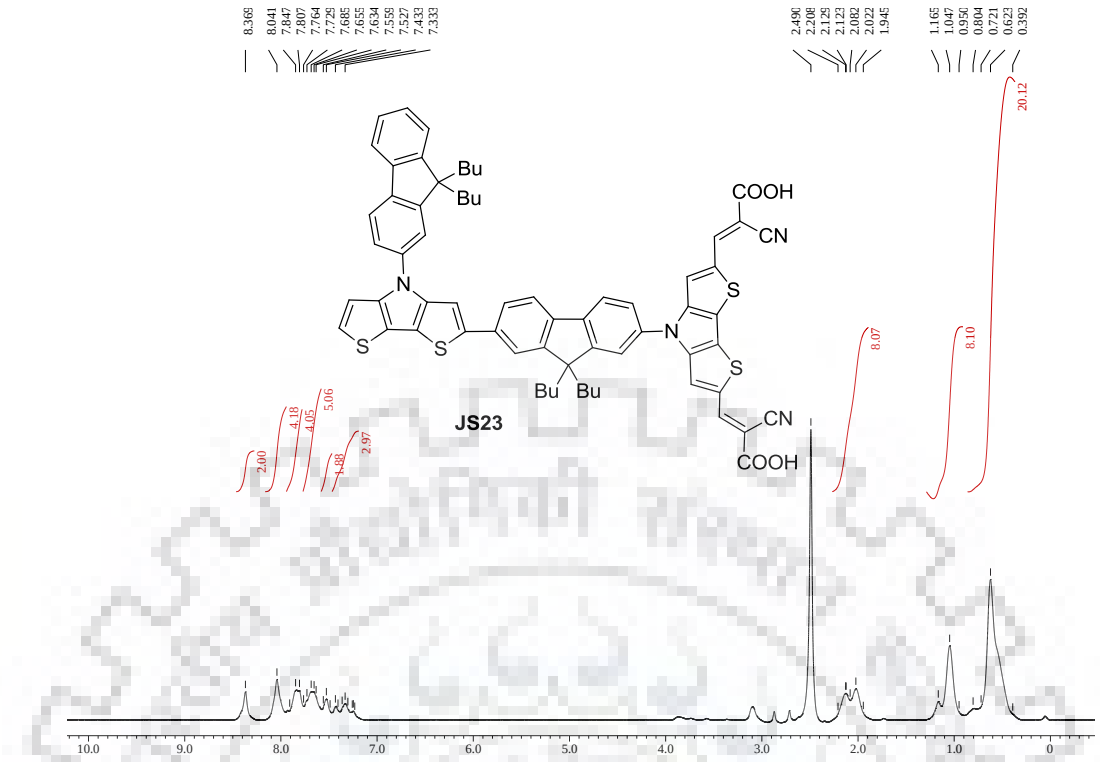

Figure S67 ^{1}H NMR spectra of **JS23** recorded in DMSO-d_6.

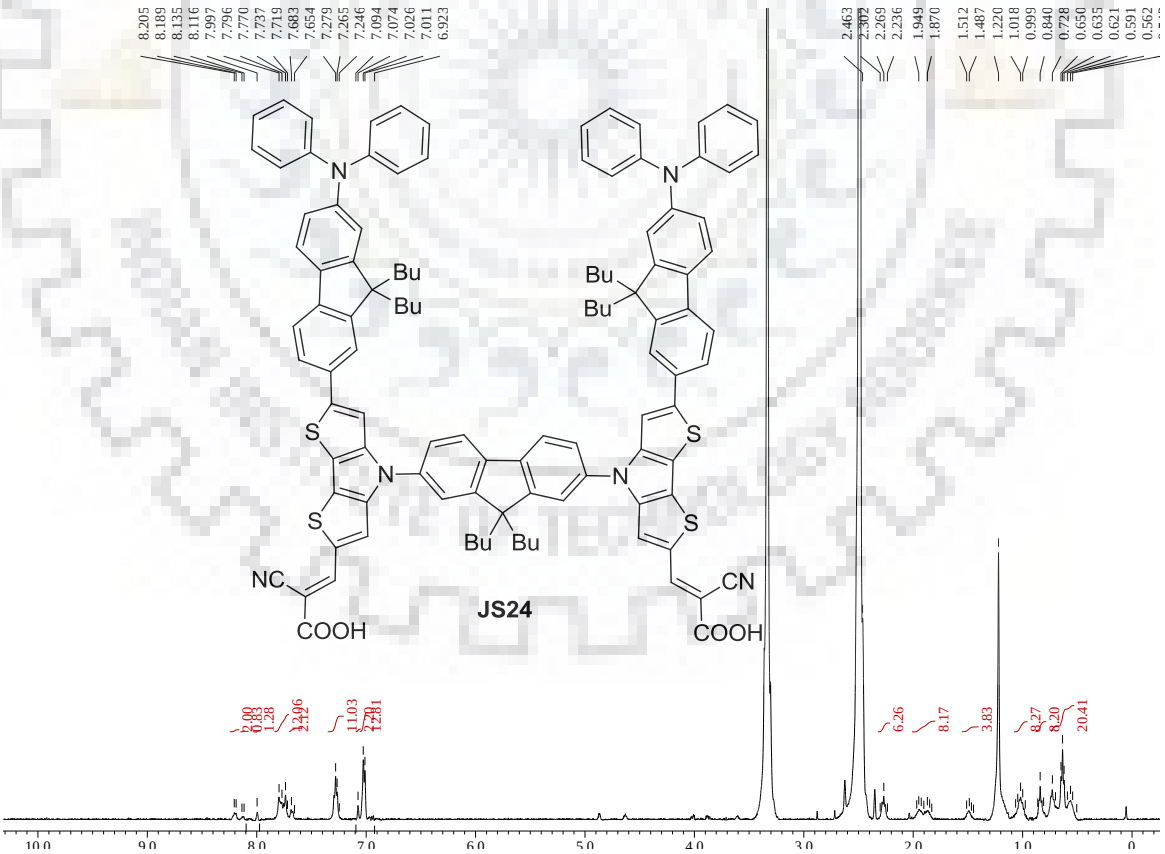

Figure S68 ^{1}H NMR spectra of **JS24** recorded in DMSO-d_6.